Characterising the transcriptional, spatial and behavioural consequences of TLR7-driven neuroinflammation

Kirstyn Gardner-Stephen BSc (Hons)

A thesis submitted in fulfilment of the requirements of the University of Glasgow for the degree of Doctor of Philosophy

School of Infection & Immunology
College of Medical, Veterinary and Life Science
University of Glasgow

July 2025

Abstract

Neuropsychiatric conditions, such as depression and anxiety, are a burden for both the people living with them and from a socioeconomic viewpoint. Traditional pharmacological interventions for these syndromes primarily focus on altering levels of monoamine neurotransmitter availability within the brain. From this patient group, a non-responsive fraction to these monoamine treatments has emerged. This calls for better understanding of alternative pathophysiology that can lead to these clinical conditions. From this search for different causative pathways of neuropsychiatric conditions, an inflammation-driven theory emerged. This neuroinflammation-focused pathophysiology proposes that raised intracerebral pro-inflammatory cytokines can alter neural circuits and ultimately result in behavioural changes.

The molecular and cellular mechanisms underpinning neuroinflammation are relatively poorly understood. To further understand these neural changes, this work uses the Aldara model of non-invasive toll-like receptor (TLR)-7-driven neuroinflammation. The Aldara model involves topically applied cream containing imiquimod (IMQ), which is a TLR7 agonist. This has been found to trigger both a peripheral dermal psoriasis-like response and cross the blood brain barrier (BBB) to directly activate TLR7-expressing CNS-resident cells. This thesis focuses on characterising the transcriptional global and region-specific TLR7-driven neuroinflammation. Both brain-resident microglia and peripheral T cell populations will be explored in respect to their cytokine production and reactive status. To characterise the interplay between microglia and mature lymphocytes, RAG2KO mice which lack B and T cells were used. Spatial transcriptomics was used to evaluate the immune cell response within the Aldara model and transcriptionally investigate brain regions linked to reward behaviours. To further characterise inflammation-driven behavioural changes, a battery of behavioural tests have been implemented to characterise anxiety-like and anhedonia-like behaviours.

This data presents a transcriptionally-validated global neuroinflammation response within the Aldara model. Both microglia and T cells are found to actively produce cytokines in the TLR7-driven neuroinflammation. Spatial transcriptomics

identified 5 potential subclusters of immune cells within the CNS. These had a primary pro-inflammatory transcriptional signature with suggestions of a potential anti-inflammatory response. Immune-rich neighbourhoods in the brain were found uniquely in Aldara-treated mice via spatial transcriptomics. RAG2KO Aldara-treated mice still displayed heightened microglial reactivity via Iba1^{+} staining. Brain regions associated with reward circuity were found to upregulate pro-inflammatory transcriptional responses and downregulate synaptic signalling-related genes. Behavioural tests documented an anhedonia-like phenotype within Aldara-treated mice. This work presents the Aldara model as a useful non-invasive tool to study neuroinflammation.

Table of Contents

List of Tables

List of Figures

Chapter 1: Introduction

Chapter 2: Methods

Chapter 3: Whole-brain transcriptomic changes following TLR7-activated neuroinflammation

Chapter 4: Microglial response and changes following TLR7-activated neuroinflammation

Chapter 5: Transcriptomic and flow cytometric analysis of $CD4^+$/$CD8^+$ T cell subsets in TLR7-driven neuroinflammation

Chapter 6: TLR7-driven neuroinflammation results in neurotransmission-related transcriptional changes and anhedonia-like behaviour

Acknowledgements

I can't believe I'm writing this! Reflecting on my academic journey overwhelms me with the amount of love and support I have received throughout. There is an endless list of people I want to thank wholeheartedly for their support during my PhD. Firstly, my supervisors Professor Jonathan Cavanagh and Dr Rhona McGonigal. Thank you for your expertise and guidance throughout this journey. Your support and feedback helped me refine my scientific approach and develop my critical thinking. Thank you to Jonathan for welcoming me into the lab and encouraging me to pursue a PhD. Rhona, you have answered my countless questions with patience and shown me what it means to be good scientist.

I would like to thank George Simpson for his generosity in supporting this research. I feel honoured to be the University of Glasgow's first Inger & George M Simpson Scholar. Thank you to the wonderfully talented staff from the facilities throughout the University of Glasgow. This includes the Central Research Facility, MVLS Flow Core Facility and the Cellular Analysis Facility. Thank you to John Cole, Robin J Carvajal-Quisilema and other bioinformatician colleagues for your guidance, time and expertise in navigating our transcriptomic datasets.

To all my lab lassies Deepika, Lilya & Jen; Lily, Zuzanna and all of level 3 peeps and the TNG group. You all have no idea how much you have taught me. My academia experience was shaped by you all and filled with memories I will cherish for years to come! Thank you for helping me navigate the academic landscape with lots of laughs and support.

Thank you to all my friends outside of the lab who have listened to all my thoughts and worries throughout this process. To my long-time friends, Cara and Shannon. You are always my go-to safe space to air out thoughts which are always met with kindness and the best advice. I feel so lucky to call you my friends and proud of every life move you make.

Everyone knows I am a homebird and I could not have done this without the support of all my family. Mum and Dad, I will never be able to express truly how grateful I am for the life you have provided for us. Mum, with your confidence and

outlook on life, you are truly the woman I strive to become. Your perspective-setting advice of ‘naebody’s deed!’ has remained central to my coping mechanism during this time. Dad, your patience and cool-headed approach to life is something I always try to adopt. Truly everything I do in life is in the hope of making you both proud. Thank you for everything.

My siblings, Ian, Cara & Laurie. I always kid on my fun fact is that I am a big sister. I think this stems from, above everything, the title of ‘sister’ is the best I’ve ever been given and I hold closest to my heart. I am forever learning from you and all your different quirks that make you *you*. Watching you grow up and forge your paths in life is an absolute privilege. I beam with pride whenever I talk about you. I won the family lottery.

To my wee dog Theo, your unconditional love and cuddles got me through more than you’ll ever know (obviously because you’re a dog). I also wish to acknowledge the animals involved in this research, whose contributions were small but significant.

Lastly, my husband Gerald. I’m taking this one opportunity to go against our nature and be lovey dovey in public. Your support and love during this ‘side quest’ has been unwavering. Your encouragement of my studies from high school to now (which is a LOT of years) makes me feel like I can achieve anything I put my mind to. You put us and our happiness above all else. I’m so proud of you and feel privileged to have found my best friend to navigate life with. This accomplishment is as much yours as it is mine. I promise I’m *neeearly* done with studying. Thank you from the bottom of my heart. I love you.

Author's Declaration

I declare that, except where reference is made to the contribution of others, this thesis is a result of my own work. This thesis has not been submitted for any other degree at the University of Glasgow or any other institution.

Kirstyn Gardner-Stephen BSc (Hons)

University of Glasgow

July 2025

Abbreviations

AADC – Aromatic amino acid decarboxylase
AAV – Adeno-associated virus
ACC – Anterior cingulate cortex
AD – Alzheimer's disease
APC – Antigen presenting cell
BAM – Border-associated macrophage
BBB – Blood-brain barrier
BP – Biological processes
cAMP – Cyclic AMP
CC – Cellular component
CNS – Central nervous system
COMT - Catechol-O-methyl transferase
CSF – Cerebrospinal fluid
CUMS – Chronic unpredictable mild stress
D-PBS – Dulbecco's phosphate-buffered saline
DA – Dopamine
DAM – Disease-associated microglia
DAMP – Damage-associated molecular pattern
DAPI – 4',6-diamidino-2-phenylindole
DAT – Dopamine transporter
DE – Differential expression
DEG – Differentially expressed gene
DEPC - Diethpyrocarbonate
DR – Dopamine receptor
EAE – Experimental autoimmune encephalopathy
EPM – Elevated plus maze
FACS – Fluorescent-activated cell sorting
FBS – Foetal bovine serum
FC – Fold change
FFPE – Formalin-fixed paraffin-embedded
FMO – Fluorescent minus one
FOV – Field of view
G-CSF – Granulocyte colony stimulating factor
GABA - gamma-aminobutyric acid
GFAP – Glial fibrillary acidic protein
GO – Gene Ontology
Iba1 – Ionised calcium-binding adaptor molecule 1
IBD – Inflammatory bowel disease
iCCR – Inflammatory chemokine receptor
IFN - Interferons
IHC – Immunohistochemistry
IL – Interleukin
IMQ – Imiquimod
IRF – Interferon-regulatory factors
ISH – *In situ* hybridisation
KO – Knock-out
LPS – Lipopolysaccharide
MAO – Monoamine oxidase
MDD – Major Depressive Disorder
MF – Molecular functions
MHC – Major histocompatibility complex
mRNA – messenger RNA
MS – Multiple sclerosis

MSN – Medium spiny neuron
NAc – Nucleus accumbens
NBF – Neutral-buffered formalin
NDRI – Noradrenaline-dopamine reuptake inhibitor
NGS – Normal goat serum
NK – Natural killer
nt – Nucleotide
NVU – Neurovascular unit
OF – Open field
ORA – Over representation analysis
p.adj – Adjusted p-value
PAMP – Pathogen-associated molecular pattern
PBS – Phosphate-buffered saline
PBS – Phosphate-buffered saline
PBST – Phosphate-buffered saline with Triton X
PC – Principal component
PCA – Principal component analysis
PD – Parkinson's disease
PFA – Paraformaldehyde
PFC – Prefrontal cortex
PL – Project licence
PMA – Phorbol 12-myrisate 13-acetate
QC – Quality check
qPCR – Quantitative polymerase chain reaction
RA – Rheumatoid arthritis
RAG – Recombination activation gene
RIN – RNA integrity number
RNA – Ribonucleic acid
ROI – Region of interest
ROS – Reactive oxygen species
RPM – Rotations per minute
rRNA – Ribosomal ribonucleic acid
SB – Sickness behaviours
scRNAseq – Single-cell RNA sequencing
SD – Standard deviation
SMI – Spatial molecular imager
SPT – Sucrose preference test
SSC – Saline sodium citrate
SSRI – Selective serotonin reuptake inhibitor
ssRNA – Single-stranded RNA
TBI – Traumatic brain injury
Tc – Cytotoxic T cell
TCA – Tricyclic antidepressants
TCR – T cell receptor
Th – Helper T cell
TH – Tyrosine hydroxylase
TLR – Toll-like receptor
TNFα – Tumour necrosis factor alpha
TRD – Treatment-resistant depression
Treg – Regulatory T cell
UMAP – Uniform manifold approximation projection
VTA – Ventral tegmental area
WM – White matter
WT – Wild type

1 Introduction

1.1 Overview

Neuroinflammation is a key biological mechanism which is implicated in many neuropsychiatric conditions including major depressive disorder (MDD), anxiety and schizophrenia. This possible pathological change within the central nervous system (CNS) involves many signalling processes and cellular contributors to carry out its damaging effects. A number of neuropsychiatric conditions, including MDD and anxiety, have an established link to pro-inflammatory cytokines. Patients living with these conditions have documented elevated peripheral cytokines levels including TNFα and IL-6 (Min et al., 2023, Cui et al., 2024, Yirmiya, 2024). This increase of pro-inflammatory molecules observed in MDD underpins the alternative pathophysiology of cytokines being a driver of the neuropsychiatric condition (Felger and Lotrich, 2013). The cytokine hypothesis of depressive behaviours is further supported by evidence of patients receiving cytokine therapy developing depressive-like behaviours. An example of this includes patients living with hepatitis C being administered interferon (IFN)-α therapy and developing depression (Smith et al., 2011). Furthermore, patients treated with Etanercept, an antagonist of TNFα commonly used to treated psoriasis, reported improvement of depression scores in both humans and rodents (Brymer et al., 2018, Yang et al., 2019). Presence of neuroinflammation in both individuals and animal models can manifest the onset of sickness behaviours (SB). This umbrella term encompasses various feelings one may experience when unwell and these include fatigue, reduced appetite and feelings of anhedonia.

This thesis uses the Aldara neuroinflammation model which is triggered by the TLR-7 agonist IMQ. To begin understanding the cellular drivers of the Aldara model and its TLR7-driven neuroinflammation, brain-resident microglia and infiltrating T cells have been selected as the research focus of this study. This is due to their fundamental involvement in initiating, mediating and possibly resolving neuroinflammation. Microglia are the primary immune cell of the CNS and possess similar abilities to their macrophage counterparts. This includes carrying out phagocytosis to remove potentially damaging pathogens and cellular debris. The

brain-resident immune cell also are key drivers and mediators of neuroinflammation in producing and responding to pro-inflammatory cytokines.

Recruitment of peripheral T cells into the brain parenchyma during neuroinflammation can both signify contribution to pro-inflammatory mechanisms and/or attempts of dampening the inflammatory insult. Characterising the presence of exogenous immune populations, such as T cells, in the CNS could highlight their role in promoting or combating the ongoing neuroinflammation present in the Aldara model.

Previous characterisation of the Aldara model has focused on the global nature of the TLR7-driven inflammation. Whilst expanding the understanding of this global transcriptional environment, work in this thesis additionally investigates regional differences. This includes particular focus on brain regions involved in reward-processing behaviours which may explain anhedonia-like phenotype present in the Aldara model. Additionally, a wider phenotypic profile is created of the Aldara model via a battery of behavioural tests to characterise the presence of anxiety-like and anhedonia-like behaviours.

1.2 Neuropsychiatric conditions

The pathophysiology underpinning MDD and other neuropsychiatric conditions is complex and multi-faceted. Several different causative events have emerged ranging from biological deficits to environmental impacts to comorbidity triggers (Cui et al., 2024, Hollander et al., 2020, Hesdorffer, 2016). Dissecting and understanding these pathophysiologies will potentially present new therapeutic targets to help relieve the burden of neuropsychiatric conditions.

It is estimated that 1 in every 5 people live with a neuropsychiatric condition. This family of diagnoses include, however are not limited to, MDD, schizophrenia, anxiety and neurodevelopmental disorders. Each of these conditions are taxing for the people living with them and upon society from a socioeconomic viewpoint (Campbell et al., 2022). Recent work shows the prevalence of MDD and anxiety stands at 12.2% and 17% in Scotland, respectively (Fernandez-Pujals et al., 2015).

Diagnosis of neuropsychiatric conditions is rarely in isolation. These conditions are prevalent comorbidities observed in several somatic conditions including cancer, diabetes, cardiovascular and respiratory diseases (Huang et al., 2024, Lloyd et al., 2018, Sartorius, 2018, Pope and Wood, 2020, Dudek et al., 2020). Considering the high prevalence and devasting impact of neuropsychiatric conditions, relatively little is understood about the underlying molecular and cellular mechanisms driving these complex and heterogenous conditions compared to other non-neuropsychiatric conditions.

One of the leading pathophysiology hypotheses underpinning MDD is the monoamine hypothesis (Potter and Manji, 1994, Lee et al., 2010). This involves an imbalance in monoamine neurotransmitters which include dopamine, noradrenaline and serotonin. The monoamine hypothesis for depression was proposed in the 1950s when patients with hypertension were treated with the drug Reserpine and concurrently developed depressive-like symptoms (Strawbridge et al., 2023). Reserpine induces a reduction in brain monoamine neurotransmitter levels (Baumeister et al., 2003), which is thought to cause this unexpected pharmacological consequence. This disease mechanism has been well explored by the neuropsychiatric field and has resulted in the design of successful therapeutics. This family of drugs include selective serotonin re-uptake inhibitors (SSRIs), noradrenaline-dopamine re-uptake inhibitors (NDRIs) and tricyclic antidepressants (TCAs).

These various pharmacological families of antidepressants generally work by increasing the bioavailability of their respective monoamine neurotransmitter in the brain. SSRIs block the serotonin reuptake transporter on the presynaptic neuronal membrane (Stahl, 1998). This results in increased levels of serotonin available in the synaptic cleft. NDRIs work in a similar mechanism except from blocking noradrenaline and dopamine reuptake transporters. Again, TCAs elicit their effects by similar means but focus on blocking both serotonin and noradrenaline reuptake.

As prescription of monoamine-related therapeutics grew in popularity, a considerable body of non-responding patients to now ‘traditional antidepressants’

also grew (Al-Harbi, 2012). The research began to uncover a fraction as high as 30% of people diagnosed with depression that did not respond clinically to these monoamine-focused interventions (Joffe et al., 1996, Al-Harbi, 2012). This presentation of treatment-resistant depression (TRD) further highlights the heterogeneity of the neuropsychiatric condition and needs for alternative therapeutics. To reveal potential novel therapeutic targets, more research is required to understand alternative molecular and cellular mechanisms driving the pathophysiology underpinning neuropsychiatric conditions.

During the late 20th century, research within the neuropsychiatric field focused on discovering different neuropsychiatric pathophysiology that deviated from the monoamine hypothesis. Depression was starting to be appreciated not only as a change to mental state and behaviour but also coupled with peripheral changes in the body, notably, elevation of circulating proinflammatory cytokines (Himmerich et al., 2019, Burrows et al., 2021). Additionally, this inflammatory bidirectional relationship was presenting in several peripheral inflammatory conditions. This comorbidity dynamic is observed in inflammatory bowel disease (IBD), rheumatoid arthritis (RA) and psoriasis (Graff et al., 2009, Matcham et al., 2013, Russo et al., 2004). Growing clinical evidence was recognising patients with peripheral inflammatory conditions also experienced a high prevalence of neuropsychiatric conditions (Wang et al., 2025). These discoveries initiated the focus on an inflammation-based cause of neuropsychiatric conditions. Resulting in a demand of novel alternative therapeutics that adopted an anti-inflammatory pharmacological approach.

A systematic review conducted in 2016, found that diagnosis of anxiety and depression in patients living with IBD doubled compared to healthy controls (Mikocka-Walus et al., 2016). Common elevated peripheral pro-inflammatory cytokines within IBD patients which correlate with worsening of depressive symptoms include interleukin (IL)-6, interferon (IFN)γ and IL-17 (Moulton et al., 2019). Following a similar pattern, diagnosis of depression within patients living with RA is significantly higher compared to the general population (Nerurkar et al., 2019). Key inflammation molecular players found to be elevated in circulation of RA patients include tumour necrosis factor alpha (TNFα), IL-6 and IL-17

(Parlindungan et al., 2023). Psoriasis again mirrors this comorbidity trend with the condition's upregulation of peripheral cytokines including IFNγ, IL-17 and TNFα. A recent review found that patients living with psoriasis experience significantly higher prevalence of neuropsychiatric conditions including anxiety and MDD (Hedemann et al., 2022, Chen et al., 2021).

Overall, this bidirectional comorbidity between peripheral inflammatory conditions and neuropsychiatric conditions highlights the interplay between peripheral and central brain inflammatory changes. The raised circulating cytokines recorded in these patient groups uncovers a potential origin of these pro-inflammatory agents which can drive negative changes to behaviour (Miller, 2009). This inflammatory link between cytokines, cellular drivers within the brain and changes to behaviour will be a focus in this thesis.

Another body of evidence that supports the role of inflammation in development of depressive-like behaviours is the onset of depression in patients administered cytokine therapy (Capuron et al., 2002). With their action inducing immune-modulatory effects, cytokines are a key area of therapeutic research. They can be used agonistically to aid cellular proliferation and harness their inflammatory effect. These therapeutics include IFNα recombinant therapy for viral infections and granulocyte colony-stimulating factor (G-CSF) in patients with neutropenia (Donini et al., 2007, Finter et al., 1991). Cytokine inhibitors are another beneficial therapeutic tool and aim to decrease the inflammation in several clinical conditions. This includes anti-TNFα therapeutics (e.g. infliximab, etanercept) for peripheral inflammatory conditions such as psoriasis and RA. Overall, these pieces of evidence further proved that altering cytokine levels can promote or attenuate depressive-like symptoms.

1.3 Sickness behaviours

Inflammation may result in the development of SB during periods of acute illness. These encompass a wide scope of signs and symptoms that individuals exhibit in times of inflammation-driven illness which are considered a protective and compensatory mechanism of the body. Some of these behaviours include malaise,

reduced appetite and anhedonia (Kelley and Kent, 2020). Manifestation of SB is considered an evolutionary mechanism to allow the body to tackle the infection (Dantzer, 2009, Dantzer, 2023). These states of mind and body have also been found to potentially precede and mirror the more chronic biology which underpins neuropsychiatric syndromes including MDD and anxiety (Turkheimer et al., 2023, Maes et al., 2012). Neuroinflammation has various key cellular players and molecular mechanisms underpinning the pathological changes associated with the tissue state. These biological components will be discussed later in this chapter with their links to neuroinflammation discussed in tandem.

One symptom common in both SB and neuropsychiatric conditions is anhedonia. Negative changes to mood and motivation are often classified as 'anhedonia' (Cooper et al., 2018). This emotional status is described as the loss of one's ability to feel pleasure or interest in activities that once were enjoyed by the individual. This change in behaviour is thought to have links to reward circuitry in the brain. One brain network which mediates reward behaviour is the dopaminergic mesolimbic pathway.

1.3.1 Depressive-like behaviours and reward circuitry

As scientific work strives to understand the neurobiological changes that lead to a development of anhedonia, these feelings of loss of interest have been linked to reward circuitry deficits (Der-Avakian and Markou, 2012, Hoflich et al., 2019). Individuals reporting anhedonic feelings may also experience reduced motivation in the initial seeking of activities that induce pleasure. In the context of depression pathophysiology, initial studies focused on serotonergic and noradrenergic pathway deficits. As discussed previously in this chapter, this body of research brought about success in the discovery of treatment options including SSRIs and SNRIs (Moncrieff et al., 2023, Gorman and Kent, 1999).

However, with anhedonia and reduced motivation being frequently documented symptoms from individuals living with depression, the relevant dopamine-driven reward pathways gained more interest within the neuropsychiatric field (Ostinelli et al., 2023, Dresp-Langley, 2023). Some of the success attributed to these common monoamine-linked depression treatments have more recently been

linked to changes in dopamine levels within the brain (Li et al., 2020). Understanding dopamine's role in reward pathways and its links to clinical success of first-line antidepressive treatment highlights the neurotransmitters importance when exploring changes to motivation-related behaviours.

As with any complex behaviour, reward and motivation encompass intricate interactions of several different neurotransmitters, neural circuits, and brain regions. Of these, dopamine is one of the primary neurotransmitters for mediation of reward-driven behaviours (Bromberg-Martin et al., 2010).

Dopamine is an example of a catecholamine neurotransmitter and present both in the brain and periphery. Dopamine exerts its myriad of effects via activation of G protein-coupled dopamine receptors (DRs) which have two major subcategories: D1-like and D2-like. The synthesis of dopamine is a two-step process involving the hydroxylation of L-tyrosine to form L-DOPA via the enzyme tyrosine hydroxylase followed by decarboxylation via aromatic amino acid decarboxylase (AADC).

The primary cell type that synthesises dopamine are dopaminergic neurons which are mainly found in the ventral midbrain. Following neuronal excitation, dopaminergic afferents release the neurotransmitter from storage vesicles into the synaptic cleft primarily in the nucleus accumbens (NAc) to modulate reward-related behaviours. Excess dopamine can be removed from the synapse either via dopamine transporters (DAT) or undergo inactivating oxidative deamination via monoamine oxidase (MAO) or *O*-methylation via catechol-*O*-methyl transferase (COMT). Understanding these biosynthesis steps and potential changes to them following neuroinflammation may explain the resulting deficits in motivation and reward.

The mesolimbic pathway is one neural circuit underpinning the coordination of reward and motivation behaviour. This pathway involves various brain regions including the ventral tegmental area (VTA), NAc, amygdala, hippocampus, and prefrontal cortex (PFC). Dopaminergic neurons mediate the effects and behaviours of the mesolimbic pathway. The thalamus is considered a major relay centre and indirect regulator of the mesolimbic pathway via its glutamatergic afferent projections into the NAc which subsequently cause the release of dopamine. The primary neurotransmitter released from NAc efferents is gamma-aminobutyric acid (GABA) via the principal cell type of the brain region medium spiny neurons (MSNs). These GABAergic efferents primarily project to the ventral pallidum which also play a role in the modulation of reward-seeking behaviours. A summary of these neural circuits can be seen in *Figure* 1 (Heshmati and Russo, 2015). These dopamine-driven pathways mediate various cognitive functions including attention, memory and behaviours involved in motivation and reward.

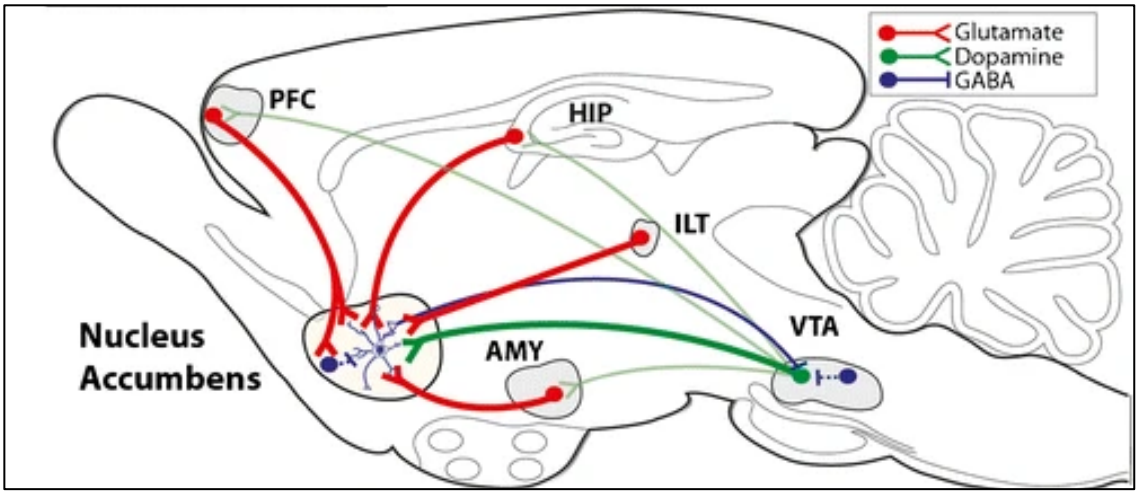

Figure 1: Anhedonia and brain reward circuitry summary on sagittal mouse brain section schematic. *Glutamatergic projections from the prefrontal cortex (PFC), hippocampus (HIP), intralaminar thalamus (ILT) and amygdala (AMY) to the nucleus accumbens. Dopamine projections from the ventral tegmental area (VTA) also to the nucleus accumbens. GABAergic inhibitory projections from the VTA to the nucleus accumbens. Figure adapted from Heshmati and Russo, 2015.*

1.4 Aldara TLR7-driven neuroinflammation model

As discussed previously, the increase of neural cytokines can lead to manifestation of depressive-like behaviours. The exact molecular and cellular drivers of these inflammation-induced behaviours are poorly understood. To begin characterising the biology underpinning these behavioural changes, this thesis will use the non-invasive Aldara model of TLR7-driven neuroinflammation.

Aldara cream is a topically applied treatment which contains the active ingredient IMQ. It is used to treat a range of skin conditions including genital warts, precancerous skin growths (actinic keratoses) and superficial basal cell carcinoma (Wagstaff and Perry, 2007). However, following topical application of Aldara cream, patients started reporting psoriasis-like dermal inflammation (Owens et al., 1998). This then led to the IMQ-containing cream to be used in mice to create an acute dermal inflammation murine model of psoriasis. The psoriasis-like model was first described in 2009 by Van Der Fits (Van der Fits et al., 2009). IMQ is a TLR 7/8 ligand which when activated generates a strong anti-viral immune response involving type I IFN, cytokines, and chemokines. The reaction to IMQ, when applied to the skin, is that similar to human psoriasis infection pathology characterised by erythema of the skin, swelling, scabbing, and itching of the affected area (Badanthadka and D'Souza, 2020). Other more widespread effects of the cream involve hyperkeratosis of the dermal skin layer, splenomegaly, and a draining effect on lymph nodes (Palamara et al., 2004).

Traditionally, this model was created as a psoriasis model and used to study the effects of peripheral inflammation and its downstream effects. The Aldara model serves a powerful tool in the study of psoriasis with its trigger of the IL-17/IL-23 signalling pathway which is harmonious with the pathophysiology detailed in the human disease (Guo et al., 2024). Additionally, the model results in the onset of neuroinflammation including raised intracerebral cytokines and glial cell activation. A pre-clinical model of psoriasis resulting in neuroinflammation would be useful to document links between the peripheral inflammatory condition leading to central brain changes. Studying the presence of neuropsychiatric-like behaviours in psoriasis was of interests due to patients living the dermal conditions reportedly 1.5 times more likely to experience depressive symptoms compared to healthy control cohorts (Hedemann et al., 2022). However, it must be considered that Aldara preparation of IMQ cream contains isostearic acid which has been shown to play a role in activating the TLR7-independent inflammasome response (Walter et al., 2013). This additional pro-inflammatory trigger may be contributing to the overall dermal response in the Aldara model.

Work using the Aldara model then shifted to studying presence of neuroinflammation in the murine model. Mass spectroscopy experiments found that IMQ is present in the brain parenchyma as little as 4-hours post-topical application of Aldara cream (Nerurkar et al., 2017b). Previous experiments also discovered that the 3-day timepoint is the peak of neuroinflammation within the model (McColl et al., 2016). This timepoint will be the one further explored within this thesis. TLR7 is expressed on several brain-resident cells including neurons, astrocytes and primarily microglia (Michaelis et al., 2019). This presented the use of the Aldara model being a non-invasive model of TLR7-driven neuroinflammation.

Previous work has established that the IMQ-driven peripheral inflammation results in central brain changes of IFN-stimulated genes alongside increased neuroinflammation and increased neuroglia activity (Sharma et al., 2024, Nerurkar et al., 2017b, McColl et al., 2016). The Aldara model additionally displays, following from IMQ entering the brain and inducing an anti-viral-like immune response, increased chemokine expression within the CNS. This results in the infiltration of peripheral blood leukocytes into the brain parenchyma including B, T, NKT cells and monocytes. Central brain changes also associated with the Aldara model include a recorded reduction in hippocampal neurogenesis. Furthermore, behavioural implications with a reduction in burrowing behaviour; a commonly used behavioural output to assess routine activity and motivation in rodents (McColl et al., 2016; Jirkof, J Neurosc Methods, 2014). A summary of the neuroinflammation present in the Aldara model and possible TLR7-driven inflammation routes are shown in *Figure 2*.

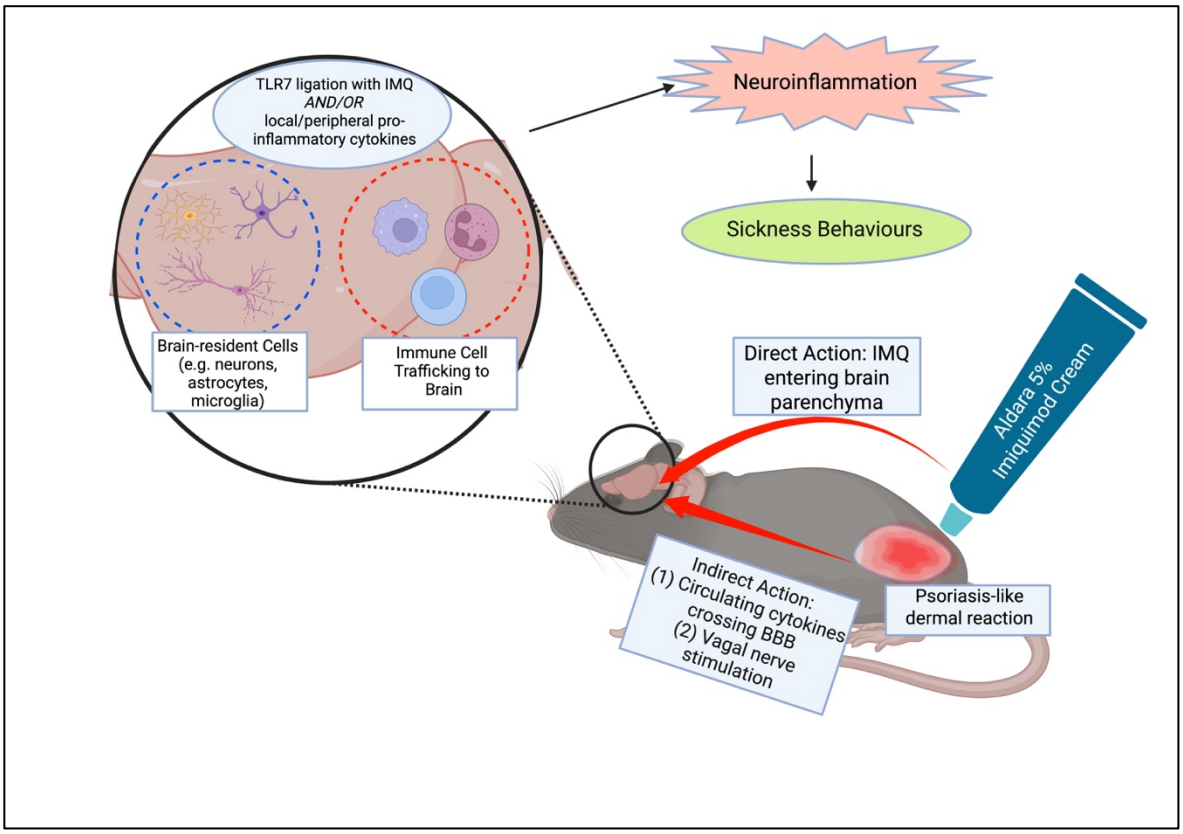

Figure 2: Aldara IMQ TLR7-driven neuroinflammatory model. *Topical application of 5% IMQ cream triggers a psoriasis-like dermal reaction. This creates a systemic pro-inflammatory response. Previous findings show, via mass spectrometry, IMQ enters the brain parenchyma following topical application. This highlights another route of neuroinflammation trigger. A neuroinflammatory response is triggered through activation of brain-resident glia, raised cerebral cytokines and infiltration of peripheral immune cells. This results in changes to behaviours termed 'sickness behaviours'. These changes include reduced appetite, weight changes, reduced burrowing and presentation of anhedonia-like phenotype. Schematic created in https://BioRender.com*

1.4.1 TLR7 signalling pathway and TLR7-activated neuroinflammation

As stated previously, mass spectrometry experiments found IMQ present in brain parenchyma 4 hours post-topical Aldara application (Nerurkar et al., 2017a). This infiltration from circulation is attributed to the chemical composition of IMQ being a lipophilic molecule with a relatively small molecular weight of 240-260kDa (Peralta et al., 2018, Bellettato and Scarpa, 2018). IMQ is a TLR7 ligand which is a modulator of the innate immune response (El-Zayat et al., 2019). TLR7's primary role is recognising pathogen-associated molecular patterns (PAMPs) via single-stranded viral ribonucleic acid (RNA) (Kawasaki and Kawai, 2014). TLR7 ligation activates transcription factors including NF-kB and IFN regulator factors (IRF) via the MyD88 pathway (Hemmi et al., 2002, Bender et al., 2020). The consequential inflammatory pathway triggered is a type I IFN and cytokine-mediated response (Wenzel et al., 2005). A summary of the TLR7 signalling pathway can be seen in *Figure 3 (Lesniak et al., 2023)*.

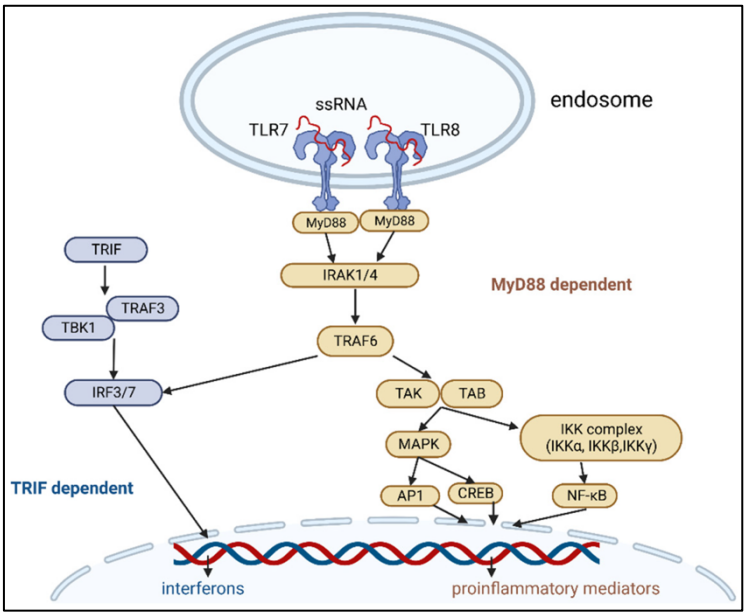

Figure 3: TLR7 signalling pathway. *TLR7/8 located intracellularly on endosomes are innately activated by single-stranded RNA viruses (ssRNA). This activates a molecular cascade results in the production of interferons and pro-inflammatory molecular mediators. Adapted from Leśniak et al., 2023.*

Circulating pro-inflammatory cells that express TLR7 include T cells, B cells, macrophages and monocytes (Li et al., 2019, Fillatreau et al., 2021). The primary cell thought to be driving the dermal TLR7-activated response in the Aldara model

is plasmacytoid dendritic cells (Holcmann et al., 2012). TLR7 expression within the CNS has also been reported in neurons, microglia and astrocytes all which are thought to contribute to neuroinflammation (Hanke and Kielian, 2011). This widespread expression of TLR7 across brain-resident and immune populations highlights different activation mechanisms possible of the TLR7 ligand IMQ. Although exact mode of activation underpinning the neuroinflammation in the Aldara model is unknown, it is important to consider the numerous possible routes of inflammatory pathways. The benefits of this model lie in its non-invasive nature (i.e. IMQ crossing the BBB and activating TLR7 on brain-resident cells directly). The Aldara model evokes a neuroinflammatory response with subsequent changes to behaviour. To further validate the use of this model as a TLR7-driven neuroinflammatory model, experiments in this thesis focus on characterising transcriptional and cellular drivers of the inflammation-induced behavioural changes.

1.5 Neuroinflammation

Neuroinflammation is a multi-cellular and molecular process which mediates pro-inflammatory responses to various pathogenic stimuli. The initiation of neuroinflammation begins as a protective defence mechanism. However, if pro-inflammatory mechanisms persist in the brain chronically, they can result in changes within the CNS. These changes may include negative effects on synaptic plasticity, cellular damage, behavioural changes and chronically elevated neural cytokines (DiSabato et al., 2016).

Presence of cytokines does not necessarily indicate damage within neural tissue. Tolerated levels of these pro-inflammatory molecules are essential for repair, protection, learning & memory (Yong et al., 2019, Bourgognon and Cavanagh, 2020). In periods of sickness, upregulation of pro-inflammatory cytokines is considered a protective adaptive response of organisms. In some cases, this inflammatory response results in the manifestation of SB.

1.5.1 Microglia

As the brain's resident immune population, microglia are a research hotspot when investigating neuroinflammation. Microglia are CNS-resident macrophages and are responsible for a myriad of immune and neural functions. These include the refining of neural networks via synaptic pruning, phagocytotic clearance of cellular debris and secretion of inflammation-mediating molecules (Colonna and Butovsky, 2017). This innate immune cell of the brain is essential for the protection of the CNS and response to any pathogens and inflammatory stimuli. A summary of their homeostatic and pathological responses can be seen in *Figure 4 (Pocock and Piers, 2018)*.

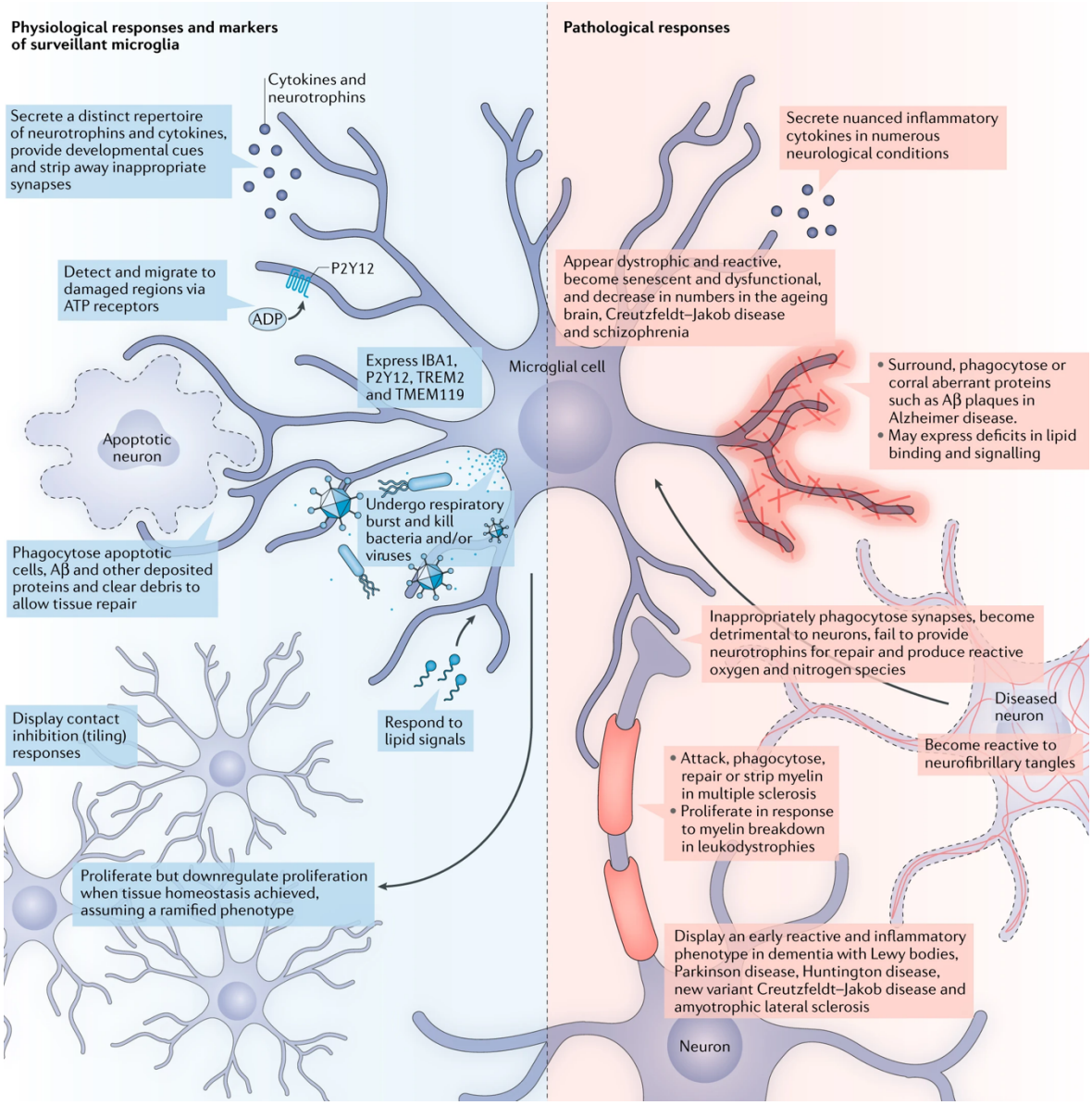

Figure 4: Summary of homeostatic and pathological microglial responses. *Schematic adapted from Pocock and Piers, 2018.*

The lineage of microglia is unique compared to other tissue-resident macrophages in originating from erythromyeloid precursors from the yolk sac (Alliot et al., 1999, Prinz and Priller, 2014). Other myeloid populations differentiate from stem cells located in the bone marrow. This difference in lineage of microglia and other myeloid populations is useful for distinguishing the 2 broad populations. The cellular origin differences allow for techniques such as cellular fate mapping to detail cells', such as microglia, precursor and development stages (Bobotis et al., 2024).

Microglia form the first-line of innate defence for the CNS with initial activation having a protective role. The brain-resident immune population actively contribute to both damaging and reparative processes through the release of both pro-inflammatory and anti-inflammatory cytokines (Piano et al., 2023). Microglia have been shown to respond both to direct brain inflammation and also immune challenges in the periphery (Dantzer et al., 2008). In systemic inflammatory lipopolysaccharide (LPS) rodent models, microglia have been identified as key cellular regulators of the consequential neuroinflammation (Geloso et al., 2024). This peripherally-induced microglial reactivity has been demonstrated via increased ionised calcium-binding adaptor molecule 1 (Iba1) staining and increase pro-inflammatory cytokines from the innate brain immune cell (Norden et al., 2016). Microglia are equipped with TLRs which aid their surveillance and responsive abilities in the CNS tissue (Jack et al., 2005). This surface and intracellular family of receptors allow for detection and recognition of damage-associated molecular patterns (DAMPs) and PAMPs. Depending on which subtype of TLR is activated, this results in a multi-molecular pro-inflammatory cascade typically consisting of cytokines and type I IFNs. As TLR7 is known to be expressed on microglia and, when activated, triggers a pro-inflammatory response, this presents the Aldara model as a useful research tool.

Following a pathogenic stimulus, microglia can change their reactive status. This shift to a reactive microglial phenotype results in various transcriptional changes and increased cytokine production (Guvenek et al., 2024, Muzio et al., 2021). Additionally, changes to microglial morphology is a primary indicator of their reactive status. When faced with pro-inflammatory triggers, microglia may alter their morphology from a complex ramified structure with many cellular processes to an ameboid structure (Adrian et al., 2023, Green and Rowe, 2024). Increased microglial processes have been imaged, via two-photon imaging, to aid immune surveillance and synaptic remodelling (Kamei et al., 2022, Nimmerjahn et al., 2005). These morphological changes highlight microglia’s goal to survey the brain parenchyma and respond accordingly.

The nomenclature surrounding the microglial field is ever-changing in pursuit of the most accurate classification of the brain-resident cell. Originally, microglia

were categorised similarly to peripheral macrophage as M1 or M2 phenotypes based on showing pro-inflammatory and anti-inflammatory properties, respectively. However, microglial reactivity states are now known to be more complex and exist in a spectrum of physiology (Wang et al., 2023a). Single-cell RNA sequencing (scRNAseq) has provided an in-depth exploration into the transcriptomic profiles of mouse microglia in various tissue environments. These experiments have revealed the true heterogeneity of the brain-resident immune population (Hammond et al., 2019). Subsets of microglia have been described in different tissue states including aged brain, diseased and post-injury (Jin and Yamashita, 2016). These differing phenotypes and functional abilities of microglia highlight the true multidimensional nature of the glial population. This evidence supports the abandonment of previous M1/M2 polarity categorisation of microglia to more accurately portray their variable reactivity status.

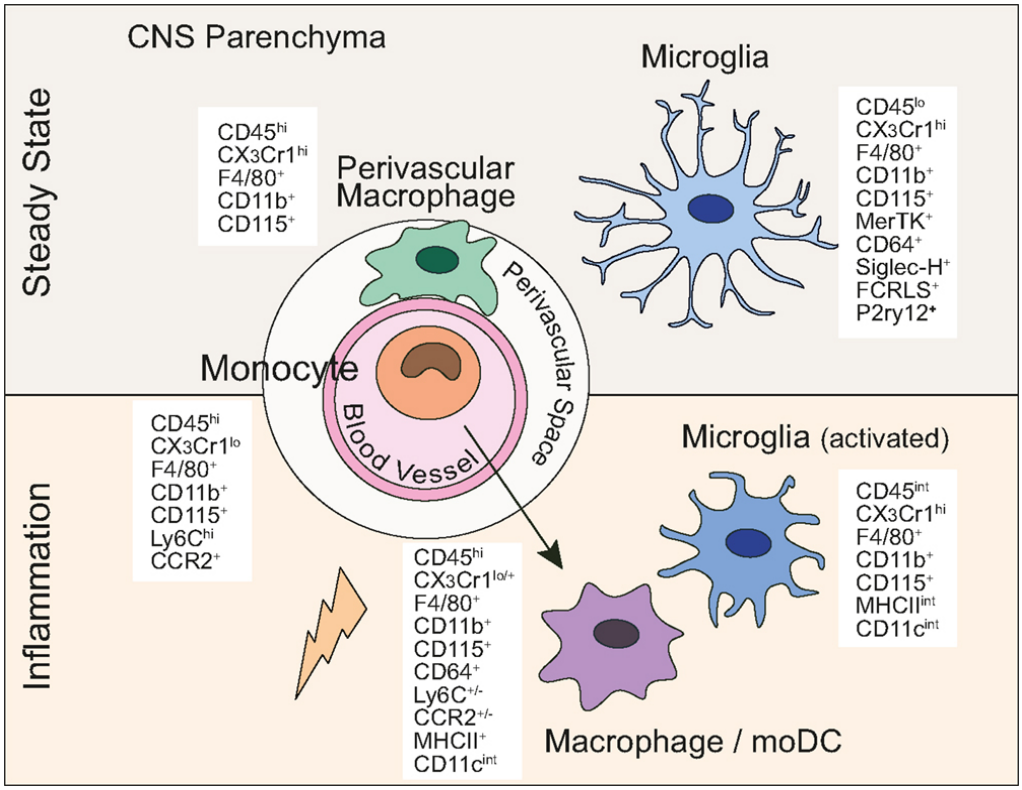

Figure 5: CNS-related myeloid cells including their unique and overlapping markers. *Adapted from (Greter et al., 2015).*

Microglia express a variety of cell surface markers with single cell experiments documenting a wide range of markers of the CNS immune population in both humans and rodents (Mrdjen et al., 2018, Yaqubi et al., 2023). A number of these

microglial markers are shared with other myeloid populations such as macrophages and monocytes as illustrated in *Figure 5 (*Greter et al., 2015).

In vitro, the cytoplasmic marker Iba1 can be used to visualise both microglia at rest and at increased levels indicating reactive microglia (Bennett and Viaene, 2021, Ito et al., 1998). Iba1 is also capable of staining other myeloid population including circulating monocytes and macrophages which needs to be considered when interpreting results (Cora et al., 2020). Using Iba1 staining can serve as a preliminary result of general microglial reactivity within the CNS. Microglia share various markers with their other myeloid cell types (*Figure 5)*. As microglia perform similarly to their macrophage counterparts and possess these shared cellular markers, teasing apart the population proves a difficult task for the neuroimmunology field. Some surface markers expressed by microglia include Tmem119, P2ry12 and Msr1 alongside pan immune markers such as CD45 and CD11b (Hammond et al., 2019). However, work with inflammatory models have demonstrated that macrophages and other myeloids can express these 'microglial markers' (Jurga et al., 2020). Additionally, the expression of these myeloid cellular markers varies depending on the biological state of the tissue. This highlights the lack of unique and specific microglial markers within the neuroimmunology field.

This restricted identification of true microglia from other myeloid populations creates a technical limitation when studying neuroinflammation. Both activation of resident microglia and infiltration of macrophages are at play in various neuroinflammatory environments including models of Alzheimer's disease (AD) and traumatic brain injury (TBI) (Minogue, 2017). This inability to reliably distinguish microglia from other infiltrating myeloid populations during neuroinflammation limits the accurate characterisation of the different cellular drivers. However, whilst maintaining this limitation in mind when interpreting results, consequential pro-inflammatory effects of both cellular population can still be characterised. Various technical methods exist to attempt to separate out the innate and infiltrating myeloid cellular drivers of neuroinflammation.

One method of separating microglial and myeloid populations is through varying expression of the immune marker CD45 via flow cytometry. Recent work has shown brain-resident microglia express relatively 'intermediate' levels of CD45 compared to 'high' expression of macrophage and other myeloid populations (Ritzel et al., 2015, Honarpisheh et al., 2020, Srakocic et al., 2022). This creates a resident microglial population identifiable by a $CD45^{int}$ $CD11b^{+}$ via flow cytometry. However, following inflammatory activation, some microglia may shift their CD45 expression to 'high' and adopt a more macrophage-like phenotype (Honarpisheh et al., 2020). This change in CD45 expression may represent microglia entering a more reactive cellular state in response to neuroinflammation. However, this $CD45^{hi}$ $CD11b^{+}$ will also contain other myeloid populations including infiltrating monocytes and macrophages. Infiltration of this population of $CD45^{hi}$ monocyte-derived macrophages into the CNS has been documented in various mouse neuroinflammatory environments including models of stroke (Ju et al., 2022). Neuroinflammation-mediated mouse stress models also demonstrate an increase of the peripherally-derived $CD45^{hi}$ myeloid populations (Wohleb et al., 2014, Mildner et al., 2007). Using additional microglial or macrophage-specific markers on these flow cytometry populations could further delineate the 2 myeloid populations from each other.

Another subset of macrophages that have been shown to be involved in the regulation of the brain's immune response are border-associated macrophages (BAMs) (Sun and Jiang, 2024b). The BAMs encompass various subsets of macrophages residing in meningeal tissue and space, choroid plexus and perivascular area. This broad category of macrophages are derived from bone marrow stem cells and reside in these CNS boundaries as seen in *Figure 6* (Sun and Jiang, 2024a). These macrophages act similar to other myeloid subset including detecting and responding to immune stimuli. Additionally, BAMs carry out their immunomodulatory role in the production of various molecular drivers including cytokines and chemokines following inflammatory stimuli including peripheral introduction of LPS (Yan et al., 2023). BAMs are another macrophage subset which express similar surface markers to microglia including CSF1R, MerTK and Iba1 (Sun and Jiang, 2024a, Utz et al., 2020). Therefore, care must be taken when interpreting microglial findings as some changes may be attributed to other non-

microglial macrophage subsets. Microglia are similar to their macrophage counterparts in carrying out immune-focused functions in the brain parenchyma. They do possess various unique function due to their resident organ including synaptic pruning and modulation of synaptic transmission.

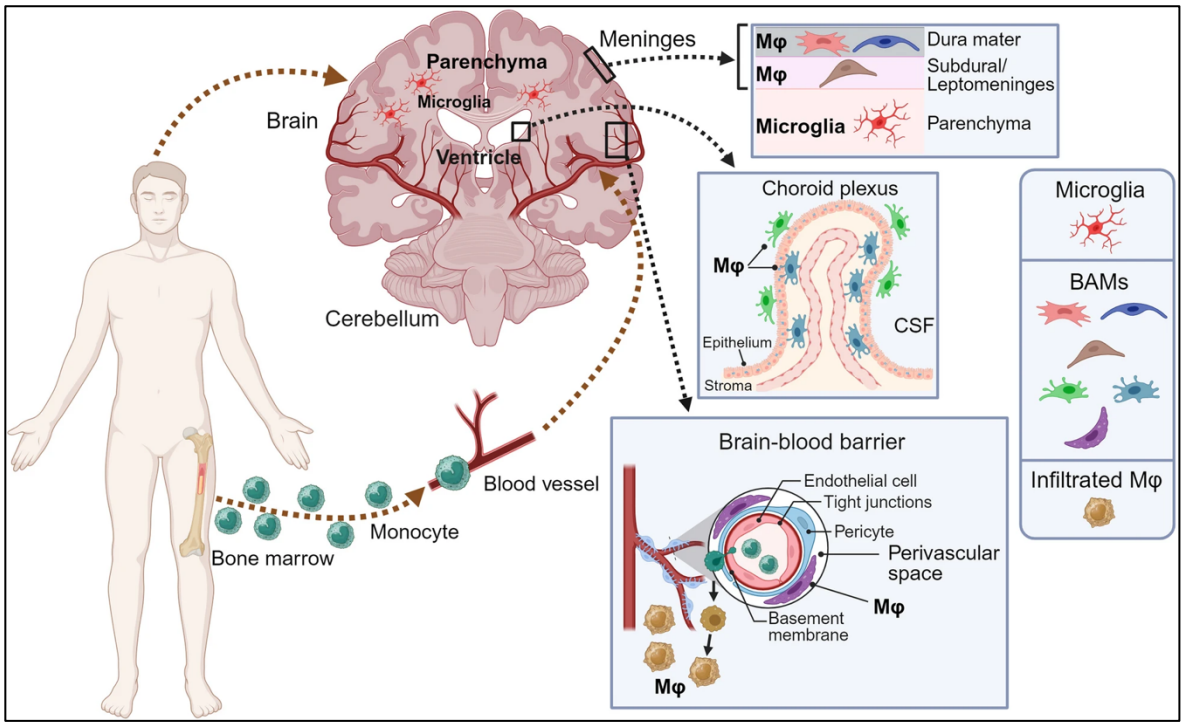

Figure 6: Border-associated macrophages (BAMs) subsets and anatomical differences of brain parenchymal microglia. *Various BAM anatomical niches including meningeal, perivascular and choroid plexus. Macrophage (Mϕ) differentiates from bone marrow stem cells and enter circulation as monocytes. CSF = cerebrospinal fluid. Adapted from Sun and Jiang, 2024.*

1.5.2 Meninges

The meninges are 3 protective layers of the CNS and, in more recent years, has become of interest to immunologists. Recent discoveries of meningeal immunological tissue-niches present the question of their involvement in neuroinflammation (Rebejac et al., 2024). From skull to brain, the 3 meningeal layers are the dura, arachnoid and pia mater. The dura mater is a dense, connective tissue which adheres tightly to the cranium and anchor at the boundaries of the foramen magnum. The dura mater has both a protective function but also organisational one with its folds forming the falx cerebri and tentorium cerebelli which aids the structuring of the cerebrum. The arachnoid mater has a branching appearance which extend into the cerebrospinal fluid (CSF)-

containing subarachnoid space. The arachnoid and its associated features create the shock-absorber feature of the meninges to protect the brain. The pia mater is directly adhered to the brain parenchyma and can be grouped with the arachnoid mater as the leptomeninges.

The meninges were originally thought to solely be responsible for forming the physical protective barrier of the CNS. However, recent work now recognises the meninges as vital regulatory components of CNS immune function (Ransohoff and Engelhardt, 2012). Even at rest, the meninges have an immunomodulatory action on the CNS without any cells trafficking to the brain parenchyma (Rebejac et al., 2024). Various RNA sequencing techniques have revealed the meningeal layers are immune-rich compartments with presence of various subtypes of CD45+ cell populations (Van Hove et al., 2019). Some of the previously discussed BAMs reside in this meningeal space (Sun and Jiang, 2024b). This meningeal myeloid subset are involved in the local immune surveillance and homeostasis of CNS tissues. However, through various transcriptomic profiling of these subtypes they have been distinguished from their brain parenchymal microglial counterparts. Experiments in this thesis have begun to detail the transcriptomic signatures of immune cells in the brain.

When investigating neuroinflammation and its effects on both resident and infiltrating immune populations, it is important to consider the meninges. As will be discussed later in chapters 4 and 5 of this thesis, care must be taken during tissue collection to ensure brain parenchyma is being harvested without meningeal tissue. This is to separate out the 2 immune niches of the CNS and meninges.

1.5.3 CNS immune cell surveillance

The now disproven belief that the CNS is an immune-privileged site was based on the idea that the blood-brain barrier (BBB) created a strict compartmentalisation of the CNS from the peripheral immune system. Now it is understood that, even at rest, there is a delicate interplay between brain-resident immune populations (i.e. microglia), CNS-associated immune niches (e.g. meningeal immune cells, BAMs) and peripheral immune cells. Immune surveillance of the CNS is vital to

maintain a healthy, homeostatic tissue environment is that of immune surveillance. This cellular system patrols the brain parenchyma to identify and eliminate potentially damaging invading pathogens and toxins from the CNS.

As previously discussed, brain-resident microglia are the main contributor to immunosurveillance specifically within the brain. Microglia are the first responders of the CNS tissues by completing phagocytosis, secreting proinflammatory cytokines and can act as antigen presenting cells (APCs) to infiltrating T cell populations into the neural niches. Immune surveillance is vital for neuron and glial function including synaptic transmission. It is now understood that other peripheral immune cells also support the surveillance and immune response within the CNS. CNS-Infiltrating T cells are now a key focus of peripheral and central immune interactions. This is due to the peripheral lymphocyte being a primary mediatory of inflammatory processes by the release of both pro-inflammatory and anti-inflammatory cytokines (Benallegue et al., 2022). These primarily infiltrating T lymphocytes are known to respond to a variety of neural immune stimuli.

1.5.4 T lymphocytes

Recent work demonstrates the importance of peripheral immune cells in modulating the neuroimmune environment. T cells, B cells and macrophages are involved in the cellular processes mediating neuroinflammation (Ni Chasaide and Lynch, 2020, Ahn et al., 2021). This thesis focuses on T lymphocytes (T cells) and their role in TLR7-driven neuroinflammation as the chosen 3-day timepoint of inflammation is relatively acute (McColl et al., 2016). Other peripheral immune cells such as B cells are more often associated with chronic states of inflammation.

The major subcategorisation of T cells is that of CD4+ (helper T cells: Th) or CD8+ (cytotoxic T cells: Tc). However, at this stage expression signalling results in the naive T cells becoming double positive for these markers (Parel and Chizzolini, 2004). Before becoming a single positive T cell, this transitional population must undergo positive selection. This process occurs when the T cells interact with thymus-resident epithelial cells which express with major histocompatibility complex (MHC) Class I or II. T cells will differentiate into CD8+ TC or CD4+ Th cells

after interacting with epithelial cells expressing MHC Class I and II, respectively (Swain, 1983). Th cells exhibit a coordinating role of immune responses including activating other immune cells including B cells and myeloid populations (Pobor et al., 1984). Tc cells carry out their functions more directly by inducing apoptosis of pathogenic harmful cells (Groscurth and Filgueira, 1998). Both subtypes are responsible for secretion of key cytokines depending on their further phenotypic characterisation. Full categorisation and mature phenotypes is a multi-molecular process which is summarised in the schematic shown in *Figure 7*.

1.5.4.1 T Cells in neuroinflammation

Infiltration into the CNS of both CD4+ and CD8+ T cells has been demonstrated in a variety of neuroinflammatory environments including mouse models of multiple sclerosis (MS), TBI and stress (Gonzalez and Pacheco, 2014, Xu et al., 2021, Shi et al., 2022). In MS lesions, infiltration of CD4+ T cells has been shown to contribute pro-inflammatory cytokines to the neuroinflammation-driven demyelinating syndrome. IFNγ and IL-17 production from Th cell subsets have been shown as one

of the pro-inflammatory drivers of the pathology in both humans and animal models of MS (Arellano et al., 2017, Domingues et al., 2010).

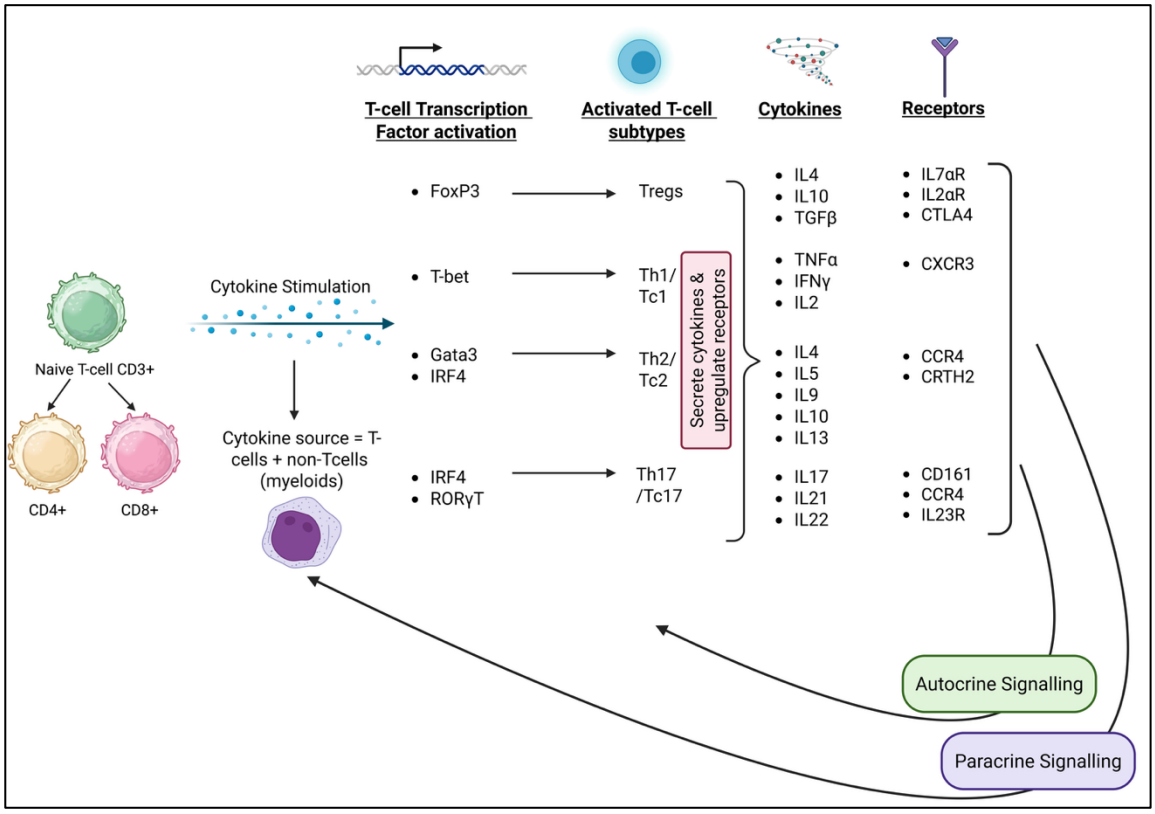

Figure 7: T Cell subset phenotypic characterisation. *Schematic summarising molecular mechanisms underpinning T Cell functional categorisation. Vital transcription factors, cytokine production and surface receptor expression of Tregs, Th1, Th2, Th17 and Th22 subsets shown. Figure created in https://BioRender.com.*

CD8+ T cells elicit a relatively more direct attack during neuroinflammation. This also involves secretions of pro-inflammatory cytokines, in addition to triggering cell death via intrinsic and extrinsic pathways (Jangalwe et al., 2019). CD8+ T cells have established interactions with various brain-resident cells. One pathogenic relationship exists with cytokines produced from astrocytes triggering CD8+ T cells to initiate caspase-3-mediated apoptosis in neurons in acute stage TBI (Wu et al., 2021). T cells and characterisation of their inflammation-mediating components is essential to understanding peripheral immune contribution to neuroinflammation.

CD4+ T cells are essential mediators of neuroinflammation. This Th subset have also been identified in the serum of patients living with anxiety (Dai et al., 2024). These lymphocytes are considered essential for maintaining the balance in neuroinflammation in the production of pro-inflammatory and anti-inflammatory cytokines. The maturation process of microglia has been found dependent on CD4+

T cells (Pasciuto et al., 2020). In the neuroinflammatory AD mouse model, CD4+ T cells have been found to promote microglia to shift to a more phagocytic phenotype with the upregulation of MHCII and P2ry12 (Mittal et al., 2019). Ultimately, this T cell subset plays important roles in the neural environment both independently and participating in glial reactivity.

1.6 Cytokines & chemokines

Cytokines are one of the primary molecular mediators of inflammation in the body. Cytokines encompass other immunomodulatory molecules of cellular response which include chemokines, lymphokines and IFNs. These secretory proteins play a crucial role in the immune system to combat pathogens. Cytokines trigger signalling cascades within cells via interaction with their relevant 7-transmembrane G-protein-coupled receptors (Lowry, 1993). Depending on what cell and corresponding receptor cytokines act upon, a single cytokine can have several differing effects. In their role as immune response regulator, they have a homeostatic role that can be either pro- or anti-inflammatory.

As with peripheral inflammation, neuroinflammation is initiated and modulated by cytokines (Konsman, 2022). These neural cytokines can originate from either resident populations (e.g. microglia, astrocytes and neurons) or responding infiltrating peripheral leukocytes. Cytokines play a key role in brain development and homeostatic mechanisms such as learning and memory (Bourgognon and Cavanagh, 2020, Mousa and Bakhiet, 2013). Initiation of a pathogenic neuroinflammatory environment triggers a cascade of damaging consequences. They range from BBB remodelling, leukocyte trafficking to the CNS, aggregation of abnormal proteins, behaviours and synaptic deficits. Detailing the molecular mechanisms that lead to these consequences would provide better understanding of potential damage-limiting therapeutic targets.

1.6.1 Pro-inflammatory cytokines

A variety of pro-inflammatory and anti-inflammatory cytokines are documented in neuropsychiatric conditions including MDD, schizophrenia and anxiety (Kim et

al., 2016, Na et al., 2014, Kronfol and Remick, 2000). However, this thesis focuses on a selected panel due to their involvement in neuropsychiatric conditions. Additionally, these cytokines have direct links to microglia and T cells via activation of these cellular populations. These cellular drivers of neuroinflammation are the primary focus on the work in this thesis.

1.6.1.1 TNFα

TNFα is a major player in the initiation and continuation of inflammation within the body. There are many cellular sources of TNFα including macrophages, B cells, activated T cells and within the CNS namely astrocytes and microglia. TNFα has a key regulatory role and can trigger different effects depending on which receptor it acts upon. TNF receptor (TNFR)-1 and TNFR2 both have proinflammatory capacity, however, the latter primarily elicits an anti-inflammatory response.

TNFα plays a homeostatic role in the brain with contributions to plasticity and myelination (Kleidonas et al., 2023, Selmaj and Raine, 1988). The classic proinflammatory cytokine has been established as a key mediator in homeostatic synaptic plasticity to maintain proper neural circuit function (Heir and Stellwagen, 2020). This cytokine has the capacity to have both protective and damaging effects within the CNS. When TNFα levels tip from homeostatic to pathological, several downstream effects occur within the CNS. Primarily via TNFR1 activation, release of proinflammatory cytokines is elicited from both brain-resident microglia and infiltrating immune populations (e.g. infiltrating activated T cells (Raffaele et al., 2020, McCulloch et al., 2024). Endothelial cells of the BBB can also secrete TNFα which may have local effects on the barrier's physiology. This may include decreasing expression of the tight junctions which may result in a breach of the integrity (Versele et al., 2022). Changes to BBB integrity is one of the consequences of neuroinflammation which can exacerbate the pro-inflammatory environment.

TNFα and microglia have an intimate relationship, namely, TNFα-induced activation and maturation of microglia into a proinflammatory phenotype. TNFα-dependent activation of microglia further promotes inflammation within the brain parenchyma, continuing the damaging cycle (Henning et al., 2023). Detailing cellular sources of TNFα in the TLR7-driven neuroinflammation in the Aldara

model aids understanding of the molecular mechanisms underpinning the sequence of pathological events.

As mentioned previously in this introduction, TNFα is one of the pro-inflammatory cytokines found to be implicated in neuropsychiatric conditions namely MDD. Raised serum TNFα levels have been shown to positively correlate with the severity of depression symptoms (Das et al., 2021). One of TNFα's proposed roles in the pathophysiology of depression include decreasing the bioavailability of the essential serotonin precursor tryptophan via stimulating the enzyme indoleamine 1,3-dioxygenase. This enzymatic depletion of tryptophan mediated by TNFα has been shown to results in depressive-like behaviours in preclinical models of stress (Liu et al., 2015). As briefly discussed in the overview section of this chapter, another piece of evidence of TNFα's involvement in neuropsychiatric conditions includes Etanercept and the drug's biological consequences. The antagonist of TNFα, administration of Etanercept has been documented to alleviate neuropsychiatric-like symptoms in both rats and humans (Bayramgurler et al., 2013, Yang et al., 2019).

1.6.1.2 IFNγ

IFNγ is one of the primary pro-inflammatory cytokines that induces glial reactivity in the CNS (Monteiro et al., 2017). Increased levels of IFNγ are typical of an anti-viral response. Literature surrounding IFNγ presents the cytokine as having both neuroinflammatory and neuroprotective effects. IFNγ-incubated cultures stimulated with LPS resulted in a heightened astrocytic neuroprotective response for neurons (Sun et al., 2017). Characterising IFNγ+ cells via flow cytometry could provide clearer understanding of the role of the cytokine. Considering type I IFN signalling is a primary molecular pathway activated within the Aldara model (Grine et al., 2015), this presents the TLR7-driven model as a useful tool for investigating this cytokine's contribution further.

IFNγ displays a similar variability in its role within various neuropsychiatric conditions. The pro-inflammatory cytokine has been documented as both increasing and decreasing in patients living with MDD (Dunn et al., 2020). The link between IFNγ and onset of depressive-like symptoms is exhibited in patients

receiving IFNγ therapy and developing these behavioural changes (Lai et al., 2023). This connection is further suggested with levels of IFNγ mRNA in MS patients positively correlating with severity of depression scores (Kahl et al., 2002). However, serum IFNγ levels have been documented to decrease within MDD patient groups (Daria et al., 2020). This brief investigation of the literature highlights the variable role of IFNγ within neuroinflammatory and neuropsychiatric clinical contexts.

1.6.1.3 IL-6

IL-6 is a common pro-inflammatory cytokine that has both damaging and homeostatic effects within the CNS. It is a key immune regulator with both microglia and astrocytes producing the molecule following viral infection. Specifically for microglial production, IL-6 has been found to have a neuroprotective effect by promoting neuronal survival in viral responses (Chucair-Elliott et al., 2014). Normal feeding behaviours is thought to have an IL-6-dependent mediation with IL-6-deficient mice showing increased eating and rapid weight gain (Lopez-Ferreras et al., 2021). IL-6 is involved in the development of inflammation-induced SB with IL-$6^{-/-}$ mice showing attenuation of systemic LPS-driven behavioural changes (Bluthe et al., 2000).

IL-6 has a well-established pathogenic role within the preclinical context which extends into the clinical conditions. A meta-analysis in 2010 documented IL-6 as one of the primary pro-inflammatory cytokines to be elevated in patients living with MDD (Dowlati et al., 2010). This pathological elevation in IL-6 within neuropsychiatric patients is important to note due to the cytokine's involvement in reduction of adult hippocampal neurogenesis (Marsland et al., 2008). Anti-IL-6 therapy is being investigated into its potential pharmacological use of alleviating depressive-like behaviours in patients living with long-term COVID-19 symptoms (Kappelmann et al., 2021).

1.6.1.4 IL-17

IL-17 is a key pro-inflammatory cytokine with various links to neuroinflammation. Th17 cells are the primary source of IL-17 with other subsets of Th1 and Th2 cells

thought to be an additional source (Xu and Cao, 2010). IL-17 has been shown to act directly on brain resident cells and further promote neuroinflammation namely in neurodegenerative disease and MDD (Chen et al., 2020, Kim et al., 2021a). BBB endothelial cells have been shown to express receptors for IL-17 and activation results in an increase in BBB disruption (Kebir et al., 2007). The presence of SB have been demonstrated to involve IL-17 in their pathogenesis with the cytokine's release from meningeal γδ17 T cells eliciting anxiety-like behaviours in mice (Alves de Lima et al., 2020). Clinical trials are currently underway to investigate the therapeutic potential of monoclonal antibodies against IL-17a in patients with treatment-resistant depression.

As detailed above, IL-17 has a significant immunomodulatory effect within the brain in the context of neuroinflammation. This pro-inflammatory role extends into the cytokine's involvement in a number of neuropsychiatric conditions. Previous studies identified elevated IL-17 serum levels and its primary cellular source Th17 cells in patients living with MDD (Chen et al., 2011). This increase in circulating and CSF IL-17 has also recently been documented in paediatric cases of neuropsychiatric conditions (Foiadelli et al., 2025). Novel therapeutic research is focusing on the use of probiotics to alter Th17 cellular and subsequently IL-17 levels in the hopes to alleviate depressive-like symptoms (Yousefi et al., 2019).

1.6.1.5 IL-21

IL-21 has been found to have a mediating role in a variety of neuropsychiatric conditions. Elevated levels of the pro-inflammatory cytokines have been documented in both humans living with AD and mouse models of the conditions (Baulch et al., 2020, Agrawal et al., 2022). Th17 cells are a major source of IL-21, and these cells have been reported in neuroinflammatory environments including the CNS of mouse AD models (Machhi et al., 2021). IL-21-driven mechanisms in neuroinflammation include the trigger of reactive microglia. Mice injected with IL-21 display heightened microglial reactivity and subsequent elevated neural cytokine levels (Oyamada et al., 2025). Identification of IL-21 including its T cell sources within a neuroinflammatory model could aid understanding in its role between infiltrating T cells and microglial reactivity.

IL-21 has a relatively understudied relationship with neuropsychiatric conditions. Significant increases in gene expression of IL-21 have been documented in patients living with MDD (Galecka et al., 2021). However, this finding is not in agreement with other studies finding no difference in the serum protein IL-21 between MDD patients and healthy controls (Davami et al., 2016).

1.6.2 Anti-inflammatory cytokines

1.6.2.1 IL-10

IL-10 is an anti-inflammatory cytokine considered to be the primary immunosuppressive cytokine in neuroinflammation (Burmeister and Marriott, 2018). Microglia carry out their protective roles through the release of IL-10 to aid resolving of pro-inflammatory environments (Lobo-Silva et al., 2016). IL-10's main producer are CD4+ T cells (Saraiva and O'Garra, 2010). This lymphocyte subset have been identified in neuroinflammatory contexts including the experimental autoimmune encephalomyelitis (EAE) model of MS (Yogev et al., 2022). Investigating cellular sources of anti-inflammatory cytokines in neuroinflammation could reveal drivers of resolution in a given animal model.

IL-10 anti-inflammatory role is also thought to be involved in the pathophysiology leading to neuropsychiatric conditions. A recent case-control study found patients living with anxiety had reduced serum IL-10 levels compared to healthy controls (Sarmin et al., 2024). This reduction in the circulating anti-inflammatory cytokine is also observed in MDD patients (Dhabhar et al., 2009). This highlights the inflammation-driven pathophysiology may be both a heighted pro-inflammatory response coupled with a dampened anti-inflammatory response within neuropsychiatric conditions.

1.6.2.2 IL-4

IL-4 is one of the anti-inflammatory cytokines that plays many roles in neuroinflammation. IL-4 is produced by a variety of immune cells including CNS-infiltrating T cells. Murine models of intrauterine growth restriction, a developmental disorder with a prevalent neuroinflammation, demonstrate a

heightened neuroprotective Th2-driven IL-4 response to restore remyelination processes (Zanno et al., 2019). Another neuroprotective effect of IL-4 is the suppression of key pro-inflammatory cytokines TNFα and IL-1 demonstrated in vitro with LPS-treated purified human monocytes (Hart et al., 1989). IL-4 enhances the phagocytic ability of microglia in a pro-inflammatory subarachnoid haemorrhagic mouse model (Wang et al., 2024).

IL-4 has gained popularity within the psychoneuroimmunology field as being presented as a potential diagnostic factor between active depressive episodes in both MDD and bipolar disorder (Lu et al., 2023a). A recent meta-analysis of patients living with depression also found reductions in circulating IL-4 protein levels (Osimo et al., 2020). This further highlights the potential loss of this anti-inflammatory compensatory mechanism within neuropsychiatric patients.

Experiments focusing on characterising a neuroinflammatory environment, including cellular sources of cytokines present possible target for therapeutic design. As neuroinflammation is controlled by several molecules and pathways and not all having damaging roles, developing drugs to target specific molecules could have a more tailored and fine-tuned treatment approach. These specific cytokine-focused interventions could alleviate the damaging side of inflammation with attempts to maintain neuroprotective aspects of neuroinflammation.

All the discussed pro-inflammatory and anti-inflammatory cytokines have established research and clinical neuroinflammatory links. Of this group of cytokines, previous work with the Aldara model has shown TNFα, IL-6 and IL-10 all to increase and peak within the brain at the 3-day timepoint of the model (McColl et al., 2016). Given these previous findings, these cytokines will be the focus of the experiments in this thesis. This will include identification of cellular origins of the cytokines, namely microglia and T cell subsets. Identification of origin and quantification of these cytokines aid full characterisation of the TLR7-driven neuroinflammatory environment within the Aldara model.

1.7 Using transcriptomics to study neuroinflammation

Transcriptomics is the field of studying an organisms' transcriptome which includes RNA, particularly messenger RNA (mRNA), within cells. RNA sequencing and its various associated branches have grown in popularity within recent years. RNA sequencing utilises isolated RNA samples from organs, tissues or cells and combines the data output with computational techniques to provide a quantified expression of transcripts from the given sample. Investigating the transcriptome provides valuable and reliable estimations of the organism's current biological state and changes following a stimuli.

However, one limitation that existed in the transcriptomic field until recently was the loss of spatial information with the data outputs. Tissue processing prior to single cell sequencing analysis removes cells from their *in-situ* context. Additionally, harvesting of single cells for sequencing can induce cellular damage and death which would alter the transcriptional output. This technical limitation stands true for brain-resident cells. Their complex morphology and proximity to one another makes it difficult to harvest single cell suspensions from brain parenchyma. This is due to cellular processes branching relatively long distances in the mouse brain. For example, microglial ramified branches have been documented to range from 200-350um in length (Reddaway et al., 2023). Therefore, this complex morphology of brain-resident cells makes cellular harvest difficult resulting in a lower yield of cells. Additionally, brain cells are in close and intertwined proximity which strengthens their inter-cell communication to maintain normal physiology. Maintaining a cell in its tissue context is beneficial for understanding proximity to other cells which may be indicative of interaction and influence on one another. This tissue context is essential to truly understanding a cell's state and overall function *in situ*.

The development of spatial transcriptomics aims to address these current limitations of other sequencing techniques (Stahl et al., 2016). Spatial transcriptomic platforms have many versions including Visium by 10X Genomics and Nanostring's contributions of GeoMx and CosMx. Experiments in this thesis have used the spatial transcriptomics platform CosMx, Nanostring's single-cell subcellular transcriptomic spatial molecular imager (SMI).

CosMx's SMI utilises molecular barcodes for its *in situ* hybridisation (ISH) of RNA from intact biological samples. The biology involved does not require any amplification of nucleic acid targets like other techniques (Williams et al., 2022). The RNA ISH probes in CosMx consist of a DNA strand that will bind to the target RNA via a target-binding domain (He et al., 2022). Alongside the target-binding domain is a readout domain which consists of 4 short DNA sequencing (10-20 nucleotides) that all are individually barcoded. Via the CosMx SMI, these ISH probes can be detected, identified and recorded in the target's original tissue location. A schematic of the CosMx RNA ISH probes can be seen in *Figure 8* (He et al., 2022). Imaging of this transcriptional output allows for single-cell and subcellular categorisation of cell type and transcript location.

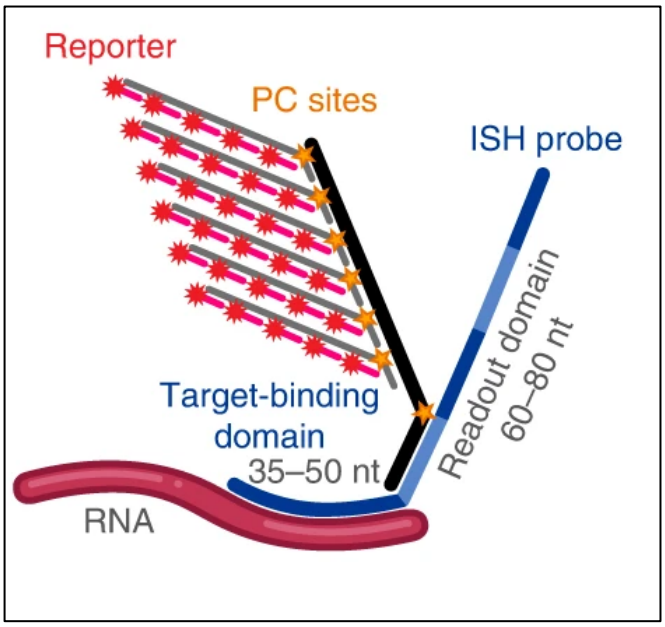

Figure 8: CosMx SMI ISH RNA probes. *Target-binding domain consisting of 35-50 nucleotides (nt). Readout domain of DNA sequence of 60-80 nt. Short DNA strands of 10-20 nt forming the report-landing domains. Each fluorescent reported is attached to DNA via photocleavable (PC) sites. These reports aid transcript in situ location determination. Figure adapted from He et al., 2022.*

For characterising the Aldara TLR7-driven neuroinflammatory model, Nanostring's CosMx Mouse Neuroscience 1000-plex RNA panel can begin to deepen our knowledge of inflammation-driven transcriptional changes. Alongside cell typing, this predefined neuroscience panel contains gene targets used to investigate a variety of changes including glial reactivity, BBB function, cytokine and chemokine signalling and neurotransmission.

1.8 Animal behavioural tests for inflammation-induced behaviours

For robust translational work in the neuropsychiatric field, there must be reliable measures of rodent behaviour via behavioural and functional testing. This becomes a difficult task when considering the heterogenous phenotypes presented in neuropsychiatric conditions such as anxiety and MDD. Furthermore, limitations arise when assuming rodents can feel and express complex human emotions and symptoms (von Mucke-Heim et al., 2023). As previously discussed in this chapter, a common symptom of neuropsychiatric conditions is anhedonia. This describes individuals reporting loss of pleasure from life's experiences. To investigate anhedonia, using reward-focused behavioural tests for rodents provides initial understanding to potential deficits resulting in this lack of pleasure.

An array of behavioural tests can be used to examine these inflammation-induced changes that may be attributed symptoms like anhedonia experiences in neuropsychiatric conditions and SBs. These tests include rotarod for motor capability as Aldara-treated mice present with observed reduced in-cage movements (*Unpublished observation, Kirstyn Gardner-Stephen)*. Before pursuing with other movement-based tests for anxiety and anhedonia-like behaviours, it was important to assess that Aldara-treated mice did not have any motor deficits. Tests used for assessing anxiety-like behaviours will include the elevated plus maze and open field. Other neuroinflammatory models including TBI, systemic LPS and stress present with anxiety-like behaviours assessed by these parameters (Fesharaki-Zadeh et al., 2020, Carregosa et al., 2024). To assess presence of anhedonia-like behaviours within the Aldara model, sucrose preference and nest building will be used as tests. These tests commonly present with deficits in other neuroinflammatory models including chronic unpredictable mild stress (CUMS) and AD mouse models (Markov, 2022, Robinson et al., 2024). Overall, this battery of behavioural tests will assess possible inflammation-induced behavioural changes within the Aldara model.

1.9 Justification and thesis aims

Neuroinflammation is increasingly recognised as a contributor towards the pathophysiology of various neuropsychiatric conditions. This involvement highlights the requirement of clear and detailed understanding of the biological processes underpinning neuroinflammation. More in-depth appreciation for these molecular and cellular drivers may potentially lead to the discovery of novel therapeutic targets for neuropsychiatric conditions. The heterogeneity displayed in neuroinflammation creates a challenging biology to study with multiple facets to its resulting damage and outcomes.

As discussed earlier in this chapter, there are many cellular drivers of neuroinflammation. To fully understand the contribution to neuroinflammation of these cell families, researching the interplay among brain-resident and infiltrating peripheral immune populations is an important mechanism to characterise. In a field lacking in non-invasive neuroinflammatory models, I present the Aldara IMQ model as a beneficial model due to its non-invasive nature. Additionally, the neuroinflammation within the Aldara model has not been described as having neurodegenerative effects. Having access to a reproducible mouse model of neuroinflammation at this sub-chronic timepoint allows for characterisation of molecular and cellular drivers of this neuroinflammation. This would allow for potential intervention at this acute time point before subsequent chronic tissue change occurs with prolonged states of neuroinflammation.

The overarching aim of this thesis is to describe the transcriptional and cellular mechanisms underpinning the TLR7-driven Aldara IMQ neuroinflammatory model. Additionally, a battery of behavioural tests will be used to further characterise the inflammation-induced functional changes within this model. To achieve this aim, I will address the following research questions concerning the Aldara IMQ model:

1. What whole-brain transcriptomic changes, characterised via bulk RNA sequencing and spatial transcriptomics, occur following TLR7-activated neuroinflammation?

2. How does microglial reactivity change in response to TLR7-driven inflammation?
3. What subtypes of T cells are present in the brain parenchyma and what is the cytokine contribution of CNS-infiltrating T cells in TLR7-driven inflammation?
4. What effects does TLR7-driven neuroinflammation have on anxiety-like and depressive-like behaviours including transcriptional changes to associated brain regions?

These experiments aim to characterise and validate the use of the Aldara IMQ model as a non-invasive preclinical model of TLR7-driven neuroinflammation. I hypothesise these forthcoming experiments will show a detailed transcriptional signature of a global pro-inflammatory TLR7-driven neuroinflammatory environment. I believe this neuroinflammatory environment will have both microglia and T cells are cellular drivers of the pro-inflammatory mechanism. Furthermore, I hypothesise from the observed in-cage behaviours of Aldara-treated mice, this neuroinflammation will exert behavioural changes which mimic neuropsychiatric-like symptoms such as anhedonia. Overall, characterising the Aldara model of TLR7-driven neuroinflammation as a useful, non-invasive research tool for the neuropsychiatric field.

2 Materials & methods

2.1 General materials, reagents & equipment

- 5mm Stainless Steel Beads (69989, Qiagen, UK)
- 70μm Cell Strainer (CLS431751, Merck, UK)
- Aldara™ Imiquimod 5% Cream (Meda AB, UK)
- BD Cytofix™ Fixation Buffer (554655, BD Biosciences, USA)
- BD GolgiPlug™ Protein Transport Inhibitor (containing Brefeldin A) (555029, BD Biosciences, USA)
- BD Horizon™ Fixable Viability Stain 510 (15873609, Fisher Scientific, UK)
- BD LSRFortessa™ Cell Analyser (BD Biosciences, USA)
- Boots Aqueous Cream (Boots, UK)
- Bovine Serum Albumin Standard Ampules 2mg/mL (23209, Thermo Scientific™ Pierce™, UK)
- Buffer RPE (1018013, Qiagen, UK)
- Buffer RW1 (1053394, Qiagen, UK)
- CosMx™ Mouse Neuroscience RNA Panel FFPE Kit (Nanostring Technologies, USA)
- Cotton (for nesting material)
- DAPI Nuclear Stain (H-1500-10, Vector Laboratories, UK)
- Debris Removal Solution (130-109-398, Miltenyi Biotec, UK)
- DeNovix DS-11 Series Spectrophotometer (DeNovix Inc., USA)
- Diethypyrocarbonate (DEPC)-treated Water (Nanostring, USA)
- Dolethal 200mg/mL Solution (Covertus, UK)
- Dulbecco's phosphate-buffered saline (D-PBS) with calcium, magnesium, glucose and pyruvate (1419044, ThermoFisher Scientific, UK)
- eBioscience™ Permeabilisation Buffer, 10X (00-8333-56, ThermoFisher Scientific, UK)
- EDTA, 0.5M (AM9260G, ThermoFisher Scientific, UK)
- Enzyme mix 1 (from Miltenyi Biotec Adult Brain Dissociation Kit, UK) = Enzyme P (50ul) and Buffer Z (1900ul)
- Enzyme mix 2 (from Miltenyi Biotec Adult Brain Dissociation Kit) = Buffer Y (20ul) + Enzyme A (10ul)

- Foetal Bovine Serum
- gentleMACS™ C Tubes (130-093-237, Miltenyi Biotec, UK)
- gentleMACS™ Octo Dissociator with Heaters (130-096-427, Miltenyi Biotec, UK)
- Goat anti-Rat IgG antibody, mouse absorbed (H&L), Biotinylated (BA-9401-.5, VectorLabs, USA)
- Haemocytometer
- IBA1 antibody (234308, Sysy Antibodies, Germany)
- Invitrogen™ eBioscience™ Cell Stimulation Cocktail, 500X (00-4970-93, Fisher Scientific, UK)
- ITC Rotarod (755, ITC Life Sciences inc., USA)
- JAX® Mice Strain: C57BL/6J Mice (Strain code: 632, Charles River, USA)
- Leica Biosystems BOND PLUS SLIDES (NC1823288, Fisher Scientific, UK)
- Miltenyi Biotec Adult Brain Dissociation Kit (130-107-677, Miltenyi Biotec, UK)
- Mouse BC Fc Block™ (553141, BD Biosciences, USA)
- Nikon Inverted AX-R Microscope (Nikon, USA)
- Normal Goat Serum (31872, Invitrogen, UK)
- Paraformaldehyde 4% (158127, Sigma-Aldrich, UK)
- PB Buffer: D-PBS with 0.5% BSA
- Phosphate-buffered saline
- *Qiagen* RNeasy Lipid Tissue Mini Kit (74804, Qiagen, UK)
- QIAzol Lysis Reagent (79306, Qiagen, UK)
- Red Blood Cell Lysis Solution, 10x (130-0940183, Miltenyi Biotec, UK)
- RNA*later*™ (AM7021, ThermoFisher Scientific, UK)
- Saline Sodium Citrate (Nanostring, USA)
- SM2010R freezing microtome (Leica, UK)
- Streptavidin, AlexaFluor™ 546 conjugate (S11225, ThermoFisher, UK)
- Sucrose (S0389, Sigma-Aldrich, UK)
- Thermo Scientific Shandon Citadel 1000 tissue processor (ThermoFisher Scientific, UK
- Thermo Shandon AS325 Manual Microtome (Fisher Scientific, UK)
- TissueLyser II (85600, Qiagen, UK)
- Triton™ X-100 (X100, Sigma-Aldrich, UK)

- Trypan Blue Solution, 0.4% (15250061, ThermoFisher Scientific, UK)
- UltraComp eBeads™ Compensation Beads (01-2222-41, ThermoFisher Scientific, UK)
- VECTASHIELD® HARDSET™ Antifade Mounting Medium (H-1400-10, Vector Laboratories, UK)

2.2 Animals

Adult female C57BL/6 mice aged 8 to 10 weeks were obtained from Charles River Laboratories (UK) and housed in University of Glasgow Central Research Facility. Animals were kept in individually ventilated and pathogen-free cages. Animals were permitted one-week to acclimatise to new housing environment prior to commencement of models and/or procedures. Animals were maintained in a 12-hour light/dark cycle in a temperature and humidity-controlled environment. Animals had *ad libitum* access to food and water. All experiments were carried out in accordance with UK Animal Scientific Procedures Act 1986 under a Home Office approved PPL. Local ethical approval was granted by the University of Glasgow Animal Welfare and Ethical Review Board.

2.2.1 RAG2KO Mice

To assess mature B and T lymphocyte contribution, the Aldara model was carried out on mice lacking the *Rag2* gene. This gene is responsible for initiating the recombination sequences essential to produce mature B and T lymphocytes (Akamatsu and Oettinger, 1998, Mombaerts et al., 1992, Shinkai et al., 1992). The transgenic mouse strain was all on a C57BL/6 background. Mice were obtained from the Maizel's laboratory at the University of Glasgow. The Aldara model was completed as described below with the addition of twice daily health checks.

2.3 Aldara 5% imiquimod neuroinflammation animal model

The Aldara™ IMQ neuroinflammation model was completed as per previous studies (Nerurkar et al., 2017a, McColl et al., 2016, Thomson et al., 2014). An

approximately 3cm^3 square region was shaved on the dorsal back region of adult mice. Following this, for 3 consecutive days, mice were weighed daily then 62.5mg of Aldara™ cream (containing 5% IMQ: *Meda AB*) or Control cream (*Boots Aqueous Cream)* was applied to the shaved skin. If mice lost 20% of the initial weight prior to topical cream application, they were culled as per the project license guidelines. Temporary weight loss is expected in the 3-day duration of the Aldara model, however, rarely reaches the 20% limit. Fresh baby food was provided *ad libitum* as a supportive measure to limit inflammation-induced weight loss. Psoriasis-like dermal inflammation was assessed daily using the scoring matrix found in *Table 2.1.* This details inflammation, erythema and scaling potentially caused by topical Aldara cream application. Typical Aldara-treated mice have small daily increments in the 3 dermal inflammation parameters demonstrating a worsening of the psoriasis-like reaction.

Table 2.1: Example psoriasis-like dermal reaction scoring matrix for Aldara-treated mice. Scores are recorded daily for duration of model.

Mouse ID	Day 1 (1st application)				Day 2			
	inflammation	erythema	scaling	Weight	inflammation	erythema	scaling	Weight
xxx	0	0	0	17.6g	1	1	0	16.8g

0: no sign - 1: pinkish skin – a little dandruff - 2: red skin – erythema visible – dandruff - 3: red skin, psoriasis-looking skin, scaling

2.4 Tissue collection & processing

2.4.1 Transcardial perfusion

Mice were terminally anaesthetised via intraperitoneal injection of pentobarbital (Dolethal, 10 µl/g of 200mg/mL solution). To remove most residual blood from brain parenchyma vasculature, transcardial perfusion was performed with 20 mL of ice-cold phosphate-buffered saline (PBS). Brain tissue harvest was performed as per requirement of proceeding experiments.

2.4.2 RNA isolation from whole brain

Following PBS perfusions, one hemisphere was collected and stored at -20°C in 1.5 mL RNA*later*™ (AM7021, ThermoFisher Scientific™). RNA extraction was completed using *Qiagen* RNeasy Lipid Tissue Mini Kit (74804, Qiagen™) and following manufacturer's instructions. Prior to RNA extraction, tissue was thawed and weighed to ensure sample did not exceed maximum weight restriction of extraction columns from Qiagen extraction kit. A summary of the protocol is as follows. Prior to RNA extraction, Buffer RPE was diluted in 100% ethanol (1:4 dilution) and used for nucleic acid purification by removing trace salts. Tissue was weighed and split to comply with 100mg tissue weight upper limit of the kit. Exceeding the weight limit results in poor RNA extraction due to columns saturation with tissue.

Tissue was placed in 2 mL Eppendorfs with 5mm Stainless Steel Beads (69989, Qiagen™) in 1 mL of QIAzol Lysis Reagent. Tissue was disrupted using TissueLyser II (85600, Qiagen™) for 3 minutes at 20 Hz. This allowed for sufficient mechanical dissociation of tissue before proceeding to RNA isolation. Tissue:lysis reagent mixture was left to incubate at room temperature for 5 minutes. 200μl of chloroform was added and then tubes were shaken vigorously for 15 seconds then left to incubate for 3 minutes. Tissue was centrifuged at 12,000 x *g* for 15 minutes at 4°C. This centrifugation separates the lysate into 3 layers: 1. upper, aqueous RNA-containing phase; 2. white lipid-containing middle phase and; 3. lower, organic DNA-containing phase. The upper, aqueous RNA-containing phase was transferred to a new 2 mL Eppendorf and equal volume (approx. 600μl) of 70% ethanol was added and the tube vortexed thoroughly.

700μl of this sample was then transferred to RNeasy Mini spin column within a 2 mL collection tube. This was the maximum volume able to be transferred to the RNeasy spin column to ensure sufficient RNA collection and avoid saturation of the silica membrane. Samples were centrifuged at 8000 x *g* for 15 seconds at room temperature. Flow-through was discarded and a second centrifugation was completed. 700μl of Buffer RW1 was added and centrifuged at 8000 x *g* for 15 seconds at room temperature. Buffer RW1 is a stringent washing reagent which

contains ethanol and guanidine salt. This buffer was used to remove potential contaminating biomolecules including carbohydrates, fatty acids and proteins. Once again to remove trace salts flow-through was discarded and 500μl of Buffer RPE was added then centrifuged. A final washing step was completed using 700μl of 80% ethanol to remove impurities. Extracted and purified RNA was collected by adding 50μl of RNase-free water to the pellet. RNA concentration and purity was measured using DeNovix DS-11 spectrophotometer (Appendix 1).

2.5 Immunofluorescence staining

To determine microglia activation status and T cell contribution to the TLR7-driven neuroinflammation, wild-type and RA2GKO brain tissue was stained with Iba1. This is a commonly used stain to identify microglia both at rest and with reactive phenotypes (Ito et al., 1998). Four treatment groups were used, wild-type Control, wild-type Aldara, RAG2KO Control and RAG2KO Aldara (n=4/treatment). Following perfusion-fixation with ice-cold PBS and 4% paraformaldehyde (PFA), hemispheres were harvested and fixed in 4% PFA overnight at 4°C. Hemisphere tissue was then cryoprotected in 30% sucrose solution at 4°C. Coronal hemisections of 10um thickness were cut using the SM2010R freezing microtome (Leica, UK). Sections were collected into in-house antifreeze solution (30% ethylene glycol, 25% glycerol and 25% 0.2M PB in ddH_2O) at -20°C until the staining process. Storage in antifreeze solutions preserve the integrity and antigenicity of the tissue prior to staining.

All staining and washing steps were completed in a 12-well plate. Prior to antigen retrieval, sections were washed with PBS 3 times to remove residual antifreeze. Antigen retrieval was completed overnight in AGR Buffer (10mM citrate, pH 6.0) in a water bath set at 60°C. Between each staining step, sections were washed in PBS with Triton X (PBST: 0.1M PBS, 0.3% Triton X) for 15 minutes. To reduce background staining, sections were incubated in 100mM glycine solution. Then to reduce non-specific binding of antibodies, tissue sections were then incubated in blocking buffer (3% Normal Goat Serum [NGS] with PBST) for 2 hours at room temperature. Primary antibody incubation of Iba1 (Anti-Iba1 [Guinea Pig], *Synaptic Systems,* 234308) was completed for 72 hours at 1:200 dilution with 1%

NGS. Biotinylated secondary antibody (BA-9401-.5, VectorLabs, USA) incubated for 4 hours at room temperature. Streptavidin tertiary antibody (S11225, ThermoFisher, UK) were incubated for 2 hours at room temperature. A final wash using PBS was completed prior to mounting with VECTASHIELD® HardSet™ with DAPI (H-1500-10, Vector Labs, UK).

10X magnification tile scan images were captured using the Nikon Inverted AX-R Microscope (Nikon, USA) at the University of Glasgow's Imaging Facility. Images were processed using Fiji imaging software (ImageJ2, v2.16.0/1.54p) (Schindelin et al., 2012). All images were set to the same Brightness and Contrast and the 'Reduce Noise' function was also applied. Representative images of full hemisphere and anterior cingulate cortex (ACC) were captured.

2.5.1 Preparation of formalin-fixed paraffin embedded (FFPE) sections for CosMx spatial transcriptomics

For immunohistochemistry and CosMx, following PBS perfusion, mice were transcardially perfused with ice-cold 4% PFA (20 ml) for tissue fixation . Brains were removed, hemisected and incubated in 4% PFA overnight at 4°C to ensure complete fixation of tissue.
Hemispheres were placed in individual embedding cassettes for paraffin embedding using a Thermo Scientific Shandon Citadel 1000 tissue processor (ThermoFisher Scientific, UK). This involved the following steps:

1. 70% Ethanol (1 hour)
2. 90% Ethanol (1 hour)
3. 95% Ethanol (1 hour)
4. 100% Ethanol (1 hour) [repeat 3 times]
5. 100% Ethanol (1.5 hours)
6. 100% Ethanol (2 hours)
7. Xylene (1 hour) [repeat twice]
8. Xylene (1.5 hours)
9. Wax (2 hours)
10. Wax (3 hours)

Total processing time = 17 hours

For steps 9 & 10, 4 mouse brain hemispheres were placed within 1 paraffin block to adhere with CosMx Scan Area boundaries as demonstrated in *Figure 1*. Thermo

Fisher Scientific™ Shandon Finesse 325 microtome was used to cut 6um thick coronal sections into water bath set at 60°C. Sections were mounted onto *Leica Biosystems BOND PLUS SLIDES* according to CosMx imaging area boundaries. Each slide held coronal hemisphere sections of 2 biological replicates from Control and Aldara mice. The total experiment had n=4/ group. For each biological replicate, 6um coronal hemisections were cut in an anterior plane (Bregma range = +1.1 to +0.78 mm) and posterior plane (Bregma range = -1.0 to -2.0 mm). Tissue sections prepared and pre-stained for morphological markers for CosMx can be seen in *Figure 2*-5 with Control (A&B) and Aldara (C&D) samples from each plane. See *Table 2.2* for slide details. Slides were baked at 37°C overnight to improve tissue adherence.

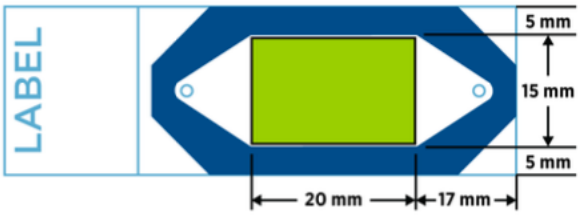

Figure 1: CosMx SMI Tissue preparation guidelines. *Scan Area (green area) represents location of tissue for successful capture by CosMx SMI. Image adapted from CosMx SMI Manual Slide Preparation Manual Page 24.*

Table 2.2: CosMx™ slide IDs and corresponding AtoMx reference slide image

Slide ID	*AtoMx* Reference Slide Image	Sample ID & treatment group (Figure ref)
1055_1	*Figure 2*	Control - 1055antbs1 (2A) Control - 1055antbs2 (2B) Aldara - 1055antbs3 (2C) Aldara - 1055antbs4 (2D)
1055_2	*Figure 3*	Control - 1055posbs1 (3A) Control - 1055posbs2 (3B) Aldara - 1055posbs3 (3C) Aldara - 1055posbs4 (3D)
1056_1	*Figure 4*	Control - 1056antbs1 (4A) Control - 1056antbs2 (4B) Aldara - 1056antbs3 (4C) Aldara - 1056antbs4 (4D)
1056_2	*Figure 5*	Control - 1055posbs1 (5A) Control - 1055posbs2 (5B) Aldara - 1055posbs3 (5C) Aldara - 1055posbs4 (5D)

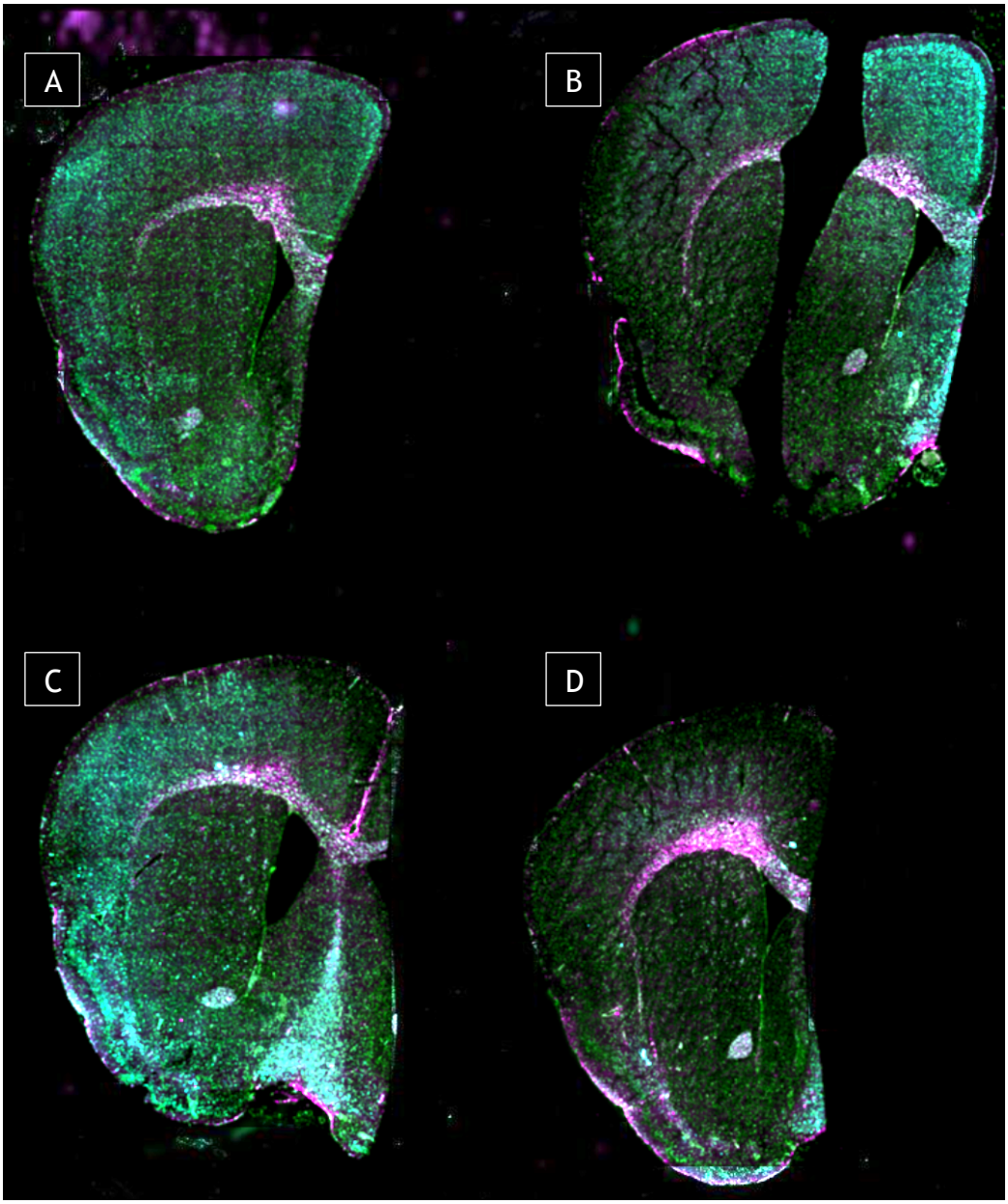

Figure 2: Image of Slide 1055_1 from Nanostring AtoMx platform showing Control (A & B) and Aldara (C & D) anterior coronal hemisphere sections. *Morphology markers shown include GFAP (Magenta), ribosomal RNA (Cyan), Histone (Green) and DNA (Grey). Images shown with altered contrast to aid visualisation.*

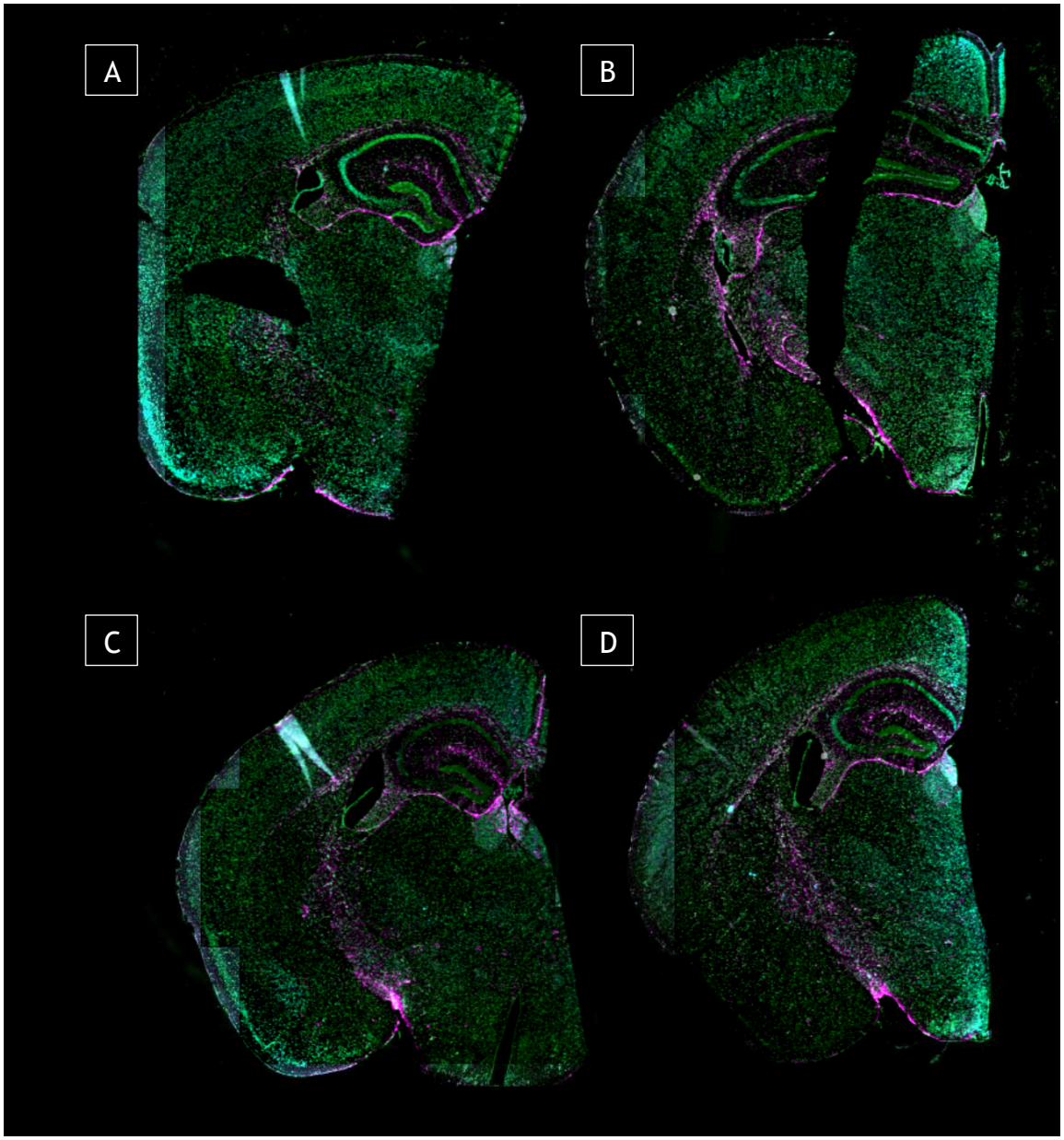

Figure 3: Image of Slide 1055_2 from Nanostring AtoMx platform showing Control (A & B) and Aldara (C & D) posterior coronal hemisphere sections. *Morphology markers shown include GFAP (Magenta), ribosomal RNA (Cyan), Histone (Green) and DNA (Grey). Images shown with altered contrast to aid visualisation.*

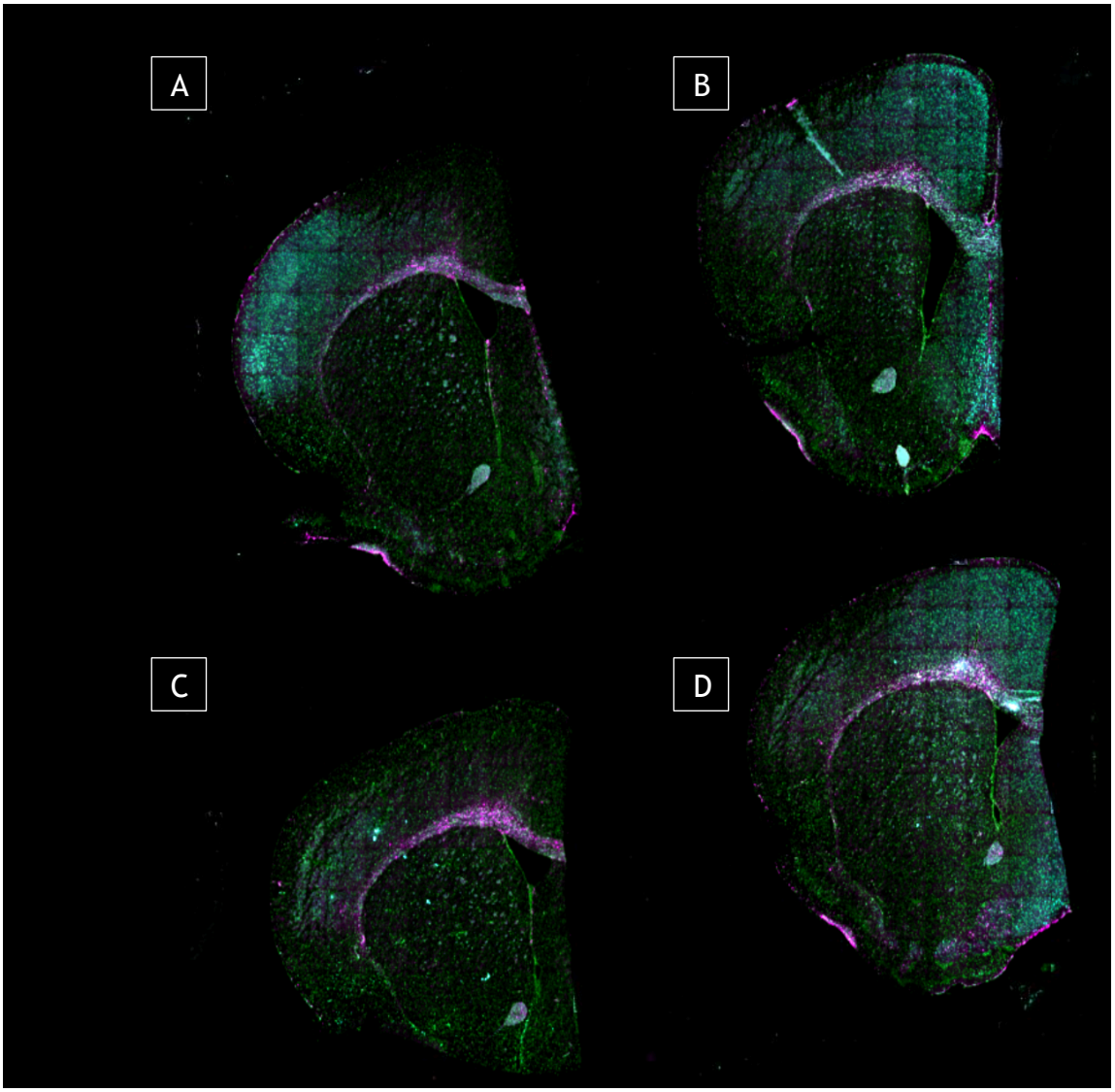

Figure 4: Image of Slide 1056_1 from Nanostring AtoMx platform showing Control (A & B) and Aldara (C & D) anterior coronal hemisphere sections. *Morphology markers shown include GFAP (Magenta), ribosomal RNA (Cyan), Histone (Green) and DNA (Grey). Images shown with altered contrast to aid visualisation.*

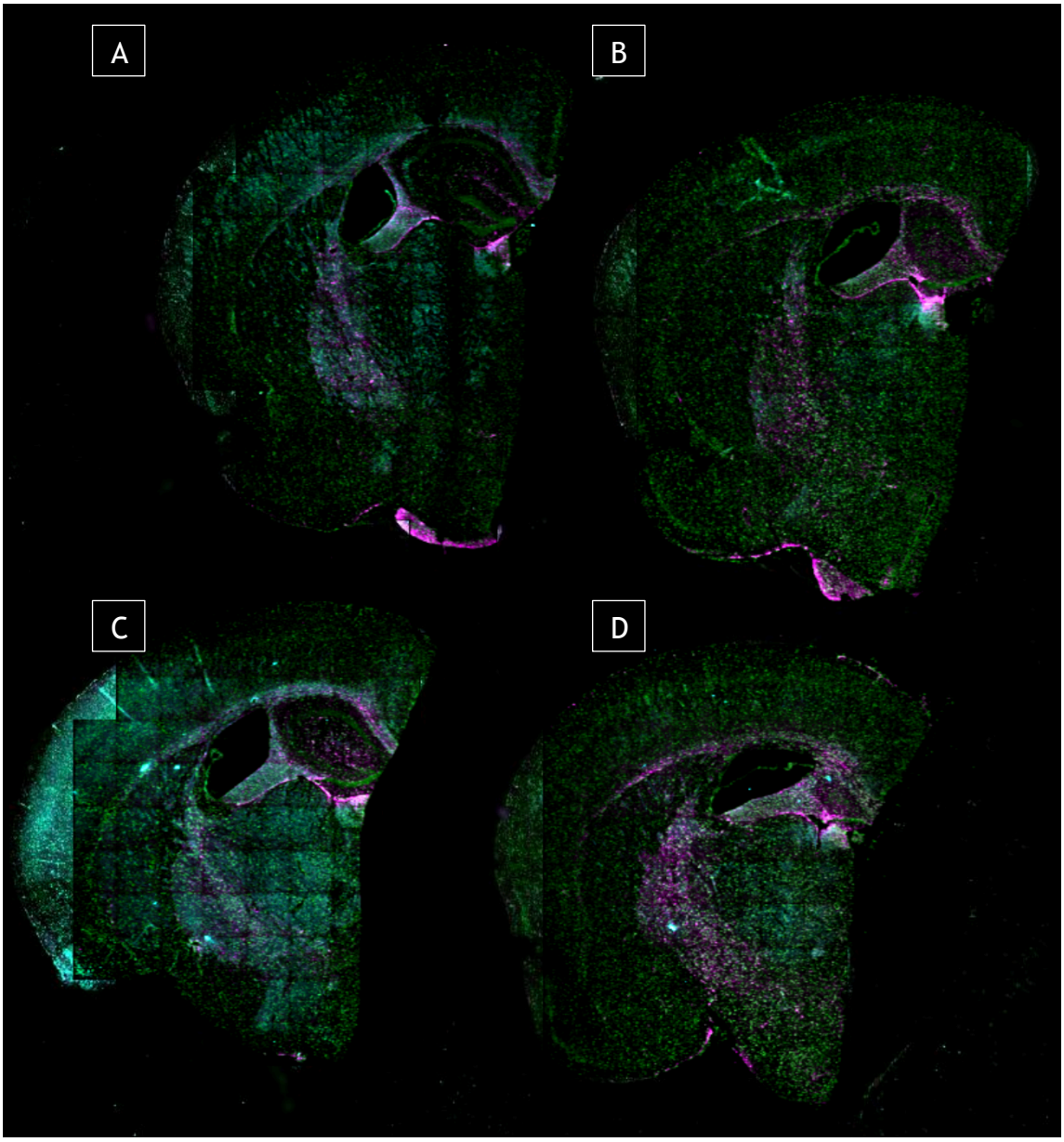

Figure 5: Image of Slide 1056_1 from Nanostring AtoMx platform showing Control (A & B) and Aldara (C & D) posterior coronal hemisphere sections. *Morphology markers shown include GFAP (Magenta), ribosomal RNA (Cyan), Histone (Green) and DNA (Grey). Images shown with altered contrast to aid visualisation.*

2.6 Flow cytometry

Brains were harvested following perfusion with ice-cold PBS. For cell-surface marker flow, 1 hemisphere provides sufficient cell numbers to complete the flow cytometry protocol. For intracellular cytokine and transcription factor staining panels, the whole brain is needed to meet cell number requirements due to additional washing and fixing steps within the protocol that results in unavoidable cell loss.

2.6.1 Adult brain single-cell dissociation

Brain tissue was dissociated using the Adult Brain Dissociation Kit for mouse (Miltenyi Biotech; 130-107-677, UK). After transcardial perfusion of ice-cold PBS to remove most residual blood and tissue harvest, brain tissue is cut into 8-10 small pieces with a scalpel before being transferred into gentleMACS™ C Tubes containing 1950 µL of Enzyme Mix 1 and 30 µL of Enzyme Mix 2. Tissue was dissociated using the gentleMACS™ Octo Dissociator with heaters and pre-defined tissue program 37C_ABDK_01. This machine mechanically disrupts tissue while maintaining samples at 37°C. This created a single-cell suspension of all the cells in the mouse brain. This single-cell suspension included all brain-resident cells (e.g. neurons, astrocytes, microglia and oligodendrocytes) and infiltrating immune populations (e.g. T cells, B cells, macrophages and monocytes). All reagents were maintained ice-cold unless stated otherwise.

2.6.1.1 Debris removal

Following mechanical dissociation, samples were mixed with 10 mL of Dulbecco's PBS (D-PBS). This balanced salt buffer is used to maintain cell viability throughout tissue processing. Samples were then filtered through 70 µm cell strainers whilst using the back of a 5 mL syringe plunger. This filtration step removes extracellular debris such as fatty connective tissue material from the myelin sheath to avoid

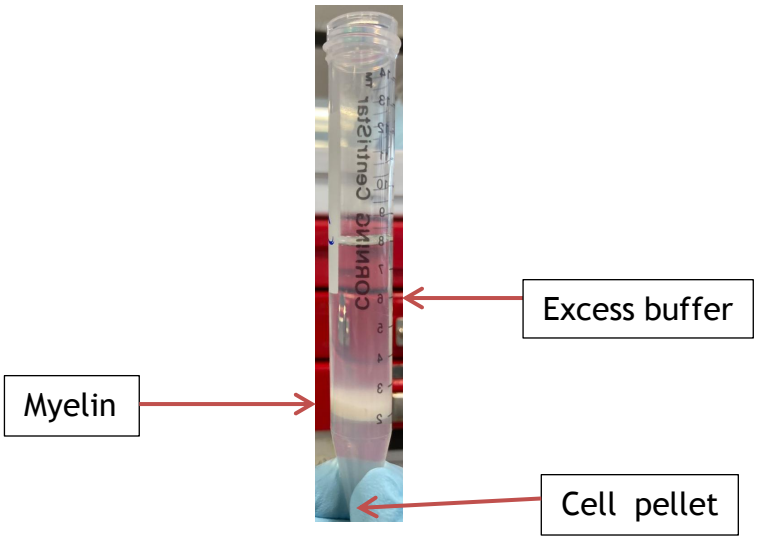

Figure 6: Representative image representing density layer separation technique for single cell flow cytometry tissue preparation. Off-white coloured myelin layer and excess buffer can be removed to continue purification of single cell samples for flow cytometric analysis

clogging of flow cytometer at later stages. Samples were centrifuged at 300 x g for 10 min at 4°C to pellet single cells. The supernatant was discarded, and cell pellet was re-suspended in 3.1 mL of D-PBS and 900μl Debris Removal Solution. Another 4 mL of D-PBS is gently overlayed to create a density gradient solution to remove myelin and isolate cells. This creates a density gradient to separate cells and myelin based on their density following centrifugation. Samples were centrifuged at 3000 x *g* for 10 minutes at 4°C with half acceleration and half brake parameters. Then the top two layers were aspirated and discarded which represent the myelin and excess debris buffer layer as seen in *Figure 6*. D-PBS was added then samples were centrifuged at 1000 x *g* at 4°C for 10 minutes. Aspirate and discard the supernatant leaving behind the cell pellet.

2.6.1.2 Red blood cell removal

To remove erythrocytes, samples were incubated in Red Blood Cell Removal Solution diluted 1:10 with double-distilled water. Cell pellets were resuspended in 1 mL of Red Blood Cell Removal solution and incubated for 10 minutes at 2-8°C. The lysis reaction was then stopped by adding 10 mL of cold PBS and centrifuge at 300x*g* at 4°C for 10 minutes. The cell pellet was then resuspended in 1 mL of D-PBS.

2.6.2 Flow cytometry staining

Trypan blue and a haemocytometer were used for cell counting (live cells exclude trypan blue, and dead cells are stained blue). These cells count were further used to count the absolute numbers of different cell types from Flow cytometry analysis. Incubations were completed in fluorescence-activated cell sorting (FACS) buffer (2% Foetal Bovine Serum [FBS], 0.4% of 50mM EDTA in 1 X PBS) unless stated otherwise. Samples were centrifuged at 400x*g* at 4°C for 5 minutes between incubations unless stated otherwise. Live/Dead staining (eBioscience™ eFluor™ 506, Cat. No.: 65-0866-14, USA) was performed to stain live cells and allow for selection and quantification of live-only cells in future gating analysis. This live/dead staining identifies cells with intact membranes as 'live' cells. 'Dead' cells are those whose membrane is not intact and, therefore, this dye can enter the cell and label intracellular components. Live/Dead staining was completed at

1:1000 dilution in PBS at 4°C for 20 minutes. To prevent non-specific staining, Fc block (Mouse BC Fc Block™: 553141, BD Biosciences, USA) was first performed in 4°C for 20 minutes, at 1:100 dilution. Extracellular marker antibodies were incubated at 4°C for 20 minutes. See Table 2.3 for flow cytometry antibody details.

Table 2.3: Antibody details for flow cytometry experiments

Marker	Fluorophore	Company	Catalogue Number	Clone	RRID	Dilution
CD11b	AF700	Biolegend	101222	M1/70	AB_493705	1:500
CD11b	APCCy7	Biolegend	101226	M1/70	AB_830642	1:500
CD11b	BV785	Biolegend	101243	M1/70	AB_2561373	1:500
CD19	PE Texas Red	Biolegend	115554	6D5	AB_2564001	1:500
CD19	APC-Cy7	Biolegend	115529	6D5	AB_830706	1:500
CD3	Bv711	Biolegend	100241	17A2	AB_2563945	1:500
CD4	Bv605	Biolegend	100451	GK1.5	AB_2564591	1:500
CD4	Bv605	Biolegend	100451	GK1.5	AB_2564591	1:500
CD4	BUV805	BD Biosciences	612900	GK1.5	AB_2739008	1:500
CD45	BUV395	BD Biosciences	564279	30-F11	AB_2651134	1:500
CD45	PCP Cy5.5	Biolegend	103132	30-F12	AB_893340	1:500
CD45	PE Texas Red	Biolegend	103146	30-F11	AB_2564002	1:500
CD45	Bv605	Biolegend	103139	30-F11	AB_2562341	1:500
CD8	FITC	Biolegend	100723	53-6.7	AB_389304	1:500
CD8	PECy7	Biolegend	100722	53-6.7	AB_312761	1:500
CD8	BV650	Biolegend	100741	53-6.7	AB_11124344	1:500
F4/80	BUV805	BD Biosciences	749282	T45-2342	AB_2873657	1:500
GATA3	BV421	Biolegend	653813	16E10A23	AB_2563220	1:100
IFNg	APC	Biolegend	505810	XMG1.2	AB_315404	1:100
IFNg	APC	Biolegend	505810	XMG1.2	AB_315404	1:100
IFNy	Bv421	Biolegend	505830	XMG1.2	AB_2563105	1:100
IL10	PCP-Cy5.5	Biolegend	505027	JES5-16E3	AB_2561522	1:100
IL10	APC	Biolegend	505009	JES5-16E3	AB_315363	1:100
IL17	AF488	Biolegend	506910	TC11-18H10.1	AB_536012	1:100
IL17	AF488	Biolegend	506910	TC11-18H10.1	AB_536012	1:100
IL17	PCP-Cy5.5	Biolegend	506919	TC11-18H10.1	AB_961385	1:100
IL4	Bv421	Biolegend	504119	11B11	AB_10896945	1:100
IL6	APC	Biolegend	504508	MP5-20F3	AB_10694868	1:100
MERTK	PE Texas Red	Biolegend	151524	2B10C42	AB_2876509	1:500
MHCII	Bv786	Biolegend	107645	M5/114.15.2	AB_2565977	1:500
MHCII	Bv786	Biolegend	107645	M5/114.15.2	AB_2565977	1:500
MSR1	BV711	BD Biosciences	268318	Clone 268318	AB_2872549	1:200
NK1.1	PCP Cy5.5	Biolegend	108916	DX5	AB_2129358	1:500
RORyt	APC	eBiosciences	17-6981-82	B2D	AB_2573254	1:100
Tbet	FITC	Biolegend	644811	4B10	AB_2287097	1:100
TNFa	PE	BD Biosciences	554419	MP6-XT22 (RUO)	AB_395380	1:100
TNFa	Bv421	Biolegend	506327	MP6-XT22	AB_10900823	1:100

For intracellular cytokine staining, single cells, post extracellular-marker staining, were stimulated with a Cell Stimulation Cocktail (eBioscience™ Cell Stimulation Cocktail 500X, Cat. No.: 00-4975-03, USA) and incubated with a protein transport Golgi blocker for 4 hours at 37°C in CO2 incubator. The cell stimulation cocktail

is a pre-made (500X) solution containing phorbol 12-myrisate 13-acetate (PMA) and ionomycin. These reagents induce cell activation and stimulate cytokine production. This cell stimulation cocktail is used with a Golgi blocker (BD GolgiPlug™ Protein Transport Inhibitor: BD Biosciences, Cat. No.: 555029, USA) which contains brefeldin A and monensin. These reagents prevent cytokines from being transported out of the cell and instead accumulate the cytokines in the Golgi apparatus and endoplasmic reticulum. This allows for antibody labelling of the cytokines within and flow cytometry analysis. Cells were fixed using Fix Buffer (BD Biosciences; Cat. No.: 554655, USA) then permeabilised with Perm Buffer (BD Biosciences; Cat. No.: 554723, USA). Detergents in the Perm Buffer are used to make small pores in the membranes of fixed cells to allow for entry and staining of antibodies targeting intracellular components. All intracellular antibodies were incubated in Perm Buffer. For all extracellular and intracellular antibody details, see *Table 2.3*.

For fluorescence minus one (FMO) staining controls, pooled sample cells received full panel of antibodies in experiment except from one antibody. These controls were used to determine true 'positive' populations in samples. FMO controls for cell types identified via flow cytometry can be seen in Appendix 3. Compensation was performed using antibody stained UltraComp eBeads (01-2222-41, Thermo Fischer Scientific, UK)

2.6.3 Flow cytometry acquisition & analysis

Flow cytometry was performed using the LSR Fortessa (BD Biosciences, USA) within the Flow Core Facility (University of Glasgow). Data acquisition was completed using BD FACSDiVaTM digital software. Data analysis was completed using FlowJo software version 10.10.0. Data on graphs was generated using absolute cell number as recorded from haemocytometer and gating strategies percentages. Statistical analysis and graphical representation were completed using Prism 10 for macOS version 10.4.0 (527).

2.7 Bulk RNA sequencing: RNA quality analysis, sequencing & data analysis

Isolated RNA samples were stored at -80°C until being shipped to Novogene for sequencing. A minimum of 7 ug per sample was sent to Novogene. After receiving isolated RNA samples, Novogene performed sample quality check (QC). Firstly, 1% agarose gel electrophoresis to assess RNA amount, size and purity. Then, Novogene perform a second round of RNA quality analysis. This was done by using a Nanodrop spectrophotometer to assess RNA concentration and purity via 260/280 and 260/230 ratios. Novogene uses widely accepted 260/280 ratio of ~2.0 and 260/230 ratio range of 2.0-2.2 as acceptable purity levels for RNA samples. Finally, Novogene uses the Agilent2100 to check samples' RNA integrity number (RIN). A sample's RIN provides a value, between 1-10, of how degraded the RNA is with 10 being fully intact RNA and 0 being completely degraded. Novogene RIN requirement is >4.0 for total RNA samples. All RNA samples passed Novogene's QC by adhering to these purity parameters.

Library preparation and bulk RNA sequencing was completed by Novogene. Pair-end sequencing was completed with 2 read per fragment at 150 base pairs. An average of 53 million reads were sequenced per sample. Data alignment was completed by HiSat2 to the mouse genome (mus_musculus) from the Ensembl Genome Browser (Yates et al., 2020). Gene raw reads were normalised followed by differential gene expression which was calculated using DESeq2 (Love et al., 2014). Significantly differentially expressed genes (DEGs) were defined as adjusted p value (p.adj) <0.05 and $\log_2$ fold change >0.5. Glasgow Polyomics Bioinformatics facility aided analysis of sequencing data with the implementation of the Searchlight analysis platform (Cole et al., 2021). This platform provides commonly used data interpretations of bulk RNA sequencing datasets. The graphs included in this thesis are principal component analysis (PCA), heatmaps, distribution of expression values, lollipop graphs and volcano plots.

2.7.1 Over representation analysis (GProfiler)

Three-day treatment timepoint DEGs from the bulk RNA sequencing data were ranked by log_2 fold change and entered on a ranked basis into the GProfiler R online system (Kolberg et al., 2023). To test for multiple corrections of bulk RNA sequencing DEGs to predefined gene sets, the recommended significance threshold algorithm provided by GProfiler developers 'g:SCS threshold' was used. User-defined p-value threshold was set as recommended 0.05. The data input was ordered against the *Mus musculus* database. Three Gene Ontology (GO) reference databases were selected for analysis: Molecular Function (MF), Biological Processes (BP) and Cellular Components (CC). KEGG, Reactome and WikiPaths were excluded due to their biological focus on disease pathophysiological and human physiology.

2.8 CosMx single molecule imaging platform

Following CosMx tissue and slide preparation as per section 1.5.1, the following tissue processing steps and CosMx SMI instrumentation protocol was completed at the Jamieson laboratory at the University of Glasgow. The full CosMx mouse neuroscience 1000-plex panel can be seen in Appendix 2.

2.8.1 Tissue processing and *in situ* hybridisation

The hybridisation cassette was prepared by wetting Kimwipes with 2X saline-sodium citrate (SSC) buffer and heating to 40°C. SSC is used as a stringent washing buffer throughout the CosMx staining protocol. Slides were removed from baking oven and deparaffinization completed via following washing steps:

1. X2 Xylene (five minutes);
2. X2 100% Ethanol (two minutes)

Slides were then left to dry in oven at 60°C for five minutes then left at room temperature prior to target retrieval. Tissue was then washed with diethpyrocarbonate (DEPC)-treated water between each change of reagents unless stated otherwise. DEPC is used throughout as an RNase inhibitor to inactivate ribonucleases and prevent RNA degradation.

Target retrieval was completed next to reveal appropriate antibody binding sites on the brain tissue. Slides were first placed into preheated 100°C 1X Target Retrieval Solution and then the slide jar was returned to a preheated pressure cooker for 15 minutes. Slides were transferred to DEPC-treated water then 100% Ethanol for 3 minutes. Slides were then dried at room temperature for 30 minutes prior to tissue permeabilisation steps.

Incubation frames are pre-cut plastic adhesive boundaries that are used to ensure all future buffers stay within the tissue area to optimise actions and binding of reagents. Incubation frames were adhered onto the slides prior to tissue permeabilisation steps. Digestion buffer was added and incubated with tissue at 40°C for 30 minutes.

Fiducial markers are used in spatial transcriptomic platform to create artificial spatial reference points for future scanning of tissue. Fiducial stock was diluted and used at 0.001% and left to incubate with tissue for 5 minutes at room temperature. Slides were washed in 1X PBS.

Tissue is incubated in Neutral-buffered formalin (NBF) for one minute at room temperature to fix tissue. Fixation was then stopped using the NBF Stop Buffer and wash with 1X PBS.

NHS-acetate is a buffer used to prevent primary amines from interfering with the future staining steps. Binding of primary amines may result in non-specific binding. Slides were then incubated with NHS-Acetate mixtures for 15 minutes at room temperature. Following with 2X SSC for a stringent washing step.

The probe mix containing 1000-plex RNA probes was firstly denatures at 95°C for 2 minutes then crash cooled. The probe mix was then applied to the tissue in the incubation frame and left to incubate overnight at 37°C. The next day, slides were washed in 2X SSC for 25 minutes.

To capture cellular nuclei, a Nuclear Stain Buffer was applied and left to incubate for 15 minutes at room temperature whilst being protected from light. Excess

nuclear stain was removed with a washing step with 1X PBS. Following washing, the CosMx Staining Mix was applied and left to incubate for one hour at room temperature whilst being protected from light. The staining mix is a combination of all 4 cell segmentation markers and blocking buffer. These cell markers include: DAPI for nuclear staining, glial fibrillary acidic protein (GFAP) for astrocytes, rRNA and histone markers. The 4 cell segmentation markers are pre-decided and a part of CosMx's Mouse Neuroscience 1000-plex RNA kit.

A second NHS-acetate application was added to the slides and left to incubate for 15 minutes at room temperature. Again, this was to block any primary amines binding and causing non-specific binding on the tissue. Slides were then washed and stored for up to 6 hours protected from light and submerged in 2X SSC at room temperature until loading on CosMx SMI instrument.

2.8.2 CosMx spatial molecular imager

Once placed into the CosMx SMI, the tissue was scanned and visualised for the four cell segmentation markers in the panel: histones, nuclear, rRNA and GFAP. This then allows for the tissue to be subdivided into 0.51mm x 0.51mm Field of View (FOVs) for image capturing and future data analysis. Each tissue section is covered by a grid of FOVs as shown in *Figure 7*. Across the entire 4 slide CosMx™ experiment, 1348 FOVs were selected. This included most of the coronal hemisphere tissue section from the anterior plane (Bregma range = +1.1 to +0.78 mm) and posterior plane (Bregma range = -1.0 to -2.0 mm).

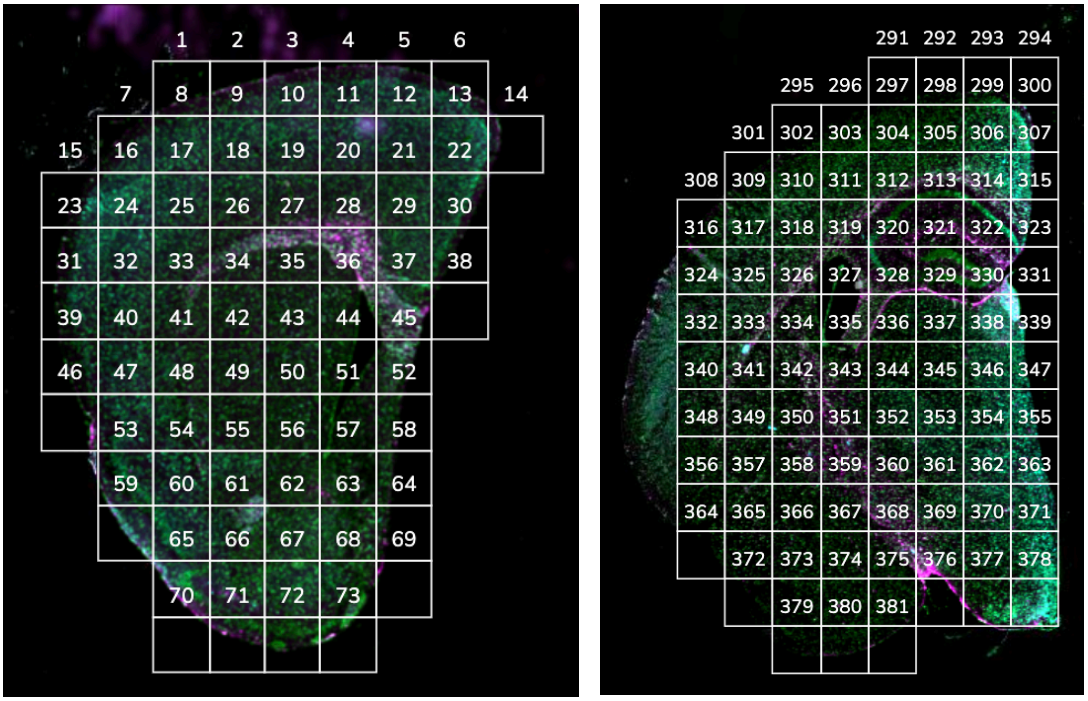

Figure 7: Representative images of CosMx anterior and posterior tissue sections illustrating FOVs grid-like placement for probe processing and capture.

2.8.3 CosMx data analysis

CosMx data processing within R was completed by bioinformaticians Megan Saathoff and Robin Carvajal Quisilema. For the analysis of CosMx data, 2 approaches were taken: first for singular cell types and their DEGs a scRNA-seq method was adopted. Secondly, for brain region analysis, a pseudo-bulk approach was adopted which involved considering all cell types (i.e. a cell agnostic approach) in the differential analysis. This involves taking all transcriptional differences from all cell types together to build a data output of one brain region. Both approaches implemented the Searchlight platform (Cole et al., 2021).

2.8.3.1 Data export, processing & quality control

Following tissue scanning and image processing, CosMx data was downloaded from Nanostring's spatial informatic platform AtoMx. All 16 sections from the 4 slides and their corresponding FOVs were exported as a scRNAseq data object for subsequent analysis using the Seurat toolkit (Hao et al., 2024). These AtoMx exports, now referred to as Seurat objects, contained all polygon and transcript coordinates. Polygon coordinates are used for cell segmentation as these

represent boundaries for individual cells. Transcript coordinates, although not used in the analysis in this thesis, allow for subcellular localisation of transcripts in single cells.

All FOVs belonging to a single brain tissue hemisection were combined to create a single Seurat object, resulting in 16 Seurat objects for the entire experiment. All Seurat objects were updated to Seurat version 5.2.0 for future analysis using this platform.

After creating Seurat objects for all 16 brain samples, QC of the spatial transcriptomic data was performed. This included controlling for number of transcripts expressed per cell (i.e. nCounts) (He et al., 2022). nCounts was set to 20 as recommended by Nanostring. This QC removed any cells from the dataset that had less than 20 transcripts in its cellular boundaries. Controlling for nCounts removed 'noise' from cells with low transcript quantity and, therefore, improving cell typing clustering during uniform manifold approximation and protection (UMAP) analysis. All data processing was completed using R programming language and RStudio (Team, 2024b, Team, 2024a).

2.8.3.2 Clustering and cell type identification

To capture all possible cell clusters and subsequent cell types, all 16 samples were merged to include all data for clustering analysis. Integration of samples for this analysis was performed to capture all shared cell populations across samples and minimize technical variation. This involved merging all 16 Seurat objects for the purpose of clustering. Merging and batch correction was completed using the Harmony software (Korsunsky et al., 2019). After merging, the Seurat object was log normalised using the NormalizeData function then scaled using ScaleData function (Seurat v5.2.0). A UMAP plot with cell clusters was created using the RunUMAP function. To identify cluster-defining markers, differential gene expression analysis was performed using the FindAllMarkers function with Wilcoxon Rank Sum test. Cluster identifier genes and spatial location of clusters were used to identify cell types in the CosMx dataset.

For identification and characterization of identified immune-like cells within the database, the 'Immune' cluster was re-clustered to produce subclusters. This was to explore subtypes from these cells that were transcriptionally different from the other subclusters. Per individual subcluster, differential gene expression analysis was completed using the Searchlight platform (Cole et al., 2021).

2.8.3.3 Regional pseudo bulk RNA sequencing CosMx analysis

To explore cell agnostic regional differences in brain areas linked to behavioural changes, pseudobulk RNA sequencing analysis was performed on hand-drawn regions of interest (ROIs). The selected ROIs included: ACC, NAc and the thalamus. ROIs were drawn using a tablet and Procreate iOS application. Regions and boundaries were identified on CosMx stained brain slices and using the Allen Mouse Brain Atlas (Wang et al., 2020b). Representative images shown in *Figure 8* detail the hand drawn ROIs for pseudobulk RNA sequencing analysis.

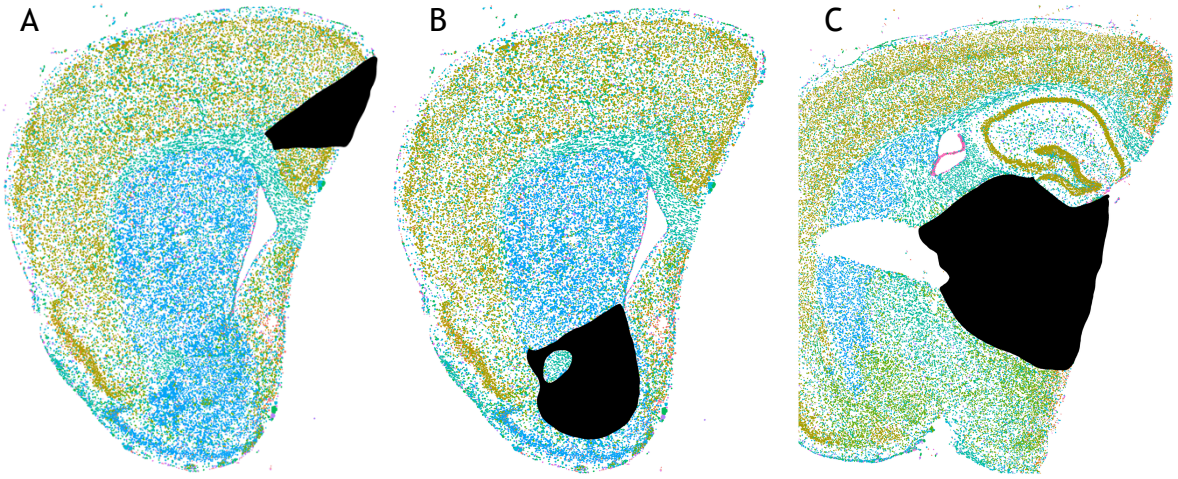

Figure 8: Representative images of hand drawn ROIs from CosMx tissue sections. *Hand drawn masks of anterior cingulate cortex (ACC) [A], nucleus accumbens (NAc) [B] and thalamus [C].*

2.9 Behavioural assessment

Excluding Rotarod testing, behavioural assessment paradigms were performed by Dr Lilya Andrianova and data was analysed by Kirstyn Gardner-Stephen.

2.9.1 Behavioural assessment animal acclimatisation

Apart from rotarod experiments in which mice were housed together in treatment groups, mice were singly housed in sterilised rat cages with running wheel for additional social enrichment. Two water-bottles were available to mice with one containing water and the other filled with 0.1% (w/v) sucrose solution. For nesting and sucrose preference test, measurements were acquired twice daily throughout the duration of the model. Elevated plus maze was completed in the morning then, following 2-3 hours of rest, open field testing was completed in the afternoon. Animals were permitted 30 minutes of acclimitisation to the room prior to the behavioural tests.

2.9.2 Rotarod

Locomotor activity was measured using an ITC Rotarod (IITC Life Sciences Inc, USA). Animals were habituated to the testing room which housed the rotarod 30 min prior to testing. Mice were acclimatised to accelerating rotarod for 3 trial runs the day before recording. Aldara model was performed as previously described and 4 timepoints were recorded per animal for rotarod: baseline (prior to first topical cream application), post-1-day topical cream application, post 2 days-topical cream application and post 3 days- topical application. Mice were placed on the stationary rotarod beam in separate lanes of the apparatus. A start speed of rotarod beams was set to 5 rpm accelerating to a maximum speed of 40 rpm. Total trial run time was 300 secs. The apparatus stops the recording when the mouse falls from the rod landing on the lever connected to the clock. Three parameters measured were: latency to fall up to 300 seconds (Time); top speed reached (rotations per minute [RPM]) and distance travelled (Distance).

2.9.3 Nesting

For nest building assessment and sucrose preference test, after 1 week of environmental acclimitisation, animals were singly housed in rat cages with a running wheel for additional enrichment and 2 drinking bottles. Cages were washed and sterilized to remove any scents from other species.

The Deacon nest building protocol was used for assessment of behavioural output (Deacon, 2006). All pre-shredded nesting, handling tubes and cardboard houses were removed from cages before study commencement. Each morning, mice were given 3g (+/- 0.05g) of unbleached cotton squares which were collected and weighed the following morning. Images of the nests were taken prior to collection and given a score out of 5, in which increasing scores indicates improving ability to nest build. A score of 5 was awarded to a fully shredded cotton square and high walled nest, whereas 1 was awarded to untouched cotton square. Low-range scores representing poor nesting behaviour indicate absence of innate in-cage nesting behaviour which are indicative of animal well-being and motivation (Jirkof, 2014).

2.9.4 Sucrose preference test

Following habituation, one bottle was filled with 0.1% (w/v) sucrose solution and the other with water. Both were available *ad libitum*. Behavioural readouts were recorded twice daily. Both water bottles, were weighed in the morning and evening. Measurements were collected 3 days prior to the model commencing and throughout topical applications. Changes of consumption were reported as a ratio of sucrose preference. Mice usually display an innate preference to sucrose solution over water. Deviation from this typical consumption is indicative of anhedonia in animals (Primo et al., 2023).

2.9.5 Open field Test

The open field test was used to assess presence of anxiety-like behaviour in the TLR7-driven neuroinflammation model. Mice were placed into an enclosed Perspex box measuring 40 x 40 x 45 cm and recorded for 1 hour using ANY-maze video-tracking software. Base of the monitoring box was white to allow for video-capturing of the black C57BL/6 mouse. The first 15 minutes of recording were analysed for average and maximum speed of animals and time spent at the centre and periphery of the arena. Apparatus was cleaned with ethanol between animals. As mice are curious in nature, exploratory behaviour of both zones is expected in healthy mice. Presence of anxiety-like behaviours in open field test would present

as preference to periphery zone rather than the central zone (Seibenhener and Wooten, 2015).

2.9.6 Elevated plus maze

Elevated plus maze was another behavioural test used to assess anxiety-like behaviour. Mice were placed into a cross-shaped Perspex arena measuring 110cm x 110cm and 65cm from the ground. Two arms were open and 2 arms were considered closed by having walls and positioning lights Recording of animals was completed by ANY-maze video-tracking software. One trial was recorded for 5 mins. Apparatus was cleaned with ethanol between animals. The following results were recorded: distance travelled, average and maximum speed and number of entries in open and closed arms. Presence of anxiety-like behaviours is considered to be exhibited by mice spending less time in the open arms and showing preference for the closed arms (Walf and Frye, 2007).

2.10 Graphical representation and statistical analysis

Individual heatmaps from bulk RNA sequencing DEGs were created using the online tool Heatmapper (Babicki et al., 2016). Venn diagrams were created using the online tool Venny (v2.1) (Oliveros, 2024). All statistical analysis and graphical representation were completed for flow cytometric, CosMx cell counts and behavioural data was completed using Prism 10 (v10.4.0). Unless stated otherwise in figure legends, data was analysed using two-way ANOVA corrected for multiple comparisons via the Šídák's correction test. All data was plotted as scatterplots with +/- standard deviation (SD). Significant findings were considered as follows: $p< 0.05$ = *, $p< 0.005$ = **, $p<0.002$ = *** and $p<0.0001$ = ****. Cell counts per CosMx immune subclusters were analysed by one-way ANOVA corrected for multiple comparisons via the Tukey's correction test.

3 Whole-brain transcriptomic changes following TLR7-activated neuroinflammation

3.1 Introduction

TLR7's signalling pathway is well characterised and triggers a type I IFN response including the upregulation of IFNα. Activation of TLR7 subsequently results in upregulation of pro-inflammatory cytokines including TNFα, IL-6 and IFN-α (Sakata et al., 2018). TLR7 is expressed within the brain parenchyma and predominantly on microglia (Michaelis et al., 2019). It has been previously shown via mass spectrometry that IMQ, a TLR7 agonist, once topically applied on the skin is able to enter circulation and passively cross the BBB (Nerurkar et al., 2017b). This is thought to be due to its small molecular composition and high hydrophobicity (Ramineni et al., 2013). This creates a non-invasive neuroinflammatory agent which is advantageous compared to other intrusive neuroinflammatory models (Aucott et al., 2018). To better understand IFN-driven neuroinflammation and its downstream pathophysiology, the TLR7-driven Aldara neuroinflammation model proves useful.

The exact mode of neuroinflammation induction in the Aldara model has various potential triggers of the neuroinflammation. Firstly, the presence of psoriasis-like dermal inflammation following topical application of the IMQ-containing cream (van der Fits et al., 2009, Wohn et al., 2014). This animal model was originally used to study the disease progression of psoriasis. When the presence of neuroinflammation was established (Thomson et al., 2014), the model was then used for studying the communication between peripheral inflammation to changes within the CNS (McColl et al., 2016). However, as it was discovered IMQ can enter the brain parenchyma directly following topical dermal application, it was noted that this model has multiple routes of initiating neuroinflammation. The scope of this thesis is to further characterise the central neuroinflammation present within this mouse model.

To begin characterising this model on a broad biological scale, whole brain bulk RNA sequencing proves a beneficial technique. Studying changes to the whole

transcriptome allows for an unbiased approach in characterising the global TLR7-driven neuroinflammation. Biological relevance of single gene findings in bulk RNA sequencing can then be used for a transcript-estimation of what biological pathways are enriched within the organ. Performing bulk RNA sequencing of the whole brain within this model identifies CNS-relevant changes following both TLR7 peripheral and central activation.

This chapter aims to transcriptionally characterise the TLR7-induced neuroinflammation within the Aldara model. This characterisation was completed for 3-days of topical IMQ application as this is the predefined 'peak' of neuroinflammation timepoint of this model (Nerurkar et al., 2017b, McColl et al., 2016).

3.2 Bulk RNA sequencing analysis

3.2.1 Distribution of expression values

Brain hemispheres were collected following PBS perfusion to remove residual plots cells from neural vasculature following 3 days of Aldara application (n=5/group). Tissue was processed and RNA was isolated prior to bulk RNA sequencing. Plotting gene expression distribution amongst all samples ensures technically high-quality RNA samples have been used in a bulk RNA sequencing experiment (Koch et al.,

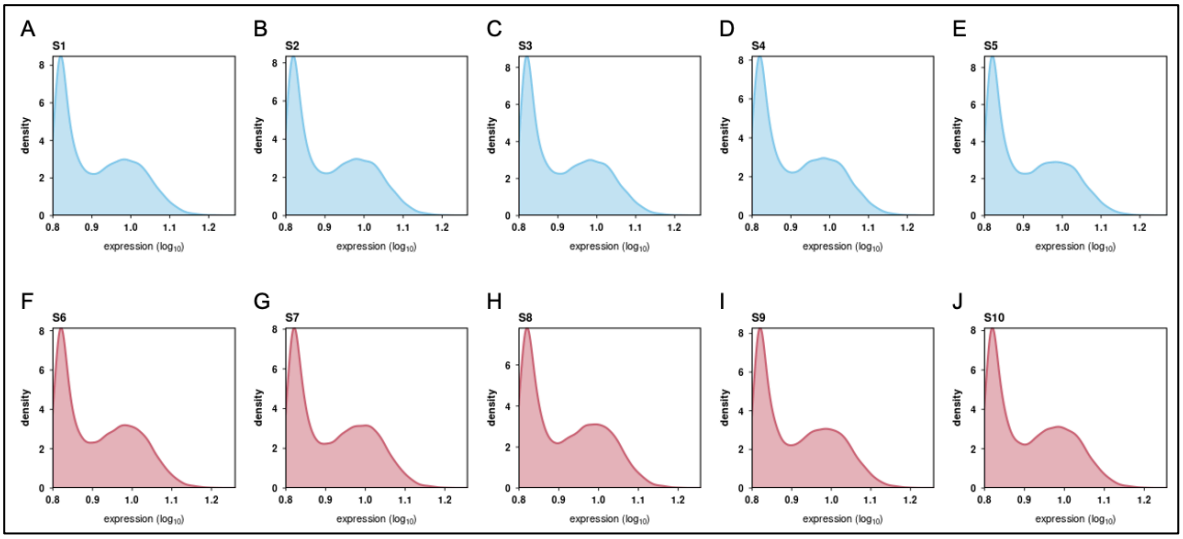

Figure 1: Distribution of expression values for Control and Treated RNA samples at three-day timepoint. *Density plots of Control Samples (A-E) and Aldara-treated samples (F-J) with expression values in log_{10} scale on x-axis and gene density on y-axis. n=5/group.*

2018). For high quality samples, density plots displaying the distribution of expression values should look similar across both treatment conditions. As seen in *Figure 1*, both Control and Aldara samples show extremely similar density plots of distribution of expression values. This demonstrates the isolated RNA from the brain tissue that was sequenced were both of high quality and low variability across all samples from both treatment groups.

3.2.2 Principal component analysis

Principal component analysis (PCA) considers all expression values within sequencing datasets and aims to identify underlying variables, termed principal components (PC), which best separate samples. To control for over representation effects of highly expressed genes, all gene expression values shown on PCA plots are scaled on a gene-by-gene basis via Z-score transformation. Z-score is determined by calculating the mean expression of a gene across all samples. A positive Z-score indicates an expression level higher than that of the gene's mean and a negative Z-score indicates an expression level lower than the mean of a given gene. If treatment groups within the experiment are separated within PCA scatterplots, this suggests that the plotted PCs are a key factor of variation within the dataset.

Figure 2A displays a waterfall plot of the gene expression data PCA and the contribution of each PC which are shown in descending order. This ranks PC1 as the highest level of variance between samples and PC10 the least. Shown in *Figure 2B*, Control (blue) and Aldara (pink) can be delineated into distinct groups. This suggests that PC1 is dependent on treatment condition. Extent of clustering within a group, shown via PC2 axis, demonstrates similar biological heterogeneity within samples from each group which is to be expected amongst mice baseline variability.

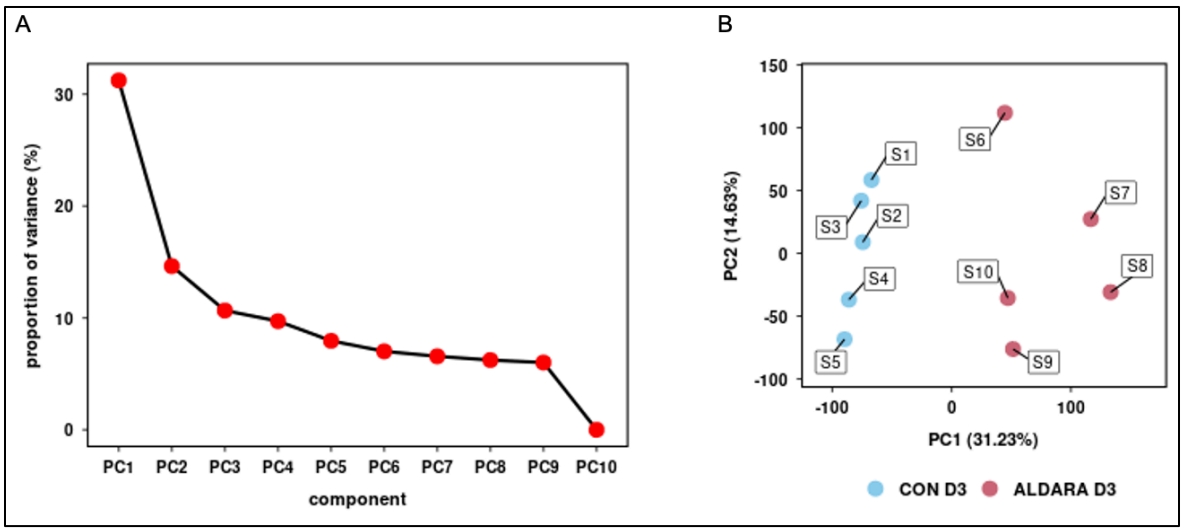

Figure 2: Principal Component Analysis (PCA) for three-day Control and Aldara samples. *(A) Waterfall plot showing PCA contribution of components of gene expression data. Components are ordered by decreasing underlying global variation between genes and samples with PC1 representing the most variation and PC10 representing the least variation. (B) Scatterplots showing PCA of gene expression with each dot representing an individual sample. Control shown in blue (S1-S5) and Aldara shown in pink (S6-S10). Percentages of total variation for PC1 and PC2 are shown on the x-axis and y-axis, representatively. n=5/group.*

3.2.3 Significant differentially expressed genes (DEGs)

At the whole-brain level, bulk RNA sequencing identified 24,732 genes in total. Of this whole transcriptome analysis following Aldara application, 2783 significantly DEG in which 2198 were upregulated and 585 were downregulated in Aldara-treated mice compared to controls, as shown in *Figure 3*. Significance was defined as p.adj value < 0.05 and an absolute log_2 fold change of >0.5 in the respective direction of change. These parameters for significance remain constant for following bulk RNA sequencing figures unless stated otherwise.

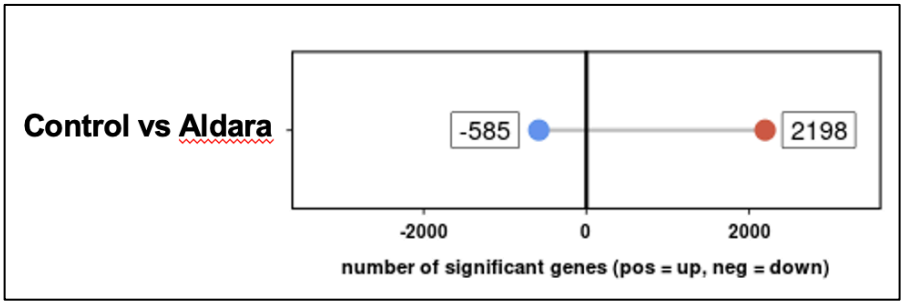

Figure 3: Lollipop bar chart showing number of significantly differentially expressed genes between 3-day treated Control and Aldara samples. *Significantly differentially expressed genes (defined as p.adj <0.05 and absolute log_2 fold change >0.5). X-axis shows number of genes with downregulated represented by a blue dot and upregulated represented by a red dot. Directional change of genes is indicative of decreased and increased expression within Aldara group compared to Control. N=5/group.*

Figure 4 shows a volcano plot of significant DEGs between Control and Aldara groups. Alongside the lollipop graph shown in *Figure 3*, the volcano plot further highlights the transcriptional changes within this model are predominantly upregulation. The 10 labelled genes on the volcano plot show the top 10 upregulated genes as ranked by adj.p-value. These ranked genes include: *C3ar1, Rac2, Ptprc, Itgam, B2m, Fcer1g, Clec4a1, H2-k1, Adgre1 and Clec4a3*. *Table 3.1* displays the top 10 upregulated genes by log_2 fold change and include the following in descending order: *Gzmb, Il1rn, Saa3, Slfn4, Gzma, Ccl5, Fcrl5, Tnf, Acod1* and *Sirpb1c*. All the stated upregulated genes indicate an increase immune response within the brain parenchyma including pro-inflammatory mechanisms.

When investigating biological relevance of bulk RNA sequencing data, one can inspect ‘top 10 DEGs’ either ranked by p.adj value or log_2 fold change. Genes ranked higher by p.adj represent the genes in which their change is most statistically reliable following data analysis and implementation of multiple testing correction. Alternatively, ranking DEGs based on their log_2 fold change represent the changes in the transcriptional biology that demonstrate the largest magnitude of change in their expression profile. Providing all top 10 genes ranked by log_2 fold change hold a significant p.adj value (*Table 3.1)*, these DEGs were focused on to examine the biological changes within this neuroinflammatory environment.

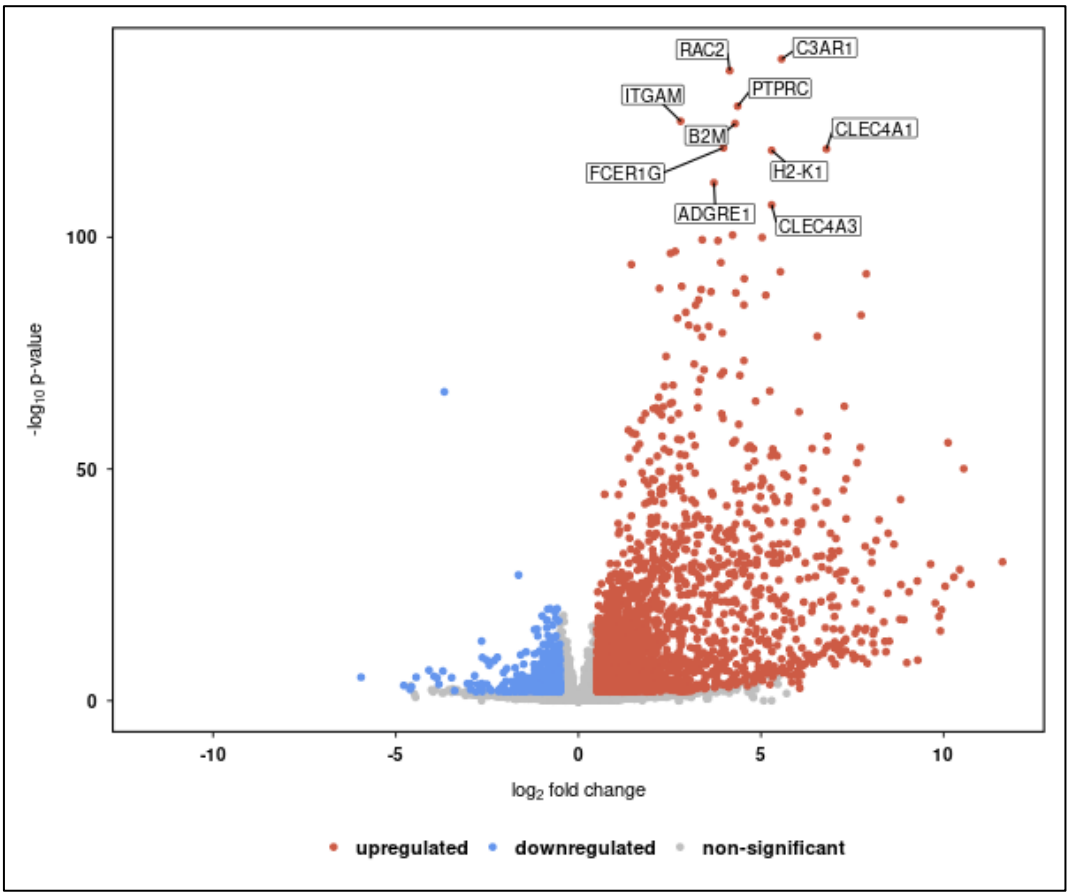

Figure 4: Volcano plot of differentially expressed genes between Control and Aldara groups. Log_2 Fold Change shown along x-axis and $-log_{10}$ p-value shown on y-axis. Upregulated significantly differential genes (p.adj <0.05, absolutely log_2 fold > 0.5) are shown in red. Downregulated significantly differential genes (p.adj <0.05, absolutely log_2 fold < 0.5) are shown in blue. Non-significant genes (p.adj > 0.05) are shown in grey. A positive (>0.5) fold change represented higher gene expression in Aldara group compared to Control. Labelled genes show the top 10 upregulated genes as ranked by p-value. N=5/group.

Table 3.1: Top 10 upregulated genes between Control and Aldara groups by log_2 Fold.

Gene	log2fold	p	p.adj
GZMB	11.61	1.139121e-30	8.599609e-29
IL1RN	10.74	7.176069e-26	3.867783e-24
SAA3	10.55	8.649130e-51	1.809097e-48
SLFN4	10.44	5.146089e-29	3.390916e-27
GZMA	10.28	2.083448e-27	1.221094e-25
CCL5	10.12	2.088124e-56	5.877424e-54
FCRL5	10.04	2.153457e-25	1.131260e-23
TNF	9.94	2.523241e-20	1.005723e-18
ACOD1	9.91	8.984901e-16	2.742259e-14
SIRPB1C	9.87	7.501168e-19	2.745090e-17

Table 3.2 displays the top 10 downregulated genes by log_2 fold change and including the following in descending order: *Cyp2g1, Scgb1c1, Cyp1a2, Gm13648, Bpifb3, Or12j5, Or4k15, Bglap, Gfy* and *Gmm44737*. Various downregulated genes are involved in olfactory functions including *Cyp2g1, Bpifb3 Or12j5* and *Or4k15* . This may be indicative of the Aldara-treated animals getting some of the topically applied cream in their noses during grooming. The downregulation of these olfactory genes could indicate a protective mechanism of the olfactory mucosal membrane (Lane et al., 2010). Some of these genes involved in drug metabolism have been found to be downregulated in other neuroinflammatory environments including *Cyp1a2 (*Nicholson and Renton, 2002).

Table 3.2: Top 10 downregulated genes between Control and Aldara groups by log_2 Fold.

Gene	log2fold	p	p.adj
CYP2G1	-5.95	9.258118e-06	9.424579e-05
SCGB1C1	-4.78	5.422900e-04	3.559940e-03
CYP1A2	-4.61	3.691193e-03	1.843898e-02
GM13648	-4.59	6.791261e-04	1.000000e+00
BPIFB3	-4.57	1.018714e-03	6.159020e-03
OR12J5	-4.49	3.312026e-02	1.067443e-01
OR4K15	-4.46	1.890901e-01	1.000000e+00
BGLAP	-4.44	8.990593e-06	9.191773e-05
GFY	-4.09	2.757957e-07	3.683577e-06
GM44737	-4.02	4.674102e-03	1.000000e+00

3.2.4 Over representation analysis (GProfiler results)

Results from bulk RNA sequencing experiments can be overwhelming when interpreting the biological significance of potentially thousands of DEGs. To gain scientific insights from sequencing results, pathway enrichment analysis can prove a powerful tool for researchers (Reimand et al., 2019). GProfiler was the online tool used to perform pathway enrichment analysis (Kolberg et al., 2023). This analysis tool implements ORA to a bulk RNA sequencing dataset. This takes the DEGs from a dataset and compares them to a predefined biological pathway reference database including Gene Ontology (GO), KEGG, Reactome and

WikiPathways. These are freely available databases which can be selected for specificity and comprise transcriptional information both of organisms at rest and in various diseased states (Drabkin et al., 2012) The analysis then defines 'enrichment' with the number of overlapping genes which are differentially expressed within the experimental dataset and a set of genes that belong to a biological pathway. For example, GO Molecular Function database 'Immune System Process' pathway contains 3050 genes. The higher number of overlapping genes within a biological pathway gene set, the higher the enrichment status of that given pathway.

Three-day Aldara treatment results in upregulated $\log_2$ fold change (FC) rank DEGs GProfiler analysis as presented in *Figure 5*. Three GO reference databases were selected for ORA: GO: Molecular Functions (MF); GO: Biological Processes (BP) and GO: Cellular Components (CC). These reference databases were selected as they focus on fundamental biological changes rather than other databases that highlight clinical relevance. The number of significantly enriched pathways from GO datasets included: GO:MF with 194, GO:BP with 1461 and GO:CC with 126. For GO:MF and GO:BP, the top enriched pathways all included immune system related hits as seen in *Figure 6* and *7*, respectively. GO:CC involved cytoplasm, membrane and other organelle-related pathways (*Figure 8)*. A full report of GProfiler analysis

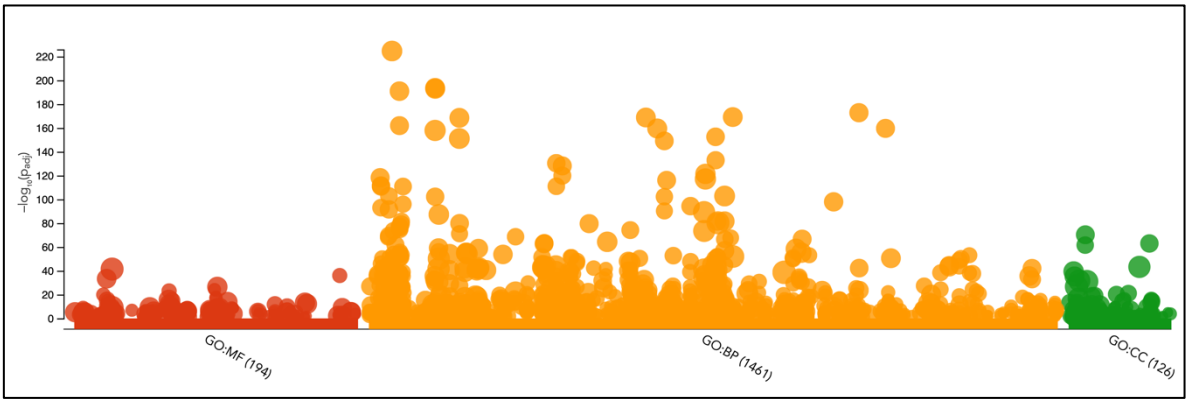

Figure 5: GProfiler over-representation analysis (ORA) overview for three-day treated bulk RNA sequencing log2FC ranked expression for upregulated DEGs. *Manhattan plots displaying enriched pathways from ORA via GProfiler analysis for upregulated genes. ORA reference databases include Gene Ontology Molecular Functions (GO:MF), GO Biological Processes (GO:BP) and GO Cellular Components (GO:CC) as shown along x-axis. Numbers within brackets represent number of enriched pathways belonging to each GO reference dataset: GO:MF - 194, GO:BP - 1461 and GO:CC - 126. Y-axis displays adjusted enrichment p-values in negative $\log_{10}$ scale.*

showing all enriched pathways, genes overlapping and pathway validation evidence can be found at https://biit.cs.ut.ee/gplink/l/0M2YRCIsTU.

GO:MF		stats	
Term name	Term ID	p_{adj}	$-\log_{10}(p_{adj})$ 0 ≤16
immune receptor activity	GO:0140375	4.873×10^{-32}	
signaling receptor binding	GO:0005102	1.616×10^{-22}	
pattern recognition receptor activity	GO:0038187	2.476×10^{-21}	
cytokine binding	GO:0019955	5.237×10^{-18}	
MHC class I protein binding	GO:0042288	1.103×10^{-17}	
cytokine receptor activity	GO:0004896	1.573×10^{-17}	
MHC protein binding	GO:0042287	1.091×10^{-16}	
catalytic activity, acting on a nucleic acid	GO:0140640	1.428×10^{-16}	
purine ribonucleoside triphosphate binding	GO:0035639	1.747×10^{-15}	
enzyme binding	GO:0019899	3.263×10^{-15}	
cytokine receptor binding	GO:0005126	1.387×10^{-14}	
carbohydrate binding	GO:0030246	2.211×10^{-14}	
protein-macromolecule adaptor activity	GO:0030674	3.081×10^{-14}	
nucleoside phosphate binding	GO:1901265	2.910×10^{-13}	
nucleotide binding	GO:0000166	2.910×10^{-13}	
GTPase binding	GO:0051020	6.018×10^{-13}	
ribonucleotide binding	GO:0032553	3.231×10^{-12}	
purine ribonucleotide binding	GO:0032555	5.797×10^{-12}	
transcription coregulator activity	GO:0003712	6.932×10^{-12}	
chemokine activity	GO:0008009	7.371×10^{-12}	

Figure 6: GProfiler Gene Ontology: Molecular Function top 20 enriched pathways from 3-day treatment upregulated log_2FC ranked results.

GO:BP		stats	
Term name	Term ID	p_{adj}	$-\log_{10}(p_{adj})$ 0 ≤16
immune system process	GO:0002376	2.516×10^{-198}	
immune response	GO:0006955	4.609×10^{-189}	
defense response	GO:0006952	2.682×10^{-174}	
defense response to other organism	GO:0098542	5.073×10^{-162}	
response to other organism	GO:0051707	4.293×10^{-158}	
response to external biotic stimulus	GO:0043207	9.340×10^{-158}	
response to biotic stimulus	GO:0009607	1.310×10^{-155}	
defense response to symbiont	GO:0140546	1.269×10^{-152}	
regulation of immune system process	GO:0002682	1.143×10^{-149}	
biological process involved in interspecies interaction b...	GO:0044419	9.619×10^{-149}	
innate immune response	GO:0045087	1.790×10^{-144}	
positive regulation of immune system process	GO:0002684	1.118×10^{-135}	
regulation of immune response	GO:0050776	9.815×10^{-135}	
response to external stimulus	GO:0009605	2.468×10^{-125}	
positive regulation of immune response	GO:0050778	2.858×10^{-118}	
regulation of defense response	GO:0031347	2.039×10^{-106}	
positive regulation of response to external stimulus	GO:0032103	4.529×10^{-98}	
regulation of response to external stimulus	GO:0032101	3.199×10^{-97}	
regulation of response to biotic stimulus	GO:0002831	4.725×10^{-97}	
positive regulation of defense response	GO:0031349	1.726×10^{-95}	

Figure 7: GProfiler Gene Ontology: Biological Processes top 20 enriched pathways from 3-day treatment upregulated log_2FC ranked results.

GO:CC		stats	
Term name	Term ID	p_{adj}	$-\log_{10}(p_{adj})$ 0 ≤16
cytoplasm	GO:0005737	5.038×10^{-99}	
nucleoplasm	GO:0005654	1.628×10^{-92}	
cytosol	GO:0005829	1.444×10^{-80}	
external side of plasma membrane	GO:0009897	1.662×10^{-54}	
cell surface	GO:0009986	5.386×10^{-51}	
organelle membrane	GO:0031090	1.210×10^{-49}	
microtubule cytoskeleton	GO:0015630	4.615×10^{-49}	
side of membrane	GO:0098552	3.068×10^{-48}	
catalytic complex	GO:1902494	6.055×10^{-46}	
mitochondrion	GO:0005739	9.229×10^{-45}	
synapse	GO:0045202	7.806×10^{-44}	
cell junction	GO:0030054	3.388×10^{-39}	
bounding membrane of organelle	GO:0098588	4.428×10^{-39}	
cell projection	GO:0042995	6.037×10^{-38}	
centrosome	GO:0005813	2.946×10^{-37}	
organelle envelope	GO:0031967	5.792×10^{-37}	
envelope	GO:0031975	5.792×10^{-37}	
microtubule organizing center	GO:0005815	4.876×10^{-36}	
plasma membrane bounded cell projection	GO:0120025	5.194×10^{-36}	
neuron projection	GO:0043005	2.278×10^{-35}	

Figure 8: GProfiler Gene Ontology: Cellular Components top 20 enriched pathways from 3-day treatment upregulated log_2FC ranked results.

Figure 9 shows 3-day treatment downregulated log_2FC rank DEGs GProfiler results. The number of significantly enriched pathways from GO datasets included: GO:MF with 26, GO:BP with 46 and GO:CC with 17. The GO:MF analysis reveals pathways involved in protein binding including haemoglobin, tetrapyrrole and haptoglobin (*Figure 10*). These are groups with oxygen-related activity including antioxidant relevant pathways. GO:BP mirrors this oxygen-related biology pathway enrichment alongside synaptic signaling pathways (*Figure 11*). More oxygen-related pathways are featured in the GO:CC analysis which are coupled with extracellular matrix processing including collagen and plasma membrane interactions (*Figure 12*). A full report of GProfiler analysis can be found at https://biit.cs.ut.ee/gplink/l/agSIW-QgkQX.

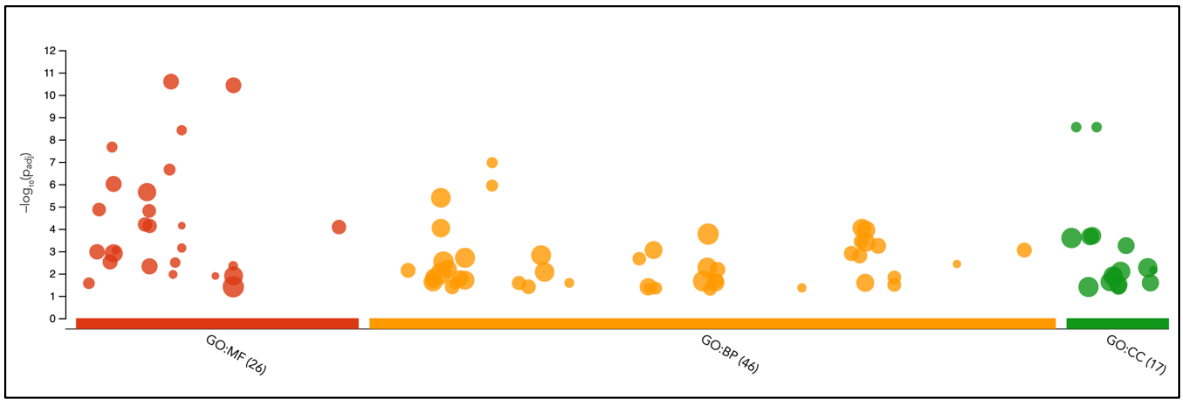

Figure 9: GProfiler Over Representation Analysis overview for 3-day treated bulk RNA sequencing log2FC ranked expression for downregulated DEGs. *Manhattan plots displaying enriched pathways from overrepresentation analysis (ORA) via GProfiler analysis for upregulated genes. ORA reference databases include Gene Ontology Molecular Functions (GO:MF), GO Biological Processes (GO:BP) and GO Cellular Components (GO:CC) as shown along x-axis. Y-axis displays adjusted enrichment p-values in negative log_{10} scale.*

GO:MF		stats	
Term name	Term ID	p_{adj}	$-\log_{10}(p_{adj})$ 0 ≤16
heme binding	GO:0020037	2.542×10^{-11}	
tetrapyrrole binding	GO:0046906	3.720×10^{-11}	
haptoglobin binding	GO:0031720	3.831×10^{-9}	
oxygen carrier activity	GO:0005344	2.171×10^{-8}	
oxygen binding	GO:0019825	2.215×10^{-7}	
iron ion binding	GO:0005506	9.739×10^{-7}	
oxidoreductase activity	GO:0016491	2.252×10^{-6}	
peroxidase activity	GO:0004601	1.362×10^{-5}	
oxidoreductase activity, acting on peroxide as acc...	GO:0016684	1.560×10^{-5}	
antioxidant activity	GO:0016209	6.299×10^{-5}	

Figure 10: GProfiler Gene Ontology: Molecular Function top 10 enriched pathways from 3-day treatment log_2FC ranked results for downregulated DEGs.

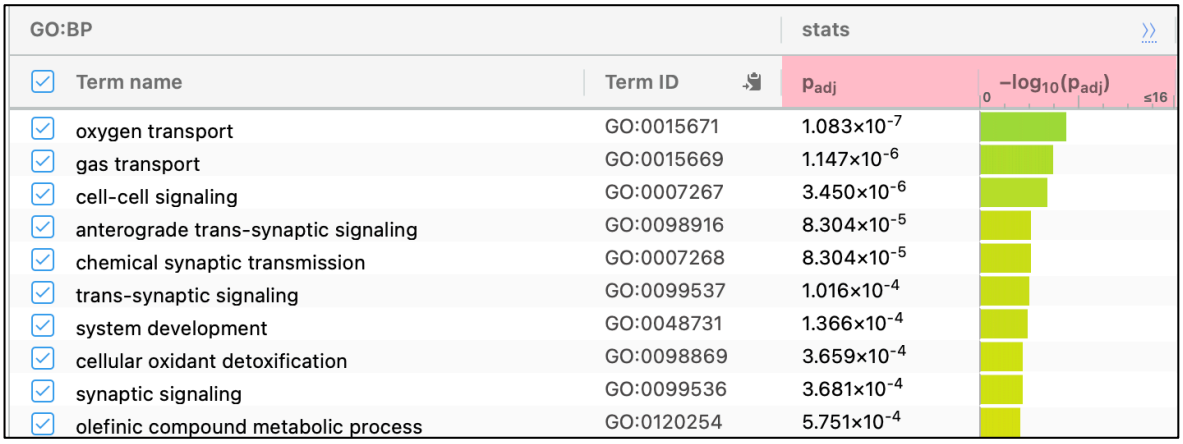

GO:BP		stats
Term name	Term ID	p_{adj}
oxygen transport	GO:0015671	1.083×10^{-7}
gas transport	GO:0015669	1.147×10^{-6}
cell-cell signaling	GO:0007267	3.450×10^{-6}
anterograde trans-synaptic signaling	GO:0098916	8.304×10^{-5}
chemical synaptic transmission	GO:0007268	8.304×10^{-5}
trans-synaptic signaling	GO:0099537	1.016×10^{-4}
system development	GO:0048731	1.366×10^{-4}
cellular oxidant detoxification	GO:0098869	3.659×10^{-4}
synaptic signaling	GO:0099536	3.681×10^{-4}
olefinic compound metabolic process	GO:0120254	5.751×10^{-4}

Figure 11: GProfiler Gene Ontology: Biological Processes top 10 enriched pathways from 3-day treatment downregulated log_2FC ranked results.

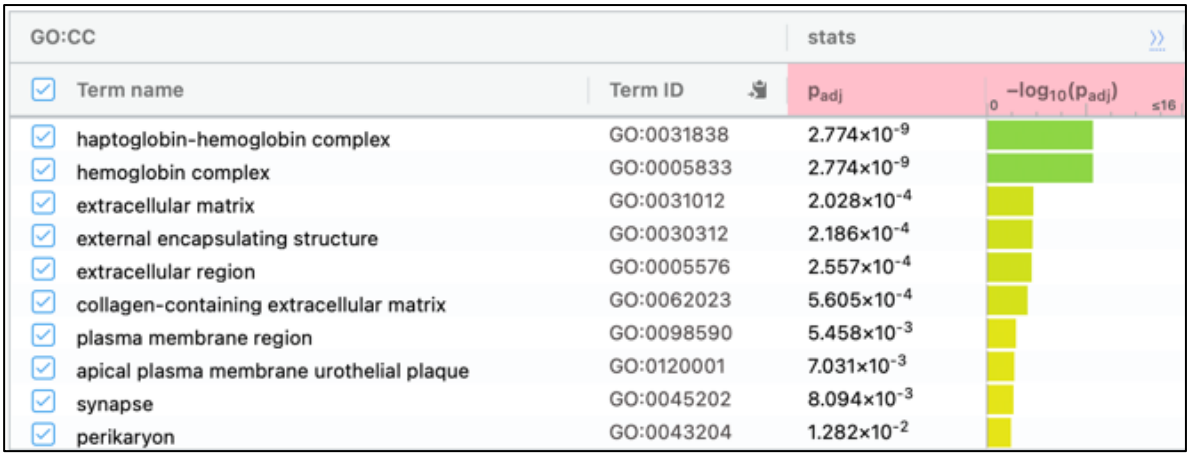

GO:CC		stats
Term name	Term ID	p_{adj}
haptoglobin-hemoglobin complex	GO:0031838	2.774×10^{-9}
hemoglobin complex	GO:0005833	2.774×10^{-9}
extracellular matrix	GO:0031012	2.028×10^{-4}
external encapsulating structure	GO:0030312	2.186×10^{-4}
extracellular region	GO:0005576	2.557×10^{-4}
collagen-containing extracellular matrix	GO:0062023	5.605×10^{-4}
plasma membrane region	GO:0098590	5.458×10^{-3}
apical plasma membrane urothelial plaque	GO:0120001	7.031×10^{-3}
synapse	GO:0045202	8.094×10^{-3}
perikaryon	GO:0043204	1.282×10^{-2}

Figure 12: GProfiler Gene Ontology: Cellular Components top 10 enriched pathways from 3-day treatment downregulated log_2FC ranked results.

3.3 Discussion

The use of whole brain bulk RNA sequencing provides a transcriptional snapshot of the inflammation present at a global scale in the CNS. This technique additionally provides an unbiased exploration into the TLR7-driven transcriptional changes. The bulk RNA sequencing results reveal a broad and expected inflammatory response. This finding is supported by both individual DEGs and enriched pathways. The gene *Tnf*, which encodes for the pro-inflammatory cytokine TNFα, features in the top DEGs following Aldara application. This inflammatory mediator

has been implicated in a variety of neuroinflammatory models including EAE and clinical conditions such as MDD (Steeland et al., 2017, Elgellaie et al., 2023).

Upregulation of *Saa3* features in the top changed genes in this model. This gene encodes for a serum protein which has been shown to increase expression in neuroinflammation including post-stroke. *Saa3* has links to upregulating another pro-inflammatory cytokine IL-1ß via inflammasome activation (Yu et al., 2019). These top DEGs upregulated following Aldara treatment provide further evidence of the prevalent neuroinflammation in the mouse model. Previous work investigated the transcriptional response to neuroinflammation by investigating pre-determined genes via quantitative polymerase chain reaction (qPCR) (McColl et al., 2016). The work in this thesis confirms these findings through a more unbiased approach of bulk RNA sequencing. Additionally, the previously quantified genes vis qPCR only featured 1 gene from the top 10 identified via bulk RNA sequencing. This further validates the importance of the unbiased approach implemented in this thesis' experiments.

Amongst the upregulated DEGs, we gain a transcript-backed insight into the possible cellular mechanisms underpinning the neuroinflammation within the Aldara model. Myeloids and T cells are presented as likely key players within this physiology through the upregulation of genes including *Gzma/b*, *Ccl5* and *Sirpb1c*. Inhibitors of Granzyme B, encoded by *Gzmb,* show neuroprotective properties with *in vivo* EAE models (Haile et al., 2015). Granzymes have also been established as potential diagnostic biomarkers of MS with presence of granzyme B^+ T cells positively correlating with disease progression (Shi et al., 2023).

Peripheral immune cells have been documented in the brain parenchyma following topical Aldara application (Sharma et al., 2024). CCL5, encoded by *Ccl5,* is a key chemokine responsible for the recruitment of peripheral monocytes and T cells. Increased levels of CCL5 play a role in the trafficking of peripheral immune cells across the BBB (Ubogu et al., 2006). This chemokine is an important cross-cell communication signal between T cells and microglia. Blocking of CCL5 was found to dampen microglia activation within the mouse hippocampus in a seizure model (Zhang et al., 2023b). *Sirpb1c* is established as a T cell marker and upregulation of the identifier gene has been found in other models of neuroinflammation

including both early and late disease stages of EAE (Brummer et al., 2023). The chemotaxis-related transcriptional changes identified support this recruitment mechanism previously identified immune populations in the Aldara model (McColl et al., 2016, Sharma et al., 2024).

To maintain homeostasis in the brain and to prevent unwanted damage during neuroinflammatory periods, it is vital the organ has a balance between pro- and anti-inflammatory mechanisms. Evidence of an anti-inflammatory cascade is present with upregulation of *Il1rn*. IL-1 is a key pro-inflammatory cytokine within the brain which is increased following Aldara treatment (McColl et al., 2016). Studies show an upregulation of its antagonist, encoded by *Il1rn*, can modulate downstream effects to suppress its actions (Gosselin and Rivest, 2007). This highlights a potential protective mechanism being initiated to combat the ongoing TLR7-driven neuroinflammation.

Another upregulated gene which is involved in potential anti-inflammatory effects is *Adoc1*. Within microglia, ACOD1, encoded by *Adoc1,* is described as having a neuroprotective effect with *Acod1* knock out (KO) mice displaying heighted spinal cord inflammation (Qian et al., 2024). Within the Aldara model, weight change is a common occurrence with initial 2 days of weight loss followed by weight gain around day 3 of the model. This positive fluctuation in weight coupled with upregulation of anti-inflammatory mechanisms may illustrate an attempt of the organism's defence against the TLR7-mediated inflammation.

Downregulation of genes may suggest a tissue's attempt to reduce its responsiveness to a stimulus. For the Aldara model, the TLR7 agonist IMQ is topically applied daily and has been shown to enter brain parenchyma 4 hours post-application (Nerurkar et al., 2017a). It can be speculated that this results in a daily reintroduction of the TLR7 agonist into the CNS resulting in continuation of its pro-inflammatory impacts. This daily insult into the brain parenchyma may explain downregulation of previously stated genes.

A common biological trend shown in the downregulated genes within this model are those related to olfactory functions including *Cy2pg1, Scgb1c1, Bpifb3, Or12j5* and *Or4k15* (Chen et al., 2019). Chronic olfactory inflammation conditions are

mediated via IFNγ proinflammatory signalling which may be heightened by the similar TLR7 IFN-mediated signalling pathway (LaFever et al., 2022). This activation of the olfactory response may be explained by the grooming habits of Aldara mice. Following topical application of Aldara cream to the dorsal back, mice groom themselves and other cage mates. This may result in the TLR7-containing cream to enter the nose which is a commonly accepted limitation of the model. The downregulation of these olfactory genes could be explained by the potential nasal mucousal TLR7 activation.

Aldara treatment results in many global transcriptional changes which encompass primarily immune-focused biology. While single gene changes may catch the eye of biased 'favourite gene' searches, there are analysis techniques which have present stronger biological relevance to transcriptional results. One of these techniques is the previously mentioned ORA to explored enriched pathways from bulk RNA sequencing data.

The analysis software GProfiler was used to complete the enriched pathways within this dataset (Kolberg et al., 2023). When setting the parameters for this analysis, reference databases must be selected from several different sources. These can include GO, which was selected, and others such as Wikipaths, KEGG and Reactome. GO databases were selected for reference material of enrichment analysis as these databases focus on fundamental biological interactions between cells rather than human-focused clinical orientated context of changes to transcriptional material.

Unsurprisingly within a TLR7-activated neuroinflammatory model, most of the enriched pathways from upregulated genes displayed immune-related properties. This includes cytokine and chemokine activity which further supports the previously shown recruitment of peripheral immune cells into the brain parenchyma within this model (McColl et al., 2016). Response to external stimuli and defence mechanisms are additionally highlighted in the enriched pathway. This shows the ongoing defence mechanisms being activated, at the transcriptional levels, following the daily TLR7 activation.

Changes to mitochondrial function is suggested by both directional transcriptional changes but primarily the downregulated enriched gene sets. The top enriched pathway analysis of downregulated genes also involved many protein-binding pathways. Multiple pathways including haem, tetrapyrrole and haptoglobin binding are related to oxygen transport and, more specifically, oxidative stress biological pathways. Downregulation of these oxidative stress-relative genes may suggest some alterations to mitochondrial function in the TLR7-driven neuroinflammation. A common consequence of mitochondrial function alteration is the release of mitochondrial-derived DAMPs. These can be recognised by innate and infiltration immune populations to trigger a pro-inflammatory response.

Mitochondrial changes have been documented in neuroinflammation as a potential precursor event in the cascade of inflammation-caused changes (Peruzzotti-Jametti et al., 2024). Downregulation of enzymes involved in oxidative-related mechanisms can also prove detrimental to cells in making them vulnerable to increases in reactive oxygen species (ROS). These ROS have been shown to promote states of neuroinflammation in different models including systemic LPS-trigger neuroinflammation (Shukuri et al., 2021). Mitochondria serve as potential checkpoints of neuroinflammation and changes to their physiology may elevate inflammation levels within the organ.

Mitochondrial disorders have been shown to results in a number of neural functional deficits including changes to mood and more chronic neuropsychiatric manifestations including MDD (Anglin et al., 2012, Ni et al., 2024). The link underpinning mitochondrial dysfunction and behavioural changes is thought to be consequential deficits in synaptic transmission and morphology. This pathological relationship has been demonstrated in a variety of clinical conditions including AD and MDD (Guo et al., 2017, Ciubuc-Batcu et al., 2024). The transcriptional evidence of mitochondrial changes within the Aldara model may be further explored with techniques focused on mitochondrial function including the Seahorse assay for cellular bioenergetics (Shaw et al., 2020).

Gene sets found to be enriched from the downregulated DEGs included ones of synaptic transmission biology. This downregulation of neural communication genes may suggest a possible dampening of certain brain circuits. Perturbations in

reward-related brain circuits have previously been documented in the Aldara model, namely the thalamostriatal circuit (Sharma et al., 2024). Potential changes to synaptic transmission are suggested globally at the transcriptional level. Further transcriptional analysis of brain regions related to specific circuits would assign more detail on this potential synaptic signalling dampening. This more focused regional approach will be explored in chapter 6 of this thesis.

One limitation of bulk RNA sequencing of a whole organ is inability to assign transcriptional changes to one cell type. This becomes even more difficult when multiple cell types are known to express similar genes. As previously discussed in the introduction chapter, this problem of shared markers is the case for microglia and other infiltrating myeloids and BAMs (Jurga et al., 2020). Upregulated gene *Acod1/Irg1* has been implicated in both types of myeloid cells (Pires-Afonso et al., 2022). Increased *Tnf* is another potential indicator of microglia activity as they are one of the primary producers of this proinflammatory cytokine (Raffaele et al., 2020, Raffaele et al., 2024). This weakness of bulk RNA sequencing highlights the need for a technique that can assign transcriptional changes to one cell type.

Whole-organ bulk RNA sequencing can be argued as too broad an exploration technique as regionality of these transcriptional changes is lost. This is especially problematic for an organ such as the brain where details regarding regional changes is crucial if interested in neural pathways and behavioural changes. However, this chapter's goal was justifying the Aldara model as a non-invasive model of neuroinflammation. It could be argued this initial whole brain approach is beneficial and reassuring that this immune-mediated neuroinflammation is evident even when combining all cells within the organ. This may suggest a global response of the TLR7-activated pro-inflammatory cascades. However, further regional validation of biological changes is required before this can be supported.

This chapter strives to provide a transcriptional snapshot of the TLR7-driven neuroinflammatory response within the Aldara model. Additionally, through proving a global response, strengthen its appropriateness as a non-invasive neuroinflammatory model. Transcriptional evidence shows the changes in this model may be primarily immune-driven with upregulation of pro-inflammatory cytokines and chemokines. To understand the intricacies of this

neuroinflammation and cellular interactions leading to cellular and behavioural changes, relatively more focussed techniques have been utilised in forthcoming chapters. These include the use of spatial transcriptomics which begins to assign these transcriptional changes to individual cell types and brain regions.

4 Microglia response and changes following TLR7-activated neuroinflammation

4.1 Introduction

As outlined earlier in this thesis, microglia have a myriad of functions within the brain. Some responsibilities of microglia include acting as the innate immune defence against invading pathogens, maintenance of neural networks specifically via synaptic pruning and have a role in early brain development (Cornell et al., 2022). These roles are essential to maintain optimal conditions for the CNS which are active both at times of rest and in response to potential threats (Colonna and Butovsky, 2017).

Similar to peripheral immune cells, microglia have the ability to produce cytokines, phagocytose, recognise pathogens via surface receptors and act as APC (Yang et al., 2010). Microglial are one of the key cellular drivers of neuroinflammation. As stated in previous chapters of this thesis, this work utilises the Aldara model with focus on characterising the TLR7-driven neuroinflammation. Microglial responses are essential to characterise as they are the primary endogenous neural cell type for TLR7 expression as shown by previous literature (Zhang et al., 2014).

Several neuroinflammatory models, including LPS and AD models, present a microglia-based responsive relationship (Surendranathan et al., 2018, Geloso et al., 2024). This change to microglial phenotype includes increased cytokine production and changes to morphology to aid phagocytic abilities. As the primary cellular driver in neuroinflammation, microglial are essential to characterise to full describe the innate brain response to inflammation.

Microglial nomenclature and their various functional states is constantly changing to strive towards the most representative portrayal of their physiology. The now outdated ‘M1’ and ‘M2’ myeloid labels, to represent proinflammatory and anti-inflammatory respectively, lay the foundations in the preliminary phenotypic understanding of these cells. It is more recently appreciated that microglia have

multiple state of activation and diverse phenotypic presentations (Wang et al., 2023a).

The microglial field has expanded in its understanding of this heterogenous cell population with a variety of different research techniques (Sousa et al., 2017). Fluorescent-activated cell sorting (FACS) was an approach that found great success in the microglial field. Initial findings discovered brain-resident microglia presented as $CD11b^{+}CD45^{lo}$ which differed from other macrophage populations being characterised as $CD11b^{+}CD45^{hi}$ (Sedgwick et al., 1991). This flow cytometric approach has been further refined to show microglial populations express more intermediate levels of CD45 compared to other macrophages.

Single-cell transcriptomic analysis have revealed unique gene signatures of the brain resident cells and identify functionally different phenotypic subsets (Yaqubi et al., 2023). These pieces of this evidence have been discovered to not only disagree with the dated M1/M2 phenotypic and physiological assignment but support the complete abandonment of this terminology. Relatively more contemporary and palatable language within the microglial field is the view of these cells being capable of a spectrum of reactivity and fluidity of this functional state (Wei and Li, 2022).

When dealing with the brain as an organ of interest, regionality holds critical value in true understanding of biological changes as the CNS displays localisation of function. Additionally, subsets of microglia with an immune-focused functions have been found to display regionality within the human brain (Li et al., 2022b). Many research techniques, including scRNAseq and flow cytometry, provide useful details about cellular biological states such as transcriptomic and surface marker changes. However, this usually comes with the sacrifice of regionality with tissue preparation including a homogenate single-cell suspension prior to analysis.

Techniques that maintain *in situ* information, such as immunohistochemistry (IHC) are usually limited to the amount of information they can provide due to technical limits (e.g. fluorescent channels available on a microscope). These technical limitations subsequently restrict the scope of biology which can be studied (e.g. number of IHC targets limited by fluorescent channel availability). Spatial

transcriptomics is a new and growing field that begins to address this gap by providing both detailed insight to cellular changes and maintenance of tissue regionality (Williams et al., 2022). This novel technique retains regionality with staining protocols being completed on intact tissue sections and provides vast cellular information with the use of high-plex RNA probe panels.

Nanostring's CosMx SMI provides a high-plex *in situ* RNA imaging platform for fresh and archival mouse and human tissue (He et al., 2022). This technique allows for RNA-determined cell typing including subcellular visualisation of transcript localisation. With its high number of microglial markers, this platform proves useful to explore cellular changes while maintaining tissue and regionality integrity. Furthermore, in using the CosMx mouse neuroscience 1000-plex panel which contains a range of microglial and functional genes, potential subtypes of the innate CNS immune cell could be identified.

As discussed previously in this thesis, the TLR7 ligand IMQ can enter the brain via crossing the BBB (Nerurkar et al., 2017b). Therefore, it may be proposed that this neuroinflammatory agent is acting directly on TLR7-expressing microglia after IMQ enters the brain parenchyma. Another mode which may result in increased microglial reactivity is the peripheral inflammatory component in the Aldara model. Topical application of IMQ induces a psoriasis-like dermal inflammation (Wohn et al., 2014, Nerurkar et al., 2017a, McColl et al., 2016). This peripheral response additionally results in a systemic inflammatory response including raised plasma cytokines and splenomegaly. Overall, this heightened immune response is another potential route of initiation of microglial reactivity.

Previous characterisation of microglia within the Aldara model found a significant increase in Iba1$^+$ cells within the hippocampus amongst the global neuroinflammatory environment established both at transcript and protein level (McColl et al., 2016, Nerurkar et al., 2017a). The stated Iba1$^+$ cells within Aldara-treated brains additionally altered their morphology in thickening of their processes and taking on a classic reactive-status ameboid shape. Further work included in this thesis focuses on expanding this initial identification of these Iba1$^+$ cells and delineation of them from other myeloid counterparts.

Additionally, previous work with the Aldara model has shown changes to microglial morphology again via Iba1^{+} staining (Sharma et al., 2024). These innate brain immune cells were also found to be actively secreting pro-inflammatory cytokines. Reactive microglia in the TLR7-driven Aldara neuroinflammatory model has been previously described. However, no microglial characterisation in the Aldara model has been completed via spatial transcriptomics.

The aim of this chapter is to identify microglia and explore their response within the TLR7-activated Aldara neuroinflammatory model. I will utilise flow cytometry for cell characterisation alongside transcriptomic technique bulk RNA sequencing of whole-brain and the spatial transcriptomic platform CosMx.

4.2 Whole-brain transcriptional changes of microglia-related genes

To provide an initial indicator of microglia presence and reactive status, expression levels of microglia-related genes were selected for analysis from the whole-brain bulk RNA sequencing dataset. These genes range from classic myeloid/microglia surface markers (e.g. CD68, Hexb, Fcrls) and other markers which indicate increased reactive status of microglia (e.g. Msr1, MerTK). This list of microglia-related genes were comprised from mainly scRNAseq experiments of the brain-resident population from the literature (Olah et al., 2020, Hammond et al., 2019, Van Hove et al., 2019, Mrdjen et al., 2018, Masuda et al., 2020b). *Figure 1* shows a clustered heatmap of key microglial genes within Control and Aldara groups at the 3-day timepoint (n=5/group). The heatmap presented in *Figure* 1 is row-scaled using gene expression Z-scores. This analysis approach and presentation involves calculating the mean expression of the given gene for all samples and representing its expression in reference to the previously calculated gene mean.

A split in the transcriptional biology is observed with a group of upregulated genes shown in yellow (positive Z-score) and downregulated in blue (negative Z-score) amongst the Aldara-treated animals. Consistently significantly upregulated genes amongst the Aldara samples include *Hexb, Tmem119, Cd68, Msr1, Aif1* and *Pros1*

*(*p.adj<0.05*)*. These genes encode for proteins which have been shown to be involved in microglial reactivity in neuroinflammation (Masuda et al., 2020b). The genes *Csf1r, Cx3cr1* and *Mertk* showed some variation between samples with some biological replicates displaying a relatively downregulated transcriptomic signature. Of these, only *Cx3cr1* and *MerTK* were significantly changed (p.adj<0.05). This variation in microglial transcriptomic signatures could display varying levels of responsiveness of the brain immune cells. Consistently significantly downregulated genes amongst the Aldara samples include *Gpr34, P2ry12*, *Trem2* and *Nr4a1A*. Downregulation of these genes may be suggestive of a dampening of microglial responses to combat neuroinflammation. The protein encoded by *Gpr34* has been found to mediate microglial shift to disease-associated cellular states (Preissler et al., 2015). Additionally, the purinergic receptor encoded by P2ry12 has links to microglial motility (Haynes et al., 2006). Downregulation of this in the TLR7-driven neuroinflammation may be indicative

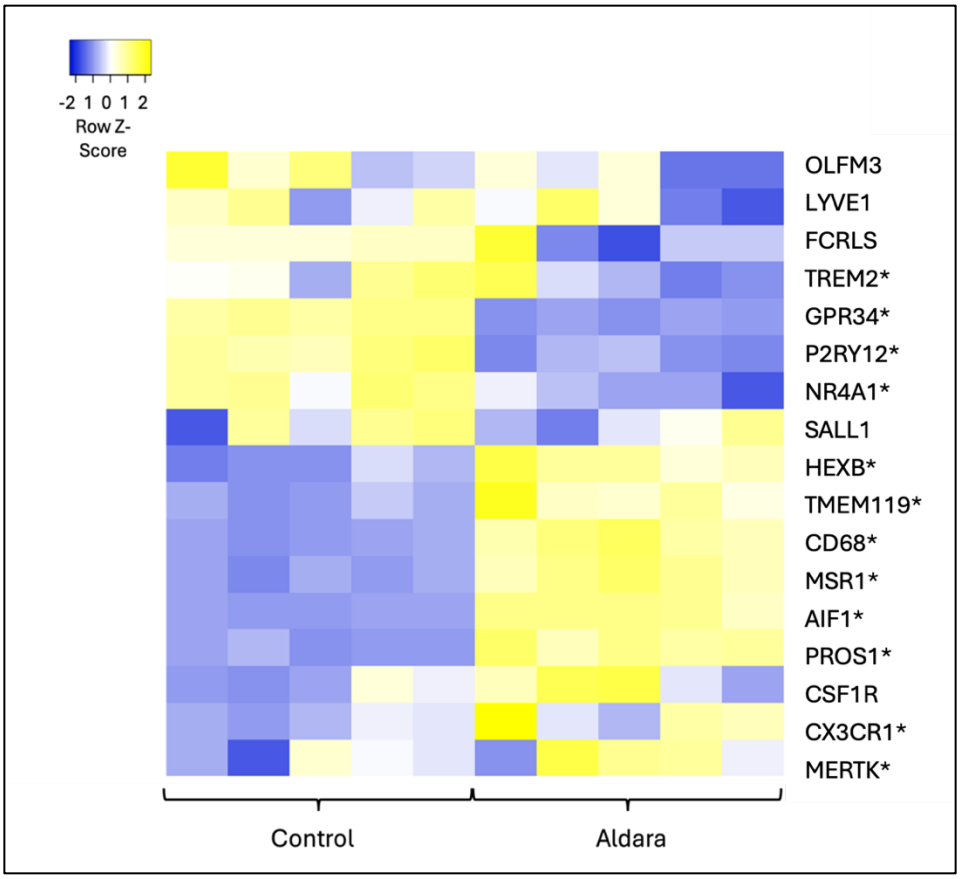

Figure 1: Aldara-treated samples display both up- and downregulated transcriptional biology of microglia-related genes at the whole-brain level. *Heatmap of microglia-related genes from 3-day treatment bulk RNA sequencing dataset. Columns indicate biological replicates within treatment groups. Expression levels of genes have been row-scaled into z-scores. Colour intensity represents expression level with yellow showing upregulated genes (positive Z-score) and blue showing downregulated genes (negative Z-score). Significantly DEGs p.adj<0.05 indicated by (*). Average linkage by rows clustering method and Pearson distance measurement method used. N=5/group.*

of a more static cell state. Several microglia-related genes that displayed varying expression levels throughout Aldara samples include *Olfm3, Lyve1, Fcrls, Trem2* and *Sall1*. However, these genes with variable expression were not significantly changed (p.adj>0.05).

4.3 Flow cytometric identification of cytokine-producing and reactive microglia within brain parenchyma

Microglia are commonly classified in flow cytometry by CD45^{int} CD11b^{+} cells (Srakocic et al., 2022). Particularly the gating separation of CD45^{int} from CD45^{hi}

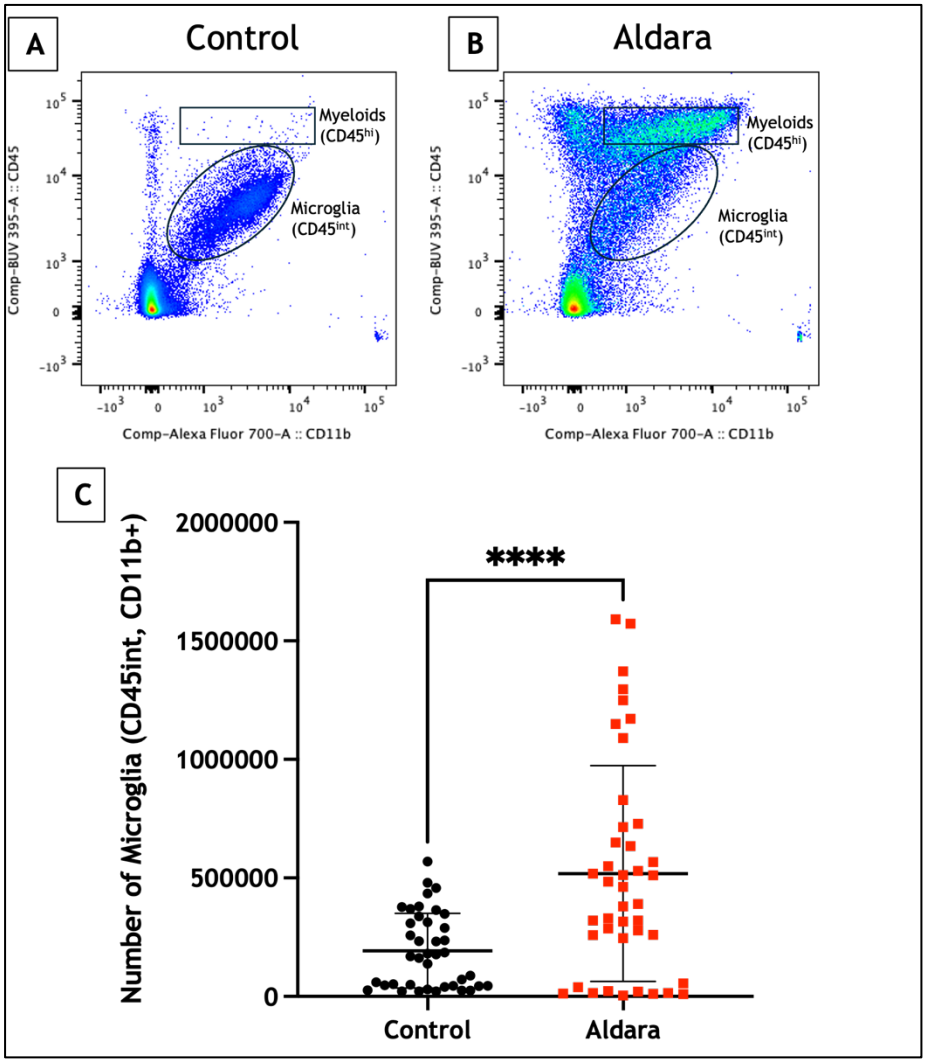

Figure 2: Number of resting microglia (CD45^{int}, CD11b^{+}) increase in whole-brain of Aldara-treated mice. *Representative flow plots of Control (B) and Aldara (C) brains showing microglial gating (CD11b^{+}, CD45^{int}) and myeloid gating (CD11b^{+}, CD45^{hi}). Scatterplot displaying total number of live cells from Microglia in Control (white) and Aldara (red) mice (C). Individual animals plotted on graph. Y-axis displayed as linear scale. Unpaired t-test shows significance for both cell groups. P<0.0001 shown as ****. Pulling of 8 experiments provided n=40 for Control and n=42 for Aldara.*

distinguishes resident microglial populations from infiltrating myeloid populations including macrophages (Brandenburg et al., 2020). This intermediate CD45 expression classification further separates resident microglia from BAMs with the latter showing high CD45 expression levels (Dermitzakis et al., 2023). Representative flow plots showing microglial gating ($CD11b^{+}$, $CD45^{int}$) and myeloid gating ($CD11b^{+}$, $CD45^{hi}$) can be seen for Control and Aldara brains in Figures 2A and B, respectively. As seen in *Figure 2C*, the number of $CD45^{int}$ $CD11b^{+}$ microglia is significantly increased in Aldara-treated mice ($p<0.0001$). On average, there is a 321% increase in $CD45^{int}$ $CD11b^{+}$ microglia in Aldara compared to Control mice. When investigating the number of microglia, some variation can be seen in *Figure 2C*. This may be explained by biological variation of microglial reactivity the TLR7-neuroinflammation.

As microglia as a relatively heterogenous population in terms of function, changes to number of microglia may not be indicative of total microglial response. To investigate microglial output during TLR7-driven neuroinflammation, their cytokine production was investigated. Additionally, to an overall increase in numbers of $CD45^{int}$ $CD11b^{+}$ microglia, their cytokine production activity is also increased. Microglia were found to significantly increase their IFNγ and TNFα pro-inflammatory cytokine production (*Figure 3A*). The third key cytokine IL-6 also presented an increasing trend without reaching significance ($p=0.0515$). This may

be explained by a smaller sample size. Representative contour flow plots of

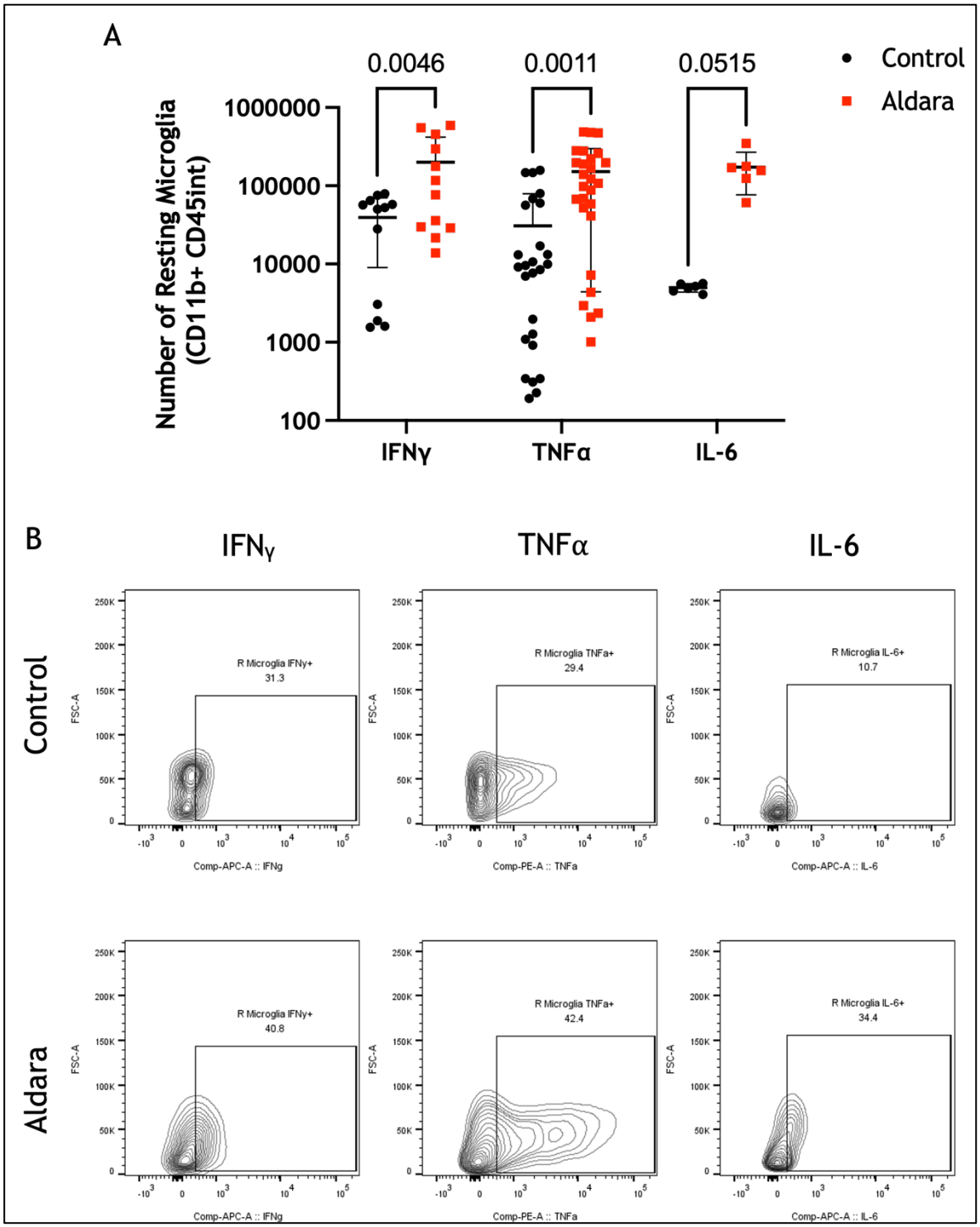

Figure 3: Increasing trend in cytokine-producing Microglia in Aldara mice. *Scatterplot displaying total number of cytokine-producing Microglia (CD45^{int}, CD11b^{+}) in Control (white) and Aldara (red) mice (A). Individual animal values shown following the key displayed. Y-axis displayed as Log10 scale. Two-way ANOVA using Šídák's statistical test for multiple comparison shows significance for both cell groups. P<0.0021 shown as ** and ns shows p>0.05. Pulled experiments and availability of marker expression explains variation observed in n number. Representative contour flow plots showing numbers of microglia for Control (upper) and Aldara (lower) mice for cytokine production (B). N number per group are as follows: IFNγ = 12; TNFα = 27 and IL-6 = 6.*

microglial cytokines can be seen for Control and Aldara brains in *Figure 3B*.

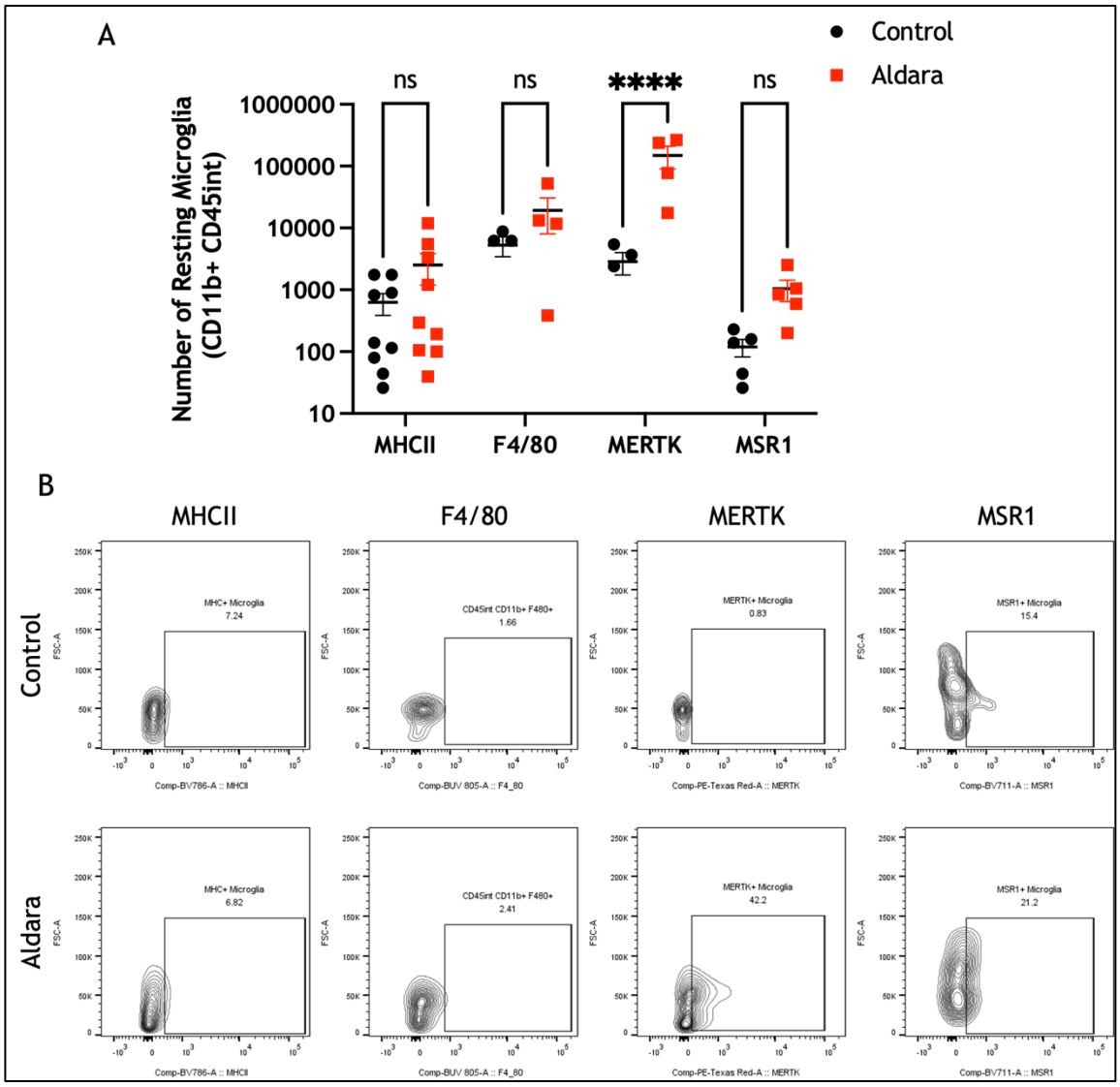

Figure 4: Increasing trend in Microglia activation markers in Aldara-treated mice. *Scatter plot displaying total number of activation marker-expression Microglia (CD45^{int}, CD11b^{+}) in Control (white) and Aldara (red) mice (A). Individual animal values shown following the key displayed. Y-axis displayed as Log10 scale. Two-way ANOVA using Šídák's statistical test for multiple comparison shows significance for both cell groups. P<0.0001 shown as **** and ns is p>0.05. Four pulled experiments and availability of marker expression explains variation observed in n number. Representative contour flow plots showing numbers of microglia for Control (upper) and Aldara (lower) mice for reactive surface markers (B). N number per group are as follows: MHCII = 9; F4/80 = 4; MERTK = 4 and MSR1 = 5.*

Further microglia changes following this TLR7 ligation is reorganisation of their surface markers indicative of a transition to reactive status. The 4 commonly used microglial reactive markers are MHCII, F4/80, MERTK and MSR1. *Figure 4A* shows all 4 of microglia reactive markers display an upwards trend in Aldara mice with MERTK being the only marker to show significance (p<0.0001). Representative

contour flow plots of microglial reactive surface markers can be seen for Control and Aldara brains in *Figure 4B*.

4.4 Identification of microglia-like population via spatial transcriptomics

As previously discussed, spatial transcriptomics allows for in situ visualisation of various cell type based on their transcriptional profile within the selected tissue (Williams et al., 2022). Here, Nanostring's CosMx SMI was chosen to further explore microglial biology following TLR7-activated neuroinflammation (He et al., 2022). CosMx 1000-plex mouse neuroscience panel provides multiple microglia-related genes for identification of the resident neural cell type. These include *Hexb, Tmem119, P2ry12, Cx3cr1 and Msr1*. Changes to these microglia-related genes were shown previously with whole-brain bulk RNA sequencing (*Figure 1)*.

Firstly, cell typing was completed with the CosMx dataset. To aid cell identification in both at rest and inflammatory tissue environments, all 16 CosMx samples, both Control and Aldara, were integrated. This was to capture all cell types regardless of their individual transcriptomic changes or reactivity status. A scRNAseq-like clustering approach revealed 18 clusters as shown in the UMAP in *Figure 5A*. The heatmap shown in *Figure 5B* involves different interpretation to classical heatmaps. These heatmaps show genes that are uniquely upregulated within that cluster. From this point, this variation of heatmaps will be termed 'inter-cluster expression heatmaps'. At this 18-cluster stage, one biological cell type may be represented by multiple clusters. This explains why 'classic' cell identifying genes may not appear in that clusters 'top 10 identifier genes' as that gene is equally expressed across all clusters that represent that cell type.

One limitation of spatial transcriptomic analysis is its minimal ability to capture complex cell morphologies. This confinement is especially true for neural cells which have many anatomical cellular processes and membrane extensions. Going forward, this may explain unusual genes being 'expressed' in certain cell types (e.g. *Gfap* is expressed in all identified CosMx cell types but is a commonly known astrocytic markers).

Of the 18 clusters, 9 cell types were identified using key cell typing genes as seen in *Table 4.1*1. These cells include glutamatergic neurons, GABAergic MSNs, astrocytes, oligodendrocytes, endothelial cells, neurovascular units (NVU; thought to be mix of astrocytes and endothelial cells), immune (predominantly microglia) and ependymal cells. Two clusters, Cluster 0 and 1, were unclassified neurons as they expressed no specific neuronal subtype identifier genes.

Table 4.1: CosMx cluster marker genes for cell type identification

Cell type	*Cluster number*	*Cell type identifier genes*
Astrocytes	7, 11, 12	*Gja1, Slc13a3, Aqp4*
Endothelial cells	14	*Cldn5, Pecam1, Flt1*
Ependymal cells	16	*Foxj1, Ttr, Htcr2*
GABAergic neurons	3	*Gad1, Gad2, Slc32a1*
Glutamatergic neurons	2, 6, 15	*Slc17a7, Camk2a*
Immune	10, 17	*Ptprc, Cx3cr1*
Medium spiny neurons	8, 13	*Ppp1r1b, Adora2a, Arpp21*
Neurovascular	4	*Plp, Apod*
Oligodendrocytes	5, 9	*Mog, Mag, Plp1, Mbp*
Unclassified neurons	0, 1	*n/a*

From the 18 initial clusters, 2 immune/microglia clusters were identified: clusters 10 and 17. Gene expression heatmaps for clusters 10 and 17 can be seen in *Figures 5C* and *5D,* respectively. Key identifier genes of these clusters which were suggestive of immune cells include complement-related genes (*C1qa-c*), *Hexb, Ctss, Tyrobp, Grn, Csf1r, Ctsd* and *Selplg* (Pettas et al., 2022). These cluster transcriptional identifiers coupled with the global spatial distribution of cells (*Figure* 6), led these cells to be classified as immune cells – including brain-resident microglia. It should be noted that cluster 10 appears as the primary microglia cluster with cluster 17 potentially representing predominantly infiltrating immune cells with their 'top' identifier genes including more classical immunological markers including *Cd6, Ctss, C1qb, Lag3, Cxcl2, Gas2, Slit2* and *Tnc* (Hsing and Rudensky, 2005, Ruffo et al., 2019, Gurrea-Rubio et al., 2025). Both

clusters were included in immune cell analysis to investigate both brain-resident and peripheral infiltrating populations.

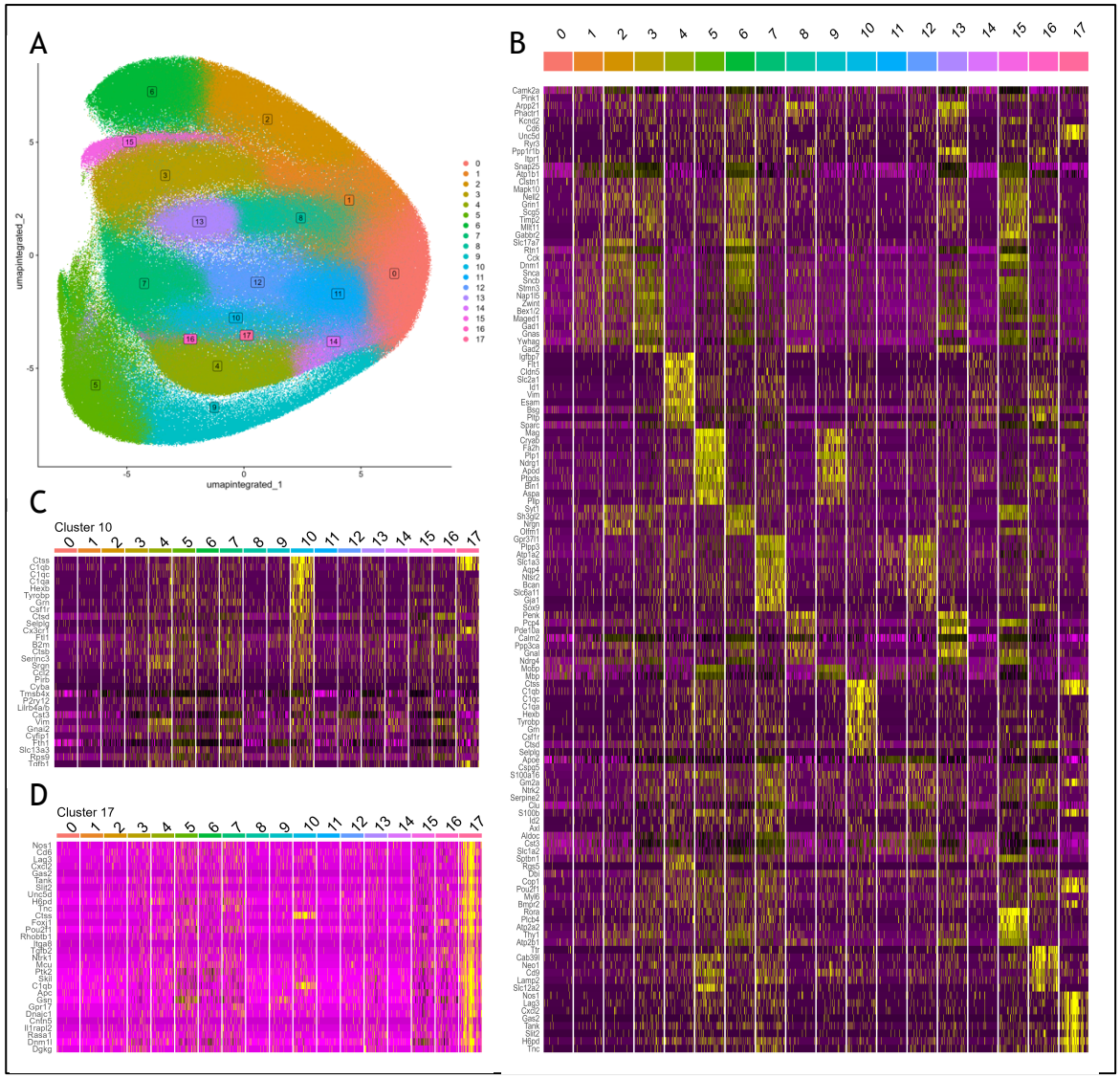

Figure 5: Two Microglia/immune-like clustered identified in initial CosMx spatial transcriptomics clustering. *(A) UMAP of 18 clusters identified from integration of all Control and Aldara samples. (B) Inter-cluster Expression Heatmap displaying relative gene expression of one cluster compared to other 17 clusters. (C) Inter-cluster Expression Heatmap showing relative gene expression indicating suspected Microglia/Immune-like cluster 10. (D) Inter-cluster Expression Heatmap showing relative gene expression indicating suspected Microglia/Immune-like cluster 17. For heatmaps shown in A-C, yellow indicates relative increased expression and purple indicates relative decreased expression.*

From the grouped clusters and biological cell types as seen in *Table 4.1*, DE analysis was performed in a bulk RNA sequencing-like approach using the Searchlight analysis platform (Cole et al., 2021). As 'anterior' and 'posterior' samples came from 1 mouse, differential analysis was performed separately to avoid oversampling improperly powered statistics.

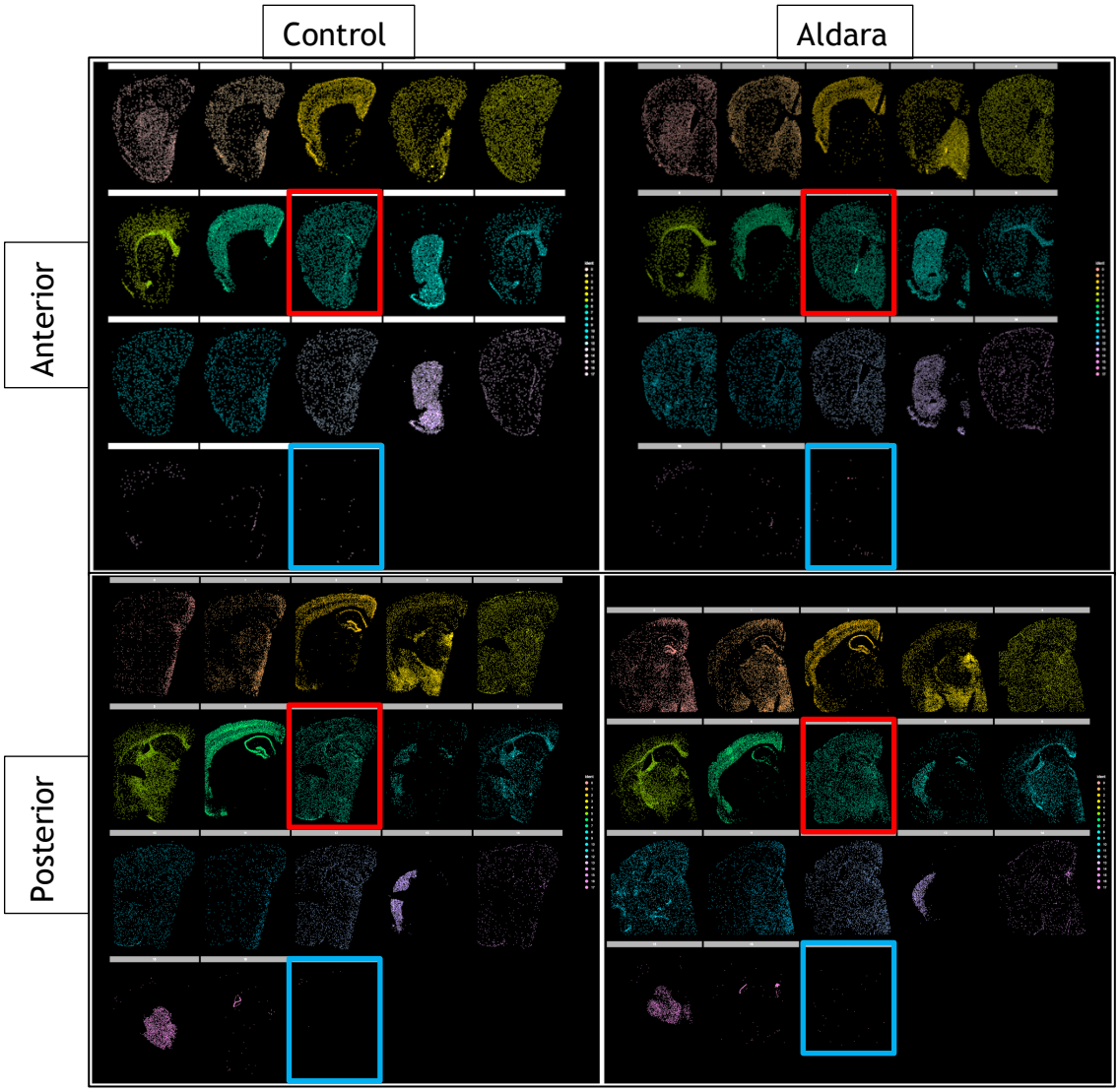

Figure 6: CosMx spatial plots of two representative Control and Aldara samples from anterior and posterior plane. *18 clusters shown correspond with 18 identified clusters from previous UMAP (Figure 5). Clusters 10 represented by red outline and clusters 17 by blue outline. One dot in the spatial plot represents one cell from the corresponding cluster.*

As the research questions for this thesis focus on the contribution of immune populations to the TLR7-driven neuroinflammation, the immune cluster was investigated. *Figure* 7 shows a summary of the DE analysis of the cells belonging to the immune cluster from anterior brain sections. PCA shows the gene expression

data Control and Aldara naturally separating into 2 distinct groups (*Figure 7A)*. This suggests PC1 may be representative of treatment and PC2 may be representative of biological variation. The lollipop graph shows 90 genes being significantly upregulated in Aldara samples compared to control and 32 downregulated (*Figure 7B;* p.adj<0.05 and absolute log^2 fold change >0.5 and <-

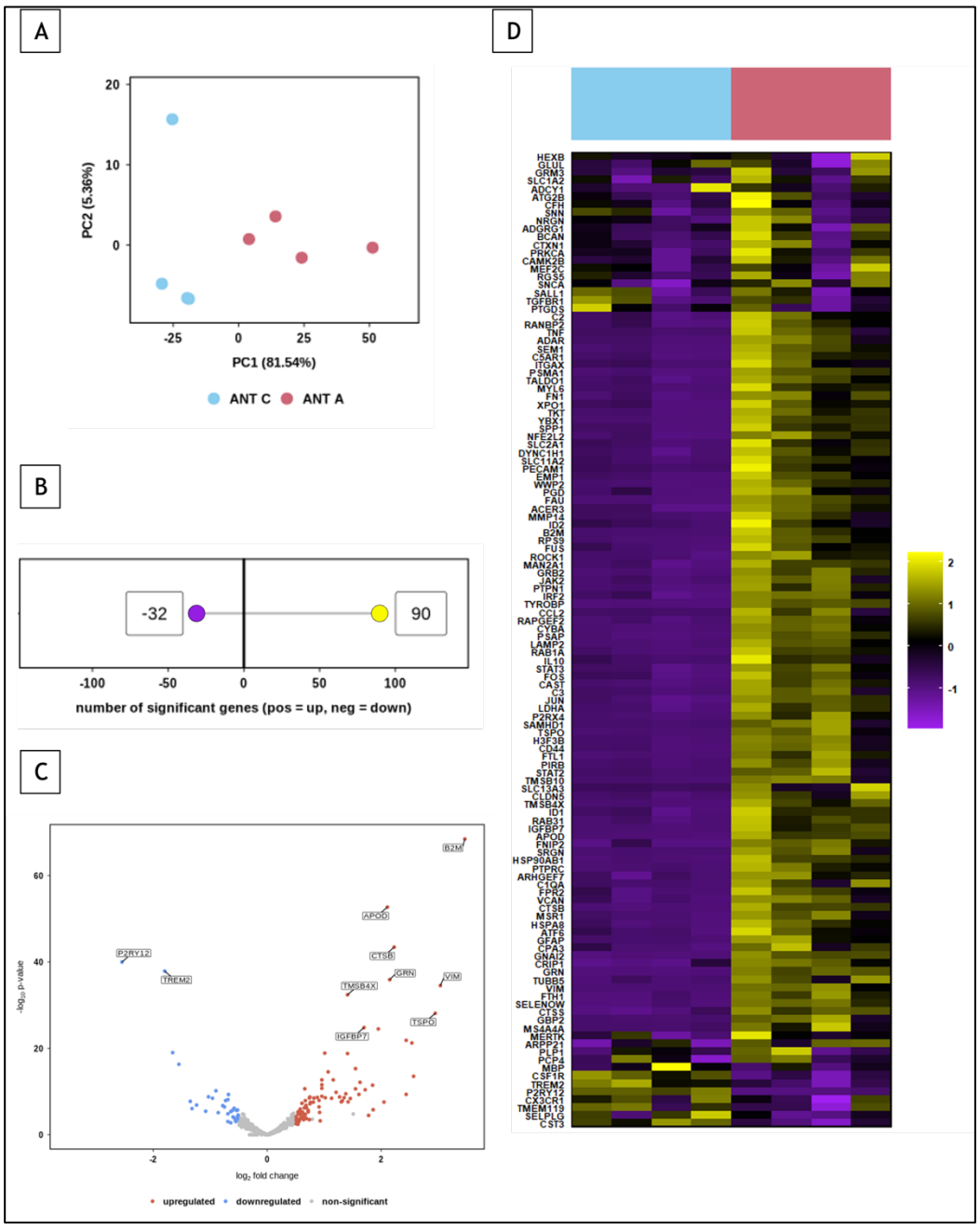

Figure 7 Differential expression analysis of Immune Cell Clusters of anterior brain sections from CosMx spatial transcriptomics platform. *(A) PCA scatterplots showing gene expression data for Control [blue] and Aldara [red]. Individual samples represented by dots. (B) Lollipop graph showing number of significantly DEGs [p.adj <0.05, absolute log_2fold >0.5]. (C) Volcano plot of significantly DEGs with upregulated shown in red, downregulated in blue and non-significant in grey. (D) Hierarchically clustered heatmap of DEGs in Control and Aldara samples. Expression levels shown are row-scaled into Z-scores with yellow representing high expression and purple representing low expression.*

0.5, respectively). The heatmap featured in *Figure 7D* highlights the DEGs and their pattern of transcriptional changes with Aldara samples primarily displaying upregulation of genes displayed in yellow. Anterior Control samples typically presented a downregulation of their transcriptional biology.

Figure 8 shows a summary of the DE analysis of the cells belonging to the immune cluster from posterior brain sections. PCA of gene expression from Control and Aldara shows a relatively less distinct grouping of treatments in posterior samples compared to anterior samples (*Figure 8A)*. This suggests more variety in the transcriptional biology of the immune cells belonging to posterior samples of both treatment groups. The lollipop graph shows 79 genes being significantly upregulated in Aldara samples compared to control and 27 downregulated (*Figure 8B;* p.adj<0.05 and absolute $\log_2$ fold change >0.5 and <-0.5, respectively). Inspecting the transcriptional biology presented in the heatmap in *Figure 8D,* most Aldara samples show significantly upregulated genes displayed in yellow.

However, for some of the significantly changes genes, there is a split between Controls with two samples displaying upregulation and the other two displaying

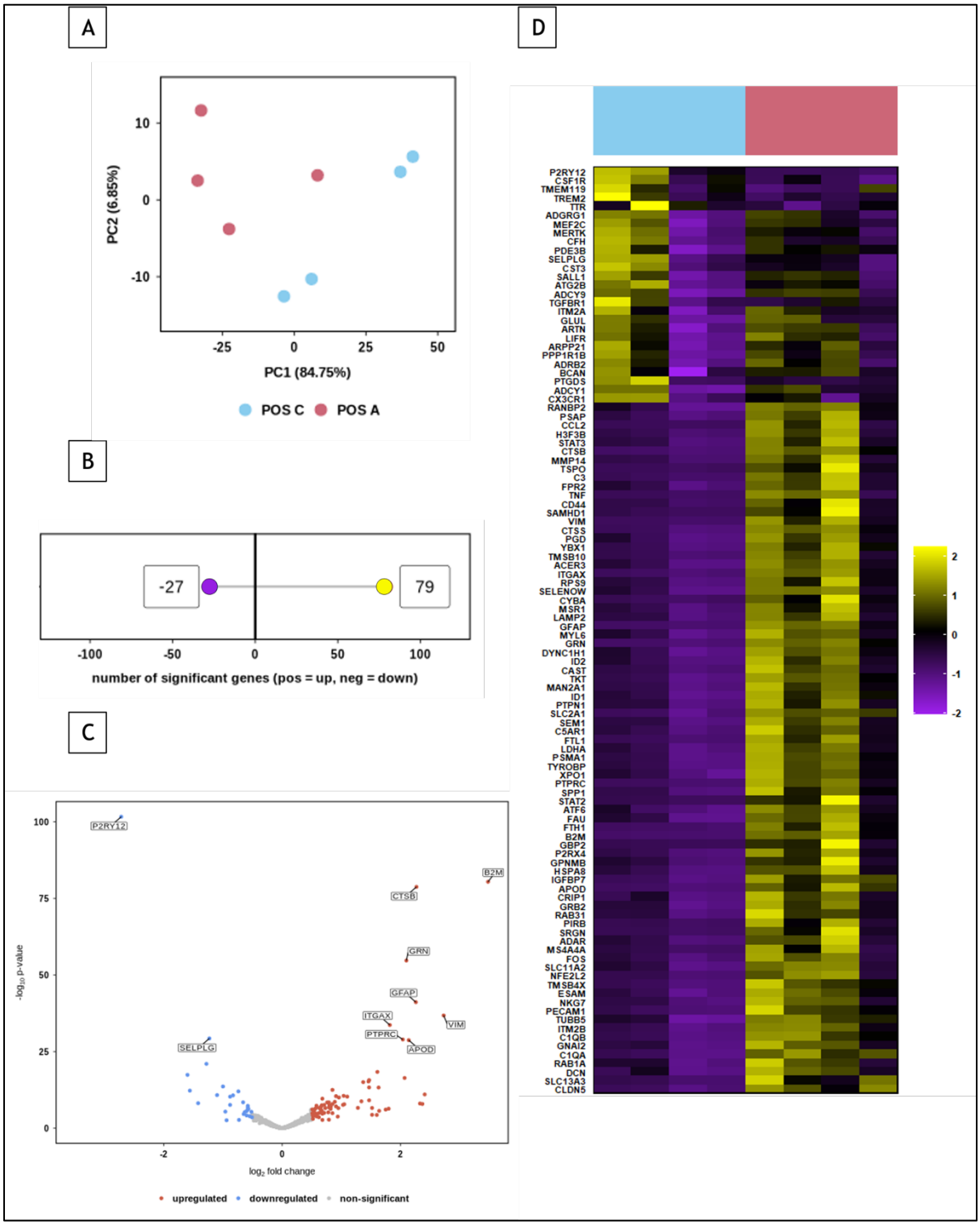

Figure 8 Differential expression analysis of Immune Cell Clusters of posterior brain sections from CosMx spatial transcriptomics platform. *(A) PCA scatterplots showing gene expression data for Control [blue] and Aldara [red]. Individual samples represented by dots. (B) Lollipop graph showing number of significantly DEGs [p.adj <0.05, absolute log_2fold >0.5]. (C) Volcano plot of significantly DEGs with upregulated shown in red, downregulated in blue and non-significant in grey. (D) Hierarchically clustered heatmap of DEGs in Control and Aldara samples. Expression levels shown are row-scaled into Z-scores with yellow representing high expression and purple representing low expression.*

downregulation of the same genes. This suggests, immune cells from posterior control brain sections may display more heterogeneity in their transcriptional biology.

From the volcano plots for anterior and posterior immune cells (*Figure 7C* and *8C),* top 10 significantly changed genes are shown. From the upregulated genes, these include key markers which have been documents as upregulated in reactive microglia. This includes the gene *Apod* which encodes for apolipoprotein D which increased levels has been shown to shift microglia from their resting homeostatic to a more secretory state and increase cytokine production (Corraliza-Gomez et al., 2023). Further suggestion of microglial reactivity comes from upregulation of *Tspo* which has been found increased in microglia within AD neuroinflammatory environments (Nutma et al., 2021). Upregulation of *Ptprc*, which encodes for the pan immune marker CD45, strengthens claims of this cell cluster being immunological. Downregulation of *P2ry12* is commonly observed in microglia in neuroinflammation and may be suggestive of decreased microglial anatomical processes (van Wageningen et al., 2019). Overall, transcriptomic signatures of these cells are suggestive of a reactive microglial subtype with potential increase in secretory processes.

To reveal all immune cell subtypes within the CosMx dataset, combination and reclustering of immune clusters 10 and 17 was performed. This was theorised to include all potential resident, infiltrating and border-associated immune cells. Reclustering revealed 5 new immune subclusters based on inter-cluster relative gene expression (*Figure 9).* The UMAP showing 5 subclusters Immune.0-Immune.4 can be seen on *Figure 9A*. The inter-cluster expression heatmap can be seen on *Figure 9B*. Representative spatial plots of all 5 immune subclusters for Control and Aldara sections on anterior and posterior planes can be seen in *Figure 10*.

Immune.0 cluster was found to have no distinct expressing genes compared to the other clusters. Of the genes shown to be relatively expressed by Immune.1, none are specific identifiers unique to microglia, but several are upregulated and related to microglial function including *Vim*, *B2m, Ftl1, Srgn, Ccl2 and Lilrb4a/b* (Hammond et al., 2019, DePaula-Silva et al., 2019, Mendes and Majewska, 2021, Kretzschmar et al., 2021). Some of these genes may also be expressed on other

cell types including astrocytes and neurons. However, this may indicate this subcluster interacting with other brain-resident population and highlight the limitation of cell segmentation within this technique. Interaction and cellular segmentation overlap with astrocytes presents as a strong possibility within this cluster with its relatively increased expression of astrocytic marker *Gfap*.

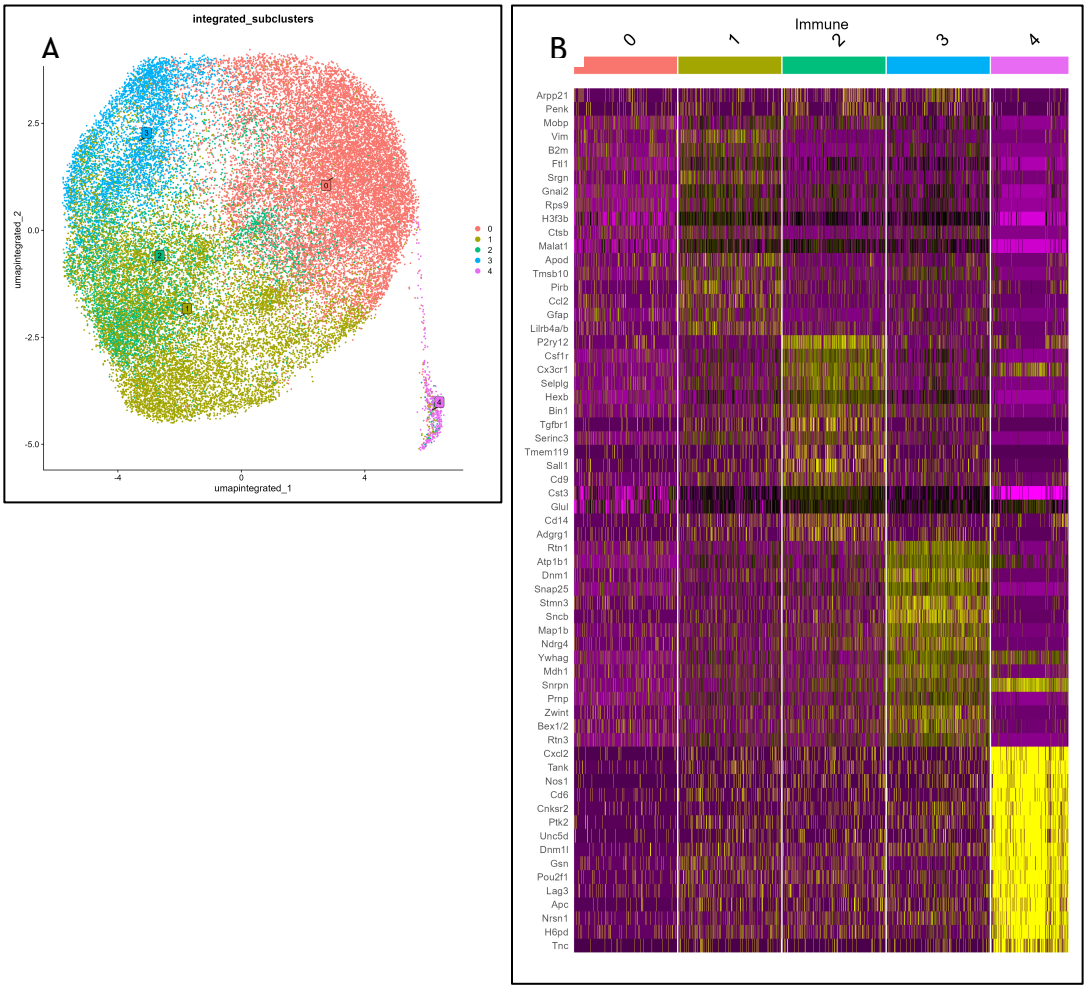

Figure 9: Reclustering of CosMx spatial transcriptomic dataset reveals five potential subclusters of microglia/immune-like cells. *(A) Integrated UMAP of five microglia/immune subclusters labelled 'immune.0', 'immune.1', 'immune.2', 'immune.3'and 'immune.4' for Control and Aldara samples. (B) Heatmap of relative inter-cluster gene expression of five microglia/immune subclusters. Yellow representing relative upregulation and purple representing relative downregulation of genes.*

Cluster Immune.2 features a collection of upregulated reliable microglia identifier genes including *P2ry12, Csf1r, Cx3cr1, Hexb, Tmem119* and *Sall1* (Hammond et al., 2019). Other upregulated transcripts that relate to microglial biology, however, may be expressed within other immune and brain-resident cells populations include *Tgfbr1, Serinc3, Cd9, Cd14* and *Selplg*. Again, potentially

indicating other brain-resident cells that this microglia-like subcluster may be interacting with.

Subcluster Immune.3 expresses the least number of microglia-related genes within this relative expression heatmap shown in *Figure 9B*. The main cell type that expresses the relatively upregulated genes within this cluster are neurons. These neuron-related genes include *Dnm1, Snap25, Sncb, Map1b, Bex1/2, Rtn1* and *Rtn3*. Some upregulated genes within this cluster, although not microglia specific, may be indicative of changes to microglial function and reactivity status include *Ywhag* and *Mdh1*.

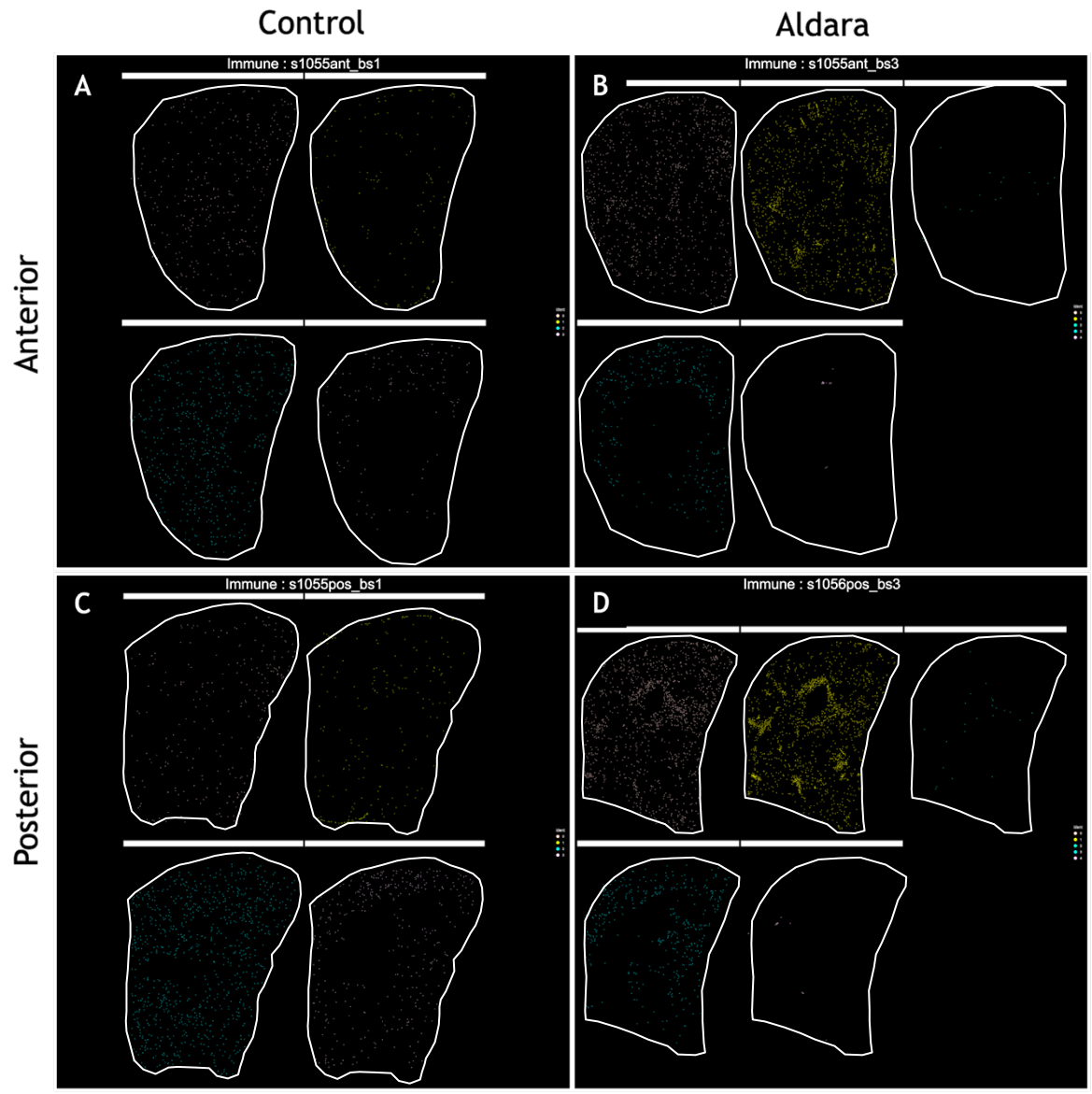

Figure 10: Representative spatial plots of immune subclusters from anterior and posterior coronal brain hemisections from Control and Aldara mice. *Spatial plots of Control brain hemisections from immune subclusters 0-3 in anterior (A) and posterior (C) planes. Spatial plots of Aldara brain hemisections show immune subclusters 0-4 in anterior (B) and posterior (D) planes. Contrast and saturation increased for visualisation. White drawn boundaries of brain tissue slice.*

The relative upregulated signal displayed by the Immune.4 subcluster features several immune-focused genes including *Cxcl2, Cd6, Lag3* and *Tnc*. This subcluster additionally displays neuron-related gene changes including *Nos1, Cnksr2, Arc* and *Nrsn1*. As seen in *Figure* 10, this subcluster was primarily present in Aldara samples. This subcluster will be further examined in relation to its immune properties in the subsequent chapter of this thesis.

As displayed in *Figure 11*, several immune subclusters experienced an increase in cell numbers following Aldara treatment. These include Immune.0 and Immune.1 which displayed significance (p<0.0001) and Immune.3 which did not reach significance (p>0.05). Immune.2 was the only subcluster to present a significant decrease in cell number (p<0.0001).

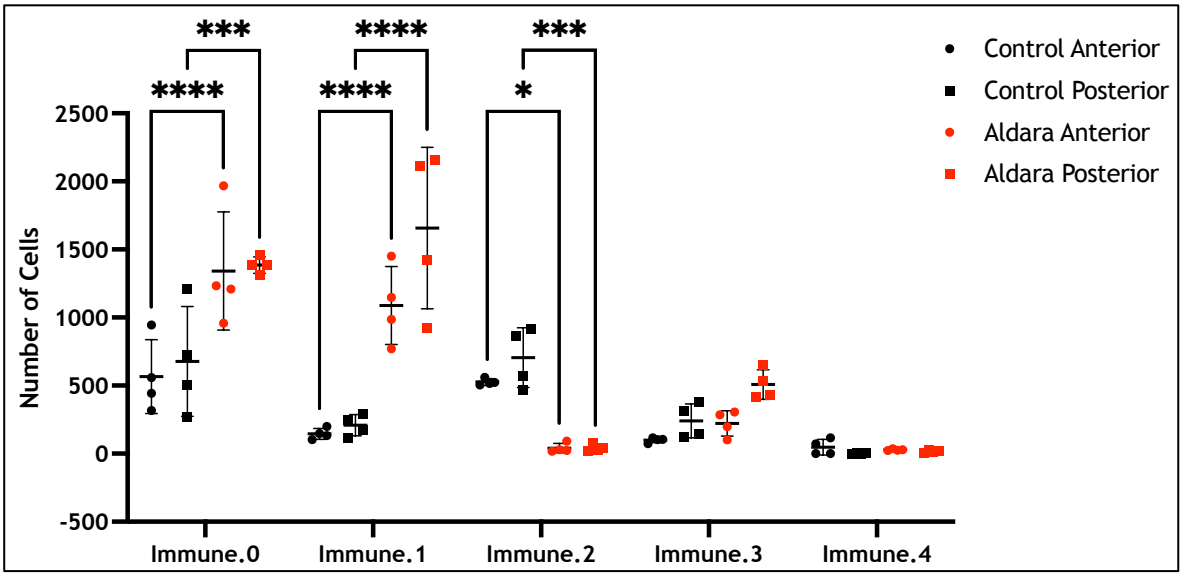

Figure 11: Changes in cell number amongst CosMx microglia/immune subclusters. *Bar chart displaying total number cells in Control (white) and Aldara (red) mice. Symbols on graphs represent one tissue section and one animal is represented by two symbols for anterior and posterior sections. Y-axis displayed as log_{10} scale. Two-way ANOVA using Šídák's statistical test for multiple comparison shows significance for both cell groups. Ns p>0.05 and not shown on graph. P<0.0332 = *, p<0.0002 = **** and p<0.0001 = ****. Data presented as mean +/- SD. N=4/group.*

To understand the transcriptional changes of the immune subclusters, DE analysis was again performed using the Searchlight analysis platform of individual subclusters in anterior and posterior tissue planes. DE analysis of cells belonging to anterior Immune.0 subcluster samples is shown in *Figure 12*. PCA shows the gene expression data of anterior Immune.0 subclusters from Control and Aldara treatment groups

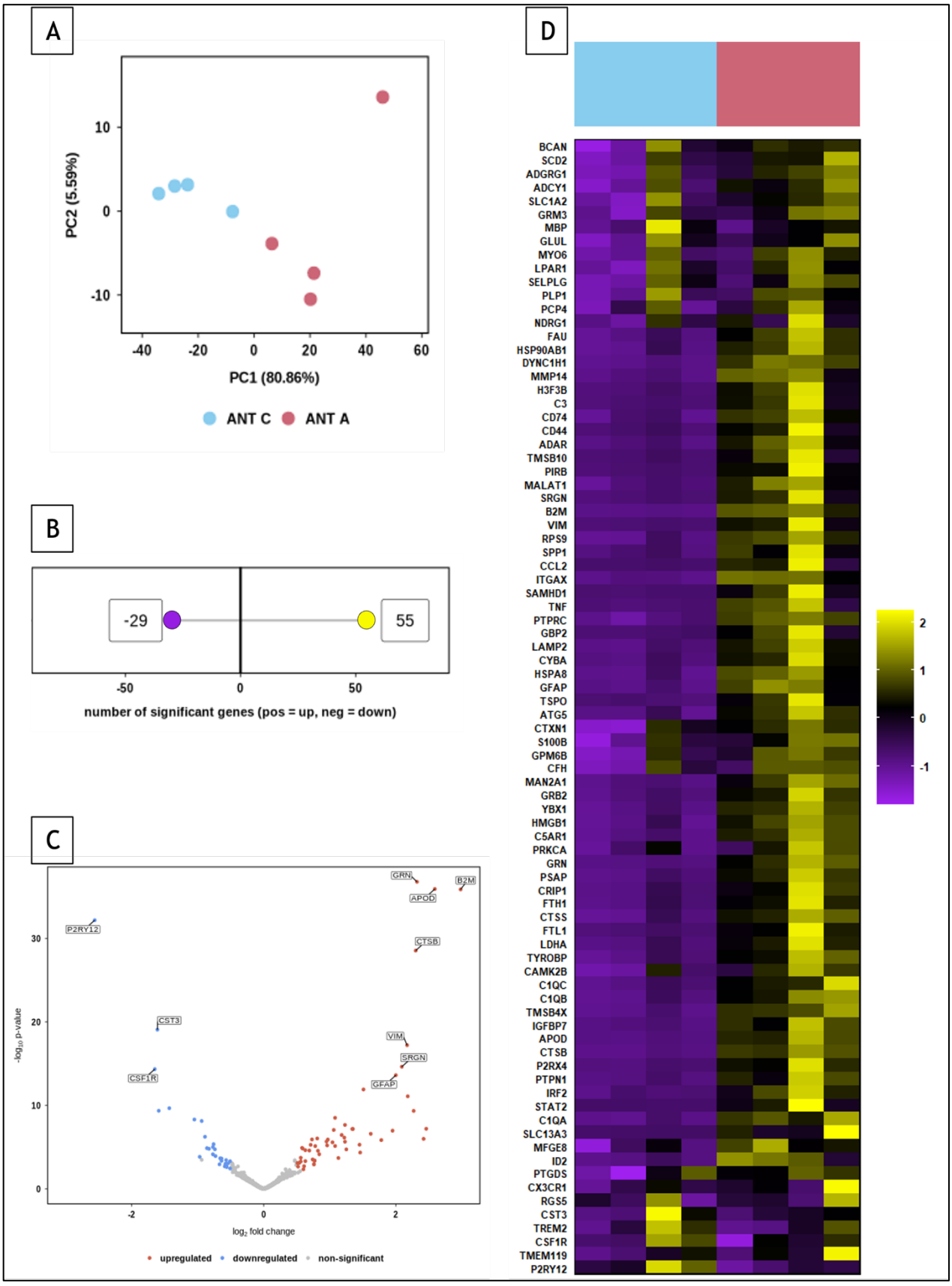

Figure 12: Differential expression analysis of 'Immune.0' subcluster from anterior brain sections. *(A) PCA scatterplots showing gene expression data for Control [blue] and Aldara [red]. Individual samples represented by dots. (B) Lollipop graph showing number of significantly DEGs [p.adj <0.05, absolute log_2fold >0.5]. (C) Volcano plot of significantly DEGs with upregulated shown in red, downregulated in blue and non-significant in grey. (D) Hierarchically clustered heatmap of DEGs in Control and Aldara samples. Expression levels shown are row-scaled into Z-scores with yellow representing high expression and purple representing low expression.*

naturally separating into 2 distinct grouping (*Figure 12)*. One Aldara sample presents as separate from the other samples with relatively higher PC1 and PC2 scorings. This sample is the third Aldara sample shown in the heatmap (*Figure 12D)* which has a relatively higher increase in the significant DEG. This slight variation among samples may be explained by the biological replicate having a strong response to the inflammatory stimulant within the Aldara model. For other samples shown in the PCA, grouping of samples via PC1 may be representative of treatment.

The lollipop graph shows 55 genes being significantly upregulated in Aldara samples compared to control and 29 downregulated (*Figure 12B;* p.adj<0.05 and absolute log_2 fold change >0.5 and <-0.5, respectively). The heatmap featured in *Figure 12* highlights the DEGs and their pattern of transcriptional changes. Aldara samples primarily display a subtle upregulation of genes displayed in yellow and some genes remaining unchanged compared to Controls as shown in black. The top significantly upregulated genes in Aldara anterior Immune.0 subclusters include *B2m, Apod, Ccl2, Slc13a3* and *Grn*. The top significantly downregulated genes in Immune.0 include *P2ry12, Csf1r, Cst3, Trem2 and Mbp*. The top 10 upregulated and downregulated genes ranked by log_2 fold change can be seen in *Table 4.2*.

Table 4.2: Top 10 upregulated and downregulated DEGs in anterior 'Immune.0' CosMx subcluster

Gene	log2fold	p	p.adj
B2M	2.98	1.342670e-36	3.168702e-34
APOD	2.59	1.188339e-36	3.168702e-34
CCL2	2.46	6.266766e-08	2.142444e-06
SLC13A3	2.42	1.011015e-06	2.385996e-05
GRN	2.32	1.646156e-37	1.165478e-34
CTSB	2.30	2.831494e-29	4.009396e-27
TSPO	2.27	4.522614e-10	2.134674e-08
ITGAX	2.18	8.003059e-12	4.721805e-10
VIM	2.17	6.082227e-18	6.151739e-16
SRGN	2.09	2.318309e-15	2.051704e-13

Gene	log2fold	p	p.adj
P2RY12	-2.56	6.515038e-33	1.153162e-30
CSF1R	-1.65	4.452999e-15	3.503026e-13
CST3	-1.61	8.414114e-20	9.928655e-18
TREM2	-1.59	4.388519e-10	2.134674e-08
MBP	-1.43	2.141623e-10	1.166361e-08
GLUL	-1.05	4.830007e-09	2.011556e-07
RGS5	-0.97	1.432749e-04	1.779625e-03
RIMS2	-0.94	3.259629e-04	1.000000e+00
PLP1	-0.94	7.334864e-09	2.885047e-07
SELPLG	-0.89	5.752842e-07	1.508523e-05

DE analysis of cells belonging to posterior Immune.0 subcluster samples is shown

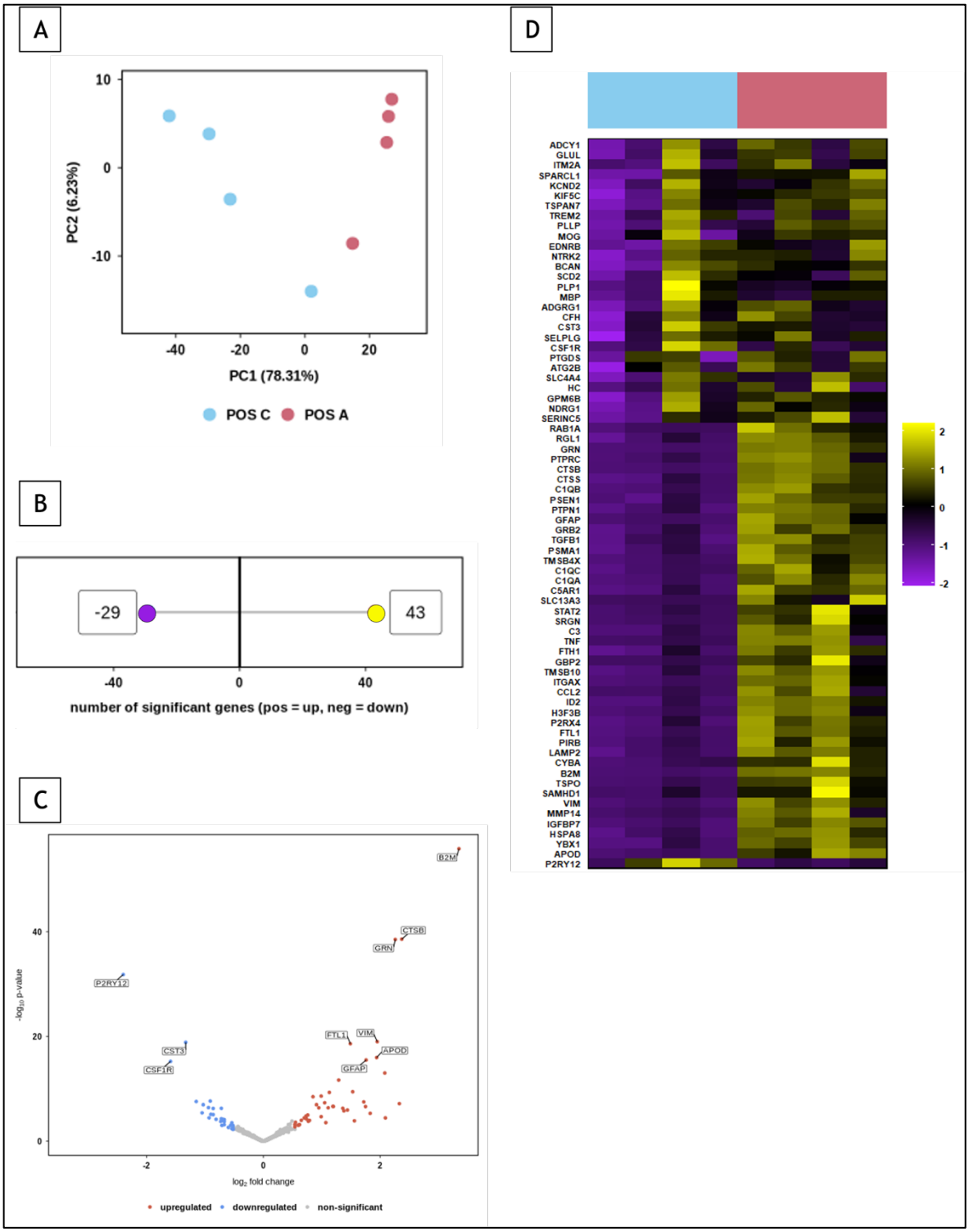

Figure 13: Differential expression analysis of 'Immune.0' subcluster from posterior brain sections. *(A) PCA scatterplots showing gene expression data for Control [blue] and Aldara [red]. Individual samples represented by dots. (B) Lollipop graph showing number of significantly DEGs [p.adj <0.05, absolute log₂fold >0.5]. (C) Volcano plot of significantly DEGs with upregulated shown in red, downregulated in blue and non-significant in grey. (D) Hierarchically clustered heatmap of DEGs in Control and Aldara samples. Expression levels shown are row-scaled into Z-scores with yellow representing high expression and purple representing low expression.*

in *Figure 13*.

PCA shows the gene expression data of posterior Immune.0 subclusters from Control and Aldara treatment groups naturally separating into 2 distinct groups (*Figure 13A)*. This suggests PC1 may be representative of treatment. The lollipop graph shows 43 genes being significantly upregulated in Aldara samples compared to control and 29 downregulated (p.adj<0.05 and absolute log_2 fold change >0.5 and <-0.5, respectively). The heatmap featured in *Figure 13D* highlights the DEGs and their pattern of transcriptional changes with Aldara samples primarily displaying upregulation of genes displayed in yellow. The top significantly upregulated genes in Aldara anterior Immune.0 subclusters include *B2m, Ctsb, Slc13a3, Grn and Gbp2*. The top significantly downregulated genes in Immune.0 include *P2ry12, Csf1r, Cst3, Plp and Trem2*. The top ten upregulated and downregulated genes ranked by Log_2 fold change can be seen in *Table 4.3*.

Table 4.3: Top 10 upregulated and downregulated DEGs in posterior 'Immune.0' CosMx subcluster

Gene	log2fold	p	p.adj
B2M	3.35	1.414962e-56	1.058391e-53
CTSB	2.37	2.677260e-39	7.589820e-37
SLC13A3	2.33	6.766112e-08	2.410025e-06
GRN	2.26	3.044045e-39	7.589820e-37
GBP2	2.09	3.574484e-05	6.076623e-04
ITGAX	2.08	9.459886e-14	6.432723e-12
VIM	1.95	1.005086e-19	1.503609e-17
APOD	1.94	1.070909e-16	1.001300e-14
CCL2	1.83	4.785188e-06	9.942557e-05
GFAP	1.76	3.092973e-16	2.570604e-14

Gene	log2fold	p	p.adj
P2RY12	-2.40	1.506545e-32	2.817240e-30
CSF1R	-1.59	5.791909e-16	4.332348e-14
CST3	-1.33	1.327711e-19	1.655213e-17
PLP1	-1.15	2.665888e-08	1.107825e-06
TREM2	-1.05	3.864810e-06	8.259652e-05
SCD2	-1.03	1.091746e-07	3.550546e-06
ADGRG1	-0.94	3.837322e-07	1.063080e-05
MBP	-0.93	3.522836e-05	6.076623e-04
GLUL	-0.91	2.185414e-08	9.615823e-07
CFH	-0.90	7.559323e-06	1.528209e-04

DE analysis of cells belonging to anterior Immune.1 subcluster samples is shown in *Figure 14.* PCA shows the gene expression data of anterior Immune.1 subcluster with the Control and Aldara naturally separating into 2 distinct grouping (*Figure 14)*. Control samples are tightly grouped together in PCA demonstrating low levels of biological variance between samples for this CosMx immune subcluster (*Figure 14A)*. Aldara samples from this group display a greater extent of biological variation as displayed with relatively diffuse spreading with respect to PC2. This suggests PC1 may be representative of treatment and PC2 of biological variance. The lollipop graph shows 84 genes being significantly upregulated in Aldara samples compared to control and 54 downregulated (p.adj<0.05 and absolute log_2

fold change >0.5 and <-0.5, respectively). The heatmap featured in *Figure 14D* highlights the DEGs and their pattern of transcriptional changes with Aldara samples primarily displaying upregulation of genes displayed in yellow. The top significantly upregulated genes in anterior tissue section Immune.1 subcluster include *B2m, Tspo, Ccl2, Srgn* and *Fth1*. The top significantly downregulated genes in Immune.1 include *Ptgds, H2-ab1, Apoe, Atp1a2 and Rgs5*. The top 10

upregulated and downregulated genes ranked by log_2 fold change can be seen in

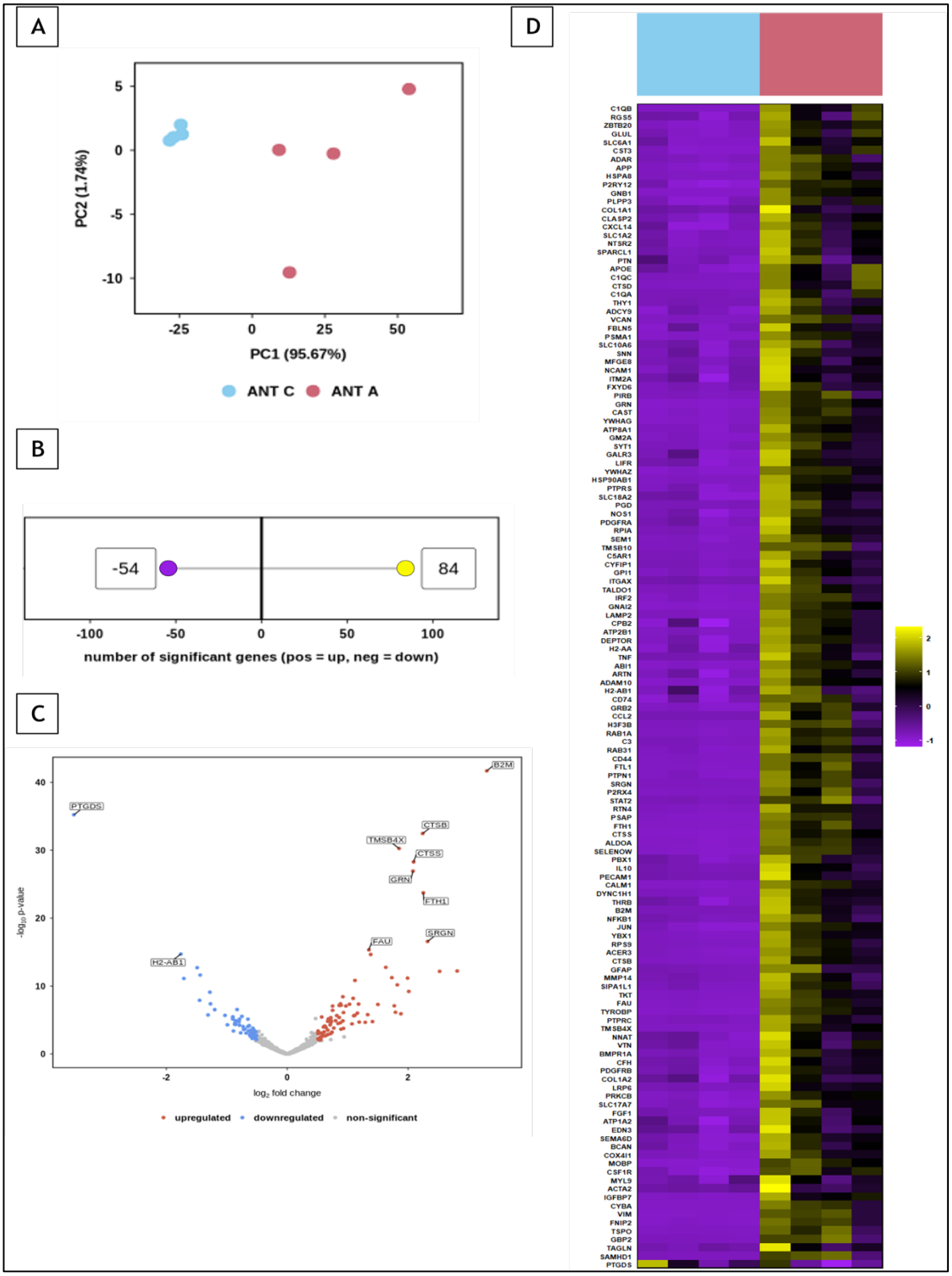

Figure 14: Differential expression analysis of 'Immune.1' subcluster from anterior brain sections. *(A) PCA scatterplots showing gene expression data for Control [blue] and Aldara [red]. Individual samples represented by dots. (B) Lollipop graph showing number of significantly DEGs [p.adj <0.05, absolute log_2fold >0.5]. (C) Volcano plot of significantly DEGs with upregulated shown in red, downregulated in blue and non-significant in grey. (D) Hierarchically clustered heatmap of DEGs in Control and Aldara samples. Expression levels shown are row-scaled into Z-scores with yellow representing high expression and purple representing low expression.*

Table 4.4.

Table 4.4: Top 10 upregulated and downregulated DEGs in anterior 'Immune.1' CosMx subcluster

Gene	log2fold	p	p.adj
B2M	3.30	2.032805e-42	1.912869e-39
TSPO	2.81	6.159137e-13	4.139820e-11
CCL2	2.52	6.965447e-13	4.369657e-11
SRGN	2.32	2.729211e-17	3.210234e-15
FTH1	2.25	1.878644e-24	2.525434e-22
CTSB	2.24	3.357696e-33	1.053197e-30
CTSS	2.09	5.206271e-29	9.798202e-27
GRN	2.08	1.162256e-27	1.822805e-25
PTPRC	2.01	6.323131e-10	2.704576e-08
VIM	1.99	7.032805e-12	3.676594e-10

Gene	log2fold	p	p.adj
PTGDS	-3.53	5.958308e-36	2.803384e-33
H2-AB1	-1.76	1.927619e-15	1.813890e-13
APOE	-1.71	7.800628e-12	3.863364e-10
ATP1A2	-1.49	1.961354e-13	1.419718e-11
RGS5	-1.45	1.264291e-08	4.575762e-07
H2-AA	-1.44	2.400053e-12	1.411531e-10
MYL9	-1.31	1.834740e-06	3.836645e-05
VTN	-1.28	8.160771e-10	3.338820e-08
EDN3	-1.27	4.269792e-08	1.434955e-06
COL1A2	-1.20	2.963688e-07	7.339028e-06

DE analysis of cells belonging to posterior Immune.1 subcluster samples is shown in *Figure 15*. PCA shows the gene expression data of posterior Immune.1 subcluster with the Control and Aldara naturally separating into 2 distinct grouping (*Figure 15)*. Control samples are tightly grouped together in PCA demonstrating low levels of biological variance between samples for this CosMx immune subcluster (*Figure 15A)*. Aldara samples from this group display a greater extent of biological variation as displayed with relatively diffuse spreading with respect to PC2. This suggests PC1 may be representative of treatment and PC2 of biological variance. The lollipop graph shows 78 genes being significantly upregulated in Aldara samples compared to control and 60 downregulated (*Figure 15B;* p.adj<0.05 and absolute $\log_2$ fold change >0.5 and <-0.5, respectively). The heatmap featured in *Figure 15D* highlights the DEGs and their pattern of transcriptional changes with Aldara samples primarily displaying upregulation of genes displayed in yellow. The top significantly upregulated genes in posterior tissue section Immune.1 subcluster include *B2m*, *Ptprc*, *Ccl2*, *Grn* and *Tnf*. The top significantly downregulated genes in Immune.1 include *Ptgds, Ttr H2-ab1, H2-aa and Cd74.* The top ten significantly upregulated and downregulated genes ranked by log2 fold change can be seen in Table 4.5.

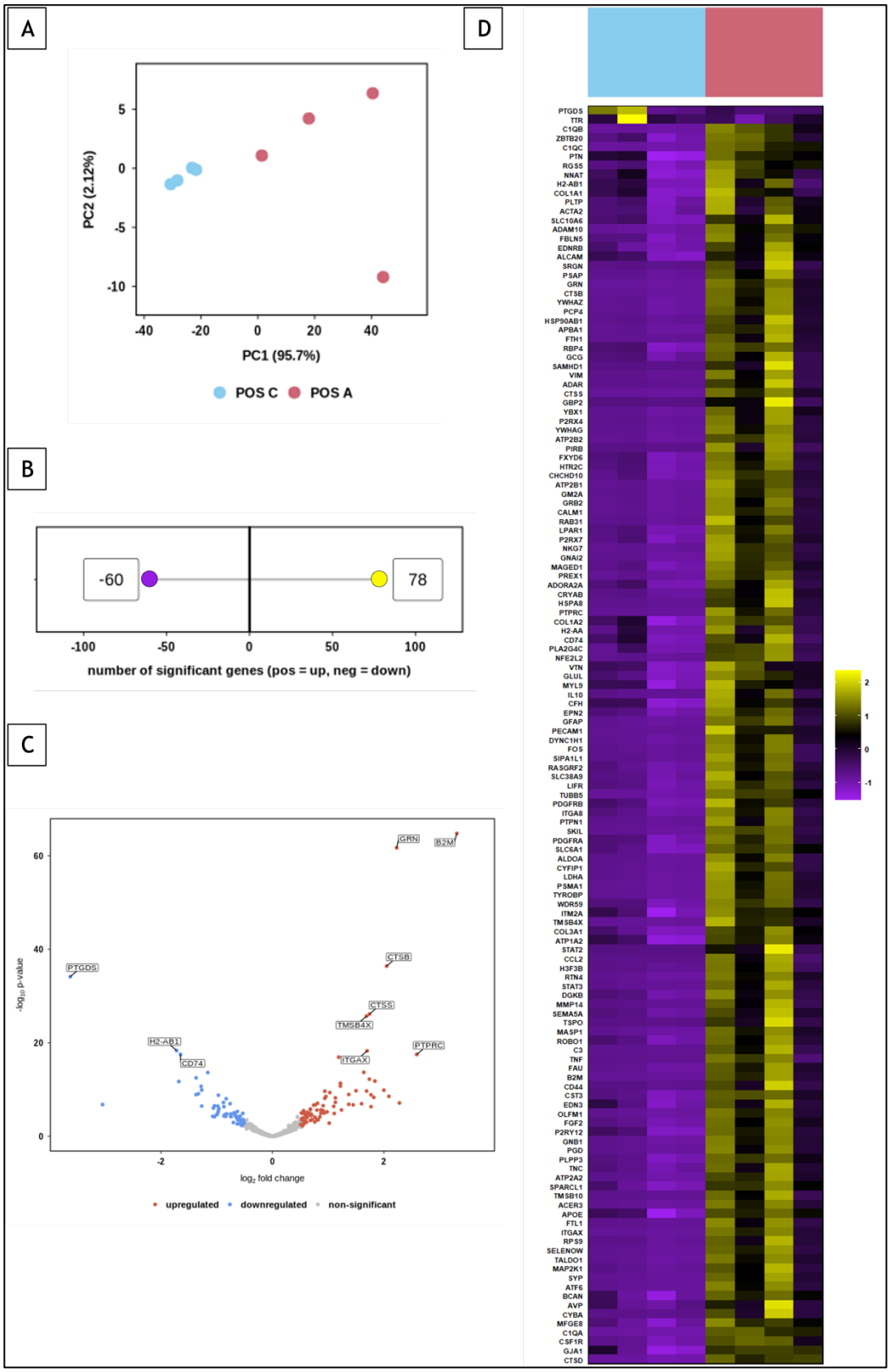

Figure 15: Differential expression analysis of 'Immune.1' subcluster from posterior brain sections. *(A) PCA scatterplots showing gene expression data for Control [blue] and Aldara [red]. Individual samples represented by dots. (B) Lollipop graph showing number of significantly DEGs [p.adj <0.05, absolute log_2fold >0.5]. (C) Volcano plot of significantly DEGs with upregulated shown in red, downregulated in blue and non-significant in grey. (D) Hierarchically clustered heatmap of DEGs in Control and Aldara samples. Expression levels shown are row-scaled into Z-scores with yellow representing high expression and purple representing low expression.*

Table 4.5: Top 10 upregulated and downregulated DEGs in posterior 'Immune.1' CosMx subcluster

Gene	log2fold	p	p.adj
B2M	3.31	1.677505e-65	1.677505e-62
PTPRC	2.59	3.184465e-18	3.184465e-16
CCL2	2.28	7.228534e-08	1.807134e-06
GRN	2.23	2.038674e-62	1.019337e-59
TNF	2.09	2.852065e-09	8.912702e-08
CTSB	2.05	4.007984e-37	1.335995e-34
TSPO	2.00	1.384406e-10	6.292753e-09
SRGN	1.84	1.557602e-12	9.735015e-11
SAMHD1	1.82	4.662452e-09	1.371309e-07
PECAM1	1.77	1.333305e-09	4.444349e-08

Gene	log2fold	p	p.adj
PTGDS	-3.63	7.470260e-35	1.867565e-32
TTR	-3.05	1.616917e-07	3.593148e-06
H2-AB1	-1.72	4.563761e-19	6.519659e-17
H2-AA	-1.68	1.890271e-12	1.111924e-10
CD74	-1.65	3.101484e-18	3.184465e-16
COL1A2	-1.37	1.199476e-09	4.136126e-08
APOE	-1.37	3.154368e-13	2.253120e-11
ITM2A	-1.33	8.145408e-10	3.016818e-08
CFH	-1.28	2.074368e-11	1.037184e-09
ATP1A2	-1.27	1.320643e-10	6.288778e-09

DE analysis of cells belonging to anterior Immune.2 subcluster samples is shown in *Figure 16*. PCA shows the gene expression data of anterior Immune.2 subcluster with the Control and Aldara naturally separating into 2 distinct grouping (*Figure 16)*. Aldara samples are tightly grouped together in PCA demonstrating low levels of biological variance between samples for this CosMx immune subcluster (*Figure 16A)*. Control samples from this group display a greater extent of biological variation as displayed with relatively diffuse spreading with respect to PC2. This suggests PC1 may be representative of treatment and PC2 of biological variance. The lollipop graph shows 14 genes being significantly upregulated in Aldara samples compared to control and 7 downregulated (*Figure 16B;* p.adj<0.05 and absolute $\log_2$ fold >0.5 and <-0.5, respectively). The heatmap featured in *Figure 16D* highlights the DEGs and their pattern of transcriptional changes with Aldara samples primarily displaying downregulation of genes displayed in purple. The top significantly upregulated genes in anterior tissue section Immune.2 subcluster include *Apod, Gfap, B2m, Ptgds* and *Slc13a3*. The top significantly downregulated genes in anterior sections' Immune.2 subcluster include *P2ry12, Cst3, Trem2, Csf1r* and *Selplg*. The top 10 significantly upregulated and downregulated genes ranked by log2 fold change can be seen in Table 4.6.

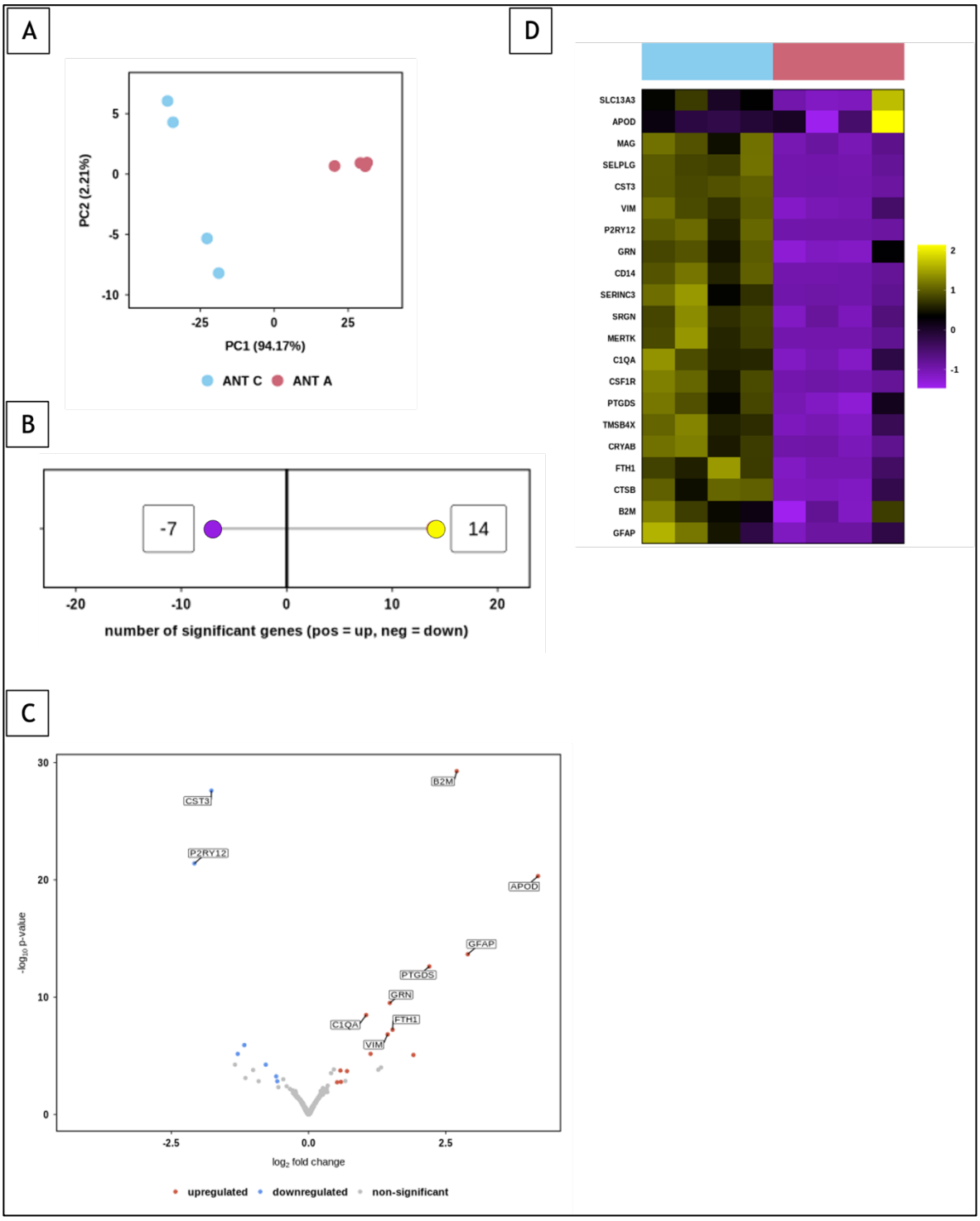

Figure 16: Differential expression analysis of 'Immune.2' subcluster from anterior brain sections. *(A) PCA scatterplots showing gene expression data for Control [blue] and Aldara [red]. Individual samples represented by dots. (B) Lollipop graph showing number of significantly DEGs [p.adj <0.05, absolute log$_2$fold >0.5]. (C) Volcano plot of significantly DEGs with upregulated shown in red, downregulated in blue and non-significant in grey. (D) Hierarchically clustered heatmap of DEGs in Control and Aldara samples. Expression levels shown are row-scaled into Z-scores with yellow representing high expression and purple representing low expression.*

Table 4.6: Top 10 upregulated and downregulated DEGs in anterior 'Immune.2' CosMx subcluster

Gene	log2fold	p	p.adj
APOD	4.18	4.819099e-21	2.710743e-19
GFAP	2.90	2.201250e-14	9.905625e-13
B2M	2.70	5.452135e-30	1.226730e-27
PTGDS	2.20	2.401230e-13	9.004614e-12
SLC13A3	1.91	8.477939e-06	1.362526e-04
FTH1	1.53	5.960469e-08	1.490117e-06
GRN	1.48	3.136004e-10	1.008001e-08
VIM	1.44	1.467434e-07	3.301727e-06
TSPO	1.32	9.780320e-05	1.000000e+00
PTPRC	1.27	1.546235e-04	1.000000e+00

Gene	log2fold	p	p.adj
P2RY12	-2.08	4.008285e-22	3.006214e-20
CST3	-1.77	2.499817e-28	2.812294e-26
TREM2	-1.34	5.690063e-05	1.000000e+00
CSF1R	-1.29	6.893264e-06	1.193065e-04
SELPLG	-1.17	1.217217e-06	2.489761e-05
RGS5	-1.15	7.796651e-04	1.000000e+00
CFH	-1.01	1.629960e-04	1.000000e+00
CRP	-0.91	1.454638e-03	1.000000e+00
SERINC3	-0.78	5.679475e-05	8.519213e-04
CD14	-0.59	5.663192e-04	6.371091e-03

DE analysis of cells belonging to posterior Immune.2 subcluster samples is shown in *Figure 17*. PCA shows the gene expression data of posterior Immune.2 subcluster with the Control and Aldara naturally separating into 2 distinct grouping (*Figure 17)*. Aldara samples are tightly grouped together in PCA demonstrating low levels of biological variance between samples for this CosMx immune subcluster (*Figure 17A)*. Control samples from this group display a greater extent of biological variation as displayed with relatively diffuse spreading with respect to PC2. This suggests PC1 may be representative of treatment and PC2 of biological variance. The lollipop graph shows 26 genes being significantly upregulated in Aldara samples compared to control and 13 downregulated (*Figure 17B;* p.adj<0.05 and absolute $\log_2$ fold >0.5 and <-0.5, respectively). The heatmap featured in *Figure 17D* highlights the DEGs and their pattern of transcriptional changes with Aldara samples primarily displaying downregulation of genes displayed in purple. The top significantly upregulated genes in posterior tissue section Immune.2 subcluster include *Apod, B2m, Ptgds, Gfap* and *Ctsb*. The top significantly downregulated genes in posterior sections' Immune.2 subcluster include *P2ry12, Cst3, Csf1r, Selplg* and *Adgrg1*. The top ten significantly upregulated and downregulated genes ranked by $\log_2$ fold change for posterior Immune.2 subcluster can be seen in Table 4.7.

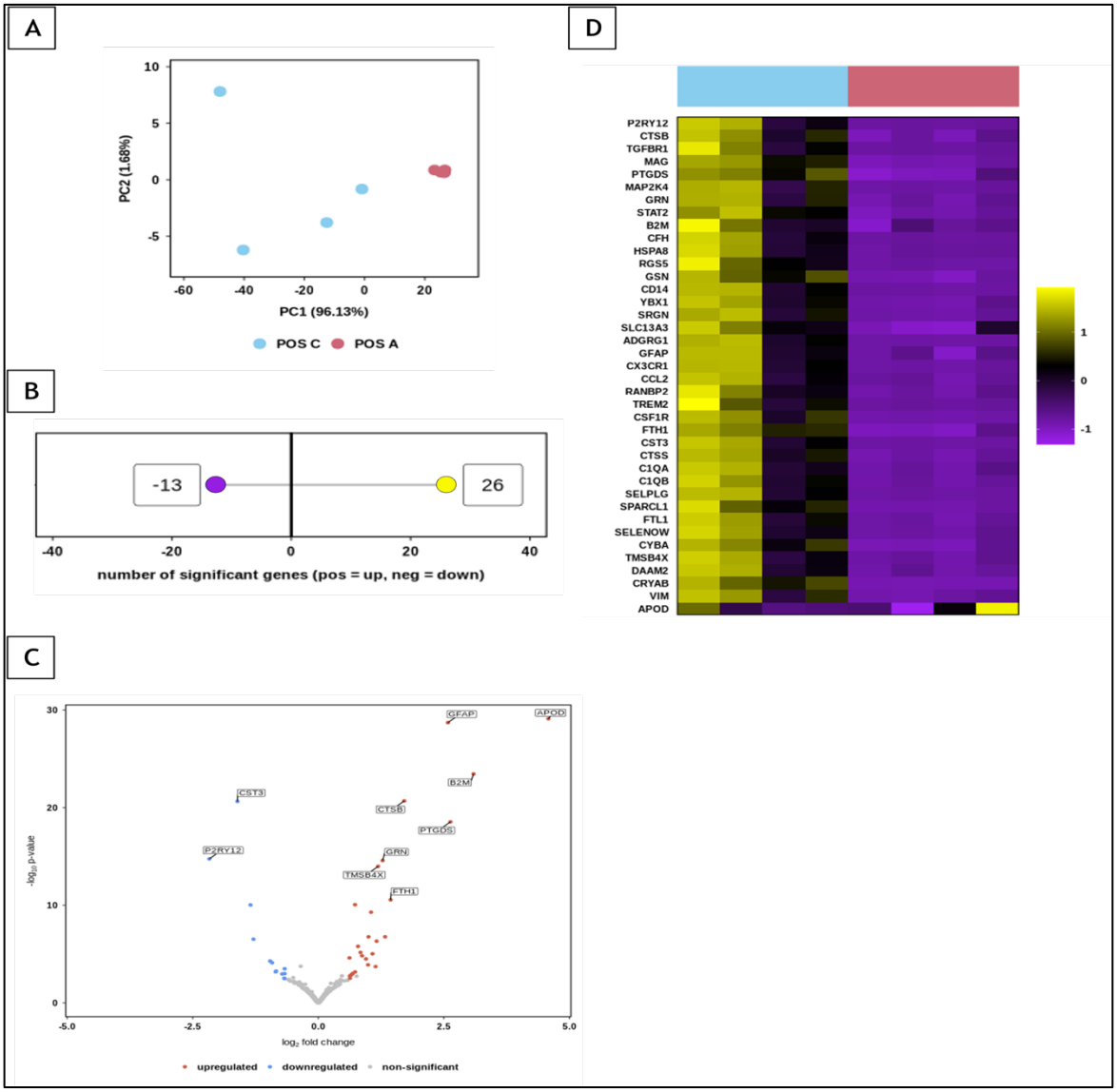

Figure 17: Differential expression analysis of 'Immune.2' subcluster from posterior brain sections. (A) PCA scatterplots showing gene expression data for Control [blue] and Aldara [red]. Individual samples represented by dots. (B) Lollipop graph showing number of significantly DEGs [p.adj <0.05, absolute log2fold >0.5]. (C) Volcano plot of significantly DEGs with upregulated shown in red, downregulated in blue and non-significant in grey. (D) Hierarchically clustered heatmap of DEGs in Control and Aldara samples. Expression levels shown are row-scaled into Z-scores with yellow representing high expression and purple representing low expression.

Table 4.7: Top 10 Upregulated and Downregulated DEGs in Posterior 'Immune.2' CosMx subcluster

Gene	log2fold	p	p.adj
APOD	4.58	7.877297e-30	4.671237e-27
B2M	3.09	3.529026e-24	6.975708e-22
PTGDS	2.63	2.853967e-19	2.820671e-17
GFAP	2.58	1.953547e-29	5.792268e-27
CTSB	1.71	2.023945e-21	2.741041e-19
FTH1	1.44	2.780895e-11	1.649071e-09
VIM	1.33	1.706385e-07	6.833524e-06
GRN	1.28	2.623241e-15	1.944478e-13
TMSB4X	1.19	1.032357e-14	6.802085e-13
MAG	1.16	4.738911e-07	1.653044e-05

Gene	log2fold	p	p.adj
P2RY12	-2.17	1.777819e-15	1.506067e-13
CST3	-1.61	2.311165e-21	2.741041e-19
CSF1R	-1.35	9.360219e-11	4.625508e-09
SELPLG	-1.29	2.969612e-07	1.100612e-05
ADGRG1	-0.96	5.133063e-05	1.268294e-03
CD14	-0.92	7.801210e-05	1.850447e-03
TREM2	-0.85	6.589096e-04	1.260430e-02
CFH	-0.84	5.547285e-04	1.096513e-02
SPARCL1	-0.72	1.090651e-03	1.847875e-02
RGS5	-0.68	2.997620e-03	4.335582e-02

DE analysis of cells belonging to anterior Immune.3 subcluster samples is shown in *Figure 18*. PCA shows the gene expression data of anterior Immune.3 subcluster for Control and Aldara samples (*Figure 18)*. Control samples are tightly grouped together in PCA demonstrating low levels of biological variance between samples for this CosMx immune subcluster (*Figure 18A)*. Aldara samples from this group display a greater extent of biological variation as displayed with relatively diffuse spreading with respect to PC2. One Aldara sample shows close grouping with the Control samples for this subcluster. This suggests for this potential cell subtype in this animal does not display typical biological responses compared to other biological repeats in the treatment group. Overall, the PCA plot suggests PC1 may be representative of treatment and PC2 of biological variance. The lollipop graph shows 35 genes being significantly upregulated in Aldara samples compared to control and 16 downregulated (*Figure 18B;* p.adj<0.05 and absolute $\log_2$ fold >0.5 and <-0.5, respectively). The heatmap featured in *Figure 18D* highlights the DEGs and their pattern of transcriptional changes with Aldara samples primarily displaying upregulation of genes displayed in yellow with exception of the previously mentioned outlier Aldara sample. The top significantly upregulated genes in anterior tissue section Immune.3 subcluster include *B2m, Gfap, Apod, Tspo* and *Vim*. The top significantly downregulated genes in Immune.3 include *P2ry12, Csf1r, Cfh, Selplg and Trem2*. The top 10 significantly upregulated and downregulated genes ranked by log2 fold change for anterior Immune.3 subcluster can be seen in Table 4.8.

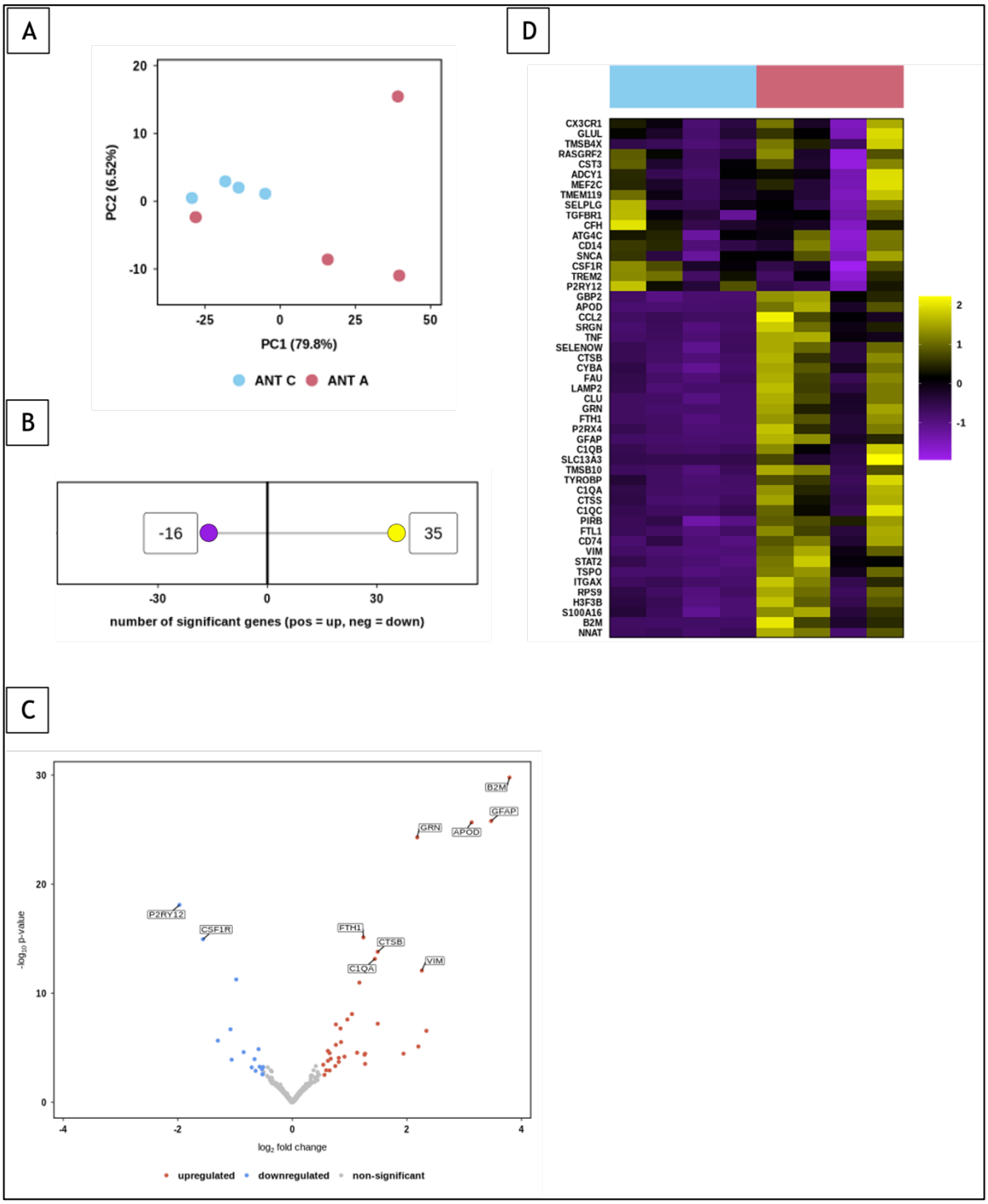

Figure 18: Differential expression analysis of 'Immune.3' subcluster from anterior brain sections. *(A) PCA scatterplots showing gene expression data for Control [blue] and Aldara [red]. Individual samples represented by dots. (B) Lollipop graph showing number of significantly DEGs [p.adj <0.05, absolute log2fold >0.5]. (C) Volcano plot of significantly DEGs with upregulated shown in red, downregulated in blue and non-significant in grey. (D) Hierarchically clustered heatmap of DEGs in Control and Aldara samples. Expression levels shown are row-scaled into Z-scores with yellow representing high expression and purple representing low expression.*

Table 4.8: Top 10 upregulated and downregulated DEGs in anterior 'Immune.3' CosMx subcluster

Gene	log2fold	p	p.adj
B2M	3.79	1.631139e-30	1.314698e-27
GFAP	3.47	1.607033e-26	5.722560e-24
APOD	3.13	2.129985e-26	5.722560e-24
TSPO	2.34	2.784605e-07	1.181259e-05
VIM	2.26	8.386576e-13	6.759580e-11
CCL2	2.20	7.695209e-06	2.696669e-04
GRN	2.18	5.047742e-25	1.017120e-22
SLC13A3	1.94	3.479249e-05	9.387554e-04
SRGN	1.49	6.273976e-08	3.371217e-06
CTSB	1.49	1.580319e-14	1.592171e-12

Gene	log2fold	p	p.adj
P2RY12	-1.97	7.903513e-19	1.274046e-16
CSF1R	-1.56	1.114125e-15	1.282836e-13
CFH	-1.30	2.225885e-06	8.970315e-05
SELPLG	-1.08	2.020644e-07	9.047996e-06
TREM2	-1.06	1.238512e-04	2.772890e-03
CST3	-0.98	5.476094e-12	4.012483e-10
RASGRF2	-0.85	2.519375e-05	7.810062e-04
TMEM119	-0.71	6.295387e-04	1.103061e-02
MEF2C	-0.66	1.105879e-04	2.546680e-03
TGFBR1	-0.64	1.307059e-03	2.025942e-02

DE analysis of cells belonging to posterior Immune.3 subcluster samples is shown in *Figure 19*. PCA shows the gene expression data of posterior Immune.3 subcluster for Control and Aldara samples which separate the 2 into distinct groups (*Figure 19)*. The PCA plot suggests PC1 may be representative of treatment and PC2 of biological variance. The lollipop graph shows 33 genes being significantly upregulated in Aldara samples compared to control and 11 downregulated (*Figure 18B;* p.adj<0.05 and absolute $\log_2$ fold >0.5 and <-0.5, respectively). The heatmap featured in *Figure 18D* highlights the DEGs and their pattern of transcriptional changes with Aldara samples primarily displaying upregulation of genes displayed in yellow. One Control sample displays unique upregulation of some genes compared to others in the treatment group. The top significantly upregulated genes in posterior tissue section Immune.3 subcluster include *B2m, Gfap, Grn, Gbp2* and *Ccl2*. The top significantly downregulated genes in Immune.3 include *P2ry12, Csf1r, Selplg, Cst3* and *Cfh*. The top ten significantly upregulated and downregulated genes ranked by $\log_2$ fold change for posterior Immune.3 subcluster can be seen in Table 4.9.

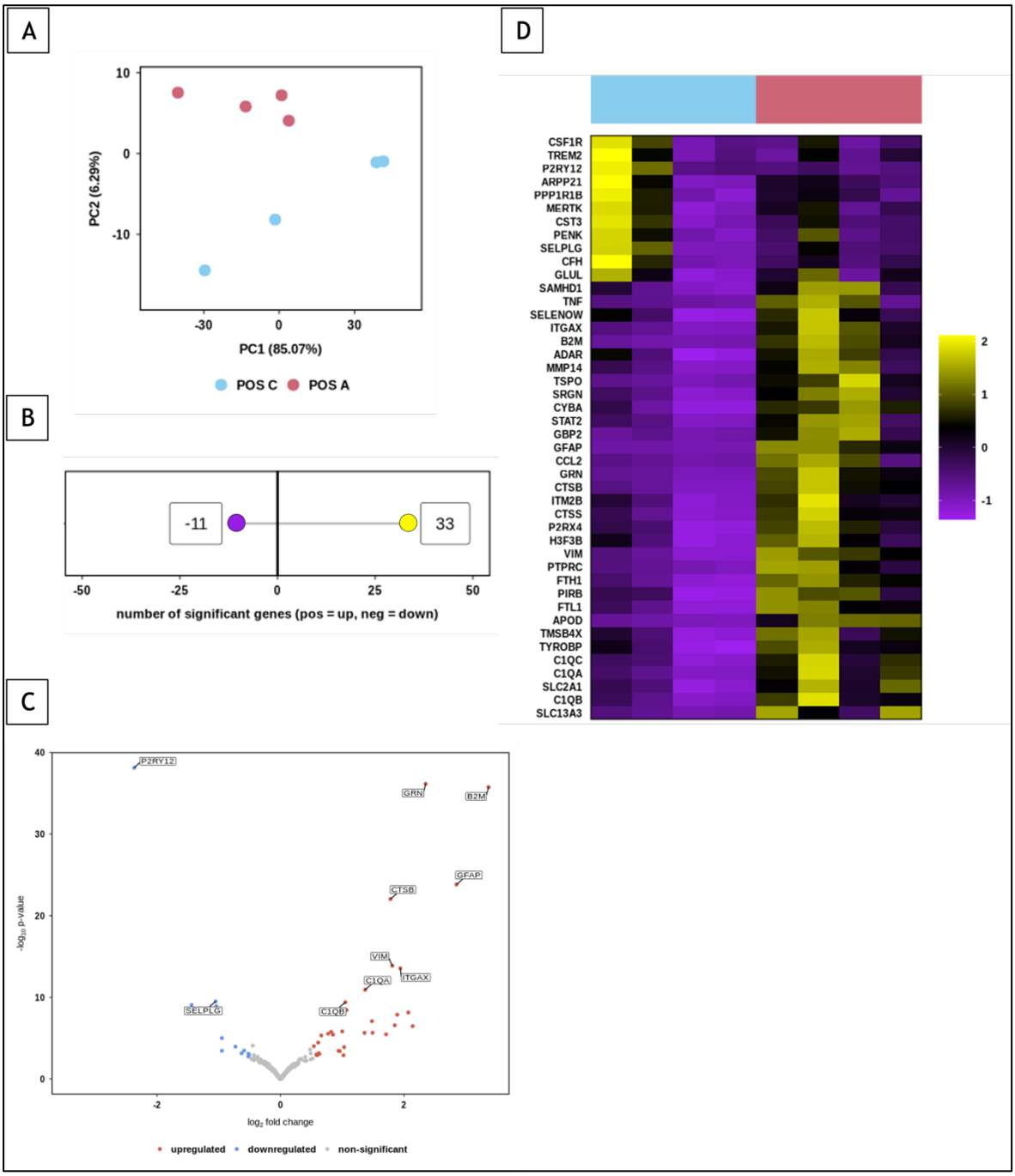

Figure 19: Differential expression analysis of 'Immune.3' subcluster from posterior brain sections. *(A) PCA scatterplots showing gene expression data for Control [blue] and Aldara [red]. Individual samples represented by dots. (B) Lollipop graph showing number of significantly DEGs [p.adj <0.05, absolute log_2fold >0.5]. (C) Volcano plot of significantly DEGs with upregulated shown in red, downregulated in blue and non-significant in grey. (D) Hierarchically clustered heatmap of DEGs in Control and Aldara samples. Expression levels shown are row-scaled into Z-scores with yellow representing high expression and purple representing low expression.*

Table 4.9: Top 10 upregulated and downregulated DEGs in posterior 'Immune.3' CosMx subcluster

Gene	log2fold	p	p.adj
B2M	3.37	1.764593e-36	5.311426e-34
GFAP	2.85	1.515925e-24	3.422201e-22
GRN	2.35	7.048500e-37	3.182398e-34
GBP2	2.14	3.311967e-07	1.574056e-05
CCL2	2.07	7.119665e-09	4.592184e-07
ITGAX	1.94	2.765058e-14	3.566925e-12
APOD	1.89	1.335375e-08	7.536521e-07
SLC13A3	1.85	2.610929e-07	1.309816e-05
VIM	1.81	1.352650e-14	2.035738e-12
CTSB	1.78	9.208826e-23	1.663114e-20

Gene	log2fold	p	p.adj
P2RY12	-2.37	7.717816e-39	6.969188e-36
CSF1R	-1.44	8.593913e-10	7.054821e-08
SELPLG	-1.05	3.118485e-10	3.128880e-08
CST3	-1.04	1.184574e-09	8.913923e-08
CFH	-0.95	9.743133e-06	3.033810e-04
TREM2	-0.95	3.421738e-04	8.350891e-03
PENK	-0.73	1.110598e-04	3.039000e-03
PPP1R1B	-0.63	7.093881e-04	1.562384e-02
MERTK	-0.59	3.334547e-04	8.350891e-03
GLUL	-0.52	1.776476e-03	3.208315e-02

To view transcriptional similarities and differences which may be indicative of cellular function, commonality of gene expression amongst immune subclusters was investigated. To allow for comparison across different subclusters, a threshold of log_2fold >1.0 was applied to capture genes largely changing their transcriptional biology following Aldara treatment.

Overlapping and unique upregulated genes, that adhere to the stated threshold, from CosMx Immune.0-Immune.3 subclusters of anterior brain sections can be seen in *Figure 20*. Eight genes are commonly expressed amongst the 4 immune subclusters: *B2m, Grn, Ctsb, Tspo, Vim, Gfap* and *C1qa*. All these genes code for proteins which have established links with pro-inflammatory tissue environments. Subcluster Immune.0 has 6 uniquely expressed genes, according to the threshold: *Mmp14, C5ar1, P2rx4, Igfbp7, Spp1* and *H3f3b*. The proteins coded by these genes are involved in immune activation. Some have been found to be expressed on reactive microglia populations particularly in states of disease responsiveness (Gomez-Arboledas et al., 2022, Vazquez-Villoldo et al., 2014).

Subcluster Immune.1 uniquely expressed 10 genes: *Ctss, Hspa8, Tyrobp, Fau, Adar, Rps9, Cd44, Lilrb4a/b, Selenow* and *Ywhag*. These genes broadly code for proteins involved in 2 branches of neuroinflammation: microglial-mediated immune processes and neuroprotective mechanisms. Subcluster Immune.2 has relatively low levels of unique gene expression with only *Ptgds* which has links to exacerbating neuroinflammation particularly through microglia and astrocyte relationships (Mohri et al., 2006). Immune.3 subcluster cells from anterior sections showed no unique gene expression in upregulated genes. Genes expressed by

Immune.3 but shared with other subclusters further demonstrate an immune-mediated pro-inflammatory subset of the cells with upregulated genes including *Ccl2*, *Tnf*, *Srgn* and *Stat2*. Genes that encode for proteins involved in iron metabolism feature in multiple subclusters namely *Ftl1* and *Fth1*. This further suggests the high cellular activity in response to the TLR7-induced neuroinflammation.

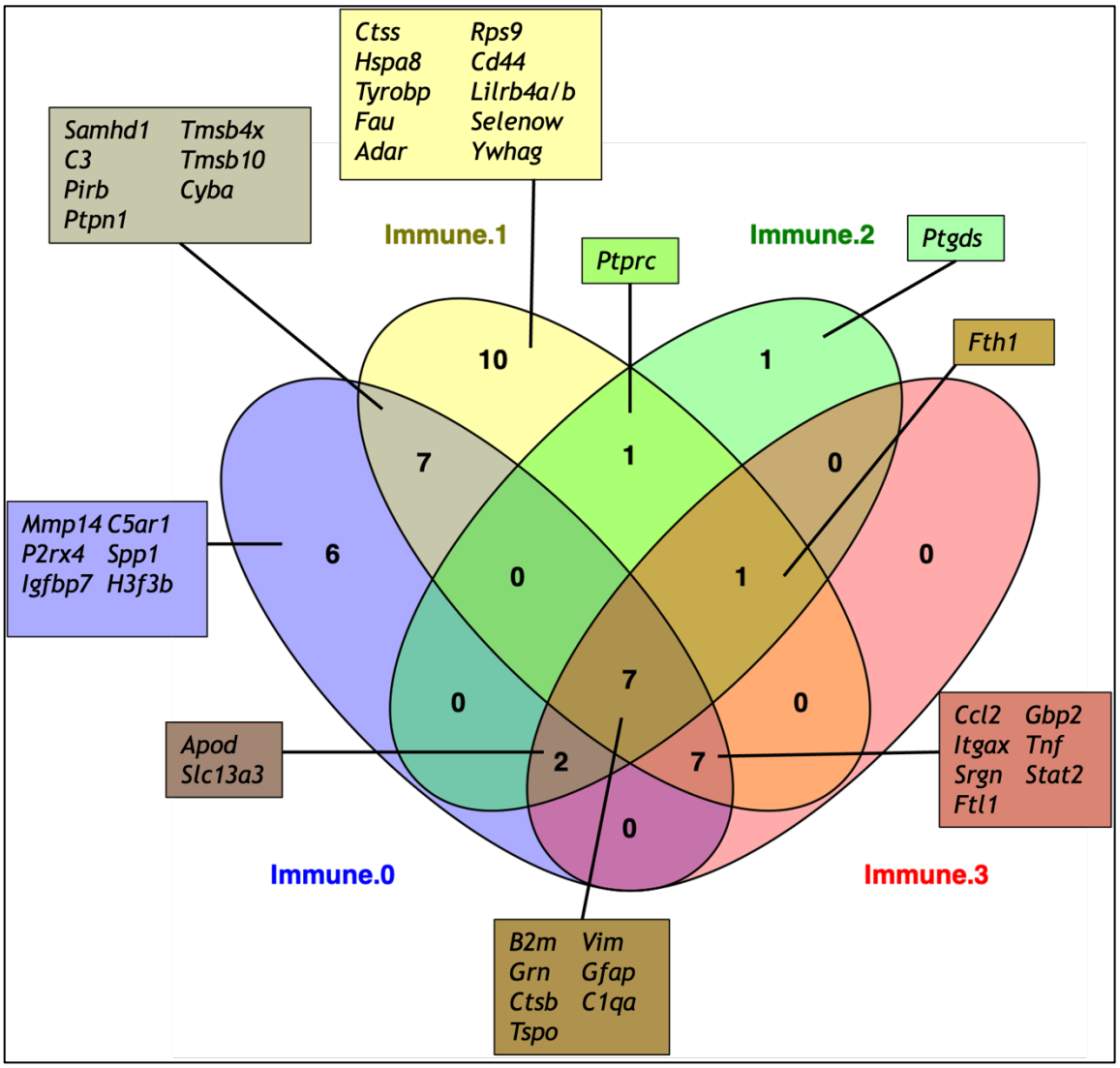

Figure 20: Commonality of top 10 upregulated genes in 4 Immune subclusters CosMx clusters from anterior brain sections. *Venn diagram representing overlap in top significantly upregulated genes in microglia/immune subclusters Immune.0, Immune.1, Immune.2 and Immune.3. Text boxes correspond with cluster's uniquely expressed genes and overlapping genes between at least 2 subclusters. Figure created using Venny 2.0.*

Overlapping and unique upregulated genes, that adhere to the stated threshold, from CosMx Immune.0-Immune.3 subclusters of posterior brain sections can be seen in *Figure 21*. Five genes are commonly expressed amongst the 4 immune

subclusters: *B2m, Grn, Ctsb, Vim* and *Ftl1*. These genes encode for proteins that could be expressed by high-activity cells in a neuroinflammatory environment.

Subcluster Immune.0 has only 1 uniquely expressed gene: *C5ar1*. This gene codes for a protein involved in the complement cascade which highlights the involvement in primarily innate immune functions in this neuroinflammatory model. Subcluster Immune.1 uniquely expressed nine genes: *Pecam1, Tmsb10, Ctss, Adar, Tyrobp, Hspa8, Ptpn1, Ywhag* and *Apba1*. Similarly to upregulated genes in the anterior sections, these genes mainly code for proteins involved in microglial-mediated immune processes and neuroprotective mechanisms. Some BBB changes may also be involved in this subcluster with *Pecam1* encoding for a cellular adhesion molecule commonly expressed by endothelial cells. Subcluster Immune.2 has 3 unique genes upregulated in its subcluster which are *Ptgds, Mag* and *Gsn*. These genes may suggest a possible relationship with myelin with upregulation of *Mag*. Mirroring the same pattern presented in the anterior sections, Immune.3 subcluster cells from posterior sections showed no unique gene expression in upregulated genes. Genes expressed by Immune.3 but shared with other subclusters further demonstrate an immune-mediated pro-inflammatory subset with featured genes coded for proteins involved in the complement cascade, microglial reactivity and chemokine/cytokine signalling.

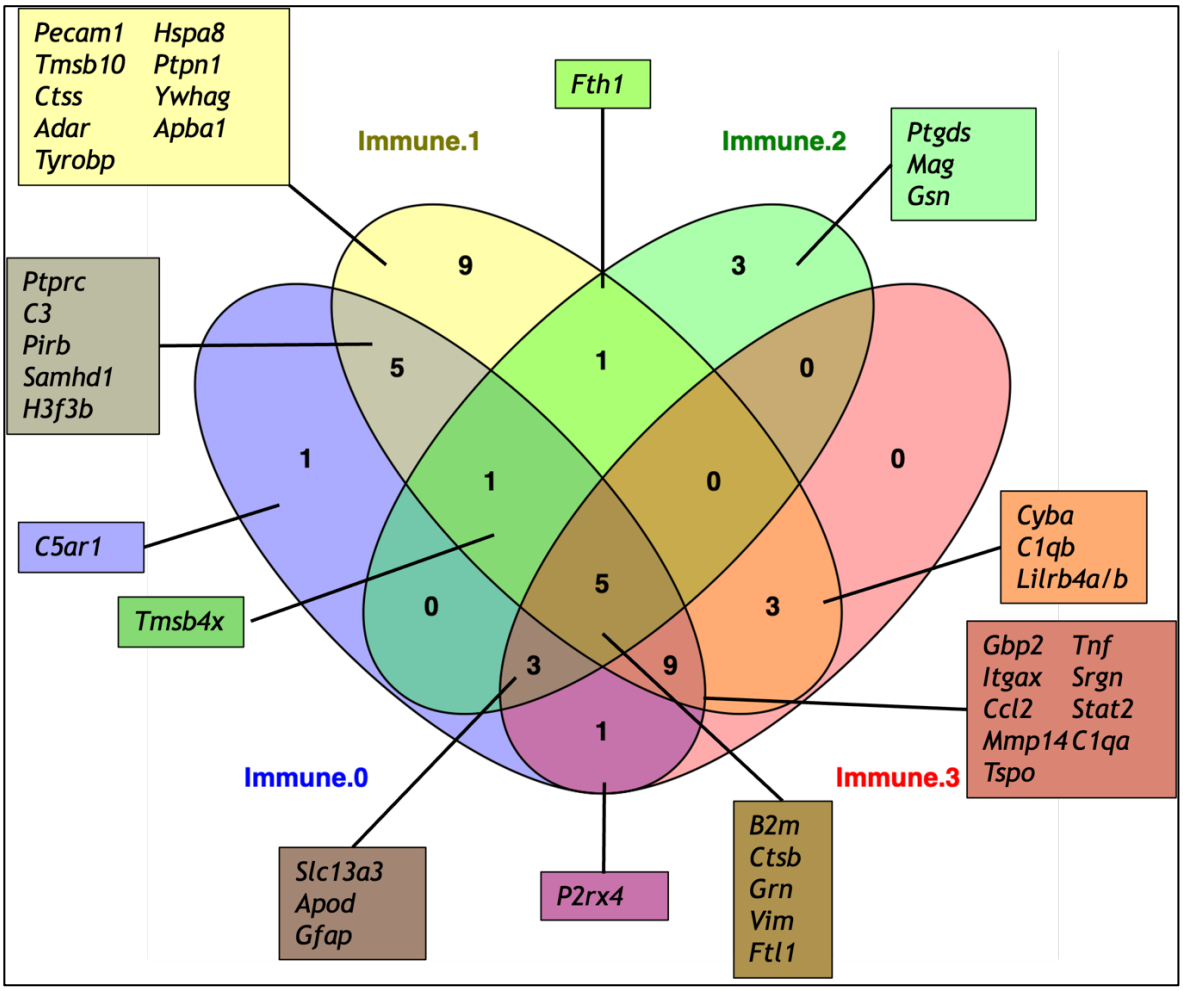

Figure 21: Commonality of upregulated genes with >1.0 log_2 fold change in 4 Immune subclusters CosMx clusters from posterior brain sections. *Venn diagram representing overlap in top significantly upregulated genes in fine microglia/immune clusters Immune.0, Immune.1, Immune.2 and Immune.3. Text boxes correspond with cluster's uniquely expressed genes and overlapping genes between at least 2 subclusters. Figure created using Venny 2.0.*

Overall, the upregulated genes, that adhered to the previously stated log_2 fold change threshold, demonstrate a similar picture regardless of plane of tissue section. All 4 subclusters of immune cells potentially represent different reactive states of microglia. All 4 present a common pro-inflammatory element with the previously stated commonly expressed genes. Elements of a potential compensatory anti-inflammatory response are present with upregulated genes such as *Selenow, Spp1, Hspa8* and *Ywhag* (Behl et al., 2023, Li and Jakobs, 2022, Dukay et al., 2019).

To compare downregulated genes of CosMx immune subclusters, a similar threshold approach was taken with genes considered if they displayed a log_2 fold change <-1.0 (*Figure 22)*. In anterior sections, relatively less commonality was

shown by downregulated genes between subclusters compared to upregulated. No genes were commonly downregulated among all 4 subclusters. Subcluster Immune.0 uniquely downregulated *Mbp* and *Glul* which are linked to myelin and glutamine synthesis, respectively. The subcluster which displays the greatest uniqueness in downregulated genes is Immune.1 with 10 genes: *Ptgds, H2-Ab1, Apoe, Atp1a2, H2-Aa, Myl9, Vtn, Edn3, Col1a2* and *Cd74*. Most of these genes have been found to be highly expressed in reactive microglia subpopulations. Both Immune.2 and Immune.3 subclusters have no uniquely expressed genes. These subclusters do co-express genes involved in microglial activity including *P2ry12* and *Csf1r*.

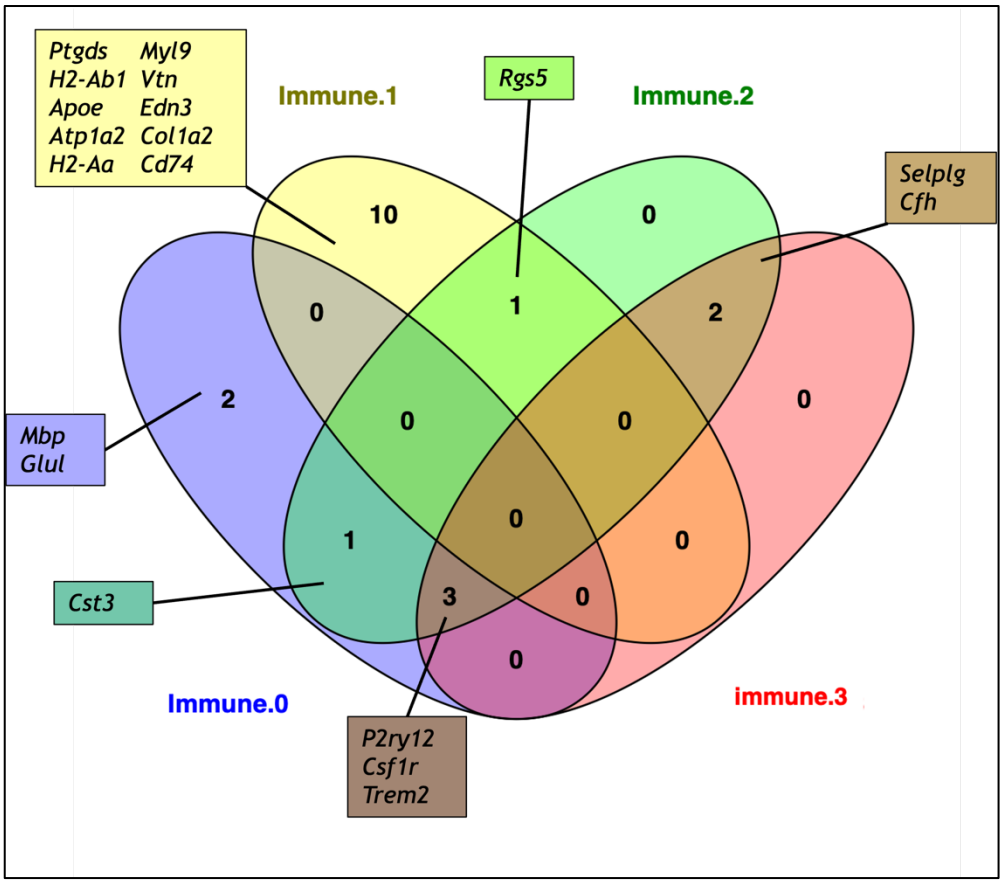

Figure 22: Commonality of top 10 downregulated genes in 4 Immune subclusters CosMx clusters from anterior brain sections. *Venn diagram representing overlap in top significantly downregulated genes in fine microglia/immune clusters Immune.0, Immune.1, Immune.2 and Immune.3. Text boxes correspond with cluster's uniquely expressed genes and overlapping genes between at least 2 subclusters. Figure created using Venny 2.0.*

Posterior sections' downregulated genes from CosMx immune subclusters can be seen in *Figure 23*. Only 1 gene, *P2ry12*, was found to be downregulated in all subclusters which has well established links to microglial reactivity. Subcluster

Immune.1 uniquely downregulated 3 genes: *Plp1*, *Trem2* and *Scd2*. These genes encode for proteins that may be involved in changes to lipid metabolism which is a key feature of neuroinflammatory tissue environments (Shippy and Ulland, 2023, Wei et al., 2024). The subcluster to display the greatest extent of uniquely downregulated genes in posterior sections was Immune.1 with 15 genes. These genes largely encode for proteins involved in microglial and astrocytic neuroinflammatory processes coupled with neuroprotective elements. No genes were uniquely expressed in subclusters Immune.2 and Immune.3.

Overall, the downregulated genes from immune subclusters of both anterior and posterior brain sections exhibit key processes and markers for both pro- and anti-inflammatory processes. Changes to lipid metabolism are suggested by some featured genes. Both the upregulated and downregulated genes presented are largely linked to microglia and peripheral immune cell activity which is further confirmatory of the cellular identification within the CosMx spatial transcriptomics system.

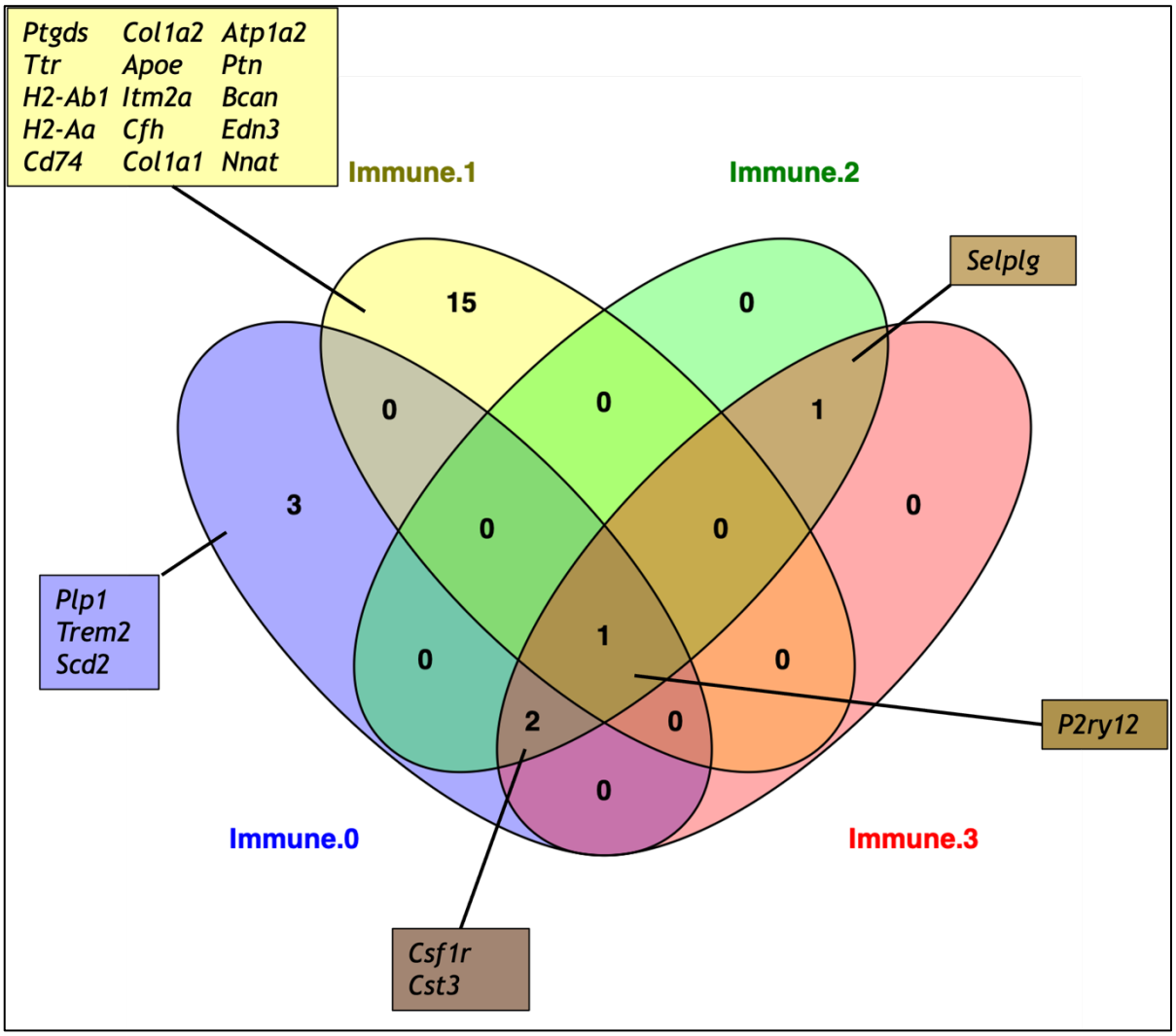

Figure 23: Commonality of top 10 downregulated genes in 4 Immune subclusters CosMx clusters from posterior brain sections. *Venn diagram representing overlap in top significantly downregulated genes in fine microglia/immune clusters Immune.0, Immune.1, Immune.2 and Immune.3. Text boxes correspond with cluster's uniquely expressed genes and overlapping genes between at least 2 subclusters. Figure created using Venny 2.0.*

To identify functionally distinct areas within the brain which encompasses all cell types, neighbourhood analysis was performed. This approach is capable of interrogating spatial transcriptomics datasets to produce unbiased cellular niches. This includes grouping together all transcriptionally-similar cells into a 'neighbourhood', with representative spatial plots seen in *Figure 24* and *26*. Assignment of cells to neighbourhoods is unbiased, however, the researcher can set the number of neighbourhoods they want the analysis to identify. The pre-determined number of niches was 5 and 8 for anterior and posterior tissue sections, respectively.

To understanded the cellular composition of the neighbourhoods, parts of a whole bar charts are shown in *Figure 25* and *27*. The 5 neighbourhoods identified in anterior Control sections included: periphery + ventricles, cortex, ventral striatum, corpus callosum + white matter (WM) and septal nuclei (*Figure 25)*. In anterior Aldara sections, the ventral striatum and septal nuclei were combined to form 1 neighbourhood. This is suspected to allow for the final neighbourhood identified in Aldara sections to be the vasculature and immune neighbourhood (*Figure 25*). The posterior Control sections contained the following 8 neighbourhoods: hippocampus, cortex, periphery + ventricles, hypothalamus + amygdala, thalamus, corpus callosum + WM, caudoputamen and midline (*Figure 27*). The posterior Aldara tissue sections contained the following 8 neighbourhoods: hippocampus (granular layer), cortex + hippocampus, cortical projections, hypothalamus + amygdala, thalamus, corpus callosum + WM, caudoputamen and vasculature + immune (*Figure 27)*.

From the cell composition analysis of the neighbourhoods, a unique predominantly immune cell neighbourhood in Aldara brains was identified. This may highlight both increased reactivity of brain-resident microglia and infiltration of exogenous immune cells. The likelihood of this neighbourhood containing infiltrating immune cells is strengthened by the anatomical location which follows the vasculature of the brain (Xiong et al., 2017). This vasculature-focused distribution of the immune neighbourhood may also be encapsulating BAMs. All other identified neighbourhoods in both planes and treatment groups appear relatively consistent and are primarily composed of other non-immune brain-resident cells (i.e. neurons, oligodendrocytes, astrocytes).

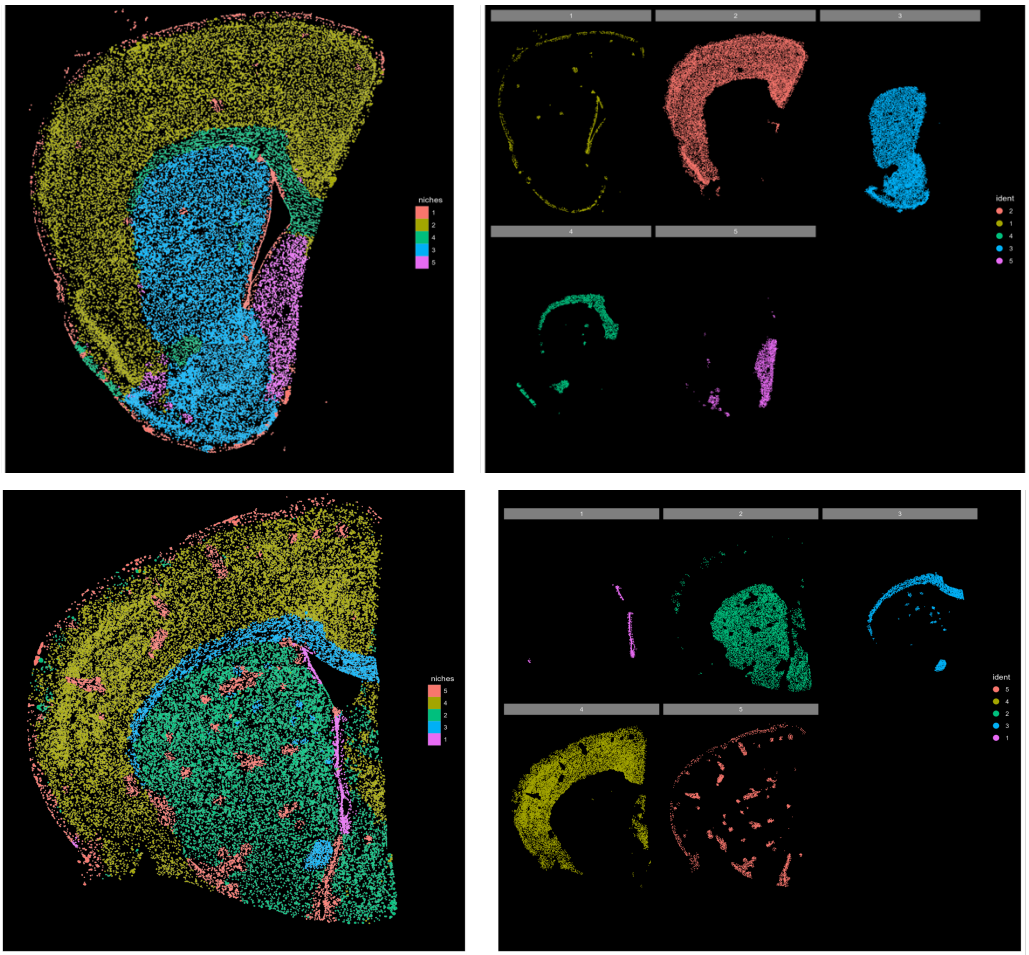

Figure 24: CosMx Neighbourhood analysis presents 5 transcriptionally determined cellular niches. *Spatial cellular plots of representative Control and Aldara CosMx coronal anterior hemisphere sections (n=1/group). (A) and (C) display combined neighbourhoods and (B) and (D) display separated corresponding individual neighbourhoods.*

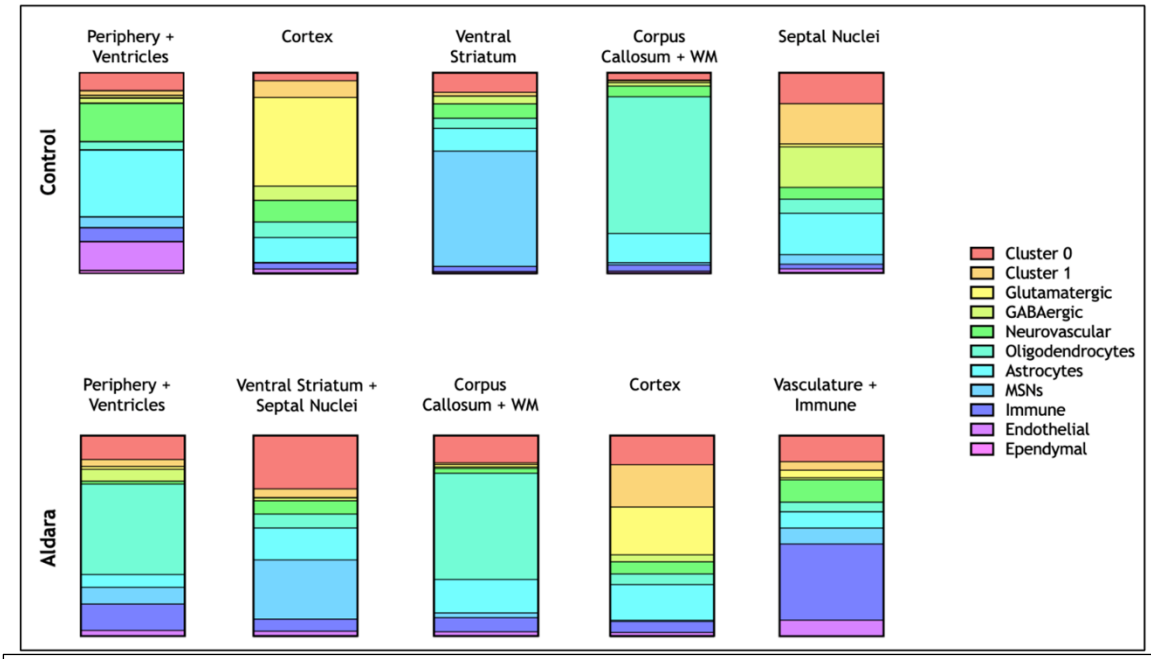

Figure 25: Cellular composition of CosMx Neighbourhood analysis niches presents Immune-dominant niche only in Aldara samples. *Parts of a whole bar charts showing cellular composition percentages of representative anterior Control and Aldara CosMx tissue sections. Control and Aldara presented n=1.*

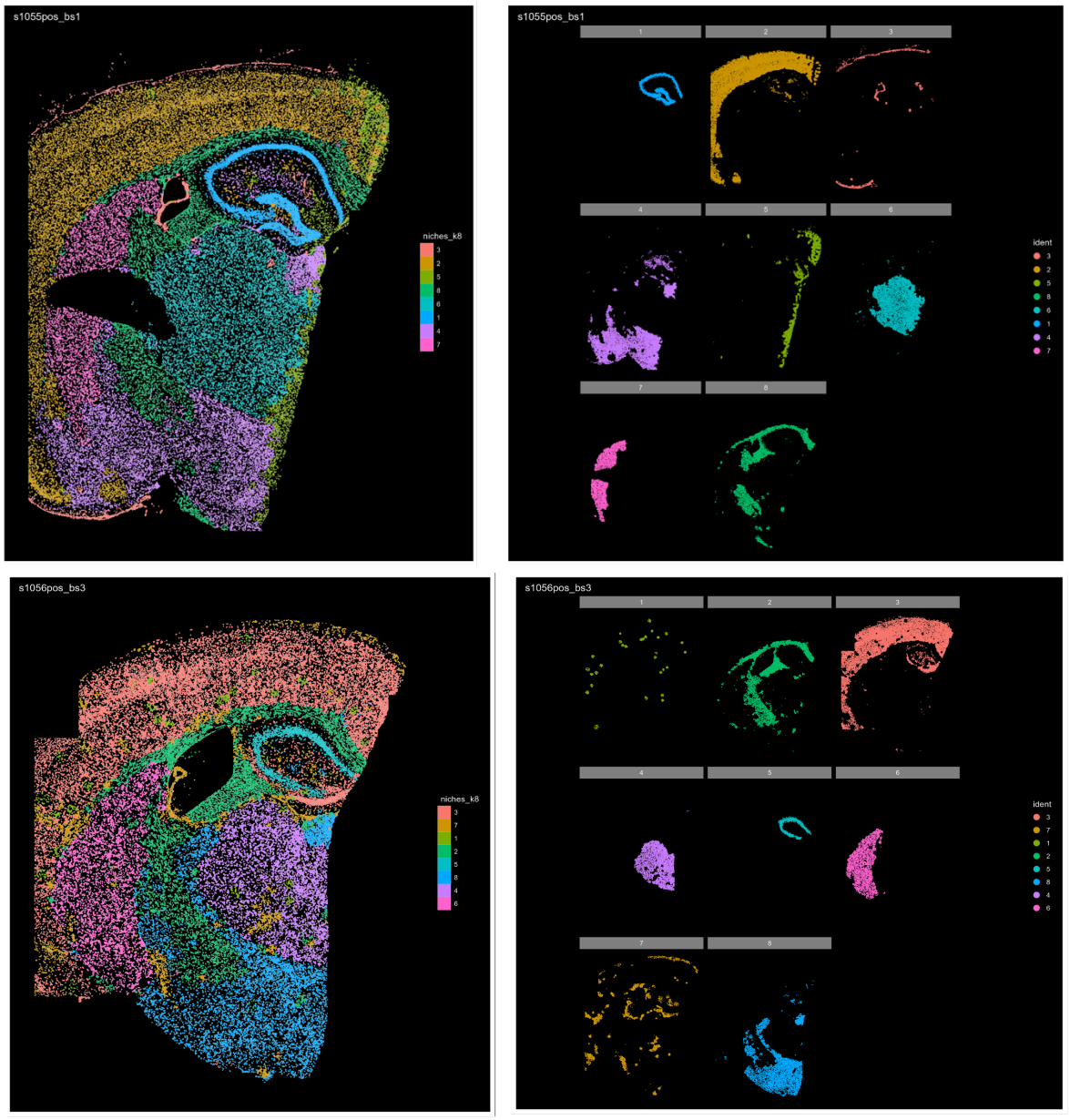

Figure 26: CosMx Neighbourhood analysis presents 8 transcriptionally determined cellular niches. *Spatial cellular plots of representative Control and Aldara CosMx coronal posterior hemisphere sections (n=1/group). (A) and (C) display combined neighbourhoods and (B) and (D) display separated corresponding individual neighbourhoods.*

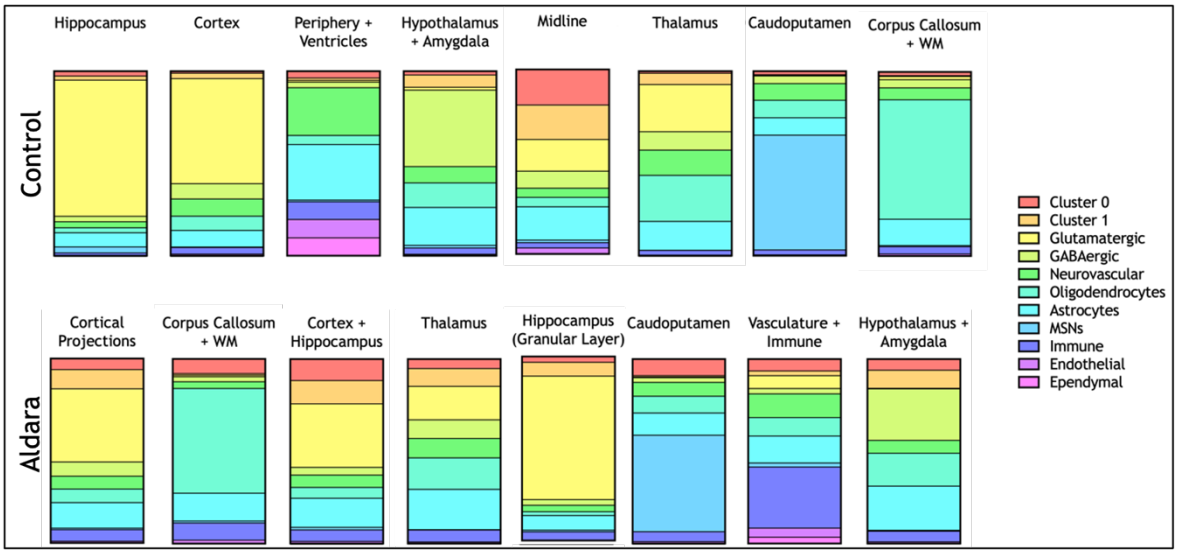

Figure 27: Cellular composition of CosMx Neighbourhood analysis niches presents Immune-dominant niche only in Aldara samples*. Parts of a whole bar charts showing cellular composition percentages of representative posterior Control and Aldara CosMx tissue sections. Control and Aldara presented n=1.*

4.5 Discussion

Following Aldara application, microglial reactivity was found to increase in both expression of reactivity surface markers and production of pro-inflammatory cytokines. Via spatial transcriptomics, 4 potential microglial subclusters were identified with a common pro-inflammatory transcriptional signature. Immune cell-rich neighbourhoods were identified uniquely in Aldara-treated mice.

Investigating microglia's role within a neuroinflammatory model is a key characterisation step of the biology underpinning the downstream consequences for an organism. Microglia are the endogenous immune cells within the brain parenchyma. As previously outlined in the introduction, their contribution is critical to the initiation, mediation and potential resolution of inflammatory processes within the CNS. Furthermore, microglia are a logical research target as they are the primary population for TLR7 expression within the brain (Michaelis et al., 2019). IMQ has previously been demonstrated, via mass spectroscopy, to be present in the brain parenchyma 4-hours post-topical application of Aldara cream (Nerurkar et al., 2017b). As the Aldara model involves daily topical applications of the TLR7 agonist IMQ, it can be postulated that microglia are receiving a daily insult and trigger to this TLR7-activated neuroinflammation.

Whole-brain bulk RNA sequencing was used as an unbiased approach to quantify transcriptomic changes underpinning this neuroinflammation. This global response was characterised in an unbiased manner in chapter 3 of this thesis. This current chapter focused on using this bulk transcriptomic dataset to identify microglial-mediated mechanisms which contributed to the TLR7-driven neuroinflammation.

Various significantly changed genes found in the bulk RNA sequencing dataset are suggestive of reactive microglia. Amongst the consistently upregulated genes, *Hexb* featured in all Aldara samples. *Hexb* encodes for the enzyme β-hexoaminidase which is an established marker of reactive microglia and claimed to not be expressed on other myeloid populations (Shah et al., 2022). This is a well-documented core microglial gene found to be upregulated in response to different inflammatory conditions including EAE (Masuda et al., 2020a). However, studies performed in *Hexb*$^{-/-}$ mice still displayed presence of activated microglia suggesting *Hexb* is a contributor to activation but not the sole mediator (Kyrkanides et al., 2012).

Hexb presents as one the most reliable delineation markers between microglia and other myeloid populations (monocytes/macrophages). The gene's unique microglial expression has been shown through various techniques including RNA sequencing of the microglial sensome (Hickman et al., 2013). Confidence in *Hexb*'s exclusive microglial expression is reinforced with research validating it as a potential target for microglia-targeted adeno-associated virus (AAV) in treatment of HIV. This includes its increased suitability for the therapy compared to other targets including *Cd68* which is limited due to its dual expression on microglia and macrophages (Shah et al., 2022). With changes to *Hexb* being strongly associated with microglial-specific changes, it is plausible that upregulation of this gene within the TLR7-driven neuroinflammatory environment suggests microglial reactivity within the Aldara model. This microglial marker was not included in the current flow cytometry experiments due to antibody availability. However, future experiments to characterise this marker expression could aid delineation between microglial and peripheral myeloid populations.

Other consistently upregulated microglial genes following Aldara treatment were *Tmem119, Cx3cr1, Msr1* and *MerTK (Hammond et al., 2019)*. However,

experiments with neuroinflammatory models including EAE have shown a downregulation of *Tmem119* for microglia (Vankriekelsvenne et al., 2022). Additionally, there are debates of the transmembrane encoded by *Tmem119* being a reliable microglial marker with recent discoveries of expression on peripheral dendritic cells. Upregulation of *Tmem119* has conflicting evidence with both homeostatic and reactive microglial populations expressing the transmembrane protein (Ruan and Elyaman, 2022). As this finding was reported at the whole-brain level, further single-cell investigation of microglia would be required to determine the reactive status upregulation of *Tmem119* may suggest in the Aldara model.

One microglia-related gene which was found to be consistently downregulated across all Aldara samples was *P2ry12*. This gene is considered an example of homeostatic microglial genes and has previously been shown to exhibit downregulation in neuroinflammatory environments including patients with MS (Zrzavy et al., 2017). In the presented bulk RNA sequencing whole-brain and single cell spatial transcriptomics dataset, the findings presented in this thesis agree with this literature.

Providing TLR7 expression is most common amongst microglia compared to other brain-resident cells, the transcriptional changes stated strengthen the likelihood surrounding microglia being a critical mediator during this inflammatory cascade. However, TLR7 expression is throughout brain-cells so this is most likely a multi-cellular response to the neuroinflammation. This adds detail to both endogenous and exogenous multi-cellular mechanism that most likely underpins the initiation and continuation of this neuroinflammation.

These whole-brain transcriptomic changes suggest the microglia within the Aldara model are shifting away from their homeostatic phenotype to a more reactive form in response to the TLR7-driven neuroinflammation. Interpretation of these results is based on these genes exclusive expression on microglia. However, studies show shared markers between the brain-resident microglia and other myeloid populations (Honarpisheh et al., 2020). Some of the ambiguous myeloid markers that can be expressed on both microglia and macrophage populations include *Cd68, Csf1r* and *Cx3cr1*. Due to these challenges of distinguishing microglia from infiltrating myeloid populations and BAMs, whole-brain gene

changes can only be interpreted reliable to a certain extent. However, further single-cell validation of these transcriptomic profiles would be required to commit them to a particular cellular origin.

To begin the single-cell characterisation of microglia, flow cytometry was used. This allowed identification of both reactive status and cytokine production of the brain-resident immune population. Once again, identification of microglia within the brain is complicated due to their similar expression profile of surface markers with their myeloid counterparts (e.g. macrophages and monocytes). However, one flow cytometric approach to separate brain-resident and other myeloid populations is by their CD45 expression level. Microglia have been shown to express the classic immunological marker CD45 at intermediate level. This creates a broad microglia classification via flow cytometry as $CD45^{int}CD11b^{+}$. This expression profile is a widely accepted and implemented classification within the microglial field (Martin et al., 2017, Marques et al., 2008, Sharma et al., 2024). Gating of the $CD45^{hi}$ population will include infiltrating myeloid cells and BAMs. Therefore, the $CD45^{hi}$ cell populations were not included in this analysis. This CD45-based separation of cell populations increases reliability that the stated flow cytometry changes are representative of microglia rather than infiltrating myeloid populations.

It is important to note that, in states of inflammation, microglia can shift their CD45 expression to a more macrophage-like 'high' phenotype (Honarpisheh et al., 2020). To fully characterise this $CD45^{hi}$ population, which contains both peripheral myeloids and microglia, more cell specific markers would be required. The $CD45^{int}$ was selected for microglial characterisation in this thesis as myeloids do not typically downregulate their expression of this immune marker. This ensured the highest confidence possible in microglial identification given the markers involved in the current experiments.

Flow cytometry showed a significant increase in cytokines, TNFα, IL-6 and IFNγ, from microglial populations. This demonstrated the brain-resident cell's active role in the mediation of the neuroinflammatory environment previously described within the Aldara model. Cytokines have diverse functions especially within the brain where they have both beneficial and damaging effects (Bourgognon and

Cavanagh, 2020). Therefore, homeostasis of these signalling molecules is essential for proper homeostatic function and prevention of prolonged periods of inflammation. TNFα is a classical cytokine with a multitude of cellular sources including other brain-resident cells (Gonzalez Caldito, 2023). Microglial activation followed by subsequent release of microglial TNFα is a hallmark of a variety of neuroinflammatory animal models including LPS, Poly I:C, AD and PD (Nazem et al., 2015).

TNFα secretion from reactive microglia has various cellular consequences (Raffaele et al., 2020). The cytokine can elicit an autocrine effect and further microglial reactivity via activation of the membrane-bound TNFR1 shown in an LPS-driven neuroinflammatory model (Kuno et al., 2005). Inducing astrocytic activation is another possible effect of TNFα which continues the pro-inflammatory environment (Liddelow et al., 2017). This microglia-driven TNFα in the Aldara model suggests a possible multi-cellular mediated neuroinflammatory environment.

TNFα is known to exhibit both pro- and anti-inflammatory effects via a variety of cellular mechanisms. In the context of cerebral ischaemia, microglia-derived TNFα is suggested to have a neuroprotective effect compared to secretion from other infiltrating leukocytes (Lambertsen et al., 2009). Consistently, the anti-inflammatory effects of TNFα is further demonstrated through microglia-specific ablation of TNFR2 causes exacerbation of EAE disease signs (Gao et al., 2017). This finding contrasted with TNFR2 ablation in infiltrating myeloid populations presents an overall suppressive effect of neuroinflammation within the animal model of MS. Microglial-derived TNFα in the Aldara model may be suggestive of either pro-inflammatory and/or anti-inflammatory mechanisms.

IL-6 is another essential cytokine underpinning neural functions, development and potential damage. The class I cytokine can be secreted from a number of brain-resident cells including neurons, astrocytes, endothelial cells and microglia (Erta et al., 2012). Microglial production of IL-6 has been described in several pathophysiological settings including viral infection and LPS-treated glial cell cultures (Chucair-Elliott et al., 2014, Zhu et al., 2018). IL-6 plays a crucial role in

neurogenesis within the brain, however, the multifaceted cytokine has also been implicated in promoting neurodegeneration in several disorders (Kummer et al., 2021). The cytokine is another of its signalling molecule family to display potential neuroprotective effects with IL-6-deficient mice displaying heightened inflammatory processes following simulated brain injury (Penkowa et al., 2000). Microglial-derived IL-6 in the Aldara model is another potential example of balance of cytokines within a neuroinflammatory environment.

IFNγ is of interest when investigating TLR7-induced inflammation as activation of TLR7 is a main mediator of production of this cytokine (Hart et al., 2005). The type II IFN family member is increased in several neuroinflammatory conditions including mouse models of AD (Mesquita et al., 2015). IFNs have been discovered to have primary links to the development of depressive-like symptoms. This is demonstrated by patients undergoing IFN-therapy reporting the onset of depression during their treatment (Pinto and Andrade, 2016). Microglial IFNγ was shown to be linked to MHCII expression of the brain-resident cells to enhance their innate immunological functions within the parenchyma (Kawanokuchi et al., 2006). Increased numbers of IFNγ-producing microglia within the Aldara model may indicate a functional shift in the brain-resident cell to more macrophage-like roles including cytokine production and acting as APCs within the CNS.

Increased microglial TNFα and IL-6 expression within the Aldara model may also highlighting a potential protective mechanism occurring in the brain parenchyma to protect the organ from this daily TLR7 activation. The increased presence of IFNγ-producing microglia may demonstrate the requirement of the relatively more macrophage-like phenotype of these brain-resident cells within the Aldara model. It proves difficult from these results to disclose a single cell populations' ability of either promoting, repairing or, most biologically likely, a combination of these homeostatic mechanisms.

For all cytokines, particularly within the CNS tissue landscape, homeostasis of these signalling molecules is crucial in maintaining balance of physiology within the organ. The presence of cytokines is not distinctly a 'bad' thing. However, when the balance of these molecules gets altered by a pro-inflammatory trigger is when damage can occur. Due to the increased cytokine production within the

Aldara model, it can be suggested that the microglial cellular state has been shifted from homeostatic to reactive in the brain following TLR7 activation. This potential pathological shift is further demonstrated through changes to microglial surface markers and recruitment of peripheral immune cells.

Microglial reactive status can initially be explored through changes to surface activation marker expression, namely MerTK F4/80, MSR1 and MHCII. These markers are traditional myeloid markers, however, have been found to feature on microglia in states of inflammation and disease (Schwabenland et al., 2021). All 4 activation markers were found to be increased in expression on microglia within the Aldara model with MerTK being the only surface receptor to show significance. MerTK is a surface receptor protein expressed on microglia which has been linked to general brain homeostasis, brain development and influence on the brain-resident cell's phagocytic abilities (Nomura et al., 2017). This MerTK-focused shift in microglia phenotype may represent the cell completing more phagocytic activities within the Aldara model. Additionally, this may highlight an increase of microglial-mediated synaptic pruning which has been shown to change in pro-inflammatory neural environments (Li et al., 2024).

To further this single-cell analysis of microglia and characterise their *in-situ* biology, the spatial transcriptomics platform CosMx was used. Utilising the CosMx 1000-plex mouse neuroscience panel allowed for microglia-like cells to be identified via characterising genes such as *Cx3cr1, Hexb, MerTK, Msr1, P2ry12* and *Tmem119*. Using a scRNAseq-like analysis approach uncovered 18 initial transcriptional-based distinct clusters. Two were identified to be the most immune cell-like and thought to encompass all microglia, infiltrating immune populations and BAMs. Subsequently after combination and reclustering of these immune clusters, 5 transcriptionally different subclusters of identified immune cells within the Aldara model were identified. Of these subclusters, 4 relatively more microglia-like presenting clusters were explored within the context of this chapter to investigate microglia's role in this TLR7-activated neuroinflammatory model.

Across all putative subclusters of CosMx identified microglia, all 4 shared common upregulated inflammation gene markers across anterior and posterior sections:

B2m, Ctsb and *Vim*. All these genes have been implicated with different neuroinflammatory and neurodegenerative conditions. This presents the 4 microglial subclusters have a fundamental pro-inflammatory transcriptional signature following Aldara treatment. The macroglobulin encoded by *B2m* is a crucial element in MHC class I-mediated antigen presentation in immunological contexts (Li et al., 2016). *B2m* has been found to mediate activation of microglial in aged mice resulting in a neurotoxic microglial phenotype (Chen et al., 2025). Additionally, *B2m* features within a group of key genes that have been found upregulated in the initial stages of microglia activation in mouse models of AD (Keren-Shaul et al., 2017). In mice displaying depressive-like symptoms, microglia NLPR3 inflammasome activation has been found and, furthermore, studies have found that *B2m* serves as an initiator of this inflammasome signalling pathway (Li et al., 2022a, Hofbauer et al., 2021). Upregulation of *B2m* within this subcluster of microglia/immune cells may highlight a key cellular population involved in the mediation of this neuroinflammatory environment within the Aldara model.

Cathepsin B, encoded by *Ctsb,* is a lysosomal cysteine protease which, in various contexts of neuroinflammation, has been shown to be elevated and carry out pro-inflammatory roles (Hook et al., 2022). Mice knock outs of *Ctsb* have been shown to improve memory and cognition in pro-inflammatory neural environments within AD mouse models (Kindy et al., 2012). Increasingly popular nomenclature for microglia in neuroinflammation is ‘disease-associated microglia’ (DAMs). This glial subset is mainly present in neurodegenerative diseases, such as Parkinson’s disease (PD) and AD, and exhibit pro-inflammatory and increased phagocytotic role. As previously stated, these diseases have a well-established neuroinflammatory component to their pathophysiology. *Ctsb* is one of the DAM-phenotypic markers and considering the upregulation in the 4 subsets of microglia within the Aldara model, it can be postulated the brain-resident immune cell is mimicking the immune-driven functions as described in the DAM literature (Wei and Li, 2022).

A potential protective mechanism in microglia is suggested by all 4 CosMx immune subclusters upregulating *Grn*. Progranulin, encoded by the gene *Grn*, has been shown to demonstrate a neuroprotective effect in neuroinflammatory contexts. Deficiencies of the glycoprotein resulted in exacerbation of injury-responding

microglial states (Martens et al., 2022). With this potential neuroprotective effect, *Grn* has become a focus of neurodegenerative treatments. This therapeutic research is validated with overexpression of the genes has shown promising protective effects in various mouse models with neuroinflammatory-mediated pathologies (Rhinn et al., 2022). This common upregulation of the protective gene *Grn* may highlight the dynamic nature of microglial reactivity in the Aldara model.

Across the 4 subtypes, Immune.0 and Immune.3 present as the most pro-inflammatory reactive microglial state. Evidence of this includes upregulation of various related genes including cytokine and chemokine signalling (*Tnf, Ccl2),* inflammation-induced vasculature changes (*Igfbp7)* and heightened cellular activity via increased iron metabolism-related genes (Wang et al., 2020a, McCarthy et al., 2018). These transcriptional changes show these microglial subclusters are performing key pro-inflammatory actions including increased cytokine production and potential vasculature changes that could heighten peripheral leukocyte ingress.

Subcluster Immune.1 presents with a shift to a neuroprotective status of microglia with evidence of BBB remodelling. Compensatory protective mechanisms against oxidative stress are suggested by the upregulation of genes such as *Selenow* and *Hspa8*. The proteins encoded by these genes have both been established as neuroprotective in various neuroinflammatory tissue environments (Wang et al., 2018a, Chung et al., 2009). This subcluster was found to increase following Aldara treatment, potentially indicating a compensatory microglial subtype to combat the daily introduction of TLR7 into the brain parenchyma.

Immune.2 is the only subcluster which was found to decrease in cell number following Aldara treatment. Additionally, this subcluster demonstrated an upregulation of genes linked to iron metabolism and downregulation of G protein signalling-linked genes. The 3-day timepoint explored in this thesis was chosen as it was previously established as the ‘peak’ of neuroinflammation in the Aldara model (McColl et al., 2016, Nerurkar et al., 2017a). The decrease in cells presenting with an Immune.2 subcluster signature may suggest these cells are the ‘first responders’ to the initial IMQ introduction to the neural environment 4-hours after the first dermal application. This 3-day timepoint may be this microglia

subpopulations' responsive time range coming to a pause to allow cellular recovery of these over-active cells. Other neuroinflammatory models including mouse models of AD have identified a chronically 'exhausted' microglial phenotype (Millet et al., 2024). However, of this transcriptomic 'exhausted' signature only 2 genes were featured on the CosMx panel. Whole transcriptomic single cell analysis of microglial would be required to query this potential exhausted phenotype further.

These findings collectively may suggest the spectrum of microglial reactivity statuses in neuroinflammation. Alongside classic pro-inflammatory signatures, a potential neuroprotective microglial role emerged from this transcriptomic analysis of TLR7-driven neuroinflammation. This potential reparative microglial subtype is a novel finding within the Aldara model. The varying microglial subclusters further highlight the balanced nature of the neural cellular response within the Aldara model. This pro-inflammatory and anti-inflammatory mixture is comparably more reflective to what is seen in human clinical conditions rather than complete ablation of homeostatic mechanisms following induction of neuroinflammation (Muller et al., 2025).

Previous work with the Aldara model has characterised various peripheral immune populations in the CNS including $CD4^+$ and $CD8^+$ T cells, (natural killer) NK and NKT cells (McColl et al., 2016, Nerurkar et al., 2017a). Method of entry of these immune cells from circulation to brain parenchyma is suspected to be trafficking across the BBB. Previous unpublished data found impaired BBB integrity following Aldara treatment via Evan's blue dye experiments (Maria Suessmilch, unpublished data*)*. Strengthening this BBB-entry point theory of peripheral immune cells to the brain parenchyma is the neighbourhood analysis of CosMx spatial transcriptomic data. This revealed Aldara-specific immune-dominant niches which appeared to follow global vasculature networks as observed in mouse brain vasculature atlas (Xiong et al., 2017). Considering IMQ is present in brain parenchyma 4-hours post-topical application, these immune-dominant niches may be encapsulating both microglia activity in proximity and potential subsequent chemokine-driven leukocyte trafficking (Nerurkar et al., 2017a). BAMs can also exercise their inflammatory effects across the neurovascular unit of the BBB. These immune-rich neighbourhoods in Aldara brain may also be identifying these vasculature-bound

active macrophages. Due to time constraints, the transcriptomic signature of these immune-rich neighbourhoods were not explored. Future work focusing on these transcriptomic changes may reveal potential immune-mediated remodelling of the BBB. This lack of barrier integrity may shed light on the method of entry for these previously identified peripheral leukocytes in Aldara-treated brains.

One limitation of the CosMx spatial transcriptomics SMI is the difficulty of accurately identifying and delineating complex cell morphology. This has proven difficult with the innate complex membrane boundaries of brain-resident cells and changes to this in neuroinflammatory contexts (Sharma et al., 2024). These intricate neural cell membranes have proved difficult to confidently complete cell segmentation within the CosMx dataset. The 'cells' captured by CosMx are only visualising the cell body of these cell populations. Disciplines which are finding great success with the CosMx platform are those of oncology and immune-prominent research (Yeh et al., 2024). These scientific advances may be attributed to peripheral immune organs and tumours display a relatively homogenous cellular architecture compared to the CNS. Immune cells are uniform in nature with relatively simple cell boundaries compared to the various processes and morphologies exhibited by brain-resident cells.

With this lack of confidence in CosMx's cell segmentation abilities, it is assumed not all transcriptional changes detected by the SMI are representative of that cell type. This is due to the exclusion of parts of the cell's processes which are inherently important and not to be disregarded when exploring neural changes. This limitation holds true for microglia with the cell type displaying essential local translation of proteins at the cellular processes beyond the nucleus to maintain their phagocytic abilities (Vasek et al., 2023). The lack of inclusions of non-soma spherical regions of neural cells may be missing important sites of transcription which will influence that cell's overall transcriptional changes following Aldara treatment.

One possibility to address this cell segmentation limitation is expansion of the panel and morphology markers included. Nanostring has expanded its RNA panels with regards to human tissue to the whole transcriptome. However, no new murine tissue panels have been announced. To expand the RNA panel to the whole mouse

transcriptome would provide greater detail of transcriptional changes within cells. This RNA information may help to identify cell boundaries due to subcellular location. For studying brain tissue, the pre-selected morphology markers in the CosMx mouse neuroscience panel included GFAP (astrocyte), rRNA, histone and DAPI (nucleus). The CosMx SMI is currently limited to 4 morphology markers due to the fluorescent channels available for visualisation of the markers. If more morphology markers were available to incorporate into the CosMx SMI, the addition of major neural cell types would prove useful. This may include NeuN for neurons, Iba1 for microglia, O4 for oligodendrocytes and CD31 for endothelial cells of the BBB (Gusel'nikova and Korzhevskiy, 2015, Lin et al., 2009, Zhang et al., 2023a). More protein cell type markers would also begin to address the complexity of brain-resident cells including the overlapping of cellular processes.

The CosMx SMI uses extremely thin tissue sections (6μm) which is not expected to capture one cell's span throughout the brain unless implementing a Z-stack approach to account for these wide spreading cellular processes. Considering dendrites of P30 mice have an average length of 11.5mm, it is understandable that CosMx using 6μm thick tissue sections will encounter limitations in its whole cell identification (Wu et al., 2014). This limited tissue thickness poses as a limitation for both brain resident and immune cells in which their total span exceeds this range (Tigner et al., 2025). Exploring spatial transcriptomic platforms that allow for thicker tissue sections, such as Deep-RIBOmap techniques, may provide more detail on cellular architecture, however, increasing tissue thickness may not resolve fundamental limitations presented by neuroanatomy (Sui et al., 2024).

One biological limitation that must be considered when studying microglial is distinguishing the brain-resident population from infiltrating monocytes, BAMs and other CNS-related tissue myeloid populations. Considering previous findings confirmed presence of both microglia and other myeloid populations within the brain parenchyma in the Aldara model, the findings presented in this thesis may be linked to both cell populations (Sharma et al., 2024). This chapter has attempted to differentiate these populations primarily using variation in CD45 expression amongst these cell populations via flow cytometry. With microglia having intermediate expression of CD45 compared to myeloid's high expression

levels allows for this distinction. A limitation to consider with this approach is microglia's fluid nature in CD45 expression particularly following microglial activation (Honarpisheh et al., 2020). Following microglia's transition into a more reactive state, they alter their CD45 expression from intermediate to high levels and present as more macrophage-like cells compared to their previous resting state. The CosMx Mouse Neuroscience 1000-plex panel does feature several microglia-related genes including *Hexb, Tmem119, Cx3cr1, Msr1* and other targets. However, some of these 'microglial' markers have been found on other peripheral myeloid populations.

Various genetic reported mouse lines have been developed in attempts to distinguish microglia from other myeloid populations. Studies using Tmem119$^{tdTomato/+}$ found, via IHC and flow cytometry, TMEM119 expression only in CNS-resident microglia and not on peripheral myeloid populations (Ruan et al., 2020). Fractalkine receptor (Cx3cr1) is another common genetic modification target for microglial mouse lines (Jung et al., 2000). However, BAMs have now been found to express this 'microglial' marker (Eme-Scolan and Dando, 2020). Carrying out the Aldara model in one of these genetic mouse lines may provide more information on contribution of microglia compared to other myeloid populations to the TLR7-driven neuroinflammation.

Ultimately, this chapter has further characterised the TLR7-activated neuroinflammatory environment within the Aldara model with respect to microglial contribution. The identified reactive and active cytokine-producing microglia has strengthened the brain-resident cell as a primary cellular driver of the neuroinflammation within the Aldara model.

Spatial transcriptomics revealed 5 potential subpopulations of immune-focused cells in which these clusters presented as transcriptionally distinct from each other. This transcriptomic-powered data also explored the proximal relationship displayed by cerebral vasculature and immune cell populations within a neuroinflammatory model. These vasculature-mapping immune-riche neighbourhood potentially highlights a leukocyte entry point into the brain parenchyma. This chapter presents the Aldara model as a neuroinflammatory

mouse model with a fundamental microglial-driven component which supports it as a favourable model to further investigate these brain-resident immune cells.

5 Transcriptomic and flow cytometric analysis of $CD4^+$/$CD8^+$ T cell subsets in TLR7-driven neuroinflammation

5.1 Introduction

T cells are one of the key immune cells which bridge the gap between the innate and adaptive immune systems (Gao and Williams, 2015, Lee et al., 2020). Their contribution to several neuroinflammatory conditions including AD, MS and PD is well established (Asamu et al., 2023, Fletcher et al., 2010, Contaldi et al., 2022) This clinical contribution is somewhat unsurprising as they are key mediators of inflammatory processes throughout the body (Sun et al., 2023).

T cell infiltration into the brain parenchyma is a research focus across a variety of neuroinflammatory mouse models and clinical conditions (Laurent et al., 2017, Kedia et al., 2024). Trafficking of T cells into the CNS is important as their relationship with brain resident immune cells, namely the activation of microglia, is a hallmark of various neuroinflammatory conditions (Gonzalez and Pacheco, 2014, Schetters et al., 2017). Peripheral immune cell trafficking into the brain parenchyma is another piece of evidence against the dated 'immune privileged' status the CNS once held (Galea et al., 2007).

Characterisation of T cells into their subsets aids both in identification and provides more information on their specialised functions including their cytokine responses. The major subcategorisation of T cells is that of $CD4^+$ (helper T cells: Th) or $CD8^+$ (cytotoxic T cells: Tc). Th cells exhibit a coordinating role of immune responses including activation other immune cells including B cells and myeloid populations (Pobor et al., 1984). Tc cells carry out their functions more directly by inducing apoptosis of pathogenic harmful cells (Groscurth and Filgueira, 1998). Both subtypes are responsible for secretion of key cytokines depending on their further phenotypic characterisation. Full categorisation and mature phenotypes is a multi-molecular process which is summarised in the schematic shown in *Figure 1*.

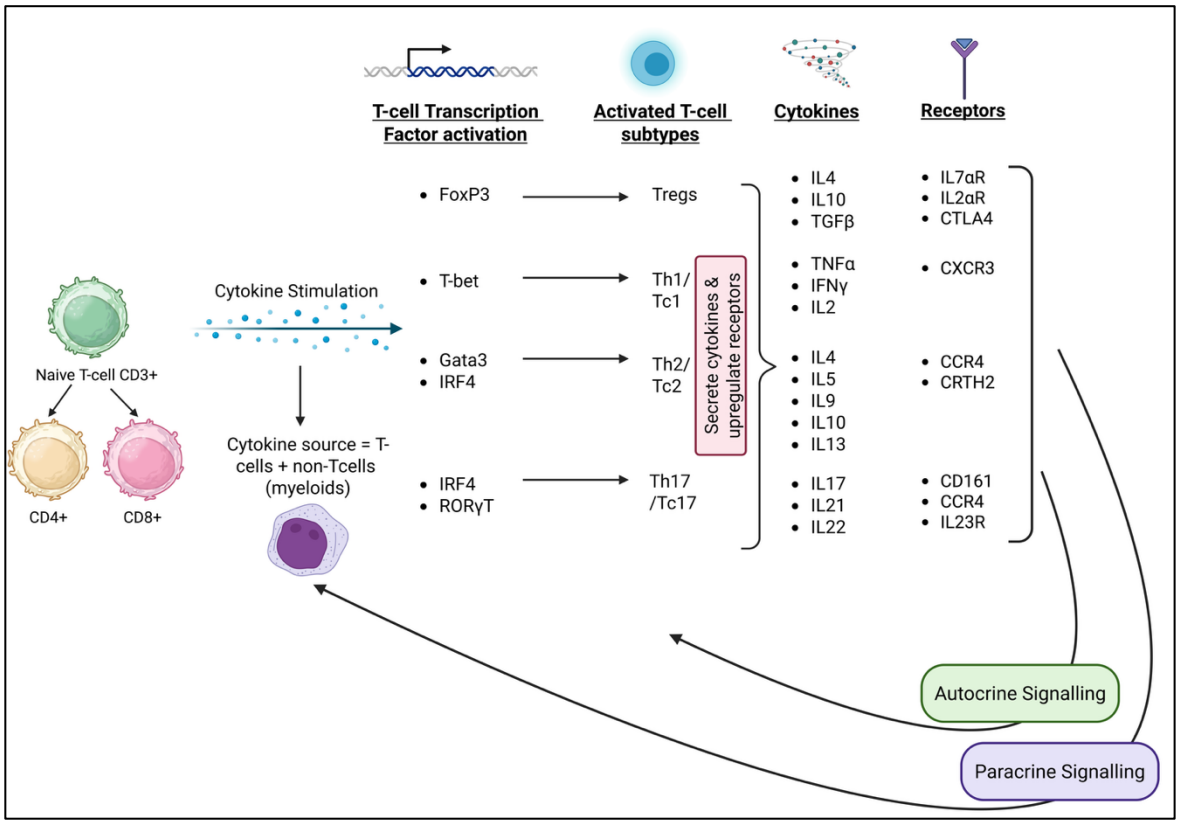

Figure 1: T Cell subset phenotypic characterisation. *Schematic summarising molecular mechanisms underpinning T Cell functional categorisation. Vital transcription factors, cytokine production and surface receptor expression of Tregs, Th1/Tc1, Th2/Tc2 and Th17/Tc17. Figure created in https://BioRender.com.*

As discussed in the previous chapter, microglia are key immune mediators during neuroinflammation. Both microglia and T cells have shown activation and pro-inflammatory properties in neuroinflammation. In mice experiencing chronic unpredictable mild stress (CUMS), both cell types become reactive and increase cytokine production (Shi et al., 2022, Wang et al., 2018c). Interactions between microglia and T cells are becoming a key research area within the neuroimmunology field. It is thought the interaction between the brain-resident microglia and infiltrating T cells could mediate the pro-inflammatory response within the brain (Schetters et al., 2017).

A $CD3^+$ T cell presence in the parenchyma has been established via immunohistochemistry in the Aldara model and their infiltration demonstrated no distinct regionality (McColl et al., 2016). This lack of regionality of T cell infiltration suggests a global immune cell-driven neuroinflammatory environment. This is important when using animal models to study changes to behaviour which

exhibits localisation of function. To further explore the T cell contribution to the neuroinflammatory environment of this model, it is pertinent to further characterise these $CD3^+$ cells as helper and cytotoxic including their cytokine profile. Detailing the presence of T cell subsets within the Aldara model may unveil how these primarily infiltrating immune cells are modifying the neuroinflammatory environment.

Whole-brain bulk RNA sequencing of T cell gene identifiers can begin to provide transcriptional evidence of infiltration of specific lymphocyte subsets. Flow cytometry allows for subcatergorisation of T cells based on transcription factors, surface markers and cytokine production. To investigate the role of T cells in microglial reactivity within the Aldara model, the RAG2KO mouse line has been used. These mice lack the RAG-2 gene which is essential for mature B and T lymphocyte production (Shinkai et al., 1992). Microglial reactivity was investigated using $Iba1^+$ cells as a marker (Lier et al., 2021).

The aim of this chapter is to further characterise the T cell subset populations as per their cytokine profiling within the Aldara model. Additionally, using RAG2KO mice, the contribution of T cells to microglial reactivity is briefly described. Furthermore, this chapter outlines the possibilities of identifying T cell-like cells using spatial transcriptomics.

5.2 Whole-brain transcriptomic changes to T cell-related genes

$CD3^+$ T cell presence in this model has been previously confirmed by the Cavanagh Laboratory (McColl et al., 2016). Their presence was global with no specific regionality observed in whole-brain transcriptomic changes to T cell-related genes. *Figure 2* shows a heatmap displaying key T cell-related genes including subsets of the $CD4^+$ and $CD8^+$ subtypes.

From this list, several genes shown here are present on all T cell subsets. Of these pan markers, the majority show consistent upregulation amongst all Aldara

samples compared to Controls. Significantly upregulated pan T cell markers include *Cd3δ (Cd3d), Cd3ε (Cd3e), Cd3γ (Cd3g), Itgal, Cd28 and Il2rg* (*Figure 2*).

As discussed previously in the introduction, the first major categorisation of T cells is into $CD4^+$ or $CD8^+$ which assigns their helper and cytotoxic phenotype, respectively. The expression levels of *Cd4* are relatively varied across Aldara samples with a primary downregulated gene expression signature of the subtype-

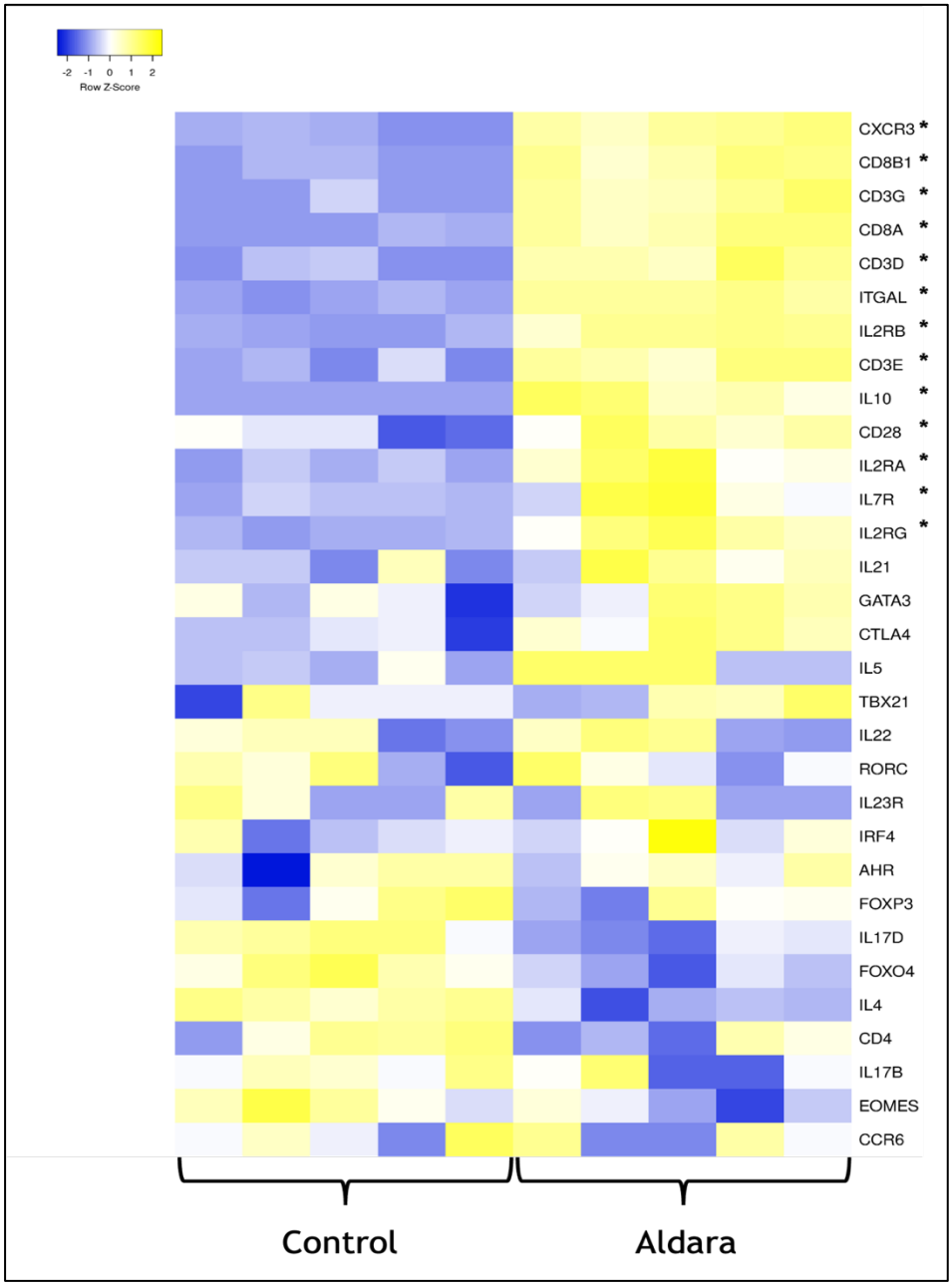

Figure 2: Heatmap of T cell-related genes from 3-day Aldara treatment bulk RNA sequencing dataset*. Significantly expressed genes (p.adj <0.05 and log_2FC > 0.5) are accentuated by (*). Columns indicate biological replicates within treatment groups. Colour intensity represents expression level with yellow showing upregulated genes and purple showing downregulated genes. Expression levels of genes have been row-scaled into z-scores. Data shown n=5 mice/group.*

specific gene ($p>0.05$). However, the CD8-related genes, *Cd8a* and *Cd8b1*, are both found to be significantly upregulated amongst all Aldara samples when compared to Control brains ($p.adj<0.05$).

T Cell subtype biology is determined through expression of transcription factors and cytokines as seen previously summarised in *Figure 1*. At the level of bulk RNA sequencing, these whole brain transcriptomic changes cannot be attributed to a single cell population. The 3 main T cell subsets, based on cytokine profiling, explored within the context of this thesis are CD4+ subsets Th1, Th2, Th17, and CD8+ subsets Tc1, Tc2 and Tc17.

Tbx21, the gene which codes for the transcription factor T-bet, is linked to Th1 and Tc1 cell subsets. This gene shows a primarily upregulated gene expression in Aldara samples; however, 2 brains present a relatively mild downregulation profile (*Figure 2)*. The transcription factor descriptive of Th2 and Tc2 cell is GATA-3 and its gene, *Gata-3,* displays a similar transcriptional biology amongst Aldara samples like *Tbx21* expression with majority of samples presenting upregulation. Two biological Aldara replicates appear to have similar downregulation patterns of the transcription factor genes. However, 2 Aldara samples again present a mild downregulated gene expression of the Th2/Tc2 transcription factor. RORγt, coded by the gene *Rorc,* and responsible for Th17 and Tc17 cell typing, displays a varied gene expression amongst Aldara samples with both downregulation and upregulation appearing across treated samples. This variation may be explained by other cells present in the brain parenchyma expressing the transcription factors listed above. As bulk RNA sequencing combines all these cells, the observed non-significant distribution may be attributed to this limitation of the technique.

Several genes which are potential markers of activated T cells *Cd28* and *Ctla4* displayed a strong upregulated gene expression profile within Aldara brains (*Figure 2)*. This collection of transcriptional changes is indicative of T cell presence including activation of these immune cells. However, as previously stated, this whole-brain expression of the T cell-related genes is inadequate to assign these changes to one subset cell.

5.3 CD4⁺ and CD8⁺ T cell characterisation in brain parenchyma following neuroinflammation

The initial whole-brain bulk RNA sequencing data of Aldara brains confirm the T cell presence within brain parenchyma, at transcriptional level. To build on and further characterise the already established presence of CD3⁺ T cells within the Aldara model, initial CD4⁺ and CD8⁺ T cell numbers were quantified using flow cytometry. Gating strategy using fluorescently-tagged antibodies for CD4⁺ and CD8⁺ T cells is presented in Appendix 3. Both populations of T cells show a significant increase within the whole brain and CD8⁺ T cell numbers are documented as relatively higher compared to CD4⁺ T cells (*Figure 3A*). Representative contour FACS plots for CD4⁺ and CD8⁺ for both treatment groups

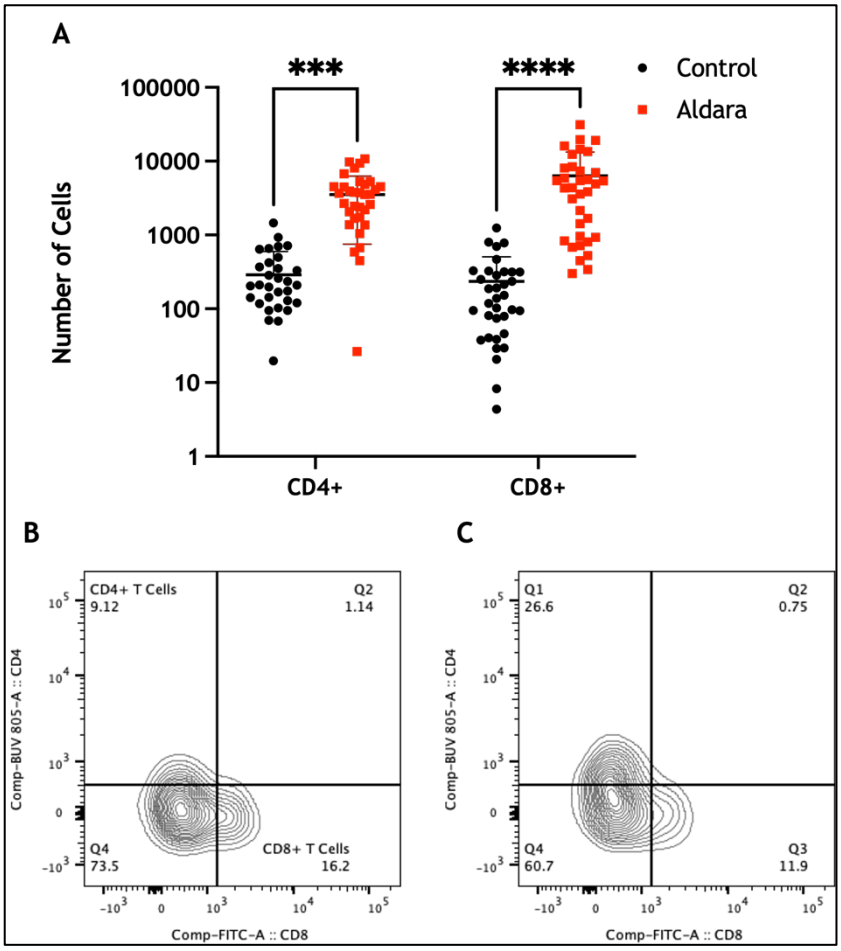

Figure 3: Number of CD4⁺ and CD8⁺ T cells increase in whole brain of Aldara-treated mice. *(A) Scatterplot displaying total number of CD4⁺ and CD8⁺ T cells in Control (black circles) and Aldara (red squares) mice. Individual animal values shown following the key displayed. Y-axis displayed as Log_{10} scale. Two-way ANOVA using Šídák's statistical test for multiple comparison shows significance for both cell groups. P<0.0002 shown as *** and p<0.0001 shown as ****. Pulling of seven experiments provided n=35/group. (B) and (C) Representative FACs contour plots showing increase in CD4+ and CD8+ T cells following Control and Aldara treatment, respectively.*

can be seen in *Figure 3B* and *C*. These representative quadrant flow plots show an increase of percentage from live cells of both $CD4^+$ and $CD8^+$ T cells following Aldara treatment. Both T cell subpopulations were present in equal numbers with no significant difference between $CD4^+$ and $CD8^+$ cells within the Control group (*p>0.05)*.

$CD4^+$ Th cells can be further categorised into Th1, Th2 and Th17 based on their transcription factor expression and cytokine production. Th1 cells express T-bet leading to pro-inflammatory cytokines IFNγ and TNFα production. Th2 cells express GATA-3 and produce anti-inflammatory cytokines IL-4 and IL-10. Th17 cells express RORγt and pro-inflammatory cytokines IL-17 and IL-21.

Figure 4 shows post-Aldara treatment brain-resident $CD4^+$ T cell characterisation via positivity for/expression of transcription factors and cytokine. Th1 & Th17 cell subsets as defined by transcription factor expression demonstrate a significant increase in number, while GATA-3 positive Th2 cells do not (*Figure 4A)*. Th1 and Th17 both demonstrate a significant increase in number with each showing more than 10-fold change from Control to Aldara groups (*p*<0.0001*)*. Representative contour flow plots for $CD4^+$ T cell expressing transcription factors can be seen in *Figure 4B*. A significant increase was found in TNFα and IL-10 (*p<0.0001)* and IL-17 (*p<0.0002)* CD4+ T cells following Aldara treatment (*Figure 4C)*. IFNγ, IL-4 and IL-21 positive cell number increased following Aldara treatment but did not reach significance (*p*<0.05). Representative contour flow plots for $CD4^+$ T Cell cytokines for both treatment groups can be seen in *Figure 4D*. The representative contour flow plots show gating strategy for discussed cell types including percentage of this cell population of live cells. Overall, all Th subsets showed an increase in Aldara mice, however, Th1 and Th17 were favoured in this biological change.

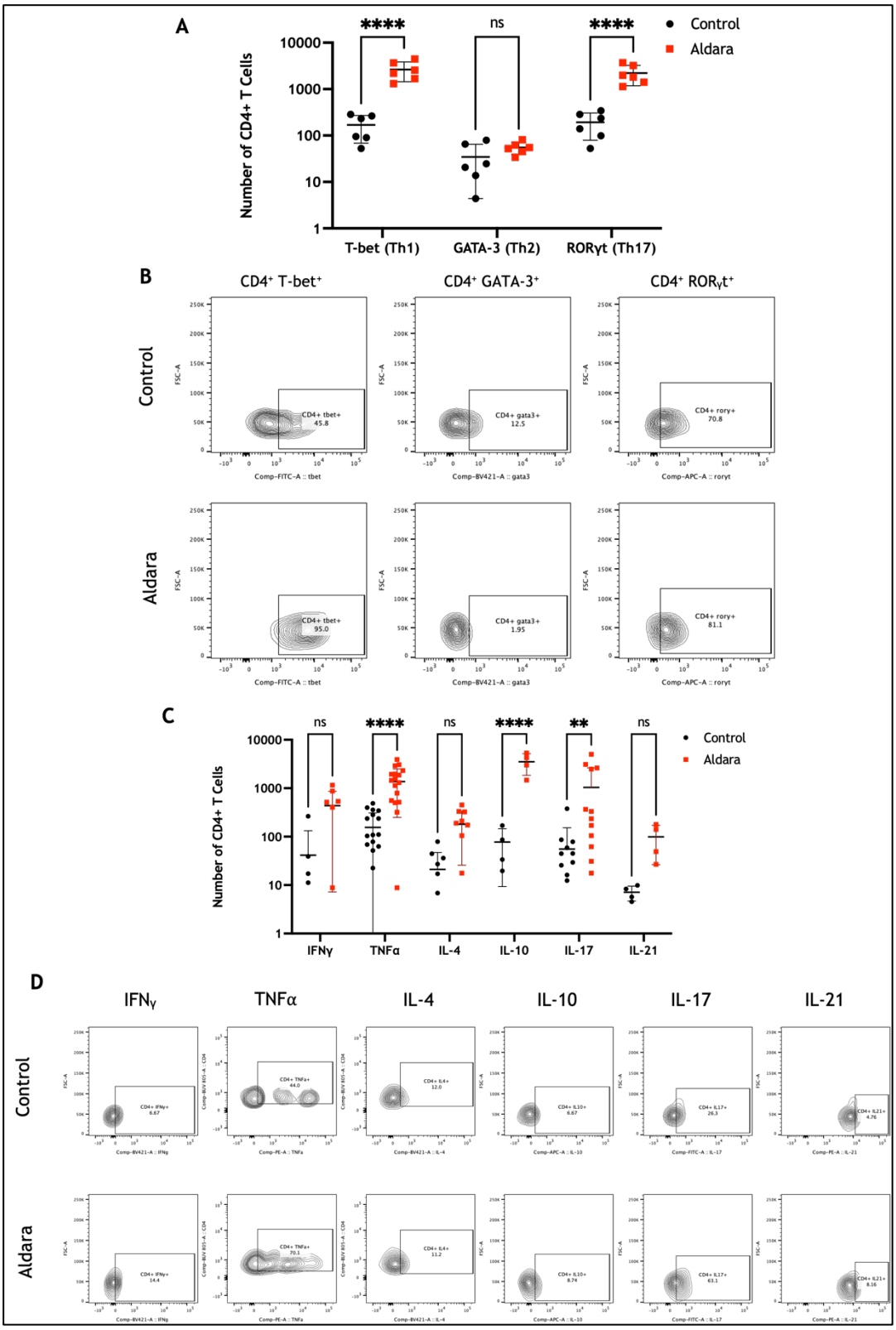

Figure 4: Increasing trend in transcription factors and cytokine-producing CD4+ T Helper cells (Th) in Aldara mice. *Scatterplot displaying total number of transcription factor-positive (A) and cytokine-producing (C) CD4⁺ T cells in Control (white) and Aldara (red) mice (individual animals represented by each point). Y-axis displayed as Log_{10} scale. Two-way ANOVA using Šídák's statistical test for multiple comparison shows significance for both cell groups. P<0.0021 shown as **, p<0.0002 shown as ***, p<0.0001 shown as **** and ns is p-value>0.05. Pooled experiments and availability of marker expression explains variation observed in n number. Transcription factor plots show one experiment n=6/group (A). N number per group for cytokine-producing CD4+ T Cells are as follows: IFNγ = 8; TNFα = 19; IL-4 = 10; IL-10 = 4; IL-17 = 14 and IL-21 = 4. Representative contour flow plots showing numbers of CD4⁺ T Cells for Control (upper) and Aldara (lower) mice for transcription factors (B) and cytokine production (D).*

$CD8^+$ Tc cells can be further categorised into Tc1, Tc2 and Tc17 based on their transcription factor expression and cytokine production. Tc1 cells express T-bet and produce pro-inflammatory cytokines IFNγ and TNFα. Tc2 cells express GATA-3 and produce anti-inflammatory cytokines IL-4 and IL-10. Tc17 cells express RORγt and pro-inflammatory cytokines IL-17 and IL-21.

Figure 5 shows post-Aldara treatment brain-resident $CD8^+$ T cell characterisation via transcription factors and cytokine production. All 2 Tc cell subsets demonstrate an increasing trend, and similarly to CD4+ Th cells, GATA-3 for Tc2 cells does not reach significance (*Figure 5A)*. Tc1 and Tc17 both demonstrate a significant increase with each experiencing an over 10-fold change from Control to Aldara groups ($p<0.0001$*)*. Representative contour flow plots for $CD8^+$ T cell transcription factors can be seen in *Figure 5B*. All cytokine positive cells were elevated in $CD8^+$ T cell populations following Aldara treatment, however, only Tc1 subset specific cells positive for cytokines IFNγ and TNFα reached significance (*Figure 5C; $p<0.05$)*. Representative contour flow plots for $CD8^+$ T cell cytokines can be seen in *Figure 5D*. Overall, all Tc subsets showed an increased in Aldara mice, however, Tc1 and Tc17 appeared to be more prevalent compared to Tc2 subpopulations.

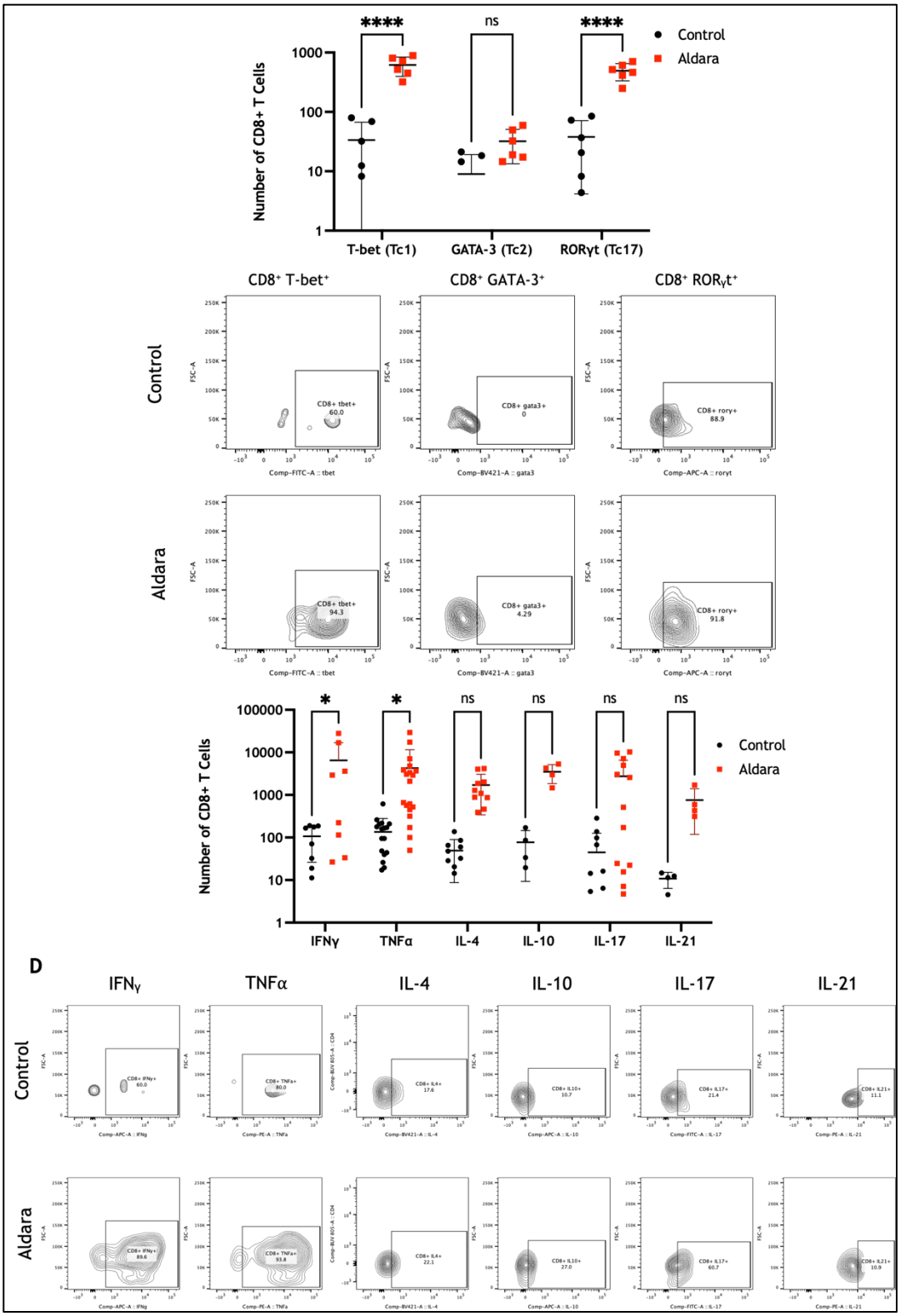

Figure 5: Increasing trend in transcription factors and cytokine-producing CD8⁺ T Cytotoxic cells (Tc) in Aldara mice. *Scatterplot displaying total number of transcription factor-positive (A) and cytokine-producing (C) CD8⁺ T cells in Control (white) and Aldara (red) mice. Individual animal values shown following the key displayed. Y-axis displayed as Log_{10} scale. Two-way ANOVA using Šídák's statistical test for multiple comparison shows significance for both cell groups. P<0.0021 shown as **, p<0.0002 shown as ***, p<0.0001 shown as **** and ns is p-value>0.05. Pulled experiments and availability of marker expression explains variation observed in n number. Transcription factor plots show one experiment n=6/group (A). N number per group for cytokine-producing CD8+ T Cells are as follows: IFNγ = 8; TNFα = 19; IL-4 = 10; IL-10 = 4; IL-17 = 14 and IL-21 = 4. Representative contour flow plots showing numbers of CD8+ T Cells for Control (upper) and Aldara (lower) mice for transcription factors (B) and cytokine production (D).*

5.4 Identifying T cell-like cells using spatial transcriptomics

To identify T cell presence and potential localisation with the CosMx spatial transcriptomic dataset, it was first explored if there were enough cells expressing CD3 subunits genes present for the platform to successfully register them. Due to the relatively low numbers of CD3+ T cells compared to brain resident cells in a coronal mouse hemisphere, an R package called *Nebulosa* was used to explore the dataset. This analysis package accounts for low data sparsity in scRNAseq experiments and was adjusted to account for spatial location for CosMx brain sections (Alquicira-Hernandez and Powell, 2021). Sparsity within an RNA sequencing dataset is defined as a high recordings of ‘zero counts’ by lowly expressed genes (Bouland et al., 2023). Presences of sparsity within a sequencing dataset would result in a high number of ‘dropout events’ which may be explained by low mRNA abundance within the processed tissue. As previously shown, CD3+ T cells are present within the Aldara brain but at relatively low cell counts (McColl et al., 2016, Sharma et al., 2024). The *Nebulosa* statistical analysis uses gene-weighted kernel density estimation which harnesses transcriptional information from neighbouring cells to recover dropout events that have been lost due to low expressed genes (Alquicira-Hernandez and Powell, 2021).

This analysis revealed areas within the brain where 3 subunits of CD3 included in the CosMx RNA panel, *Cd3δ, Cd3ε* and *Cd3γ,* were found to all be expressed on a cell in anterior and posterior sections (*Figure 6 & 7)*. These results found $CD3^{+}$ areas within both Control and Aldara samples, with treatment group showing no relatively higher signal than control. This analysis package is designed for 1 dataset at a time. Since each brain slice is treated as a standalone dataset when visualising the data at the spatial level, the package did not allow for the 'Joint Density' scale to be standardised to allow for accurate inter-sample comparison.

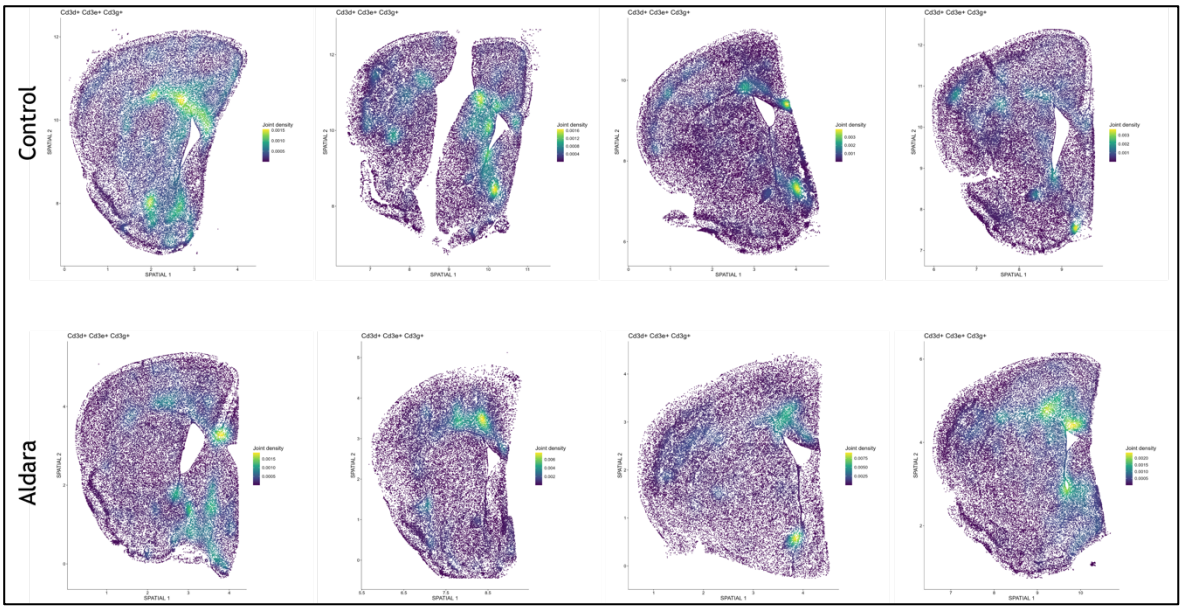

Figure 6: Nebula density plot of co-expression of transcript-based Cd3δ⁺ Cd3ε⁺ Cd3γ⁺ cells identified via anterior tissue sections CosMx spatial transcriptomic dataset. *Anterior coronal slices of Control and Aldara treated hemispheres with high joint density of three CD3 subunits shown as yellow and low joint density shown as purple. N=4/group.*

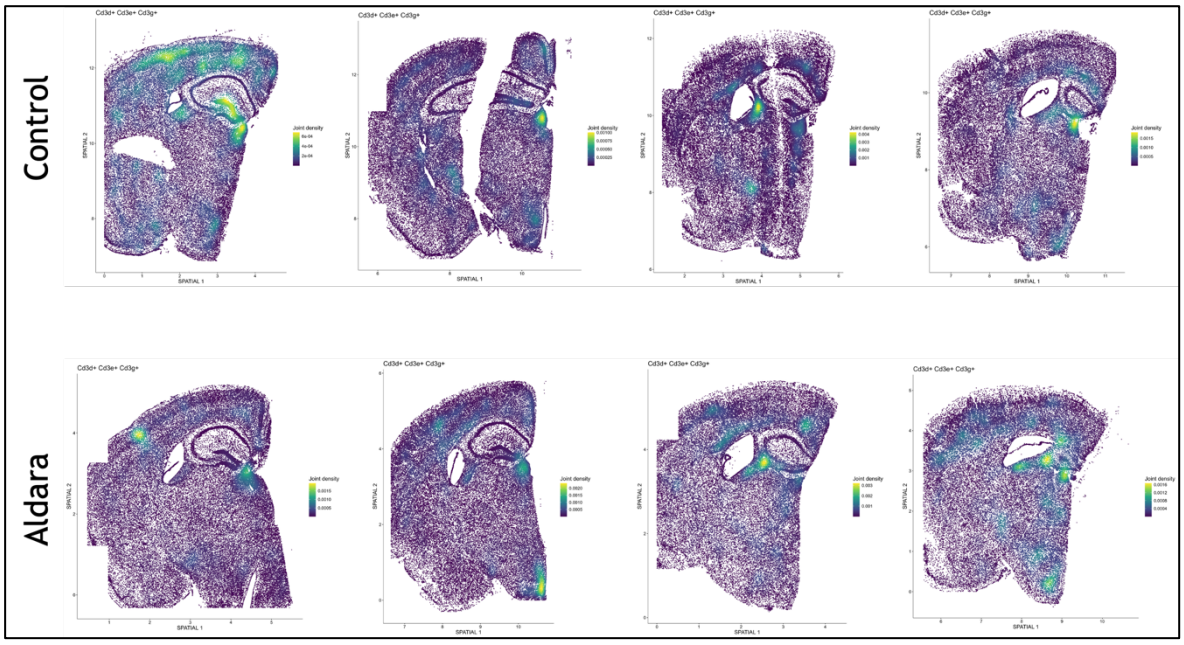

Figure 7: Nebula density plot of co-expression of transcript-based Cd3δ⁺ Cd3ε⁺ Cd3γ⁺ cells identified on posterior tissue sections CosMx spatial transcriptomic dataset. *Posterior coronal slices of Control and Aldara treated hemispheres with high joint density of three CD3 subunits shown as yellow and low joint density shown as purple. N=4/group.*

As described in the previous chapter, 5 immune clusters were identified in the 3-day Aldara CosMx spatial transcriptomic dataset. Of these potential subsets of immune cells in the brain, clusters Immune.0-Immune.3 were theorised as varying reactive subtypes of microglia, as discussed in the previous chapter. Subcluster Immune.4 appeared to be transcriptionally unique to the other 4 subclusters (*Figure 8)*. From this list of genes presented in the inter-cluster heatmap (*Figure 8B)*, some T cell markers *Lag3* and *Cd6* were identified (Ruffo et al., 2019, Santos et al., 2024).

Within the CosMx mouse neuroscience 1000-plex panel, 3 subunits of CD3 are included in the panel: *Cd3δ, Cd3ε* and *Cd3γ*. When analysing the expression of these 3 CD3 subunits amongst the 5 immune subclusters, Immune.4 is the only to show significant change of expression in any of the subunits. Notably, an increased expression of *Cd3ε* (*Figure 9*). This subcluster also shows an increased expression of *Cd3γ*, however, this change did not reach significance. The other immune

subclusters, Immune.0-Immune.3, showed non-significant (p>0.05) relatively minimal fold changes in the 3 CD3 subunits.

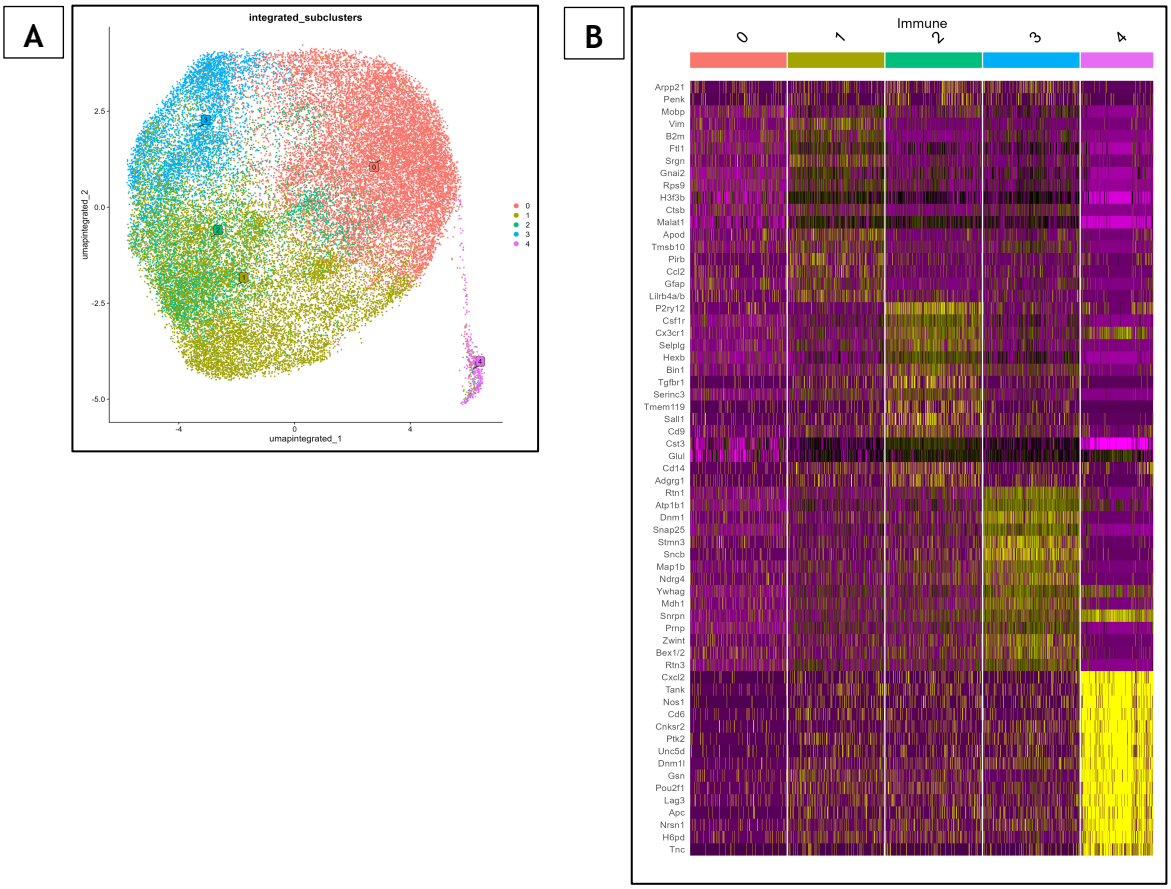

Figure 8: Reclustering of CosMx spatial transcriptomic dataset reveals 5 potential subclusters of microglia/immune-like cells. *(A) Integrated UMAP of five microglia/immune subclusters labelled 'immune.0', 'immune.1', 'immune.2', 'immune.3'and 'immune.4' for Control and Aldara samples. (B) Heatmap of relative inter-cluster gene expression of five microglia/immune subclusters. Yellow representing relative upregulation and purple representing relative downregulation of genes.*

To understand the transcriptional changes of the immune CosMx subclusters (*Figure 8)*, DE analysis was again performed using the Searchlight analysis platform approach presented in the previous chapters (Cole et al., 2021). This current chapter discusses the final CosMx immune subcluster, Immune.4. It should be noted that only 4 Control slices contained cells that belong to Immune.4 and all 8 Aldara tissue sections contained cells belonging to the subcluster. This results in 2 biological replicates for Control group as 'S1056 ANT BS1 C' and 'S1056 POS BS1 C' are different tissue planes belonging to the 1 animal (*Figure 10:* n=2). Aldara has all 4 biological replicates involved in the experiment (n=4).

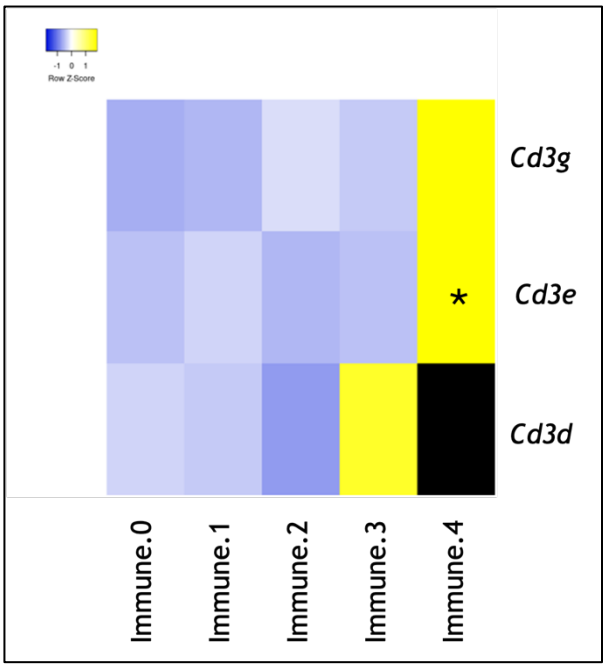

Figure 9: Heatmap showing CD3 subunit gene expression across CosMx immune subclusters. *Gene expression of Cd3 subunits (Cd3g, Cd3e and Cd3d) across CosMx immune subclusters. Only significantly changed gene shown is increased Cd3e in subcluster Immune.4 indicated by (*). Columns indicate CosMx Immune subclusters Immune.0-Immune.4. Colour intensity represents expression level with yellow showing upregulated genes and blue showing downregulated genes. Black expression shows no expression*

DE analysis of cells belonging to anterior Immune.4 subcluster samples is shown in *Figure 10*. PCA shows the gene expression data of anterior Immune.4 subcluster with the Control and Aldara naturally separating into 2 distinct grouping (*Figure 10A)*. With respect to PC2, both treatment groups display a spread across the PCA scatterplot. This suggests PC1 may be representative of treatment and PC2 of biological variance. The lollipop graph shows 129 genes being significantly upregulated in Aldara samples with no genes found to be significantly downregulated (*Figure 10B;* p.adj<0.05 and absolute $\log_2$ fold change >0.5 and <-0.5, respectively). The heatmap featured in *Figure 10D* highlights the DEGs and their pattern of transcriptional changes with Aldara samples primarily displaying upregulation of genes displayed in yellow. The top significantly upregulated genes in anterior tissue section Immune.4 subcluster include genes involved in iron metabolism (*Fth1* and *Ftl1),* immunomodulation (*Slc13a3)* and innate immune responses *(Cpa3* and *Tlr4)*. The top 10 significantly upregulated genes ranked by log2 fold change can be seen in Table 5.1.

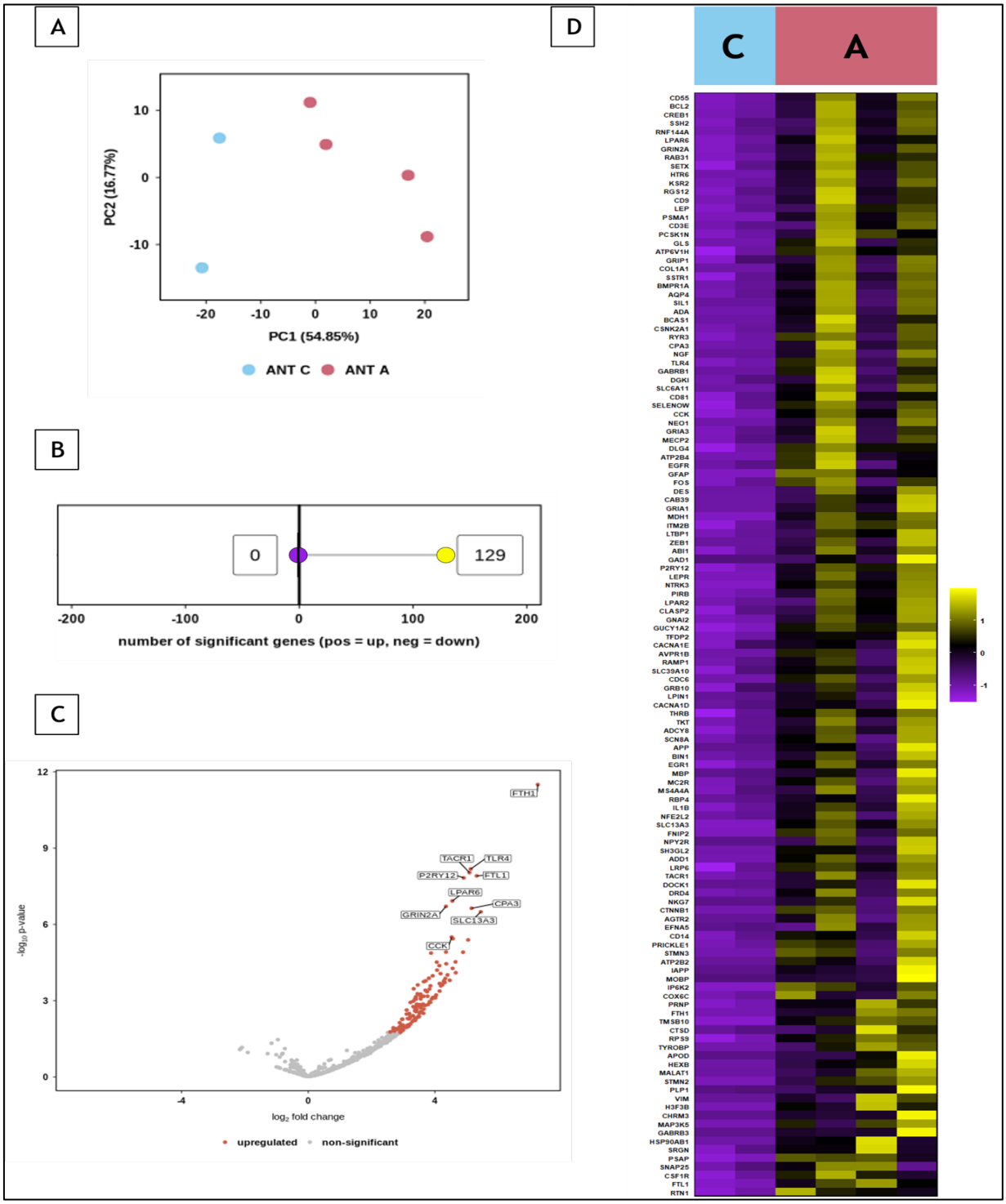

Figure 10: Differential expression analysis of anterior Immune.4 subcluster cells from CosMx spatial transcriptomics platform. *(A) PCA scatterplots showing gene expression data for Control [blue] and Aldara [red]. Individual samples represented by dots. (B) Lollipop graph showing number of significantly DEGs [p.adj <0.05, absolute log_2fold >0.5]. (C) Volcano plot of significantly DEGs with upregulated shown in red and non-significant in grey. (D) Hierarchically clustered heatmap of DEGs in Control and Aldara samples. Expression levels shown are row-scaled into Z-scores with yellow representing high expression and purple representing low expression. Control n=3, Aldara n=4 (biological replicates).*

Table 5.1: Top 10 significant upregulated DEGs in 'Immune.4' CosMx subcluster

Gene	log2fold	p	p.adj
FTH1	7.25	3.159192e-12	1.159424e-09
SLC13A3	5.45	3.214679e-07	1.310875e-05
FTL1	5.32	1.233949e-08	1.087442e-06
CPA3	5.16	2.326794e-07	1.067417e-05
TLR4	5.13	6.639275e-09	1.087442e-06
TACR1	5.09	9.186708e-09	1.087442e-06
GFAP	5.05	4.080132e-06	1.247840e-04
P2RY12	4.91	1.481529e-08	1.087442e-06
COL1A1	4.89	1.240133e-05	3.250920e-04
MOBP	4.66	7.971045e-05	1.329715e-03

No genes were found to be significantly differentially expressed between posterior Control and Aldara tissue samples.

The number of Immune.4 cells is slightly higher and consistent in Aldara samples compared to Controls (*Figure 11)*. Across both treatment groups, the number of Immune.4 cells is relatively lower in posterior sections compared to anterior sections. No trends displayed significance (p>0.05).

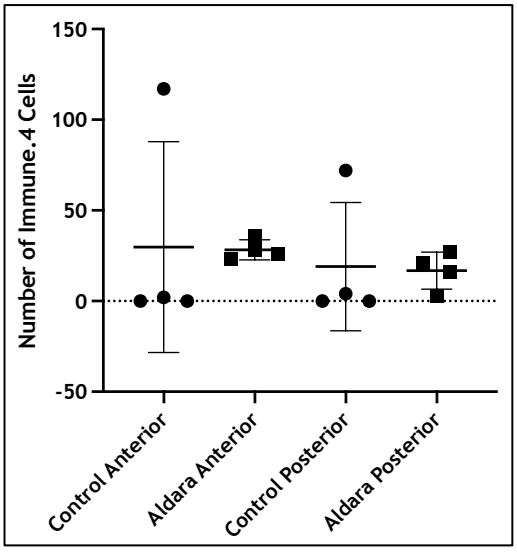

Figure 11: Number of Immune.4 cells variation across treatment groups and anatomical tissue planes. *Scatter plot showing number of Immune.4 cells in each treatment group and anterior/posterior tissue sections. One-way ANOVA corrected for multiple comparisons with the Tukey test. Data shown mean +/- SD, n=4/group.*

When the cells belonging to Immune.4 subcluster are plotted spatially in their respective hemisphere, Aldara sections are the primary treatment group that contain these cells (*Figure 12)*. In the anterior plane sections of Aldara treated mice, common brain regions that contain the caudoputamen, corpus callosum, various cortical regions and NAc. In the posterior plane sections of Aldara treated mice, common brain regions that contain

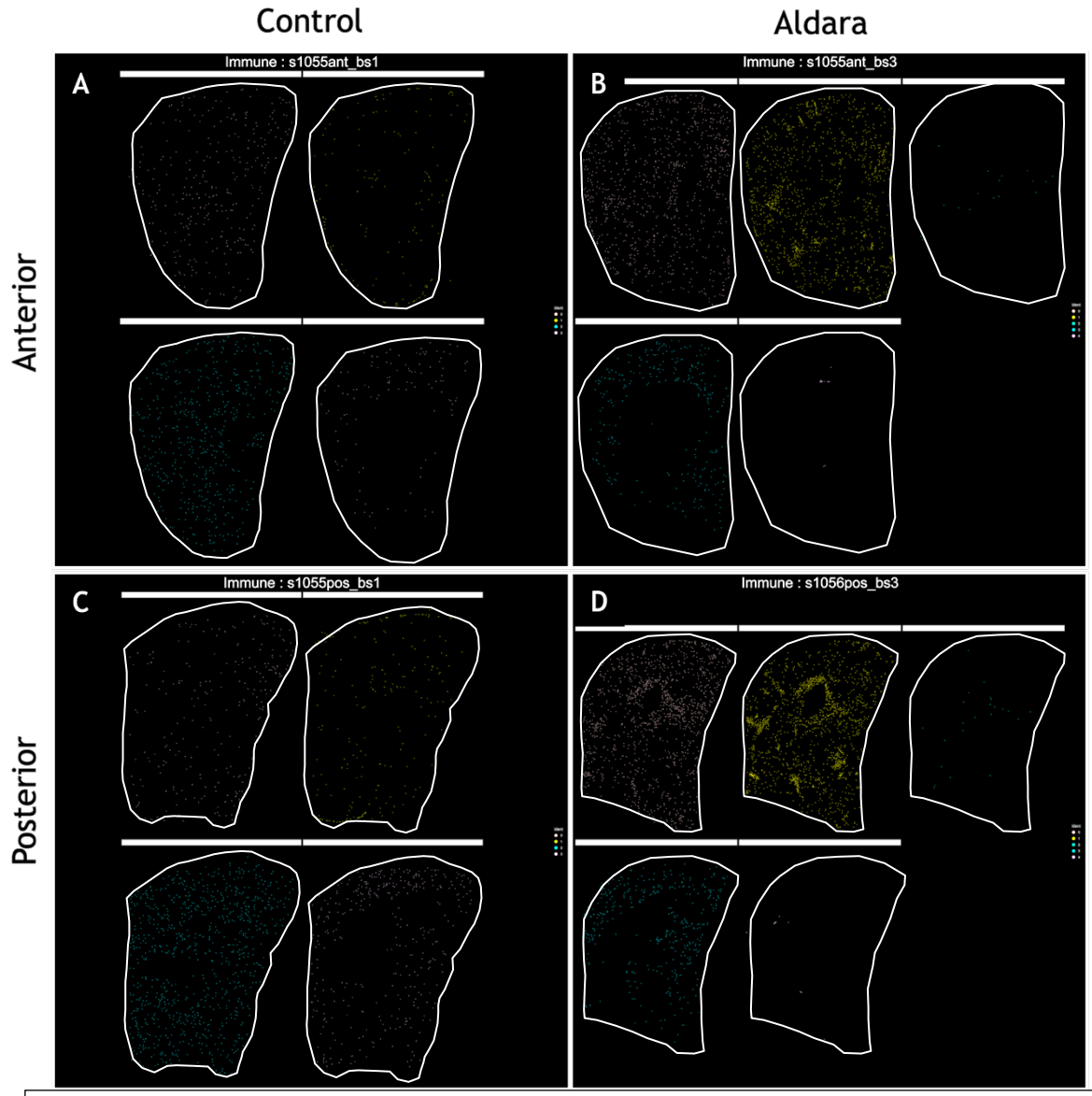

Figure 12: Representative spatial plots of immune subclusters from anterior and posterior coronal brain hemisections from Control and Aldara mice. *Spatial plots of Control brain hemisections from immune subclusters 0-3 in anterior (A) and posterior (C) planes. Spatial plots of Aldara brain hemisections show immune subclusters 0-4 in anterior (B) and posterior (D) planes. Contrast and saturation increased for visualisation. White drawn boundaries of brain tissue slice.*

Immune.4 cells include peripheral boundaries of the hippocampus, thalamus and various cortical regions. This regional infiltration of these T cell-like cells may indicate areas in the brain which are more susceptible to the effects of the TLR7-

driven neuroinflammation. Region specific infiltration of these immune.4 cells, suspected to potentially be Tregs, could be attempting to combat the ongoing TLR7-driven inflammation.

Examining the Immune.4 cell expression in Control slices reveals these cells follow white matter tracts in the brains including the corpus callosum and anterior commissure. There is some cortical expression of these cells in Control brains. These may represent a population of CNS-resident T cell populations used for immune surveillance of the vital organ. A subpopulation of T cells in brain parenchyma have been documented at rest in both mice and humans (Nevalainen et al., 2022). These reported at rest T cells primarily have a memory T cell phenotype (Ayasoufi et al., 2023). However further characterisation of these Control-present T cells would be necessary including memory T cell-specific markers.

5.5 Using RAG2KO mice to evaluate contribution of mature lymphocytes to microglial reactivity in TLR7-driven neuroinflammation

To investigate contribution of T cells to microglial reactivity in the Aldara model, RAG2KO mice that do not produce mature T and B cells were used. Iba1$^+$ staining was completed in coronal hemisections from WT and RAG2KO brains treated with control cream or Aldara (*Figure 13)*. Both control-treated groups at anterior and posterior tissue planes, wild-type and RAG2KO, have minimal Iba1$^+$ staining (*Figures 13A, C, E* & *G)*. Aldara-treated wild-type and RAG2KO anterior and posterior brain sections display observed increased Iba1$^+$ staining intensity which may suggest increased microglial reactivity following treatment (*Figures 13B, D, F* & *H)*. It is important to note, quantitative analysis was not completed for Iba1$^+$ IHC.

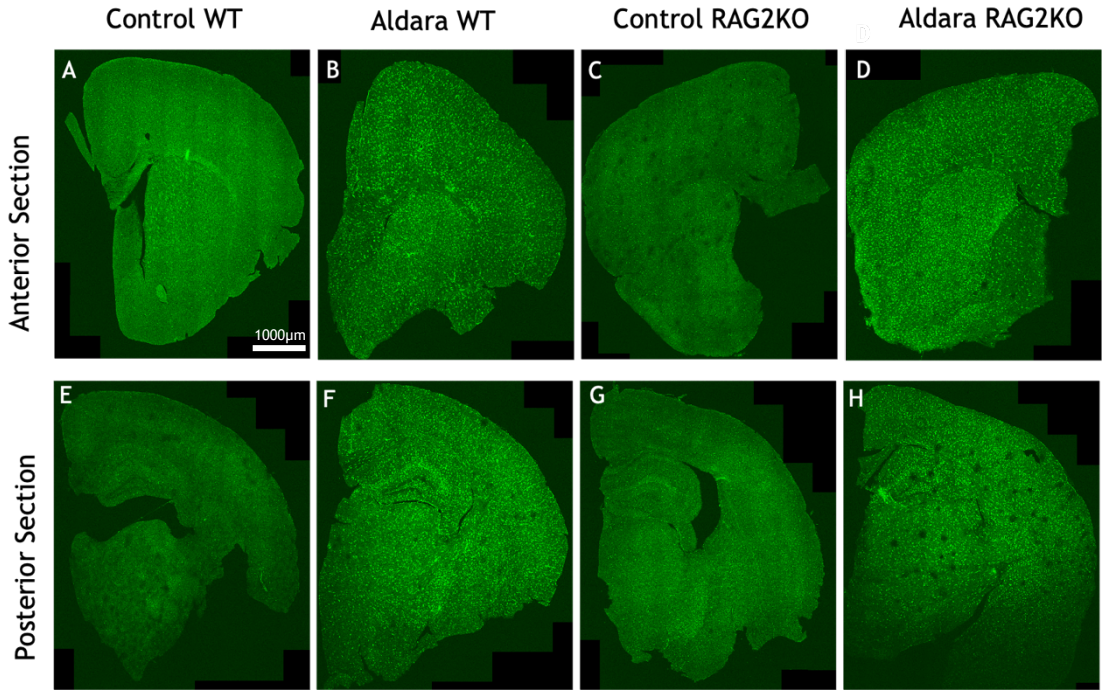

Figure 13: Iba1$^+$ staining in anterior and posterior sections from Control and Aldara-treated wild type (WT) and RAG2KO mice. *Four treatment groups: Control WT anterior and posterior (A&E), Aldara WT anterior and posterior (B&F), Control RAG2KO anterior and posterior (C&G) and Aldara RAG2KO anterior and posterior (D&H). Scale bar of 1000µm shown in FigA.*

Magnified sections of the Iba1$^+$ staining from ACC of all 4 treatment groups can be seen in *Figure 14*. Both control treated tissue, wild type and RAG2KO, have iba1+ cells with minimal cellular processes and relatively round morphology (*Figure 14A*

& *C)*. This suggests minimal to no microglial reactivity. Both Aldara-treated tissue, wild type and RAG2KO, display Iba1+ cells with extensive cellular processes typical of reactive ramified microglia (*Figure 14B* & *D)*. It could be argued that wild type Aldara-treated mice display increased Iba1^{+} cells compared to RAG2KO. This suggests a possible dampening of the microglial-driven neuroinflammation in the absence of mature lymphocytes. Overall, this suggests that in organisms lacking mature B and T cells, microglial reactivity remains a prominent feature of the TLR7-driven neuroinflammation in the Aldara model. However, further quantitative analysis would be required to increase reliability in these conclusion.

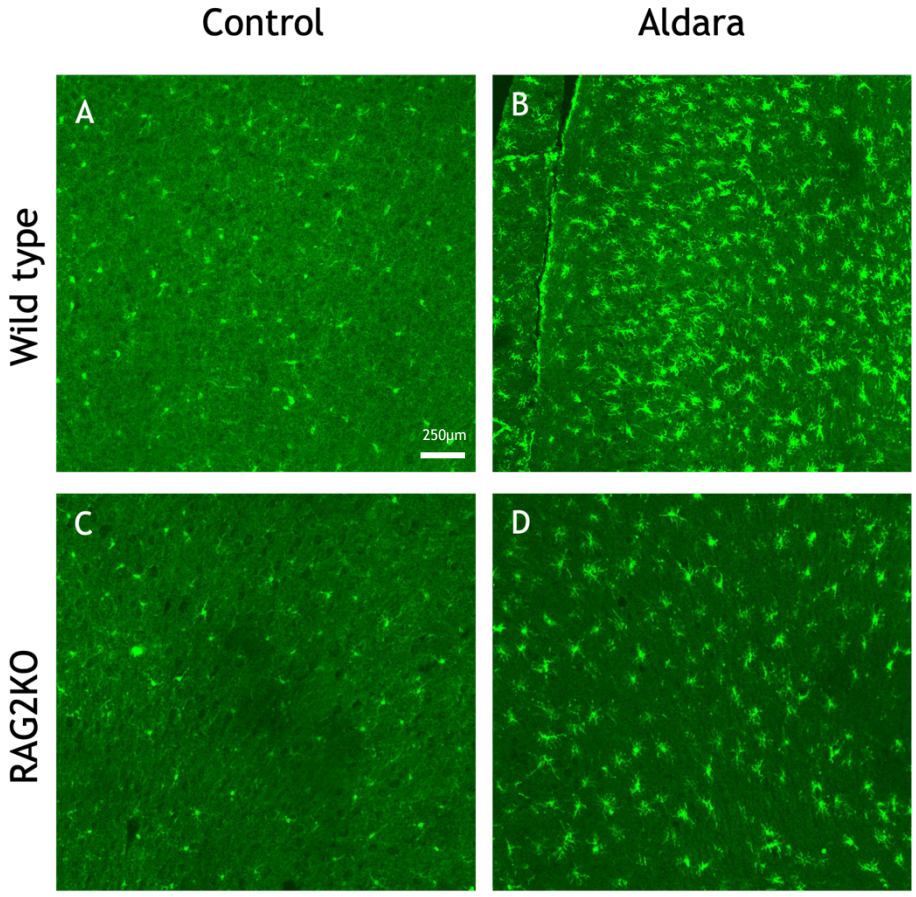

Figure 14: Iba1^{+} cells in Control and Aldara-treated WT and RAG2KO mice in ACC. Immunofluorescent staining of Iba1^{+} as a microglial reactivity marker. *Scale bar shown in Fig A for 250 µm.*

5.6 Discussion

The identification and characterisation of T cells in this chapter details another cellular mechanism actively contributing to the neuroinflammation within the Aldara model. Over previous decades, experimental evidence proves T cells are not only key mediators in a variety of CNS-focused conditions but also their importance at rest for homeostasis of this vital organ (Evans et al., 2019). This chapter provides a T cell-focused exploration of their contribution and mediation of TLR7-activated neuroinflammation.

Previous evidence of IHC $CD3^+$ T Cells and $CD4^+$ and $CD8^+$ T cells within the Aldara model via flow cytometry has been presented (McColl et al., 2016, Sharma et al., 2024). However, no further detail on subcategorisation or biological contribution to neuroinflammation was documented. The aim was to explore if the reported global presence of $CD3^+$ T cell in Aldara-treated mice results in whole brain transcriptional changes of pan and specific subset T cell markers. As presented in this chapter, several T cell-related genes exhibit consistent upregulation in Aldara compared to Control. Three subunits of the CD3 pan T cell marker, *Cd3*δ, *Cd3*ε and *Cd3*γ, express consistent and significant high levels of expression in Aldara samples.

Some of the genes stated in the above heatmap present a more varied transcriptional change across treated samples. This may be explained by specific involvement of T cell subsets or the gene expression of other non-T cell cells which may be controlling the gross transcriptional changes including NK and B cells (Wong et al., 2023, Voss et al., 1992, Finkelman et al., 1986). Increase of these nonspecific T cell markers at the whole brain level would reflect the previous findings of increase in NK and B cells in the CNS following Aldara treatment (McColl et al., 2016). Another reason for this varied T cell-related gene expression could be due to the relatively small numbers of infiltrating populations compared to the brain-resident cell types.

Of the 2 major categories of T cells, CD8-related genes are more consistently upregulated within the whole-brain bulk RNA sequencing dataset compared to CD4-related genes. This transcriptional evidence suggests that the T cell

contribution within the neuroinflammatory environment of the Aldara model is CD8-focused.

An increase in both $CD4^+$ and $CD8^+$ T cells via flow cytometry was discovered in Aldara treated brains. This was a relatively more equal documentation of $CD4^+$ and CD8+ T cells via flow cytometry compared to the bulk RNA sequencing results. However, there was still a significant increase in $CD8^+$ compared to $CD4^+$ T cells identified in the flow cytometry results. This lower $CD4^+$ T cell number identified in Aldara-treated mice may explain the weaker transcriptional signal of this subset in the bulk RNA sequencing dataset. Overall, presence of both major T cell subsets suggests a potential balance in contribution to the underlying neural biology within this model including both pro- and anti-inflammatory mechanisms.

$CD4^+$ Th cells mediate their effects indirectly on potentially damaging cells by activating and promoting other immune cells including B cells, macrophages and $CD8^+$ Tc. The Th cell subset have been implicated in several neuroinflammatory models and clinical conditions. A mouse model of PD was shown to exhibit a protective effect against dopaminergic cell loss when using CD4-deficient mice suggesting their pathological involvement with α-Synuclein-focused disease progression (Williams et al., 2021).

To investigate specific T cell-originating cytokines in the TLR7-driven neuroinflammatory model, further lymphocyte characterisation was carried out based on cytokine production. Further categorisation of $CD4^+$ T cell subsets within the Aldara model revealed a significant upregulation of cytokines related to Th1, and Th17 phenotypes and not Th2. Th1 cytokines include IFNγ and TNFα which have been demonstrated as key inflammatory mediators in a variety of physiological changes. IFNγ^+ $CD4^+$ T cells have been shown to be beneficially involved in the promotion of neurogenesis and synaptic plasticity within models of AD (Wu et al., 2022b). This suggests a potential anti-inflammatory reparative mechanisms being initiated in the TLR7-mediated neuroinflammation. This further highlights the dynamic nature of T cells in the inflammatory process.

TNFα was the only Th1-derived cytokine found to be significantly increased in Aldara-treated brain. This classic pro-inflammatory cytokine can initiate a multi-

cell response within an organ with activation of their receptors TNFR1 and TNFR2. Both TNF receptors' expression have been documented in brain-resident populations and immune cells (McCoy and Tansey, 2008). TNFR1 and TNFR2 can both exhibit pro-inflammatory effects within the brain, however, TNFR2 has showcased a neuroprotective role namely against excitotoxicity within the parenchyma (Papazian et al., 2021). This increase in TNFα neural levels is suggestive of promoting inflammation, but specific receptor binding would have to be determined before ruling out potential anti-inflammatory effects of the cytokine.

Another Th subset found significantly upregulated within the Aldara model was Th17 cells in cytokine IL-17 and transcription factor RORγt increased significantly. Cytokines originating from Th1 and Th17 cells have been found to promote a pro-inflammatory response amongst astrocytes. This includes increased Th1/17-specific chemokines such CCL20 and CXCL10 from astrocytes to further promote transendothelial recruitment of the $CD4^+$ T cell subset into the CNS (Prajeeth et al., 2017, Kunkl et al., 2022). Additional importance of Th17 cells in neuroinflammatory environments has been established in their interaction with microglia serving as a key component of disease progression in the murine MS model EAE (Xiao et al., 2025). The pro-inflammatory cytokine IL-17 has gained attention in recent years with established links to neuropsychiatric conditions including MDD and anxiety (Lu et al., 2023b). Increased circulating IL-17 levels has been suggested as a biomarker for treatment-resistant depression (Nothdurfter et al., 2021). The pro-inflammatory cytokine has been found upregulated in stressed mice which exhibit depressive-like behaviour (Kim et al., 2021b). These results suggest an IL-17-driven pro-inflammatory response within the Aldara model which could explain previous finding of reduced burrowing in treated mice (McColl et al., 2016).

Within the context of neuroinflammation, $CD8^+$ T cells can differentiate into their Tc subclass to mediate direct cell death processes against potentially harmful cells. Similarly to their Th counterpart, Tc cells can differentiate further into subtypes including Tc1, Tc2 and Tc17. Investigation of T cell subsets within the Aldara model revealed a $CD8^+$ biology across all subsets with Tc1 cells being the biggest relative change following the TLR7-activated neuroinflammation.

$CD8^+$ T cells are shown to be critical in the body's antiviral immune response with their immediate role in initiation of apoptotic pathways (Reagin and Funk, 2022). Presence of $CD8^+$ T cells have been identified in AD mouse models with an ablation of these infiltrating immune populations found to heighten $Iba1^+$ microglia and, arguably, heighten microglia activation (Unger et al., 2020). Reactive microglial have been found to promote CXCL10-mediated recruitment of $CD8^+$ T cell populations in murine neuroinflammation (Groh et al., 2025).

This contribution of $CD8^+$ T cells has been observed to shift towards more damaging effects contrasting with the previously described potential neuroprotective goals. Accumulation of $CD8^+$ T cells has been discovered in post-TBI mouse models, a well-documented condition with a neuroinflammatory element, with depletion of $CD8^+$ T cells in the model revealing an improvement in neurological outcome (Daglas et al., 2019, Chiu et al., 2016).

Presence of active cytokine-producing $CD8^+$ T cells within the Aldara model places it amongst the previously stated neuroinflammatory models with a T cell-mediated component. Both T cell populations, CD4 and CD8 can operate in balance within the neural environment in their efforts to resolve and/or amplify the tissue inflammation.

Exploration of brain-resident T cell subsets following Aldara treatment uncovers a predominantly Tc1/Th1 and Tc17/Th17-like profile which are typically pro-inflammatory. Given the global nature of the TLR7-driven neuroinflammation in this model, this pro-inflammatory T cell biology skew is expected. However, a potential regulatory mechanism is suggested by the presence of Tc2/Th2 cells actively producing anti-inflammatory cytokines. This T cell subset balance potentially suggests a homeostatic role of the infiltrating immune population. One subset of T cells which play a role in immune homeostasis are Tregs. Although not identified in this set of flow cytometry experiments, this subset is theorised with the final CosMx immune subcluster identified.

To distinguish this final immune subcluster from the previous 4 microglial-like ones discussed in the previous chapter, CD3 expression was explored. As previously discussed, CD3 is a classic pan-T cell surface antigen used for identification of T

cells. With only one subcluster from our CosMx showing significant changes in *Cd3* subunits, it can be proposed that this immune subpopulation is the most T cell-like population within the spatial transcriptomic dataset. The only other cell in the mouse that potentially may express *Cd3* are the Purkinje cells in the cerebellum, however, this brain region was not included within the examined tissue sections (Gerloff et al., 1993).

The T cell-related genes that featured on the top DEGs within the proposed T cell-like CosMx subcluster also included *Fth1* and *Egfr* which suggest a potential Treg subset of the immune cell (Wu et al., 2024, Zaiss et al., 2013). Tregs are a subset of mainly CD4+ T cells and exhibit primarily suppressive immune effects including maintaining peripheral immune tolerance and avoidance of autoimmune states (Vignali et al., 2008). There are many mechanisms Tregs can use to implement suppression within an organism including the secretion of certain cytokines and granzymes.

Tregs presence is typically associated with a relatively more chronic neuroinflammatory timeline. However, recent work proposed Tregs as potential mediators of innate and anti-inflammatory processes in a variety of conditions (Ou et al., 2023, Liston et al., 2022). Given the relatively acute timepoint of the Aldara model, 3 days topical IMQ application, this may be too short a time course for classic recruitment of peripheral Tregs into the brain parenchyma. However, brain-resident Tregs have been identified at rest in the mouse previously. Several studies have found Tregs to be protective in neuroinflammation via suppressing astrogliosis, improve cognitive outputs and decreased expression of neural pro-inflammatory cytokines (Ito et al., 2019, Wang et al., 2023c, Huang et al., 2020). This *Fth1*$^{+}$ *Egfr*$^{+}$ T cell-like population identified via CosMx in the Aldara brain tissue may highlight the development of a protective anti-inflammatory environment to combat the TLR7-activated neuroinflammation. Presence of these immune.4 subcluster cells in Control mice highlight the T cell subsets homeostatic role in both health and neuroinflammation (Liston et al., 2022). To confirm presence and numbers of these potential brain-resident Tregs, a flow cytometric analysis of the population would be beneficial. This could involve a panel including Treg-specific markers such as CD103, CD69, CTLA4 and FoxP3 which have

previously been shown to identify the brain-resident immune population (Liston et al., 2024).

However, this CosMx immune subcluster's top DEGs presented a variety of possible cellular origins namely T cells, neurons, oligodendrocytes and astrocytes. This dataset and spatial transcriptomic approach are weakened particularly by confidence of assigning these transcriptional changes to one cell population due to the technical limitations regarding cell segmentation. This list of DEGs of multi-cell origin genes may represent a snapshot of the interactions occurring within this neuroinflammatory context which has been previously documented in other experimental settings (Barcia et al., 2013, Kaya et al., 2022, Yshii et al., 2015).

The CosMx mouse neuroscience panel used in the experiments is focused on brain-resident cells and neural biological pathways. However, when focusing on peripheral immune populations including T cells, the markers to identify these cell populations are limited within this panel. Additionally, because of the relatively small number of T cells which have been identified previously in this model, this spatial transcriptomic technique is working with a small subcluster of cells for its reference. A more robust approach to investigating these brain-resident T cell populations would be scRNAseq. This would provide a whole transcriptomic picture of this relatively sparse cell type within the brain.

Results from this chapter provide evidence of brain-resident T cells following Aldara treatment. Although not one of the experimental aims of this thesis, one questions arises on *how* these peripheral immune cells penetrate the brain parenchyma. One theory of how T cells enter brain parenchyma is by crossing the BBB. Disruption and remodelling of the BBB is a common biological consequence of neuroinflammation. Damage to this tissue barrier has been documented in animal neuroinflammatory models including LPS and CUMS (Banks et al., 2015, Shi et al., 2024). Previous unpublished data of the Aldara model shows potential remodelling of the BBB with infiltration of peripheral intravenously injected Evans blue dye entering the brain tissue (*Maria Suessmilch, unpublished)*. This possible TLR7-mediated disruption of BBB integrity could suggest a weakened barrier system and present an opportunistic pathway of T cell passage to the CNS. Additionally, cytokines from these brain-resident T cells populations in the Aldara

model may be contributing to this inflammation-mediated BBB disruptions. Other cytokine-producing cells, such as the microglia detailed in the previous chapter, also may be adding to this BBB remodelling. These results agreed with previous findings of T cell-mediated BBB disruption assisting in the trafficking of the immune cells to the CNS (Aydin et al., 2023).

As discussed earlier in the first introductory chapter, the meninges are an immune niche. During tissue collection for all the techniques described in this chapter, extra precautions were taken to remove any dura mater and leptomeningeal tissue from the harvested brains. This was to exclude the T cell niches that exist within this extra-cerebral meningeal anatomy (Abbaoui et al., 2023). This was to ensure results were obtained from brain parenchyma and not surrounding supportive meningeal tissues. T cells are a part of diverse immunological populations within the meninges with some other key players from the lymphocyte and myeloid families. The meningeal immune landscape is a popular area of interest with evidence showing links between changes in behaviour, namely meningeal T cells found to regulate anxiety-like behaviours in mice via IL-17 production (Alves de Lima et al., 2020). Direct skull channel systems between the meningeal compartments and CNS have been described which further supports the direct communication between the 2 tissue environments (Mazzitelli et al., 2023). This justifies separation of meningeal tissue from brain parenchyma as both tissues hold importance and impact on a neuroinflammatory environment and warrant investigative separation.

The importance of the general T cell population has been highlighted in work with RAG2KO mice. These genetically modified mice, which lack mature B and T cells, present with worsened depression-like behaviours in mice following an inflammatory stimulus (Laumet et al., 2020). Considering T cell presence has been found to increase with continual Aldara applications; this may suggest a potential T cell-mediated resolution component within the CNS. Findings presented in the current chapter show microglial reactivity remains in RAG2KO treated with Aldara. However, as previously stated in this chapter, the Iba1^{+} IHC data presented for RAG2KO tissue was not subject to quantitative analysis due to limitations of time. To strengthen understanding of what the lack of mature lymphocytes has on the

TLR7-driven neuroinflammation, further analysis such as intensity quantifying or cell counts would be a beneficial future step.

This highlights one of the lymphocyte-independent microglial mechanisms mediating the TLR7-driven neuroinflammation. Relatively small numbers of T cells throughout the brain can have great impacts on promoting pro-inflammatory mechanisms. T cells may be promoting microglial reactivity in the Aldara model, through cytokine production, but this may not be essential to maintain the TLR7-inflammation. Furthermore, as shown in chapter 3 of this thesis, microglia are the primary TLR7-expressing cell type in the brain. Providing IMQ enters the brain 4-hours-post topical application (Nerurkar et al., 2017b), it can be speculated the microglia have direct and early activation at this earlier timepoint. This is strengthened with T cell infiltrating reaching its peak at day 3 of this model (McColl et al., 2016). The microglia must be ready to respond to this acute TLR7-mediated insult as soon as it enters the brain parenchyma and not wait for infiltrating T cells to help.

However, a full morphological and cytokine-production analysis of microglia in RAG2KO mice would be required to comprehensively detail the innate brain's cell contribution to the TLR7-driven neuroinflammation. Additionally, as previously mentioned, RAG2KO mice lack both mature B and T lymphocytes. To assess these true cellular contributions to neuroinflammation, separation depletion studies would be required of the lymphocytes. Work in this area has been explored in the Aldara model with antibody-depletion of $CD4^+$ and $CD8^+$ T cells (Sharma et al., 2024). This removal of the 2 major T cell subsets from the Aldara model did not alter the other immune cells at play in the TLR7-driven neuroinflammation including microglia, monocytes and other lymphoid populations (e.g. NKT and B cells). Future experiments would aim to deplete other immune populations to parse out their sole contribution to the TLR7-driven neuroinflammation in the Aldara model.

As discussed in previous chapters of this thesis, the 1000-plex CosMx mouse neuroscience panel is limited with respect to immune markers. Although a Treg transcriptional signature was suggested in this chapter's findings by the upregulation of *Cd6* and *Lag3,* some other cell types could be a possibility. This

cluster upregulated some neuronal genes including *Nos1* which has been documented as having roles in GABAergic neurotransmission (Wan et al., 2024). Other upregulated immune.4 neuronal-specific genes include *Cnksr2* and *Nsrn1* (Suzuki et al., 2007, Ito and Nagata, 2022).

Another reason for multicellular transcriptional changes within this CosMx subcluster may be attributed to the previously discussed limitation of this platform of accurate cellular segmentation. Due to the complex morphology of non-immune cells within the brain parenchyma, accurate cellular boundaries have proven difficult to capture with the CosMx SMI. For the posterior brain hemisections in CosMx, no significant gene changes were observed in the immune.4 subcluster between Control and Aldara. This could be due to relatively limited number of the subcluster-belonging cells being captured by the spatial transcriptomic system. Future experiments would incorporate whole-transcriptomic analysis of brain-resident T cells to provide a wider immune marker range and single cell-specific changes. These technical improvements would aim to be more accurate in immune cell-subset classification at the transcriptomic level and, in doing so, potentially capture more of this infiltrating population for differential analysis.

This chapter has identified a cytokine-producing T cell presence within the Aldara neuroinflammatory model. The T cell response within the Aldara model has been found to be primarily, however, not strictly a pro-inflammatory response. Evidence of a T cell-mediated anti-inflammatory response is also supported by this chapter's findings with a potential Treg-driven element. A potential T cell-like population was identified via spatial transcriptomics. However, an RNA and flow cytometry panel containing more Treg cell markers would be beneficial to further investigate this subcluster of brain-present immune cells. Aldara treatment of RAG2KO highlighted that presence of Iba1^{+} microglia does not rely on mature lymphocyte population. Collectively, these findings add the Aldara model onto the list of neuroinflammatory models with a T cell-driven element which is intertwined with the neuroinflammatory pathogenesis.

6 TLR7-driven neuroinflammation results in neurotransmission-related transcriptional changes and anhedonia-like behaviours

6.1 Introduction

As discussed previously in the introduction of this thesis, inflammation has an established link to affect different facets of behaviour in humans. Acute periods of inflammation in response to pathogens can manifest SB (Dantzer, 2023). This pro-inflammatory response is thought to be a protective mechanism adopted by organisms. A variety of SB can present which may include changes to appetite, malaise and anhedonia (Rademacher et al., 2021). Some of these behaviours are thought to be a results of inflammation-perturbed reward circuitry (Volkow et al., 2011, Der-Avakian and Markou, 2012). Relatively more chronic neuropsychiatric conditions such as anxiety and MDD can also display these suspected inflammation-driven behavioural changes. Patients living with depression who display raised levels of peripheral inflammation experience disturbed neural circuitry which mediate reward-driven behaviours (Felger et al., 2016, Goldsmith et al., 2023).

As previously stated, anhedonia is one of the possible behavioural changes following increased inflammation. Anhedonia is described as a loss in pleasure from activities which were previously enjoyed (Cooper et al., 2018). Anhedonia encompasses various types of the depressive-linked symptoms including consummatory and motivational anhedonia. The distinction between these two manifestations of anhedonia lies within what part of the individual's reward processing may be altered. Consummatory anhedonia describes when individuals lack the capacity to enjoy or find pleasure in the 'reward'. Motivational anhedonia describes individuals that lack the drive or motivation to seek out the reward (Treadway, 2023).

Anhedonia is a common symptom described by patients living with MDD, other neuropsychiatric conditions and chronic peripheral inflammatory conditions including psoriasis and IBD (Der-Avakian and Markou, 2012, Carpinelli et al., 2019,

Lada et al., 2022). Anhedonia is thought to have a strong link to reward processing deficits coupled with a reduction in dopamine (DA) transmission (Dresp-Langley, 2023). Indeed, DA neurotransmitter production and signalling has been found to be reduced in several neuroinflammatory environments in both humans and animal models (Mancini et al., 2023, Wang et al., 2018b).

Key brain regions and pathways thought to be implicated in anhedonia due to their involvement in the reward circuit include the mesolimbic areas, namely VTA, ACC and NAc (an area within the ventral striatum) (Der-Avakian and Markou, 2012). The thalamus has also been found to show changes to connectivity in individuals living with anhedonia (Leonard et al., 2024). The corticostriatal and thalamostriatal circuits have been found to play a crucial coordinating role in reward-driven behaviours and the brain regions output for these activities (Lee et al., 2019). Further understanding the regional neuroinflammation-driven molecular mechanisms underpinning anhedonia could aid comprehension of how these pathways fit into the wider, multi-symptomatic picture of neuropsychiatric conditions.

The relationship between neuroinflammation and behavioural changes resulting in anxiety and depressive-like behaviours in rodents is well-established (Remus and Dantzer, 2016). The psychoneuroimmunology field has revealed several mechanisms that may be underpinning these inflammation-induced SB. This is suspected to be a mechanistic combination of raised levels of intra-cerebral cytokines from activate endogenous immune and neural cells, such as microglia and astrocytes, and result in recruitment of exogenous immune cell populations into the brain parenchyma. The previous chapters of this thesis have shown increased cytokine production of both microglia and $CD4^+$, $CD8^+$ T cells following Aldara treatment. This multicellular-driven global neuroinflammation alters the neural circuits responsible for the mediation of different behaviours including that of reward and anxiety (Huwart et al., 2024, Won and Kim, 2020, Salcudean et al., 2025).

Animals treated with Aldara display peripheral inflammation-related changes including the psoriasis-like dermal reaction, splenomegaly, and increased lymph node weights (McColl et al., 2016, Nerurkar et al., 2017b). During *in vivo* models,

it has been reported anecdotally that the mice within the treatment group eat less of the baby food provided as a supportive measure (i.e. inappetence). As previously found by our laboratory group, Aldara-treated mice exhibit a reduction in burrowing (McColl et al., 2016), which is an innate and reward-driven behaviour of the animals. Changes to this behaviour indicate the presence of inflammation-induced reward-related behavioural change that may be indicative of anhedonia-like changes in treated animals. However, to fully characterise the TLR7-driven behavioural changes within this model, a more in-depth behavioural assessment is crucial.

Behavioural tests to characterise anxiety-like behaviour in rodents can be split into 3 categories: approach-avoidant behaviours, vigilance and defensive behaviours (Lezak et al., 2017). There is an overlap in test interpretation of these different brackets of anxiety-like behaviours in rodents. Two common behavioural tests to examine the presence of anxiety-like behaviours in both the literature and this thesis include open field and elevated plus maze (Belovicova et al., 2017). The open field and elevated plus maze tests the innate exploratory and curious nature of a mouse in open environments. A healthy mouse will display a preference to the closed arms of elevated plus maze. Furthermore, in the open field the animal's exploratory nature will be displayed with them exploring all areas within the test arena. A mouse experiencing anxiety-like behaviours will not showcase these typical behaviours and, instead, show an aversion to open arms of the elevated plus maze and central arena of the open field. Additional read-outs from these behavioural tests include assessing an animal's motivation and the test to explore novel environments (Chen et al., 2024).

As described previously in this chapter, there are 2 main forms of anhedonia: consummatory and motivational. Two branches of behavioural testing can be used to characterise anhedonia in rodents which evaluate interaction with either aversive or positive stimuli (Scheggi et al., 2018). Tests using aversive stimuli interaction involve the forced swim test and tail suspension test. It is believed this characterises behavioural phenotype more representative of despair within rodents. Presence of anhedonia and reward deficits can be measured using sucrose preference test and investigating changes to innate in-cage behaviours such as nest-building. The experiments in this thesis used positive stimuli behavioural

tests to characterise anhedonia, particularly the sucrose preference test and examining nesting behaviours. Testing sucrose-preference explores anhedonia as mice typically choose sweetened water. Changes in these behaviours following neuroinflammation may indicate pathological changes in neural pathways within the Aldara model. From this viewpoint, implementing these behavioural tests allow for a more detailed depiction of the reward-related changes observed following TLR7-activated neuroinflammation. The sucrose preference test can be argued to investigate both consummatory and motivational facets of anhedonia-like behaviours in rodents (Gencturk and Unal, 2024).

The aim of this chapter is to further characterise subsequent neuroinflammation-triggered behavioural changes which may be related to deficits in reward pathways within the Aldara model. A battery of behavioural tests will investigate changes to treated mice in relation to anxiety-like behaviours, anhedonia and motor functional outputs. To investigate region-specific transcriptomic changes, spatial transcriptomics platform CosMx will be utilised to investigate changes to neurotransmission-related genes in reward-related brain areas: NAc, ACC and thalamus.

6.2 Results

Previous studies using the Aldara model have documented changes to behaviour specifically burrowing deficits (McColl et al., 2016). Additionally, observational findings while carrying out the Aldara model report a reduction in in-cage movement and innate social behaviour between treated animals. To fully characterise these inflammation-induced behavioural changes, a battery of behavioural tests were used to study manifestation of motor capabilities, anxiety-like and anhedonia-like behaviours in Aldara mice.

6.2.1 Rotarod

Prior to implementing behavioural tests for anxiety-like and anhedonia behaviours, general mobility and motivation was assessed via rotarod testing. Furthermore, this initial exploration of movement was essential as Aldara-treated mice appear less mobile and exhibit less exploratory behaviour in their cages

compared to control animals (*Unpublished data, Kirstyn Gardner-Stephen)*. Rotarod behavioural testing provides details on whether treated animals can move normally if prompted compared to healthy counterparts.

No significant differences were reported in rotarod latency to fall (*Figure 1A)* and top speed (*Figure 1B)* when comparing Aldara and Control mice ($p > 0.05$). Aldara animal groups presented a slight decrease in recordings at each timepoint, however, this difference never reached significance. Aldara-treated mice were able to stay on the rotarod apparatus for an extended period that was equal to control mice. Therefore, this proved that the animals could move when prompted and exhibited no detectable locomotor deficits. This finding suggests the reduction in observed in-cage movement could be lack of motivation or possible conservation of energy in response to the presence of inflammation within the organism.

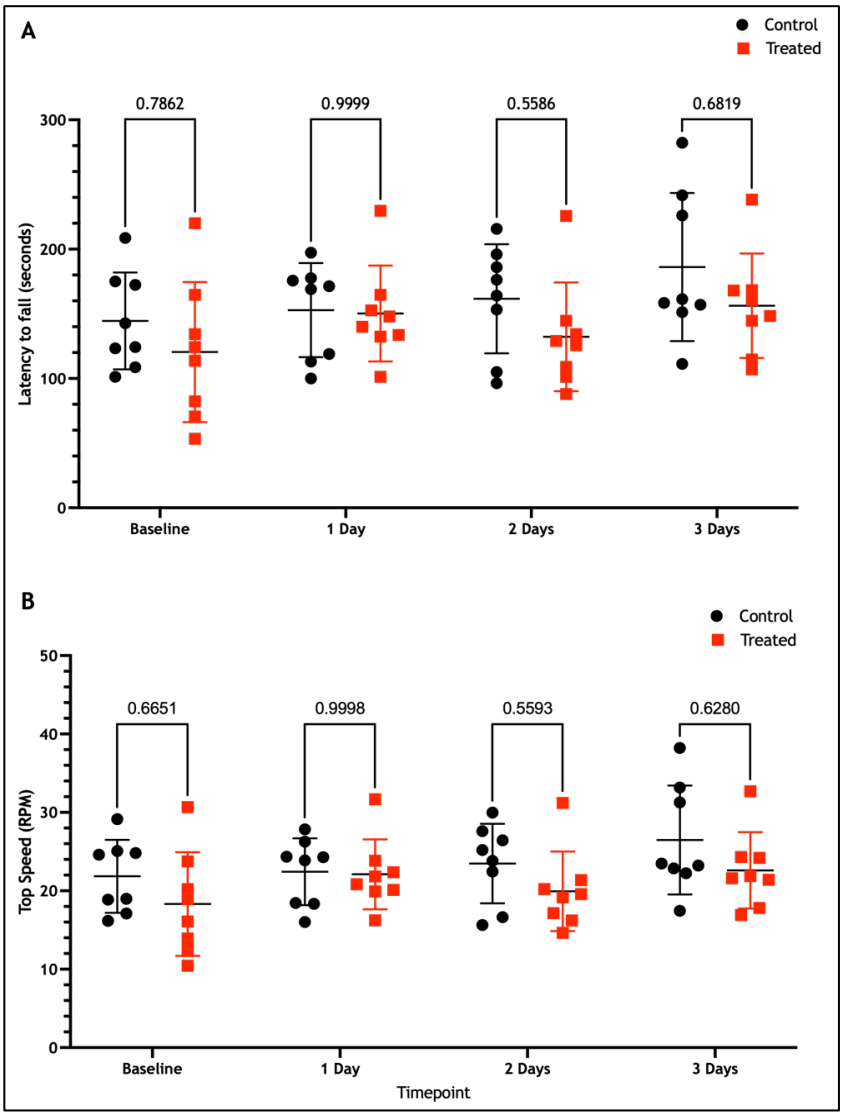

Figure 1: No significant changes in Rotarod latency to fall and top speed recordings between Aldara and Control mice. *Scatterplot displaying individual animals' latency to fall (seconds; A) and top speed (RPM: B) for Control and Aldara groups. Two-way ANOVA with Dunnett's correction for multiple comparisons revealed no significance (p>0.5). Data presented as mean +/- SD, n=8/group.*

6.2.2 Elevated plus maze

Elevated plus maze is a behavioural test for recording anxiety-like behaviours in rodents. This behavioural test uses rodent's innate aversion to open spaces when anxious. Animals exhibiting anxiety-like behaviours will spend more time in the closed arms compared to the exposed open arms (Walf and Frye, 2007). This test was used to further explore the inflammation-induced changes to behaviour, including reduced burrowing previously documented in the Aldara model (McColl et al., 2016).

Individual automatic mouse tracking for elevated plus maze and open field was completed using the ANY-maze video tracking software. Representative images of Control and Aldara mice tracking heatmaps representing duration spent in different areas of the behavioural apparatus can be seen in *Figure 2A-D*. From the individual animal tracking plots (*Figure 2A-D),* it appears both treatment groups displayed a preference to the closed arms. However, there was no significant difference in arm preference shown between closer or open arms within the Control and Aldara groups (*p>0.05: Figure 2E)*. Aldara-treated mice displayed no difference in number of entries into open and closed arms of EPM (*Figure 2E)*. Control mice showed an increasing trend in the number of entries of into the closed arms; however, this did not reach significance (*Figure 2E; p>0.05)*. Aldara mice presented a significant decrease in the number of entries in closed arms compared to Controls (*p<0.05)*.

There was no significant difference in maximum speed displayed by both treatment groups which indicates Aldara-treated mice still possess the capability of movement (*p>0.05: Figure 2F)*, similar to the results for rotarod. However, even though Aldara mice have the capability, a significant decrease in total distance travelled was recorded in Aldara mice compared to Controls (*Figure 2G)*. This overall significant reduction of movement in treated animals was further observed with a decrease in time mobile and increase in time spent immobile ($p<0.005$ and $p<0.05$, respectively: *Figures 2H and I)*. It is possible that this overall reduction in movement within the EPM recordings may explain the reduction in closed arm entries. Rather than links to anxiety-like behaviour, this may be more suggestive of a reluctance for unprompted movement of Aldara-treated mice like observed in-cage.

Overall, the results from the elevated plus maze behavioural test further supports the observation that in-cage spontaneous movement is reduced in Aldara-treated mice compared to Controls. Aldara-treated mice do not display typical anxiety-like behaviour as assessed by elevated plus maze. However, the results suggest an immobility of treated mice with reduced motivation to explore new environments. This contrasts with rodents' innate exploratory behaviour and suggests a change

to this post-Aldara treatment. This potential change to innate behaviour may be suggestive of a rodent manifestation of inflammation-induced SB.

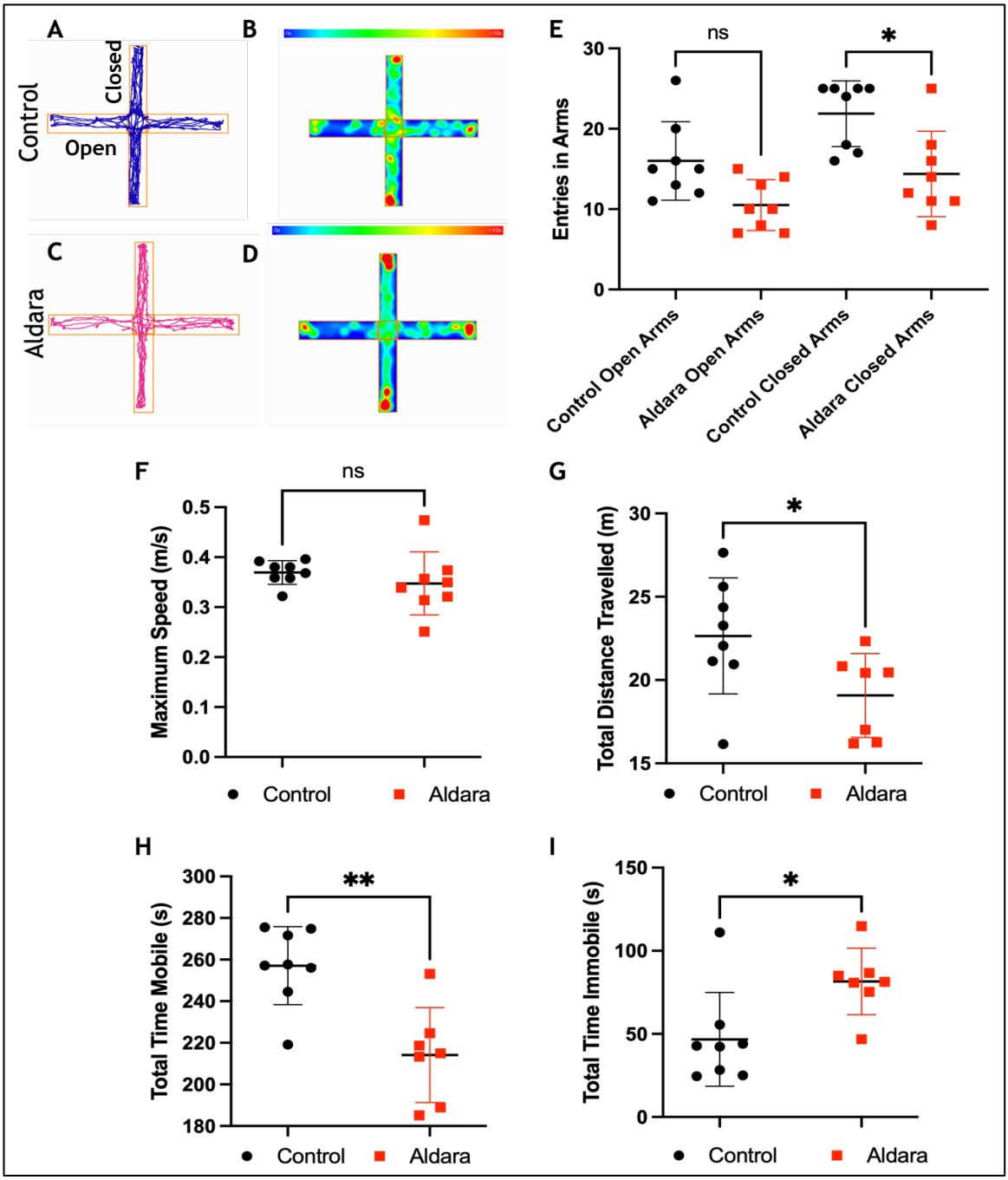

Figure 2: Elevated plus maze behavioural test to investigate presence of anxiety-like behaviours in Aldara-treated mice. *Representative animal tracking plots (A, C) and heatmaps (B, D) for Control and Aldara mice, respectively. Tracking plot shown in (A) shows open and closed arms which was consistent throughout plots. Scatter graphs showing number of entries in open and closed EPM arms with data points representing individual animals (E). Statistical testing via two-way ANOVA with Tukey's correction test for multiple comparisons. EPM recordings for Maximum Speed (m/s: F), Total Distance Travelled (m: G), Total Time Mobile (s: H) and Total Time Immobile (s: I). Statistical testing via unpaired t-test performed (* = p<0.05, ** = p <0.005 and ns>0.05). Data presented as mean +/- SD, n=8/group. EPM behavioural testing carried out by Dr Lilya Andrianova and analysed by Kirstyn Gardner-Stephen.*

6.2.3 Open field

The open field behavioural test is another method for assessing anxiety-like behaviours in rodents. Open field is rooted in rodents' innate exploratory behaviour and healthy mice would naturally investigate both central and peripheral zones of the arena. Mice displaying anxiety-like behaviour would show an aversion to exploring the centre zone and spend most time around the perimeter of the apparatus (Kraeuter et al., 2019).

No significant differences were observed in the recordings from open field tests between Control and Aldara mice for any test parameter ($p>0.05$: *Figure 3)*. Representative single mouse tracking and heatmaps of both treatment groups show a varied exploration across both centre and perimeter zones (*Figure 3A)*. No changes were recorded in the number of entries into the centre and perimeter zones between Control and Aldara groups. ($p>0.05$: Figure *3B)*. Aldara mice mirrored expected preference to perimeter zones compared to the centre with accumulative time significantly increasing in both treatment groups ($p<0.0001$: *Figure 3C)*. No significant differences were found in average speed in all zones and total distance travelled between treatment groups ($p>0.05$: *Figures 3D and E*). The matched speed and distance between treatment groups shows Aldara-treated mice still have the motor ability to complete this test. Overall, no anxiety-like behaviours are displayed by Aldara-treated mice with assessment by the OF test.

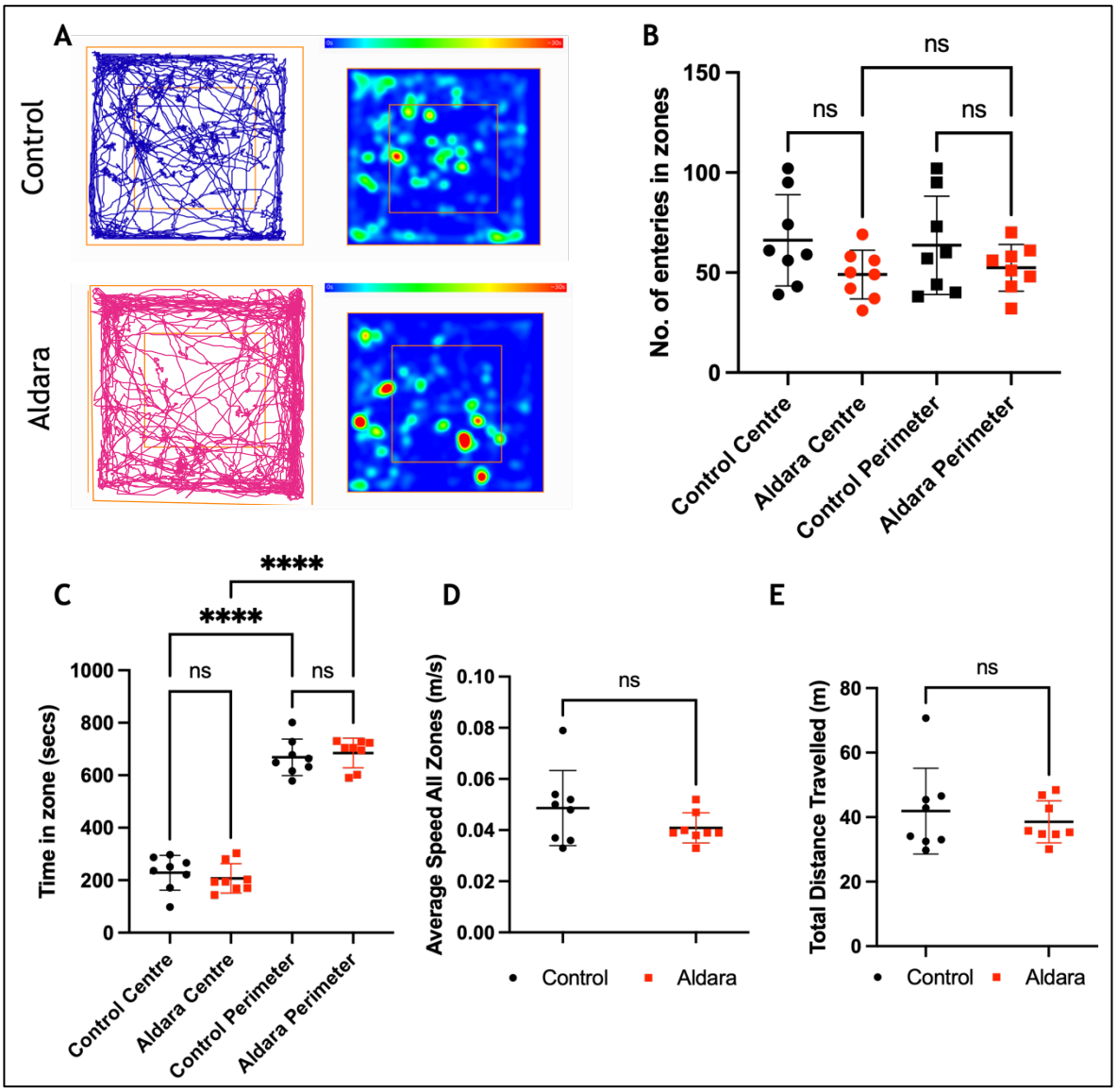

Figure 3: Open field behavioural test to investigate presence of anxiety-like behaviours in Aldara-treated mice. *Representative animal tracking plots (A, C) and heatmaps (B, D) for Control and Aldara mice, respectively. Scatter graphs showing number of entries in centre and perimeter zones with data points representing individual animals (B). Total time spent in centre and perimeter zones (s: C). Statistical testing via one-way ANOVA with Tukey's correction test for multiple comparisons. OF recordings for Average Speed in all zones (m/s: D), Total Distance Travelled (m: E). Statistical testing via unpaired t-test performed (**** = p <0.0001 and ns>0.05). Data presented as mean +/- SD, n=8/group. OF behavioural testing carried out by Dr Lilya Andrianova and analysed by Kirstyn Gardner-Stephen.*

6.2.4 Sucrose preference test

The sucrose preference test provides an assessment of an animal's engagement with a typically rewarding stimuli such as sucrose solution and assesses presence of anhedonia-like behaviours in rodents (Primo et al., 2023). Animals experiencing anhedonic behaviour will stop presenting a sucrose preference over water

consumption. Outputs from the sucrose preference test is presented as a sucrose/water ratio. No preference is indicated by a score of 1, while sucrose preference will be a score of more than 1. A score of 1 or a decrease in this ratio, indicative of reduced sucrose consumption, suggests deficits in reward-seeking behaviour within rodents (Markov, 2022). Morning (AM) and evening (PM) recordings of water and sucrose consumption were noted to account for any circadian rhythm impacts to measurements.

Prior to Aldara cream application, both groups display a preference of sucrose solution compared to water consumption overnight (*Figure 4)*. As Aldara is applied, the treatment group display a continual decrease in sucrose/water ratio compared to the controls. The treated animals are still drinking the same volume with Control mice drinking 1.34ml (*p>0.05:* range = 5.3-0.6 ml) of water on average daily and Aldara-treated mice drinking 1.37ml (range = 4.7-0.7 ml). However, the Aldara-treated mice are lacking the innate preference for sucrose. A significant decrease in sucrose preference in Aldara-treated mice is observed on the morning of day 3 of the model (*p=0.0003:* following 2 topical applications of Aldara). This decrease is also observed on cull day however this difference did not reach significance (*p=0.0576)*. This loss of sucrose preference in Aldara-treated

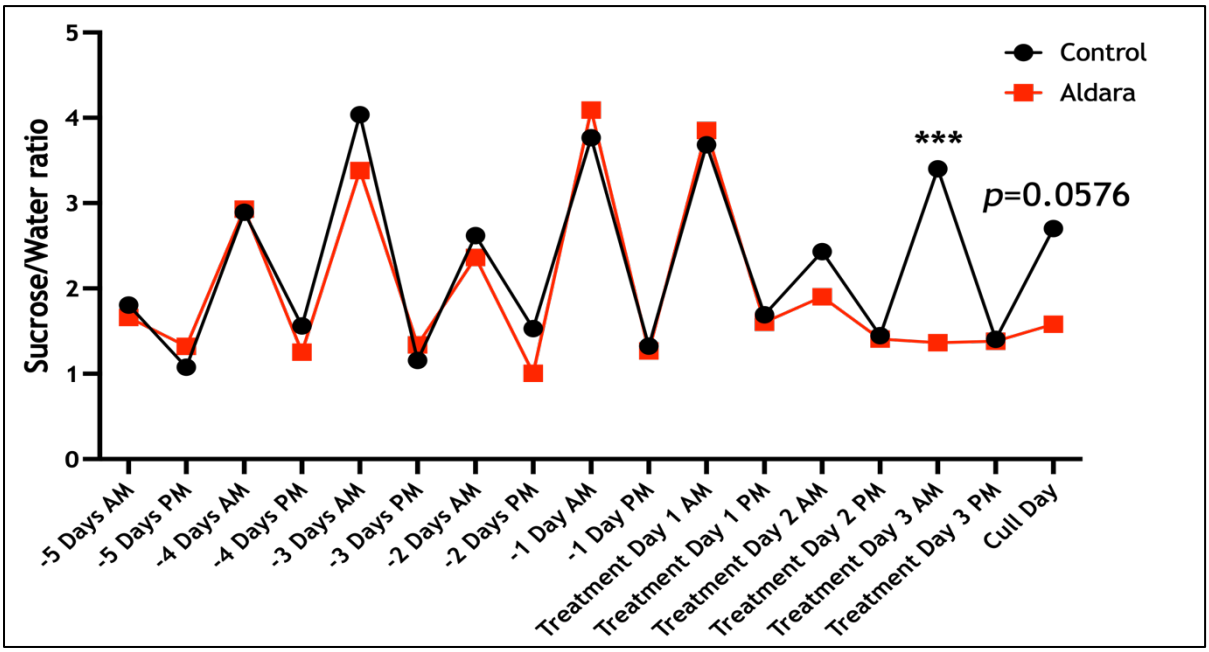

Figure 4: Sucrose preference test shows decrease in sucrose/water ratio after commencement of Aldara treatment compared to Control mice. *Line graph of summary data from Control and Aldara treatment group of sucrose/water ratio prior and after treatment. Two recording taken daily: morning (AM) and evening (PM). 2-Way ANOVA performed with Šídák's test for multiple corrections. ***: p=0.0003, ns>0.05. Statistical testing performed on non-summary data. Data presented as mean +/- SD, n=4/group.*

animals suggests they are experiencing anhedonia-like behaviour, which is a potential change to reward-pathways because of the persistent neuroinflammation in the model.

6.2.5 Nest building

To further investigate relatively more innate in-cage behaviours, nest building abilities of Control and Aldara mice was explored. Typical in-cage behaviours include animals building well-structured nests with pre-shredded nesting material. The act of nest building for mice is both for protective and rewarding goals (Deacon, 2006). Studies have found that assessing nest building abilities of rodents can be an indicator of overall health of the animal (Gaskill et al., 2013). To investigate if Aldara treatment effects reward, animals were provided with equal squares of non-shredded nestlet material with which to shred and build a nest and this was assessed daily.

Nest scores were rated out of 5 as per the grading matrix as presented in *Figure 5A*. This scoring matrix was devised by Dr Lilya Andrianova from the Cavanagh Laboratory and adapted from the Deacon nest building protocol (Deacon, 2006). The highest score of 5 was awarded to high-walled nests constructed with fully shredded material. The lowest score of 1 was awarded for cotton material which remained untouched by animals. Before topical Aldara treatment, both Control and Aldara mice consistently had high ratings of their daily nest building with most animals being scored 5 out of 5 (*Figure 5B)*. No significant difference was found between treatment group prior to topical cream application ($p>0.05$). Following Aldara treatment, Aldara mice display a sudden and maintained decrease in nest rating with average daily ratings amounting to 2 out of 5. This scoring is awarded for mice which have shredded the nesting material but not made a typical nest shape with sufficient wall height. Each daily application results in a significant decrease in Aldara mice nesting scores compared to Controls (*Figure 5B; $p<0.05$)*. Control mice consistently scored high values of 4 or 5 for nest building. Overall, this reduction in quality of nests built by Aldara-treated mice suggest a possible reduction in reward from the activity. This decreased interaction with the reward activity may be suggestive of anhedonia within Aldara-treated mice. Additionally, due to the ongoing peripheral and central inflammation in Aldara-treated mice,

there may be a lack of motivation demonstrated by the nesting behaviour deficits (Xeni et al., 2024).

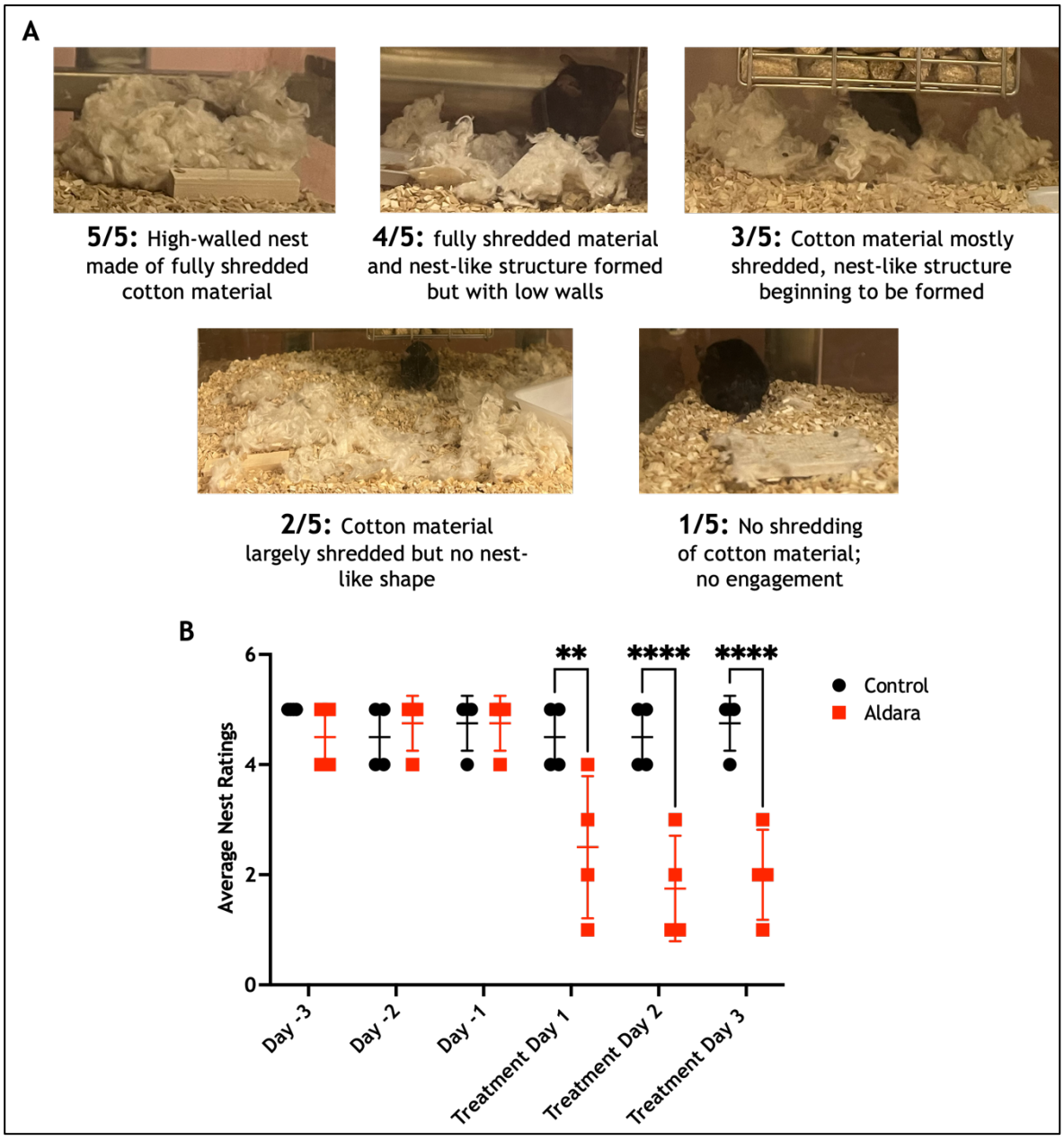

Figure 5: Aldara-treatment diminishes quality nest building ability. *Representative images of 5 possible scores for nest building behavioural assay (A). Scatterplot displaying average nest ratings (out of 5) for Control and Aldara treatment groups (B). Two-way ANOVA with Šídák's correction test for multiple comparisons. Ns comparisons not shown on graph ($p>0.05$). ** = $p<0.0021$, **** = $p<0.0001$. Data presented as mean +/- SD, n=4/group.*

6.2.6 Transcriptional changes to dopamine-related and reward network-related genes

Localisation of functional change is important when assessing behaviour. Changes to transcription in neural pathways were observed at the whole brain level previously shown by bulk RNA sequencing in chapter 3. Next, to assess changes specifically to dopamine neurotransmission-related underpinning reward behaviours, transcriptional dopamine-related biology in the whole brain was explored. A list of dopamine-related genes determined for whole brain transcriptional analysis can be observed in the heatmap presented in *Figure 6*. Only one gene from this list was found to be significantly changed and downregulated in Aldara-treated mice: *Th (Figure 6: p*<0.05*)*. This gene is involved

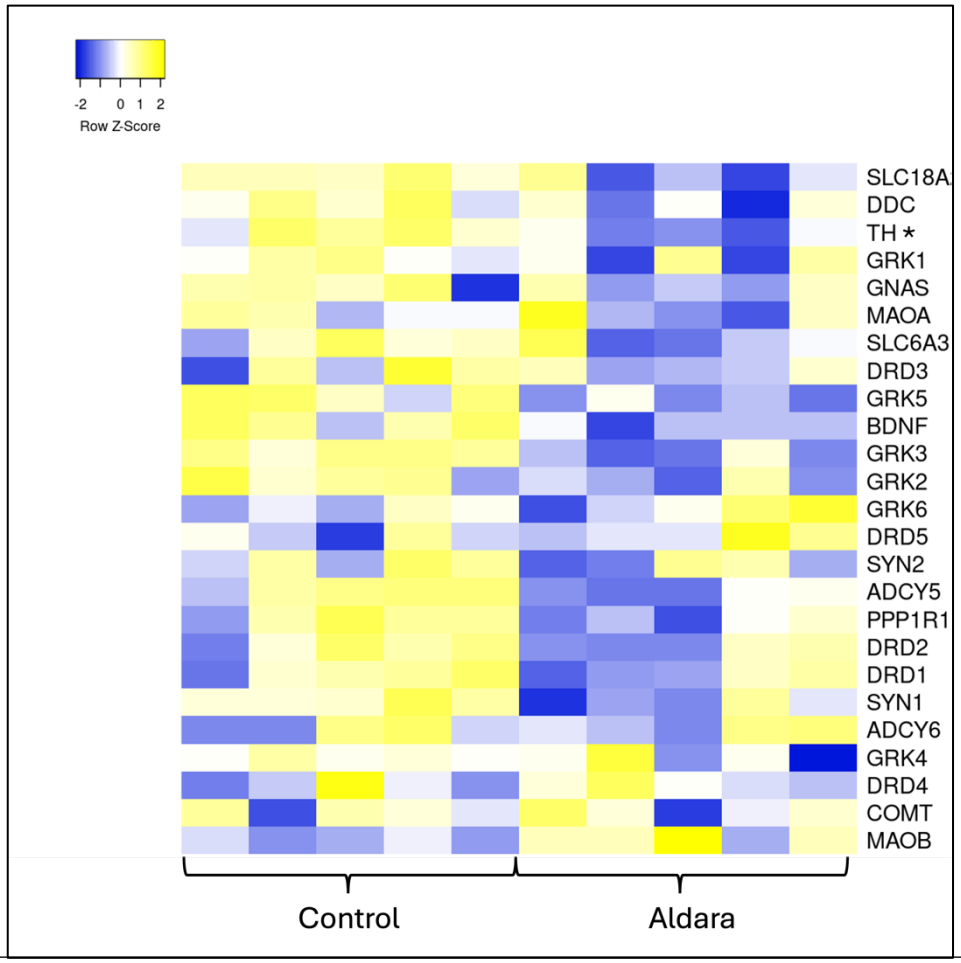

Figure 6: Gene which codes for enzyme tyrosine hydroxylase (TH) is the only significantly changed dopamine-related gene change at whole-brain bulk RNAseq following Aldara treatment. *Heatmap of dopamine-related genes from three-day treatment Bulk RNA Sequencing dataset. Columns indicate biological replicates within treatment groups. Expression levels of genes have been row-scaled into z-scores. Colour intensity represents expression level with yellow showing upregulated genes (positive Z-score) and blue showing downregulated genes (negative Z-score). P.adj < 0.05 shown by (*). Average linkage by rows clustering method and Pearson distance measurement method used. N=5/group.*

in dopamine signalling as it codes for the protein tyrosine hydroxylase (TH) which is the rate-limiting enzyme producing dopamine (Daubner et al., 2011). This suggests a global decrease in dopamine synthesis via downregulation of this key enzyme. This potential reduction in bioavailability of dopamine may result in deficits in reward circuitry. No other significant changes to genes related to dopamine transmission were observed ($p>0.05$). Although previously behavioural tests suggest a change to the reward-driven behaviours, this lack of significant changes at the whole brain shown that the CNS is still maintaining dopamine neurotransmission. A complete disruption of dopamine neurotransmission is not entirely expected at this relative acute timepoint of neuroinflammation (3-days).

6.2.7 Spatial transcriptomics of reward-related brain regions

Both in previous studies and earlier in this chapter, changes to suspected reward-driven tasks is observed following Aldara treatment. This includes changing to burrowing behaviour (McColl et al., 2016), decreased nest building ability and sucrose preference. To begin to explain these changes of reward behaviour documented within the Aldara model, transcriptomic changes within brain regions linked to reward were explored using the spatial transcriptomic CosMx mouse neuroscience 1000-plex RNA panel. A cell agnostic, pseudo-bulk analysis approach allowed for analysis of region-specific transcriptomic changes. This pseudo-bulk approached involved all cell types and resembled more of a 'bulk' readout from the regions of interest (ROI). Considering the literature discussed previously in this

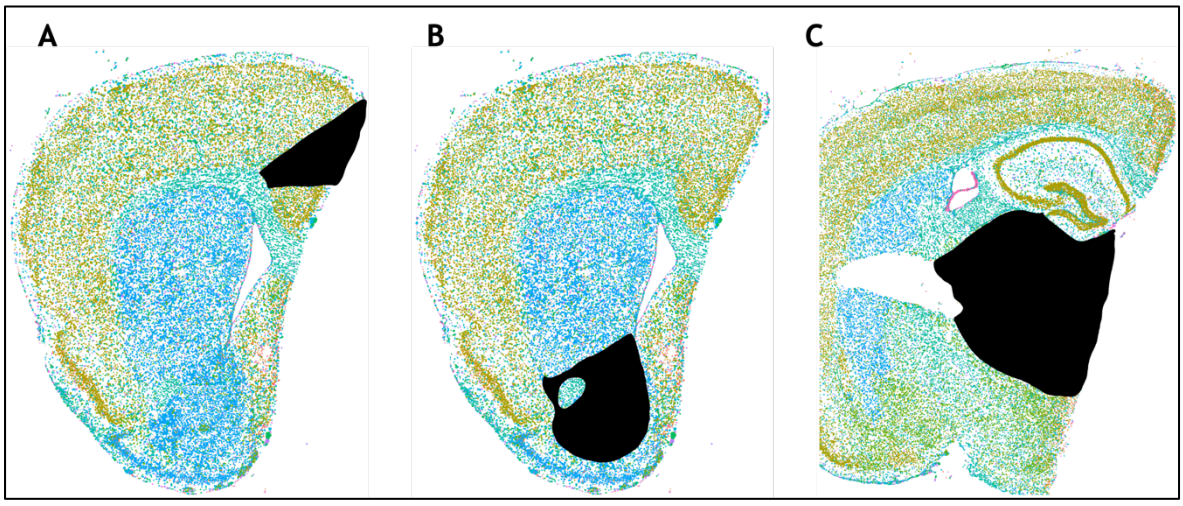

Figure 7: Representative ROI masks of brain regions associated with reward behaviour used for CosMx pseudo-bulk analysis. *ROI masks drawn using Allen coronal mouse brain atlas as reference. ROIs include ACC (A), NAc (B) and thalamus (C). Masks drawn using iPad application Procreate.*

chapter surrounding the NAc, thalamus and ACC in relation to reward, these brain regions were selected for ROI analysis. These were determined using the Allen Coronal Mouse Brain Atlas (Xu et al., 2024, James et al., 2021, Xiao et al., 2024). A representative image of the hand-drawn ROI 'masks' can be seen in *Figure 7*.

PCA shows the gene expression data of cell agnostic pseudo-bulk analysis from NAc with the Control and Aldara naturally separating into 2 distinct groups (*Figure 8A)*. This suggests PC1 may be indicative of treatment and PC2 represents expected biological variability among animals. The lollipop graph shows 47 genes are significantly upregulated in Aldara samples compared to control and 14 downregulated (*Figure 8B:* p.adj<0.05 and absolute log_2 fold change >0.5 and <-0.5, respectively). The heatmap featured in *Figure 8D* highlights the DEGs and their pattern of transcriptional changes across treatment groups. Aldara samples displaying a distinct set of both significantly upregulated and downregulated genes compared to Control (*p.adj<0.05*). The top significantly upregulated genes in NAc include primarily neuroinflammation-related genes such as *B2m, Gfap, Apod, Gbp2* and *Tspo*. The top significantly downregulated genes in the NAc relate to both neurotransmission and immune functions which include *Snca, Itm2a, Cartpt, Pcp4* and *Phactr1*. The top ten upregulated and downregulated genes ranked by Log_2 fold change can be seen in *Table 6.1*.

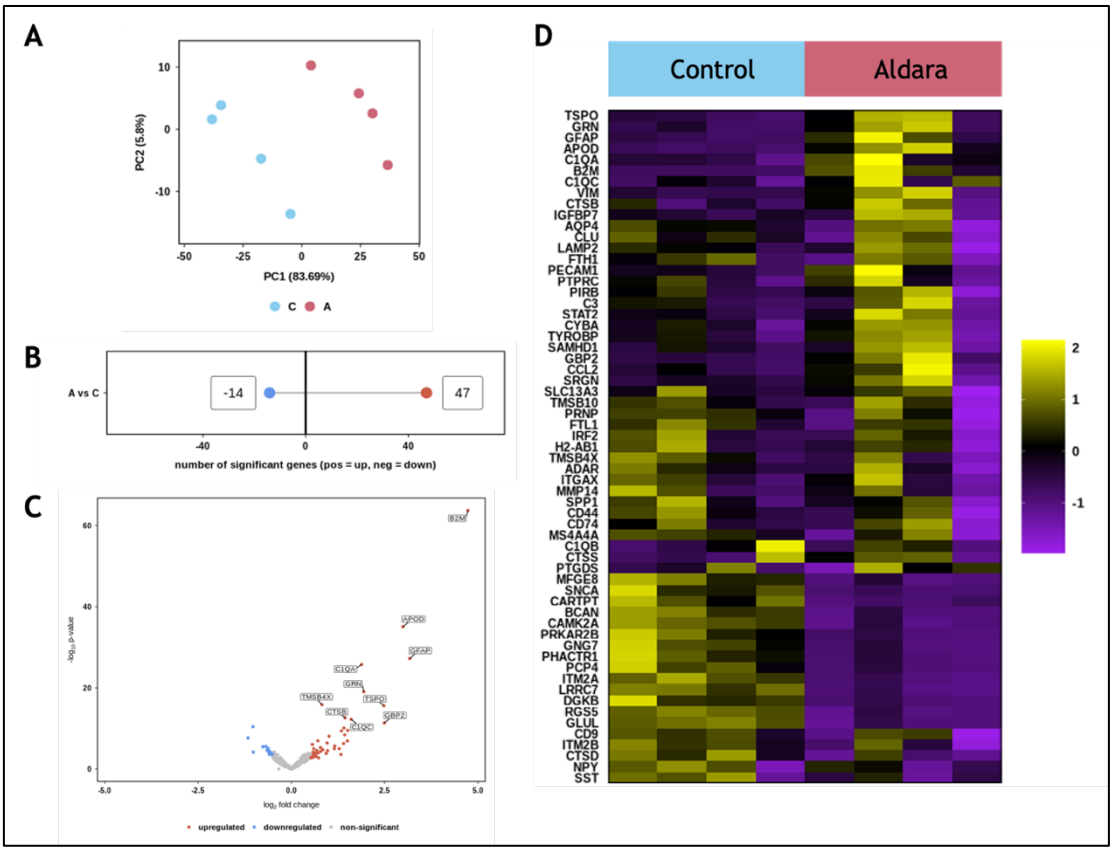

Figure 8: Pseudo-bulk cell agnostic differential expression analysis of NAc ROI from CosMx spatial transcriptomics platform. *(A) PCA scatterplots showing gene expression data for Control [blue] and Aldara [red]. Individual samples represented by dots. (B) Lollipop graph showing number of significantly DEGs [p.adj <0.05, absolute log_2fold >0.5]. (C) Volcano plot of significantly DEGs with upregulated shown in red, downregulated in blue and non-significant in grey. (D) Hierarchically clustered heatmap of DEGs in Control and Aldara samples. Expression levels shown are row-scaled into Z-scores with yellow representing high expression and purple representing low expression.*

Table 6.1: Top 10 upregulated (left) and downregulated (right) DEGs in NAc

Gene	log2fold	p	p.adj
B2M	4.73	1.972888e-64	1.970915e-61
GFAP	3.17	6.042108e-28	2.012022e-25
APOD	2.99	8.860275e-36	4.425707e-33
GBP2	2.49	4.888851e-12	4.883962e-10
TSPO	2.48	2.625936e-16	3.747586e-14
GRN	1.94	9.331840e-20	1.864502e-17
C1QA	1.88	1.788883e-26	4.467735e-24
VIM	1.83	1.278697e-10	9.826294e-09
C1QC	1.60	5.822879e-13	6.463395e-11
PECAM1	1.51	3.183497e-10	2.271653e-08

Gene	log2fold	p	p.adj
SNCA	-1.16	2.408340e-08	1.336629e-06
ITM2A	-1.03	3.843433e-11	3.490536e-09
CARTPT	-1.02	7.434452e-05	1.710253e-03
PCP4	-0.76	3.288452e-06	1.216727e-04
PHACTR1	-0.68	2.835581e-06	1.089517e-04
RGS5	-0.65	2.699454e-05	7.490985e-04
MFGE8	-0.65	2.014378e-05	5.749610e-04
BCAN	-0.62	8.168900e-06	2.814045e-04
DGKB	-0.61	6.267364e-05	1.527097e-03
GLUL	-0.59	2.578728e-04	4.600267e-03

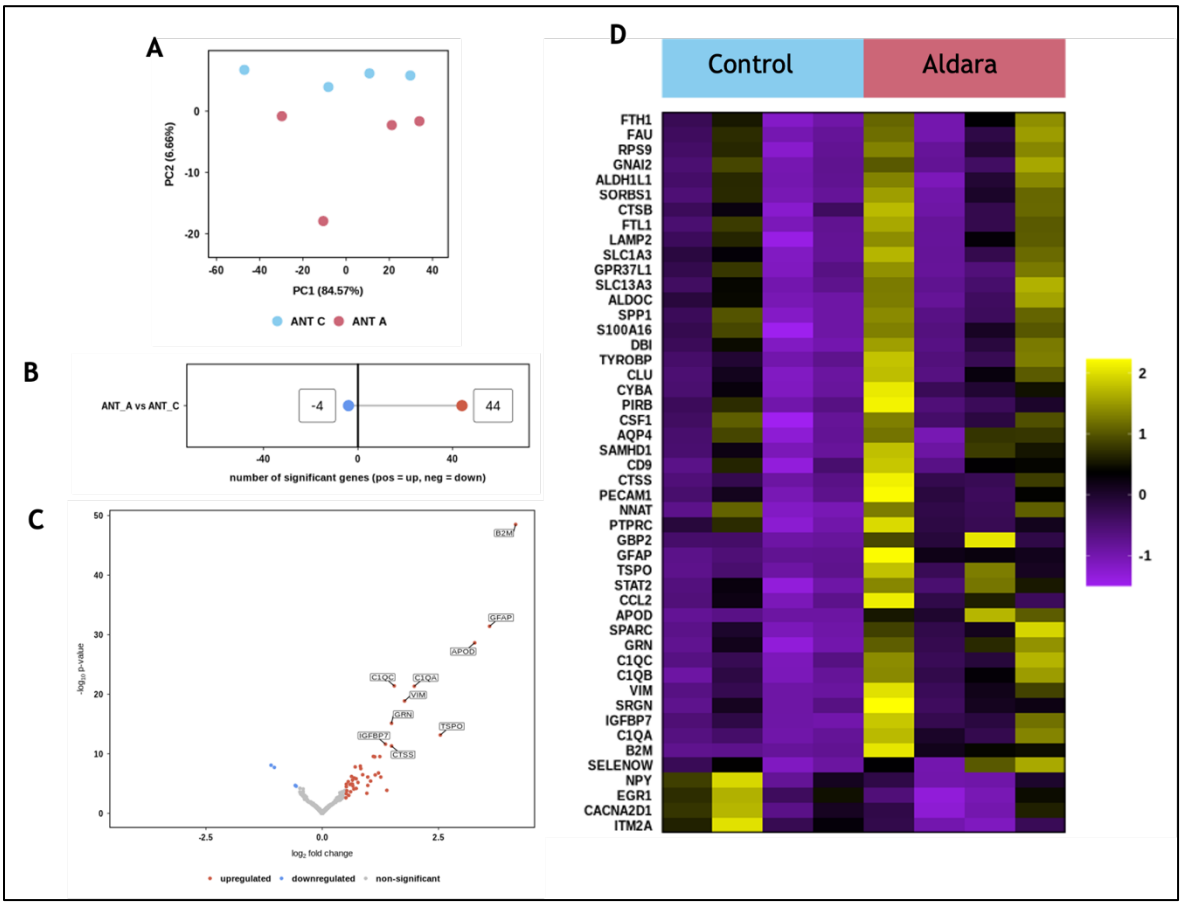

Figure 9: Pseudo-bulk cell agnostic differential expression analysis of ACC ROI from CosMx spatial transcriptomics platform. *(A) PCA scatterplots showing gene expression data for Control [blue] and Aldara [red]. Individual samples represented by dots. (B) Lollipop graph showing number of significantly DEGs [p.adj <0.05, absolute log_2fold >0.5]. (C) Volcano plot of significantly DEGs with upregulated shown in red, downregulated in blue and non-significant in grey. (D) Hierarchically clustered heatmap of DEGs in Control and Aldara samples. Expression levels shown are row-scaled into Z-scores with yellow representing high expression and purple representing low expression.*

PCA shows the gene expression data of cell agnostic pseudo-bulk analysis from ACC with the Control and Aldara separating into 2 groups (*Figure 9A)*. One Aldara sample, "S1055BS3 ANT A", is displayed as distinctly different in the PCA with respect to PC2. This variation may be explained with the biological replicate displaying larger effects of biological variability. This animal is represented by the second Aldara column in the heatmap in *Figure 9D*. Providing this animal's neural transcriptional response with relatively decreased compared to other Aldara-treated mice suggests a possible dampened biological response overall. For other samples, PC1 represents expected biological variability between animals and PC2 may be indicative of treatment. The lollipop graph shows 44 genes being significantly upregulated in Aldara samples compared to control and 4

downregulated (*Figure 9B:* p.adj<0.05 and absolute log_2 fold change >0.5 and <-0.5, respectively). The heatmap featured in *Figure 9D* highlights the DEGs and their pattern of transcriptional changes with Aldara samples displaying a relatively variable expression pattern of upregulated and downregulated genes. The top significantly upregulated genes in ACC include primarily neuroinflammation-related genes such as *B2m, Gfap, Apod, Tspo* and *C1qa*. The top significantly downregulated genes in the PFC relate to neurotransmission and synaptic plasticity and these include *Itm2a, Egr1, Npy* and *Cacna2d1 and Atp2b4*. The top ten upregulated and downregulated genes ranked by log_2 fold change can be seen in *Table 6.2*

Table 6.2: Top 10 upregulated (left) and downregulated (right) DEGs in ACC CosMx ROI

Gene	log2fold	p	p.adj
B2M	4.16	3.094699e-49	3.094699e-46
GFAP	3.60	3.893699e-32	1.946850e-29
APOD	3.28	2.268683e-29	7.562277e-27
TSPO	2.54	6.941640e-14	8.677050e-12
C1QA	1.98	4.573908e-22	9.147817e-20
VIM	1.77	1.360607e-19	2.267678e-17
C1QC	1.55	4.021170e-22	9.147817e-20
GRN	1.49	7.510814e-16	1.072973e-13
CTSS	1.49	4.727504e-12	4.727504e-10
GBP2	1.39	1.334613e-04	3.033211e-03

Gene	log2fold	p	p.adj
ITM2A	-1.10	8.175381e-09	5.839558e-07
EGR1	-1.03	1.935004e-08	1.138237e-06
NPY	-0.58	2.052361e-05	5.703254e-04
CACNA2D1	-0.56	2.714774e-05	7.144141e-04
ATP2B4	-0.48	2.427581e-04	4.759964e-03
PRKCB	-0.48	6.076526e-05	1.519131e-03
HOMER1	-0.47	3.837686e-04	7.240917e-03
ARPP21	-0.46	5.883584e-04	1.014411e-02
SST	-0.45	6.035445e-04	1.022957e-02
STMN2	-0.44	4.745873e-04	8.474774e-03

PCA shows the gene expression data of cell agnostic pseudo-bulk analysis from thalamus with the Control and Aldara naturally separating into 2 distinct groups (*Figure 10A)*. This suggests PC1 may represent expected biological variability between animals and PC2 may indicate treatment. The lollipop graph shows 29 genes being significantly upregulated in Aldara samples compared to control and 4 downregulated (*Figure 10B:* p.adj<0.05 and absolute log_2 fold >0.5 and <-0.5, respectively). The heatmap featured in *Figure 10D* highlights the DEGs and their pattern of transcriptional changes with Aldara samples which displays a broad increase of gene expression compared to Control mice. Similar to the NAc, the top significantly upregulated genes in thalamus include primarily neuroinflammation-related genes such as *B2m, Gfap, Apod, Gbp2* and *Tspo*. The top significantly downregulated genes in the thalamus relate to synaptic signalling, myelin biology and immune functions. This includes *Adcy1, Bcan, Pllp, Shc3 and Itm2a*. The top

ten upregulated and downregulated genes ranked by log_2 fold change can be seen in *Table 6.3*.

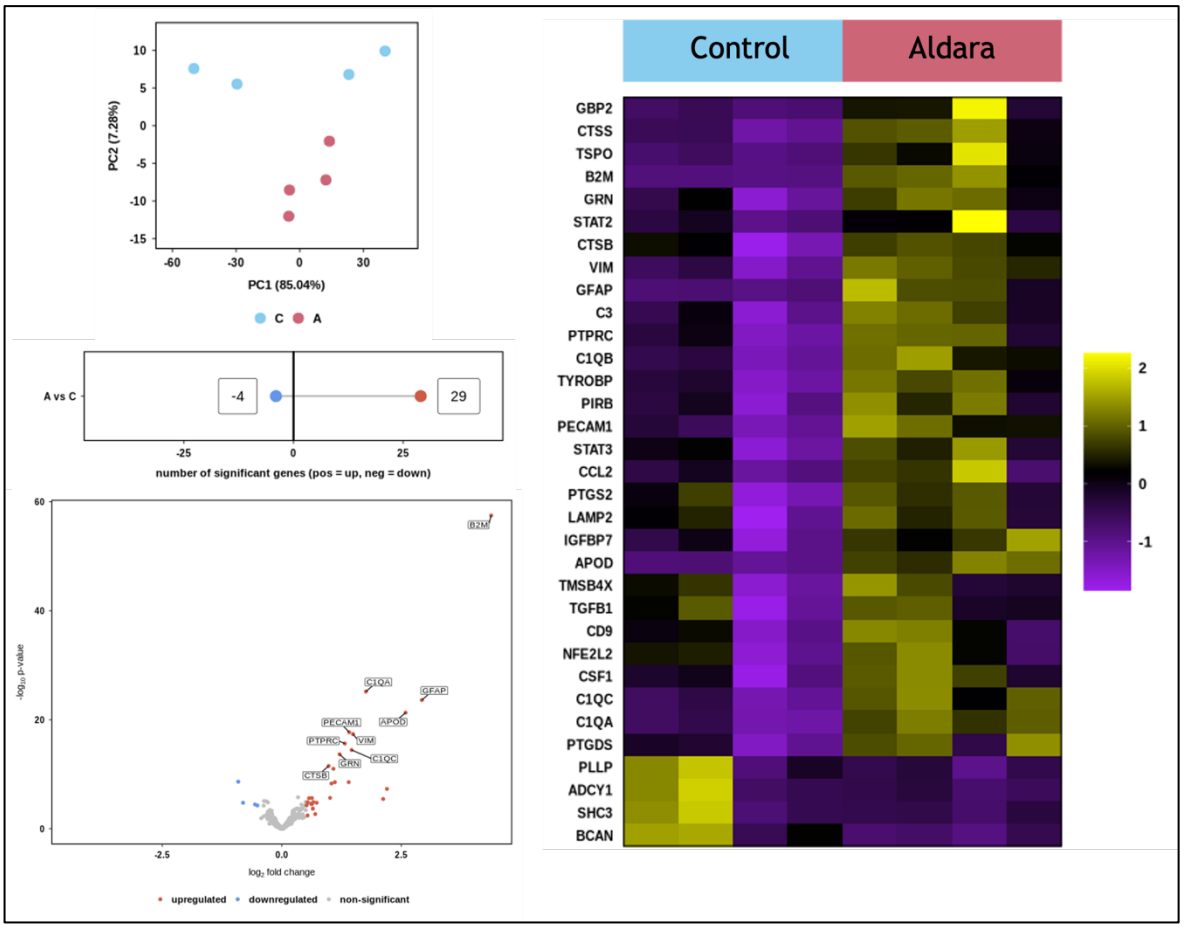

Figure 10: Pseudo-bulk cell agnostic differential expression analysis of thalamus ROI from CosMx spatial transcriptomics platform. *(A) PCA scatterplots showing gene expression data for Control [blue] and Aldara [red]. Individual samples represented by dots. (B) Lollipop graph showing number of significantly DEGs [p.adj <0.05, absolute log_2fold >0.5]. (C) Volcano plot of significantly DEGs with upregulated shown in red, downregulated in blue and non-significant in grey. (D) Hierarchically clustered heatmap of DEGs in Control and Aldara samples. Expression levels shown are row-scaled into Z-scores with yellow representing high expression and purple representing low expression.*

Table 6.3: Top 10 upregulated (left) and downregulated (right) DEGs in Thalamus CosMx ROI

Gene	log2fold	p	p.adj
B2M	4.38	3.326743e-58	3.326743e-55
GFAP	2.93	2.404949e-24	8.016498e-22
APOD	2.59	4.857314e-22	1.214328e-19
TSPO	2.20	4.830367e-08	2.841392e-06
GBP2	2.12	3.401410e-06	1.546095e-04
C1QA	1.76	6.621262e-26	3.310631e-23
VIM	1.49	4.132720e-18	6.887867e-16
C1QC	1.46	3.487744e-15	4.359680e-13
PECAM1	1.41	1.931629e-18	3.863258e-16
CTSS	1.40	2.745173e-09	1.864547e-07

Gene	log2fold	p	p.adj
ADCY1	-0.91	2.278434e-09	1.752641e-07
BCAN	-0.81	1.668628e-05	5.562094e-04
PLLP	-0.56	3.396683e-05	9.990246e-04
SHC3	-0.51	5.181243e-05	1.400336e-03
ITM2A	-0.43	1.177109e-02	1.023573e-01
GNAL	-0.38	5.509168e-05	1.449781e-03
PLTP	-0.38	5.391125e-03	6.196695e-02
P2RY12	-0.37	8.109214e-06	3.525745e-04
PCDH15	-0.32	9.228860e-06	3.845359e-04
ARPP21	-0.32	2.634289e-03	3.817810e-02

To explore patterns of commonality and uniqueness in transcriptional change across reward-related ROIs, a similar approach implemented as in chapter 4 of this thesis. A threshold of significant gene expression was set to log_2fold >1.0 for upregulated and log_2fold <-0.5 for downregulated.

As seen in *Figure 11* and *12*, Venn diagrams show upregulated and downregulated genes from the CosMx panel which met this log_2fold change threshold stated above. *Figure* 11 shows the common and uniquely upregulated genes across the ACC, NAc and thalamus. Twelve genes were commonly upregulated across all 3 reward-related ROIs. These genes encode for proteins primarily involved in immune activation and pro-inflammatory processes (*B2m, C1qa, C1qc, Ctss, Gbp2* and *Tspo),* glial reactivity (*Gfap, Vim* and *Tyrobp)* and cellular adhesion (*Pecam1)*.

The ACC uniquely upregulated *Sparc* which codes for a cell-matrix protein which has been found to be involved in maintenance of BBB integrity *in vitro* (Alkabie et al., 2016). The NAc uniquely upregulated 5 genes which code for proteins involved in immune responses (*Ctsb, Ccl2, Samhd1* and *Pirb)* and *Slc13a3* which codes for a Na^+-dependent dicarboxylate transport protein. The thalamus had no uniquely expressed genes and only expressed the 12 inflammation-related genes common throughout all 3 ROIs.

Some transcripts were commonly shared between 2 of the 3 reward-related ROIs. Three genes commonly shared between the ACC and NAc were *Cyba, Stat2* and *Srgn*. The proteins encoded by these genes are involved in immune processes including IFN signalling and secretory processes underpinning inflammation. Common upregulation of the genes *Ctss* and *C1qb* in the ACC and thalamus is further suggestive of complement-driven inflammatory processes and antigen presentation. More immune processes are suggested by the NAc and thalamus upregulating *Ptprc* and *C3* which encode for the pan immune CD45 and another complement signalling protein, respectively.

Overall, the upregulated genes across all 3 ROIs primarily present an immune-focused biology including pro-inflammatory processes including cell adhesions and astrocyte and microglia reactivity. Immune cell presence and antigen presentation processes are suggested at this transcriptional level. This supports the suggestion of global neuroinflammation present in the Aldara model shown by the whole-brain bulk RNA sequencing data presented in chapter 3 of this thesis.

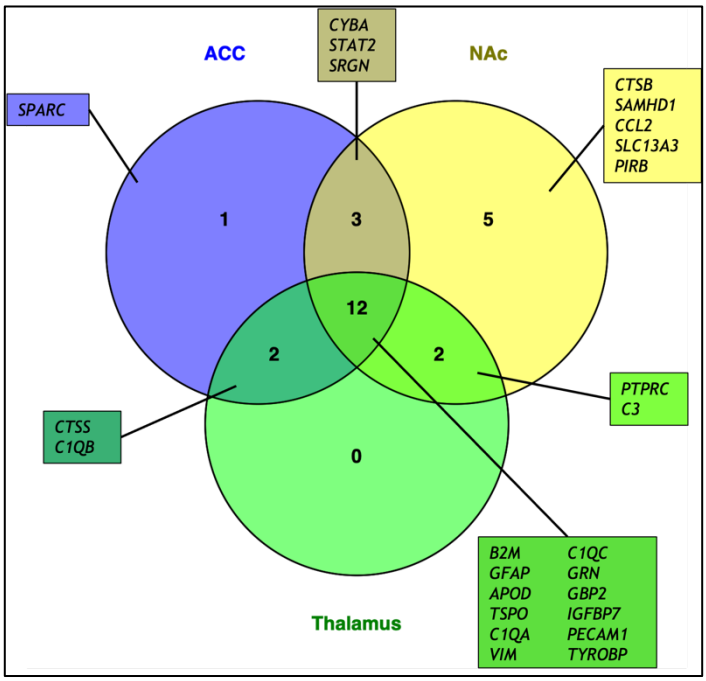

Figure 11: Commonality of top 10 pseudo-bulk upregulated genes in three ROIs (NAc, ACC and thalamus) from CosMx. *Venn diagram representing overlap in significantly upregulated genes log_2 fold change>1.0 in three ROIs. Text corresponds with commonly shared genes between ROIs. Figure created using Venny 2.0.*

Downregulated genes across the 3 reward-related areas demonstrate relatively more uniqueness compared to upregulated genes (*Figure 12)*. No common genes were found to be downregulated across the ACC, NAc and thalamus. The ACC uniquely downregulated 3 genes which code for proteins involved in both homeostatic and pathological inflammatory processes (*Egr1) (*Yang et al., 2024*)*, calcium signalling (*Cacna2d1)* and appetite signals and potential neuroprotective properties (*Npy) (*Stanley et al., 1986*)*. The NAc uniquely downregulated 11 genes which code for proteins involved in synaptic vesicle trafficking (*Snca) (Burre, 2015)*, neuronal signalling (*Camk2a, Ppkar2b* and *Dgkb)* (Kool et al., 2019, Hozumi and Goto, 2012), reward pathway (*Cartpt)* (Rogge et al., 2008) and glutamine synthesis (*Glul)*. The thalamus uniquely downregulated three genes which code

for proteins in dopamine signalling and dopaminergic neuronal health (*Adcy1) (Hwang et al., 2013)* and myelin sheath functions (*Pllp)*. Overall, the downregulated genes across reward-related ROIs present a relatively more neuronal-focused biology including signalling, neuroprotective and dopaminergic changes. This suggests a regional specific depression of neurotransmission-related genes which may explain changes in reward-driven behaviours exhibited in Aldara-treated mice.

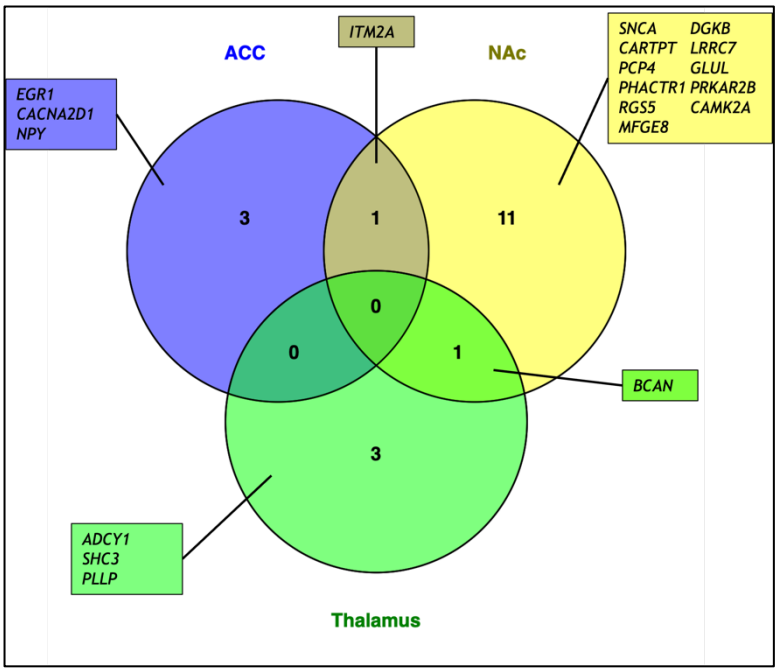

Figure 12: Commonality of top 10 pseudo-bulk downregulated genes in 3 ROIs (NAc, PFC and thalamus) from CosMx. *Venn diagram representing overlap in top significantly downregulated genes log_2 fold change <-0.5. in three ROIs. Text corresponds with commonly shared genes between ROIs. Figure created using Venny 2.0.*

6.3 Discussion

Several neuropsychiatric conditions, including MDD, commonly present with anhedonia as a clinical symptom (Der-Avakian and Markou, 2012). Individuals experiencing anhedonia report a loss of pleasure in activities and decreased engagement with the world. The neurobiology underpinning anhedonia is not fully understood. This lack of mechanistic knowledge resulting in anhedonia leaves minimal condition-specific targets for novel therapeutics. Animal models cannot fully recapitulate these complex human emotions/behaviours (Barroca et al., 2022). However, they can be investigative tools to begin detailing the molecular

mechanisms potentially causing these neuropsychiatric symptoms. Here the Aldara model has been used as a TLR7-driven neuroinflammatory model to study possible pathways leading to anhedonia-like behaviours.

Previous evidence of potential reward circuitry deficits within the Aldara model were presented by reduction of burrowing behaviour (McColl et al., 2016). Changes to in-cage innate behaviours allow for the assessment of overall animal wellbeing and may be indicative of inflammation-induced behavioural changes within mice but are not quantitative (Jirkof, 2014, Aubert, 1999). To further characterise the inflammation-induced behavioural changes specifically induced by the Aldara model, a battery of behavioural tests were used to establish anxiety-like behaviours, anhedonia and motor capability.

Following Aldara treatment, mice did not display any significant changes to motor functional via rotarod testing. Open field and elevated plus maze did not reveal presence of anxiety-like behaviour in Aldara-treated mice. However, a significant decrease in total distance in the elevated plus maze was recorded for Aldara-treated mice. Anhedonia-like behaviours were present in Aldara mice with a significant decrease in sucrose preference recorded during the model's time course.

For the decrease in total movement in elevated plus maze, this mirrors observations of a reduction in in-cage movements and exploratory behaviour by Aldara-treated animals compared to Control mice (*Unpublished observation, Kirstyn Gardner-Stephen*). Reduction in elevated plus maze distance travelled has been recorded in other neuroinflammatory models which highlights potential centrally controlled functional deficits (Wagnon et al., 2023). This may suggest an overall reluctance to move by animals experiencing neuroinflammation and is potentially a functional deficit caused by both the peripheral and central inflammation exhibited within the Aldara model. This reduced movement may also be a conservatory action exhibited by Aldara mice as a result of presence of SB.

Two behavioural tests which focus more on characterising presence and changes in reward-driven tasks are the sucrose preference test and nest building (Primo et al., 2023). The decrease of sucrose preference observed in Aldara treated mice

may indicate reduced pursuit of typically rewarding stimuli. The sucrose preference test and changes in its functional output are commonly associated with the NAc due to the behavioural test investigating reward-related behaviours (He et al., 2020, Primo et al., 2023). This is a well utilised and validated anhedonia test with other mouse models, including CUMS, showing presence of this depressive-like symptom in a decrease of sucrose preference (Markov, 2022).

Nest building is a behavioural assay routed in investigating in-cage innate behaviours of mice. Deficits in this ability may be indicative of reduced well-being of animals and reward circuit deficits. Aldara mice display a significant decrease following topical cream application of the TLR7 agonist IMQ. This may be indicative of an overall reduction in reward-seeking behaviour consequential of the ongoing peripheral and central TLR7-driven inflammation. These reward circuit deficits are observed in other neuroinflammatory models including systemic LPS treatment (Teeling et al., 2007).

Mice from this neuroinflammatory model do not present with anxiety-like symptoms as observed in other neuroinflammatory models such as systemic LPS and CUMS models (Yin et al., 2023a, O'Connor et al., 2009, Alqurashi et al., 2022). However, mice from the Aldara model present with a considerably more inflammation-based sickness phenotype including reduced spontaneous movement, sucrose preference and observed in-cage innate behaviours. This reduced movement and lack of engagement in typically rewarding stimuli in Aldara mice mirror human equivalent SB. These functional changes following Aldara treatment may be a conservatory response following the onset of peripheral and central inflammation (Dantzer, 2023). This disengagement and presence of SB may be linked to reward deficits in Aldara-treated mice. Other inflammatory models and human equivalents, such as peripheral injection of LPS, trigger a reduction in effort exerted for rewarding stimuli (Draper et al., 2018, Vichaya et al., 2014). This evidence suggests the use of the Aldara model as a TLR7 inflammation-driven SB model with presence of potential reward-deficits.

Across all selected reward-related brain regions from the spatial transcriptomic dataset, despite the limitations of the panel, a clear inflammation and immune-related transcriptional environment is presented with upregulated genes. This is

consistent with the previously presented whole-brain slice CosMx cell cluster changes in chapter 4 of this thesis and the whole-brain bulk RNA sequencing results which both reveal an immune-focused upregulated biology at the transcript level.

Classic inflammatory markers which were upregulated across all 3 reward-related brain regions include genes encoding proteins involved in the complement cascade (*C1qa* and *C1qc)* and microglia reactivity (*Gbp2)* and including promotion of anti-inflammatory phenotype of the brain-resident myeloid population (*Trem2)* (You et al., 2024, Xue and Du, 2021, Zhou et al., 2024*)*. At this regional level, this transcriptional evidence again suggests a multi-cellular mechanisms underpinning the neuroinflammation.

Two other commonly upregulated genes within the NAc, thalamus and PFC included *Gfap* and *Vim* which both have been linked to astrocyte reactivity in neuroinflammatory environments (Liu et al., 2014). Reactive astrocytes and microglia exhibit crosstalk within neuroinflammatory environments and both promote proinflammatory mechanisms (Liddelow et al., 2017). Therefore, this is a potential mechanism demonstrated in the Aldara model via upregulation of *C1qa* and *C1qc* in the selected CosMx reward brain regions (Liu et al., 2024). This upregulation of several pro-inflammatory mechanisms can directly target and alter neuronal function resulting in changes to neurotransmission, as shown in AD mouse models (Gomes et al., 2024, Edison, 2024). The regionally indiscriminative increase of inflammation within the reward-related brain regions further demonstrates the global pro-inflammatory nature of the Aldara. Additionally, transcriptional evidence for glial modulation of this neuroinflammation is present.

The presence of neuroinflammation has been established as a factor of behavioural changes in a number of both pre-clinical and clinical contexts including rodent models of chronic social stress and patients with MDD (Vichaya and Dantzer, 2018, Rengasamy et al., 2023, Zhang et al., 2024). Increased inflammation in brain regions controlling reward behaviours can result in disturbed neural circuitry and changes to the functional outputs (Greene et al., 2019). Inflammation present in the NAc has been found to underpin depressive-like behaviours in mice which further demonstrates the importance of changes to these brain regions within the Aldara model (Decarie-Spain et al., 2018). Work

with the neuroinflammatory CUMS models demonstrate the role of the thalamus, specifically the paraventricular nucleus, in the presence of depressive-like symptoms in mice (He et al., 2024). Optogenetic stimulation of the ACC highlights the modulatory role of depressive-like behaviour in rodents (Bissiere et al., 2006). Collectively, the 3 selected reward-related brain regions for the experiments in this chapter have established links to neuroinflammatory-induced depressive-like behavioural changes.

Another upregulated gene across the 3 reward-related brain regions which has connections to both glial reactivity and functional outputs is *Ctss.* The gene that codes for cathepsin S, is upregulated in the thalamus and ACC. Cathepsin S has previously established links with neuroinflammation and subsequent cognitive decline in mouse models of AD (Liu et al., 2025). Neuronal upregulation of *Ctss* has been found to induce microglial activation via the CX3CR1 axis which leads to promotion of neuroinflammation. This neuronal and microglial reactivity status is plausible within the Aldara model. Previous studies present TLR7-mediated microglia activation being demonstrated through increased Iba1+ staining and increased production of pro-inflammatory cytokines from the innate CNS immune population (McColl et al., 2016, Sharma et al., 2024). Therefore, highlighting a microglial reactivity component to the transcriptional evidence of neuroinflammation present in the thalamus and ACC regions. This evidence presents a possible molecular and cellular mechanism driving behavioural changes controlled by these brain regions.

Myeloid-mediated inflammation is suggested to be present throughout the brain both from previous bulk RNA sequencing and regional transcriptional changes. The NAc upregulated key immune genes including markers (*Ptprc)* and microglia-specific regulators of ferroptosis indicating a cellular population exhibiting high activity (Lu et al., 2024, Butovsky and Weiner, 2018). The upregulation of *Ccl2,* encodes for monocyte chemoattractant protein-1 an essential chemokine, suggests an increase in peripheral leukocyte trafficking to the NAc. This supports previous findings of peripheral leukocyte trafficking to brain parenchyma following Aldara treatment (Sharma et al., 2024, McColl et al., 2016). Additionally, chapter 5 of this thesis proved a subset of these peripheral immune cells, T cells, are actively producing pro-inflammatory cytokines in the brain of

Aldara-treated mice. This evidence further highlights the likelihood of the TLR7-driven neuroinflammation following Aldara treatment is a multi-cellular process.

The ACC presents 3 uniquely downregulated genes compared to the NAc and thalamus. *Npy* encoding for neuropeptide Y is involved in the modulation of feeding behaviours via dopamine transmission (Jin et al., 2023). Aldara-treated mice experience temporary weight loss in the duration of the model and observational data records a decreased consumption in baby food provided to animals (McColl et al., 2016). Decreased NPY levels have been reported in other rodent models in which it precedes periods of weight loss in animals (Eitmann et al., 2024). This ACC-specific decrease in NPY may indicate a depression of the dopamine-driven feeding behaviours typically exhibited by healthy mice and serve as a possible explanation for the weight fluctuations and disinterest to food by Aldara animals.

NPY has additionally gained increasing interest as an inflammatory modulatory target within the enteric nervous system (Chandrasekharan et al., 2013). Via receptors located on immune cells, increased NYP levels have been found to lower inflammation through decreasing cytokine production. Downregulation of *Npy* within the Aldara model may show a dampening of one anti-inflammatory mechanism which allows for the continuation of the TLR7-trigger neuroinflammation.

Another downregulated gene found within the NAc with links to neuropeptides and feeding behaviour was *Cartpt* (Rogge et al., 2008*)*. The neuropeptide encoded by *Cartpt* has displayed regional effects with influence on feeding behaviours: in fasted rats presenting decreased levels in the NAc (Yang et al., 2005). The similar decrease in *Cartpt* within the NAc following Aldara treatment may be highlighting a mechanism, similar to that of *Npy,* which explains the weight changes observed in the neuroinflammatory model. Additionally, changes to *Cartpt* may be indicative of the inappetence documented about Aldara-treated mice (*Unpublished observation, Kirstyn Gardner-Stephen)*. *Cartpt* encodes for CART which is a neuropeptide that has been found elevated in patients who respond positively to traditional antidepressants (Funayama et al., 2023, Mao, 2011). This neuropeptide has been found to mediate the reward behaviours underpinning drug

addiction via CAMKII and G-protein coupled signalling (Yu et al., 2017). Considering *Cartpt* was first described as being upregulated in response to individuals exhibiting signs of drug abuse, this highlights the neuropeptides' role in reinforcing the reward pathway. *Cartpt*'s links to feeding and reward may represent a depression of reward-driven behaviours towards food consumption. This potential loss of feeding behaviours is observed in Aldara-treated mice and includes decreased consumption of the provided baby food and subsequent weight loss in the model's duration.

Genes that are upregulated and mainly involved in tissue damaging processes during neuroinflammation are *Rgs5* and *Mfge8*. These genes were both uniquely downregulated in the NAc. Regulator of G-protein signalling 5, encoded by *Rgs5*, has been found to increase in expression, particularly in astrocytes, and heighten inflammation (Yin et al., 2023b). By inducing neuronal death specifically in rat striatum, upregulation of *Mfge8* following peripheral LPS injection was found to promote phagocytosis of healthy neurons (Fricker et al., 2012). Both pro-inflammatory genes being downregulated in Aldara-treated mice may suggest a compensatory mechanism to combat the ongoing inflammation.

Within the NAc, various genes were uniquely downregulated compared to the ACC and thalamus. These code for proteins involved in neural transmission such as presynaptic vesicle trafficking and enzymatic synthesis of neurotransmitter components. One of these genes is *Glul* which codes for the enzyme glutamine synthetase. This enzyme is responsible for catalysing the reaction between glutamate and ammonia to produce glutamine. A common consequence of neuroinflammation is excitotoxicity, via excess glutamate, which can be damaging to the neural cells and further exacerbate the pro-inflammatory tissue conditions. This glutamate disturbance via increased neuroinflammation is a common finding in various mood disordered including MDD (Haroon et al., 2017, Dantzer and Walker, 2014). Changes to this gene encoding for this rate-limiting enzyme may be evidence of the brain attempting to combat glutamate excitotoxity as a result of the TLR7-driven neuroinflammation.

Alpha synuclein, encoded by *Snca*, is another gene found to be uniquely downregulated within the NAc. The proteins accumulation has pathogenic links to

several synucleinopathies including PD and Lewy body dementia (Calabresi et al., 2023). A silencing of *Snca* in striatal dopaminergic neurons in mice results in T cell accumulation and increase in inflammation which suggests a mediatory and potential protective role of the synuclein (Benskey et al., 2018). Decrease of *Snca* in the NAc of Aldara-treated mice may indicate a loss of this protective mechanism for dopaminergic neurons. Consequential results may be a decrease in dopamine levels which could explain the lack of typical reward behaviours observed in treated mice. Overall downregulation of these genes may highlight deficits in the neuronal pathways underpinning these anhedonia-like behavioural changes exhibited in the Aldara model.

The thalamus uniquely downregulated genes involved in neurotransmission and myelin production. *Adcy1* was one gene found to be downregulated in the thalamus and codes for the protein adenylate cyclase 1. This enzyme is involved in the catalysation conversion of ATP to cyclic AMP (cAMP) which are crucial second messengers in several signalling pathways. These signalling molecules are involved in the downstream dopamine receptor D4 (DRD4) which is one of dopamine's receptors that has demonstrated strong links to reward behaviours, particular risk-taking in individuals (Muda et al., 2018). However, these are very common signalling molecules and may be involved in a variety of different receptor pathways. Additionally, DRD4 are expressed in the thalamus but at low levels compared to other brain regions namely the ACC.

Collectively, the upregulated genes across these reward-related brain regions suggest a primarily pro-inflammatory tissue environment with contribution of both brain-resident and infiltrating immune populations. Some anti-inflammatory compensatory mechanisms are hinted but overwhelmed by the pro-inflammatory processes at play in these areas. Downregulated genes primarily related to neurotransmitter and receptor activation with some anti-inflammatory mechanisms presented. Several genes were downregulated that exhibit links to reward-seeking networks, suggested a possible depression of this circuitry within the CNS following TLR7 activation in the Aldara model.

The NAc displayed the greatest transcriptional change, with respect to the limited 1000-plex CosMx panel, compared to the PFC and thalamus. This may suggest this

brain region was most affected by the TLR7-driven neuroinflammation which could explain the anhedonia-like behaviours shown by treated animals. Other animals experiencing raised levels of inflammation which display these depressive-like behaviours, have also found molecular changes in the NAc (Sharma and Fulton, 2013, Floris et al., 2024). The NAc is appreciated as a central brain region involved in the pathogenesis of depressive-like behaviours (Jiang et al., 2023). Other neuroinflammatory rodent models displaying both NAc changes and depressive-like behaviours include CUMS and social defeat (Song et al., 2024, Qian et al., 2020). The transcriptional changes in the NAc following Aldara treatment combined with manifestation of anhedonia-like behaviours highlights the importance of this brain region in the TLR7-driven neuroinflammatory environment.

A current limitation that stands in the behavioural assessment of depressive-like symptoms in pre-clinical models is the fundamental ability of animals to express these complex human emotions (von Mucke-Heim et al., 2023). Assessing changes to an animal's innate behaviour provides a broad picture of their well-being. However, attributing these changes to clinical symptoms or conditions may be over-interpretation of the changes. For the interpretation of the anhedonia-like phenotype in Aldara-treated mice to be strengthened, increasing the number of animals would be beneficial.

The battery of tests utilised in the behavioural characterisation of the Aldara model primarily focused on anxiety-like and anhedonia behaviours. For true presence of anhedonia and reward deficits to be established in rodent models, integration of aversion-based behavioural assays such as the tail-suspension and forced swimming tests aid identification of 'despair' in rodents which is considered another facet of MDD (Scheggi et al., 2018, Mavrogiorgou et al., 2025). Incorporation of other non-food rewarding tasks for rodents, such as foraging, is another measure of these changes which may be indicative of anhedonia-like feelings in rodents (Xeni et al., 2024). Expansion of the behavioural assessment of Aldara-treated mouse will aid a fuller understanding of this anhedonia phenotype. This presents the Aldara model as a neuroinflammation-induced behavioural change model and a potential anhedonia research tool.

For true understanding of functional outputs and inflammation-driven changes to them, recording of neuronal circuits is mandatory via electrophysiology. This would allow specific circuit detailing of changes within the Aldara model and explain changes in the connectivity following the induction of the neuroinflammation.

Although time and careful consideration was given, the selected anatomical brain regions for CosMx pseudo-bulk analysis were hand-drawn. All drawing were completed by the same researcher and minimise variability, however, some inaccuracies may exist in the selected areas being true to the neural anatomy. A brain atlas and anatomical landmarks of the tissue sections were used to guide the region masks. However, to improve this technique, an atlas could be overlaid directly on the image for more accurate drawings.

Once more, limitations are met with the restricted 1000-plex CosMx panel. This confines the transcriptional understanding of the biology in this model to what is included as RNA probes in the fixed panel. To fully understand regional differences at the whole transcriptome level, platforms such as GeoMx (another spatial transcriptomic platform by Nanostring) or brain regional dissection followed by bulk RNA sequencing would suffice (Zollinger et al., 2020). As with any transcript-based technique, the full comprehension of true biological change is only guaranteed with proteomic changes. To validate transcriptomic findings presented in this and previous chapters, protein-based assays, such as IHC and ELISA, would be vital to confirm translated changes between treatment groups.

Ultimately, the Aldara model serves as a useful tool in phenotypic exploration of more subtle inflammation-induced behavioural changes including ones linked to reward and depression. Presence of anhedonia-like behaviours were present in Aldara-treated mice. Through transcriptional analysis of fundamental brain areas controlling these behaviours, presence of an active inflammatory environment may explain the changes exhibited in this murine model. Furthermore, a potential protective anti-inflammatory mechanism was discovered in these brain regions presenting an attempt of the tissue to halt and repair the current damage induced by the TLR7-activated neuroinflammation.

7 Discussion

The aims of this thesis were to further characterise the Aldara neuroinflammatory mouse model with particular focus on the TLR7-driven global and spatial transcriptomic changes. This included identifying and describing cellular drivers of this model, namely microglia and $CD4^+$ and $CD8^+$ T cell subtypes. Additionally, functional changes were investigated via a battery of behavioural tests and exploring transcriptional changes in regions linked to the control of the anhedonia-like behaviours seen in Aldara-treated mice.

7.1 Summary of findings

This thesis presented the Aldara model as a transcriptionally-validated mouse model of global TLR7-driven neuroinflammation. Bulk RNA sequencing and spatial transcriptomics revealed a global presence of neuroinflammation. Both endogenous microglia and exogenous $CD4^+$ and $CD8^+$ T cells were found to be actively contributing to increased cerebral cytokines levels. Subsets of T cells identified were primarily Th1/Th17 and Tc1/Tc17 rather than their Th2/Tc2 counterparts. This suggests a skew to pro-inflammatory T cell-mediated processes compared to anti-inflammatory subsets (Annunziato et al., 2015). Previous experiments using the Aldara model focused only on identification of these cell types via flow cytometry and $CD3^+$ staining (McColl et al., 2016, Nerurkar et al., 2017b). The daily TLR7 stimulus triggered an anhedonia-like phenotype within treated animals with deficits in nesting and sucrose preference. Additionally, pro-inflammatory changes were identified in brain regions controlling the neural circuits mediating these reward-linked behaviours.

Bulk RNA sequencing allowed for an unbiased approach to analyse the transcriptional response of the whole brain to TLR7 stimulus. This whole transcriptome-investigation of the brain's response was novel in its understanding of the TLR7-driven inflammation. Previous studies explored limited and pre-selected transcriptomic changes via qPCR and microarray analysis (Nerurkar et al., 2017b, McColl et al., 2016). This showed a global pro-inflammatory transcriptional

response including enrichment of classic immune-related biological pathways and downregulation of oxygen and iron-related metabolism components.

Previous experiments using the Aldara model identified raised intracerebral cytokines, however, did not identify the cellular source (McColl et al., 2016). Flow cytometry experiments from this current work confirmed presence of reactive, cytokine-producing microglia following Aldara treatment. Via spatial transcriptomics, 5 transcriptionally distinct subclusters of brain-resident immune cells were identified. Using transcriptional signatures, 4 subclusters were indicative of varying microglia reactive phenotypes and 1 subcluster suggestive of infiltrating T cells. From the proposed 4 microglia subclusters, 3 presented a pro-inflammatory and one a possible anti-inflammatory compensatory phenotype of microglia. This transcriptional snapshot of neuroinflammation at day three of the Aldara model highlights the dynamic nature of microglia. The range of transcriptional subclusters identified for microglia further supports these cells exhibiting a spectrum of reactive states rather than the binary M1/M2 dichotomy (Nahrendorf and Swirski, 2016, Ma et al., 2023).

Presence of $CD4^+$ and $CD8^+$ T cells within the Aldara model is a well-established finding (McColl et al., 2016). However, specific helper/cytotoxic subtypes and the extent to which these infiltrating immune cells contributed to the TLR7-driven neuroinflammation was unknown. T cells were shown to be an actively contributing cell to the neuroinflammation in the Aldara model both previously and within the current experiments (Sharma et al., 2024). The lymphocytes were cytokine-producing and relatively more pro-inflammatory in nature with a skew to their Th1/Tc1 and Th17/Tc17 subtypes compared to Th2/Tc2. Identification of cytokine-producing microglia and T cells highlights the multi-cellular mechanism involved in neuroinflammation. This heterogeneous cellular response observed in the Aldara model is representative of the biology controlling human neuropsychiatric conditions (Dunn et al., 2020).

To build on the previous characterisation of behavioural changes displayed within the Aldara model including reduced burrowing (McColl et al., 2016), a battery of anxiety-like behavioural assays were performed including elevated plus maze, open field, sucrose preference and nest building. This behavioural analysis showed

that Aldara-treated mice appeared to lack anxiety-like behaviours assessed by these parameters. However, treated mice presented with anhedonia-like behaviour with loss of interest in innately rewarding tasks, including decreased sucrose preference and nest building. Additionally, brain regions involved in reward-seeking behaviours displayed an upregulation of pro-inflammatory-related genes, a downregulation of several neurotransmission-related genes, coupled with dampening of potential anti-inflammatory processes. Combining the functional deficits with transcriptional changes in reward-linked brain regions reveals potential inflammation-driven behavioural changes in Aldara mice. Upregulation of pro-inflammatory mechanism, such as increased neural cytokine levels and infiltrating of exogenous immune populations, may result in dampening of neurotransmission underpinning reward behaviours. These results support the Aldara model as a neuroinflammation-driven model of anhedonia-like phenotypes.

Overall, the findings of this thesis further characterise the Aldara model as a potential pre-clinical model of anhedonia with TLR7-driven global neuroinflammation composed of active microglial and T cell contribution. In a field of relatively severe, acute and invasive pre-clinical models, the Aldara model serves as a non-invasive and replicable global neuroinflammatory model in addition to being a technically easy animal model to carry out. The Aldara model may be used to begin to understand the molecular mechanisms mediating inflammation-induced behavioural changes such as anhedonia.

7.2 Aldara as a non-invasive neuroinflammation model

The Aldara model and interpretation of its experimental findings remains complicated by the multiple triggers of neuroinflammation. These include the peripheral psoriasis dermal inflammation, possible vagal stimulation and relatively more direct induction of neuroinflammation via TLR7 agonist IMQ entering the brain parenchyma (Nerurkar et al., 2017a). Additionally, TLR7 is expressed in a wide range of organs in the mouse which presents multiple binding targets for the agonist IMQ (Smith et al., 2018). Differentiation of the peripheral and central neuroinflammatory stimuli fell outwith the scope of this thesis. However, results from this thesis further support presence of global neuroinflammation following

topical application of Aldara cream and reinforces use of the model as a non-invasive neuroinflammatory model.

Other models adopting an invasive approach to induce neuroinflammation include intracerebral injections of pro-inflammatory agents such as LPS and cerebral artery occlusions to mimic ischaemic stroke (Vasconcellos et al., 2021, Campbell et al., 2012, Ma et al., 2020, Qin et al., 2007). These methods of triggering neuroinflammation have several drawbacks. This includes introducing local tissue injury to the animals at the injection site which may trigger an innate immune response. The severity of the LPS is another limitation of the endotoxin-driven biology. These extremely damaging effects for the animals include gait changes, lung inflammation and general SB (Tsikis et al., 2022, Carregosa et al., 2024, Bassi et al., 2012).

Additionally, other neuroinflammatory models such as systemically delivered LPS are an acute mimic. The Aldara model can be used to explore impacts of a relatively more chronic timepoint of neuroinflammation. Previously work has explored this model at a 5-day timepoint which still displays raised neural cytokine levels and infiltration of peripheral blood leukocytes (McColl et al., 2016). Other studies have documented a 7-day timepoint which mice have survived (Sakai et al., 2016). No exploration of neuroinflammation at these timepoints has been conducted. In terms of invasiveness, severity and possibility to extend chronicity to mirror the patient condition, the Aldara model is a preferable mouse model in its topical cream application and minimal discomfort to the animals other than the inflammation.

The Aldara model exhibits similar mechanisms to other neuroinflammation models, such as LPS and CUMS, including raised intracerebral cytokines, glial activation, inflammation-induced behavioural changes and peripheral immune cell trafficking to the brain parenchyma (McColl et al., 2016, Nerurkar et al., 2017a, Sharma et al., 2024, Jung et al., 2023, Johnson et al., 2019, Wohleb et al., 2014). This highlights the Aldara model as an easy to execute animal model for laboratory groups to study effects of global neuroinflammation.

7.3 Cellular interactions driving TLR7-induced neuroinflammation

The experiments within this thesis identified 2 cellular drivers of neuroinflammation: brain-resident microglia and infiltrating T cells. Both cell populations carry out important functions alone but also their interaction is a well-researched area in the neuroimmunology field (Schetters et al., 2017). Interactions between T cells and microglia are mediated through both cell populations producing and responding to chemokines and cytokines. The identified reactive microglial populations identified in this thesis may be acting as APCs towards the infiltrating $CD4^+$/$CD8^+$ T cells. This antigen-presenting interaction between microglia and T cells have been shown to further promote infiltration of $CD8^+$ T cells into brain parenchyma (Goddery et al., 2021). Both $CD4^+$ and $CD8^+$ T cells have been documented to promote microglial reactivity which furthers the pro-inflammatory cytokine production from the innate brain immune population (Kedia et al., 2024, Benakis et al., 2022). This reciprocal activation between the brain-resident microglia and suspected infiltrating $CD4^+$ and $CD8^+$ T cells highlights a key cellular mechanism documented within neuroinflammatory environments (Schetters et al., 2017).

In the context of EAE, a model with a well-characterised neuroinflammatory component, microglia have been established as key recruiters of T cells into the brain parenchyma and subsequent activation (Jie et al., 2021). Subsets of Th cells have also been identified in EAE, namely Th1 and Th17 cells, which displayed links to microglia activation resulting in release of classical pro-inflammatory cytokines including IL-6 and TNFα (Murphy et al., 2010).

Investigating interaction between T cells and microglia was not a specific aim of this thesis. However, to investigate the cellular populations influence on one another, the Aldara model was run within the RAG2KO mouse line that lack mature B and T cells. Aldara treated RAG2KO mice still exhibited microglial reactivity via increased $Iba1^+$. This demonstrates that even though infiltrating T cells are actively producing cytokines in the Aldara model, their presence is not vital for an increase in microglial reactivity. One limitation of RAG2KO to study T cell

contribution is this mouse line also lacks mature B cells. B lymphocytes have been shown to significantly increase following Aldara treatment (Sharma et al., 2024). However, as the focus on this thesis was to characterise the pro-inflammatory environment, T cells were selected as the primary mature lymphocyte producer. More focused and separate B and T cell depletion studies would allow for a more accurate account of the individual lymphocyte's contribution to the neuroinflammatory environment in the Aldara model. Work for this lymphocyte characterisation has started with antibody depletion $CD4^+$ and $CD8^+$ T cells within the Aldara model. Removal of both T cell subsets did not rescue the Aldara behavioural phenotype with mice still experiencing similar weight loss and sucrose preference test deficits compared to wild-type mice (Sharma et al., 2024).

The removal of mature lymphocytes was the only cellular KO mechanism investigated in this thesis. To reciprocate this approach for microglia is a relatively more difficult task. This is due to microglia being a relatively more complex cell type to remove from *in vivo* models due to their shared markers with other myeloid populations. An indirect approach to evaluate microglia contribution would be using *Csf1r*$^{\Delta FIRE/\Delta FIRE}$ (FIRE) mouse which lack microglia from embryonic to adult life (Rojo et al., 2019, Kiani Shabestari et al., 2022).

These FIRE mice retain BAMs including meningeal and perivascular macrophages (Rojo et al., 2019). Performing the Aldara model upon these microglia-deficient mice would provide an estimate of the microglia-only response within the TLR7-driven neuroinflammatory model. Utilising KO mice to investigate T cells and microglia's contribution to the Aldara model would answer their sole cellular responsibilities and begin to answer presence of interaction. Furthermore, removing both innate and peripheral immune cells simultaneously from an organism would allow for non-immune cellular drivers within the Aldara model to potentially be discovered. Both astrocytes and neurons have been shown to respond to and produce pro-inflammatory cytokines in both animal models and neuropsychiatric conditions (Zhao et al., 2024).

Another estimate of cellular interaction would be ligand-receptor analysis of spatial transcriptomic data. This transcript-based interaction studies proximity of one cell type expressing a 'ligand' and another expressing a receptor near each

other (Li et al., 2023). This interaction approximation is also possible with bulk RNA sequencing data but *in situ* information is lost with this technique (Villemin et al., 2023). However, the poor cellular segmentation of neural tissue with spatial transcriptomic software limits the reliability of this analysis. Considering cell boundaries of brain-resident cells are inaccurately defined with CosMx, assignment of ligands and receptors would therefore also be unreliable. If in situ information was sacrificed, scRNAseq would be a potential alternative to study cell ligand-receptor interactions. This will be discussed in the limitations section of this chapter.

7.4 Balance between pro-inflammatory and anti-inflammatory mechanisms

Although cross-talk between peripheral and central immune systems is now a well-established concept that challenges the dated 'immune privileged' label of the CNS, the brain remains as a tightly regulated tissue environment via the BBB. The brain has a specific pathophysiological response with the possibility of catastrophic consequences when this finely tuned environment is overwhelmed. The immune-related neurobiology underpinning neuropsychiatric conditions includes a disrupted balance of pro- and anti-inflammatory mechanisms. Utilising anti-inflammatory drugs in treatment of neuropsychiatric conditions is a growing pharmacological avenue in the field (Ballaz and Bourin, 2023). Evidence of endogenous anti-inflammatory and protective mechanisms within the Aldara model detailed earlier in this thesis highlight the homeostatic mechanisms at play in TLR7-driven neuroinflammation. In studying a model that has active anti-inflammatory properties, this could widen understanding of successful neuroprotective mechanisms and provide novel signalling pathways that may be investigated for pharmaceutical targets in treatment of inflammation-driven neuropsychiatric conditions such as MDD and anxiety.

7.5 Inflammation-induced anhedonia-like phenotype

As discussed throughout this thesis, anhedonia is a common symptom experienced by people living with neuropsychiatric conditions. Work in this thesis revealed no

anxiety-like phenotype in Aldara mice. However, discovering that our model primarily exhibits anhedonia-like symptoms creates a vital tool which can be used to characterise inflammation-induced behavioural changes including those which may be translated understand anhedonia-like phenotypes.

Models to characterise anhedonia and the biological mechanisms underpinning this behavioural change are vital to our understanding of syndromal depression (Barthel et al., 2020). No focused pharmacological treatments exist for anhedonia and the symptom is indirectly managed through antidepressants and psychological therapies (Serretti, 2023). The core neuropsychiatric symptom has been found to respond poorly or not at all to traditional antidepressant therapeutics (Cao et al., 2019). Pharmacological intervention for anhedonia has mainly focused on modulation of monoamines (Serretti, 2025). The Aldara model could be used to investigate inflammation-related changes resulting in anhedonia-like behaviours as the model shows pro-inflammatory processes in brain regions involved in reward circuitry and anhedonia-like behaviours. This model could form the basis of tests of novel inflammation-focused therapeutic targets for anhedonia treatment which is a growing pharmacological research field (Lee et al., 2018).

The battery of behavioural tests in the current experiments included assessments of anhedonia-like behaviour and anxiety-like behaviours. There was evidence of an anhedonia-like phenotype with mice displaying a reduction in preference to typically rewarding sucrose stimuli and not displaying natural innate nesting behaviours. Future experiments to monitor in-cage social interaction, such as interaction with a novel item or stranger, would be a useful way to evaluate potential reward deficits in treated animals (Kim et al., 2019). Implementing motivation-based foraging tasks would provide details if the anhedonia phenotype has a motivational deficit attached to it (Xeni et al., 2024). Further characterisation of the behavioural phenotype in the Aldara model would be useful in strengthening its use as a preclinical model of inflammation-induced anhedonia. Non-invasive in-cage monitoring systems via video recording could provide an assessment of the mice's natural behaviours and inflammation-induced changes to these. In-cage video monitoring systems such as MouseVUER allow for tracking of mouse behaviours with minimal disruption to their in-cage life (Salem et al., 2024). This better understanding of TLR7-induced anhedonia would determine if

the Aldara model would be suitable for therapeutic assessment of the neuropsychiatric symptom.

7.6 Cellular characterisation of TLR7-driven neuroinflammation

The CosMx spatial transcriptomic platform provided spatial information lacking in whole brain bulk RNA sequencing results. Additionally, it was possible to assign changes to single cell-types and adapt a pseudo-bulk cell agnostic approach to brain regions involved in reward processing. This pseudo-bulk approach involved taking all cell types into account for regional analysis (e.g. one brain region data output includes all identified cell types in the CosMx dataset). After quality control, the spatial transcriptomic dataset captured and analysed an estimated 750,000 cells. Considering a whole-brain MERFISH dataset identified 4.3 million cells (Yao et al., 2023), our QC-passed 750,000 cells seems reasonable for 16 6μm coronal hemisphere tissue sections. From spatial plots of our CosMx data, some blank spaces exist. This may highlight again the limitation of poor cellular segmentation of neural cells by CosMx with these complex morphologies not adhering to aspects of the quality control protocols and inaccurately being discounted.

As this thesis is focused on detailing the immune cell drivers of this model, only immune cells were explored in depth using this platform. Microglia were explored specifically as previous work with the Aldara model showed a reactive and cytokine-producing population of this resident immune cell (McColl et al., 2016, Sharma et al., 2024). The 4 possible immune subclusters identified via CosMx agrees with the range of phenotypes and functionality of the brain-resident immune populations observed both at rest and in other neuroinflammatory environments (Vidal-Itriago et al., 2022, Xu et al., 2022). These 4 microglial subclusters were primarily pro-inflammatory in their transcriptional signature. However, some transcriptional evidence did suggest a neuroprotective status of some of the CosMx-identified microglia. These microglial findings support within the confines of the 1000-plex CosMx panel, the known heterogeneity displayed by this brain-resident cell population (Healy et al., 2022). Expanding the RNA panel

for CosMx would provide more confidence in the identification of microglia from other myeloid populations. Inclusion of a morphology stain such as Iba1 would strengthen microglia separation. However, the success of morphology markers in the CosMx platform remains limited by the poor cellular segmentation of the platform.

Other CNS-resident cells were identified in this dataset including neuronal subtypes, oligodendrocytes, astrocytes and NVU cells of the BBB. For a comprehensive cellular characterisation of this model, future work aims to analyse all transcriptionally identified CosMx cell types as with the immune cells in this thesis. Investigating neuronal subtypes and their responses in TLR7-driven neuroinflammation would be important given the changes to neuronal networks documented in the Aldara model (Sharma et al., 2024). CosMx may also reveal changes to neurotransmitter-related genes that could explain neural pathway perturbations following Aldara treatment.

Only 3 regions of interest were explored in this thesis due to their links to reward behaviour. Future analysis of this spatial transcriptomic dataset could also explore other brain areas to further understand different behavioural changes. Other areas which may be of interest for reward behaviours could include the amygdala and hippocampus (Hu et al., 2021, Duarte et al., 2024). The 2 tissue planes were selected for CosMx analysis as they contained the largest collection of brain regions linked to inflammation-induced behavioural changes. To fully understand the reward processing in Aldara mice and changes to this, it would be beneficial for future experiments to include the VTA in tissue collection.

BBB changes have been observed within the Aldara model demonstrated by permeability of the brain to systemically injected Evan's blue dye and changes to BBB-associated tight junction proteins *(Maria Suessmilch, unpublished*). These results suggest inflammation-induced BBB changes and possible remodelling of the interface. Interrogating the endothelial and NVU cell clusters in the CosMx dataset may expand our understanding of BBB permeability. It is hypothesised that endothelial cells may exhibit upregulation of pro-inflammatory genes from the CosMx panel in response to the TLR7-triggered neuroinflammation. This pro-inflammatory state of NVU cells may highlight a mechanism resulting in the

dynamic remodelling suspected within the Aldara model. Characterising single cell type changes in response to TLR7-driven neuroinflammation via the CosMx platform provides insight to the cellular mechanisms governing the inflammation and its consequences. Detailing transcriptional changes to the BBB-associated cells may indicate an entry mechanism for the previously established infiltration of peripheral immune cells into the brain following TLR7-driven inflammation (Sharma et al., 2024).

Due to time constraints, the subcellular characterisation of transcriptomic changes using the CosMx platform following TLR7-induced neuroinflammation was not possible. Transcripts can be localised to allow for subcellular granularity of expression. This could be a useful tool to identify areas of high transcription within cells following a stimulus. Identifying subcellular regions of high transcriptional turnover of pro-inflammatory molecules may present an inhibitory target for novel drugs (Wang et al., 2023b). However, as previously discussed earlier in this thesis, there is the limitation of poor cellular segmentation for neural cells with the CosMx platform. This questions the reliability of this subcellular analysis approach as cellular processes are not included in the estimated membrane boundaries. Additionally, CosMx tissue sections are only 6μm thick so will not capture neural cells which have processes that project across several hundred micrometres (Han et al., 2013, Nimmerjahn et al., 2005).

Improvements of CosMx cellular segmentation for neural cells is vital before reliable interpretations are possible at subcellular analysis. The CosMx mouse neuroscience 1000-plex panel contains 4 morphology markers which are fixed. These contain protein markers for nuclei, rRNA, histones and GFAP. Although not currently available, incorporating cell membrane markers for main neural cell types may increase accuracy to membrane boundaries within the CosMx system.

For a broader transcriptomic single-cell analysis of CNS-resident cells in the Aldara model, single-nuclei RNA sequencing would be an attractive next step in the characterisation of the transcriptomic profile of the model. This combination of transcriptomic techniques has shown success in other neuroinflammation models including LPS-induced encephalopathy to create more detailed transcriptomic profiles of brain-resident cells (Zhu et al., 2024). Further targets of interest may

be validated via proteomic analysis including the implementation of spatial proteomic software.

Nanostring's alternative whole transcriptome spatial platform GeoMx may also prove useful in addressing neural questions (Zollinger et al., 2020). GeoMx has a more detailed transcriptional readout compared to the limited 1000-plex panel of CosMx. However, these results can only be assigned to a pre-defined region of interest and not one single cell type. For questions regarding cell-specific changes, CosMx is superior to GeoMx.

7.7 Limitations

The main limitation of the Aldara model is the multiple possible triggers of neuroinflammation. Although important questions exist surrounding which method of induction for neuroinflammation is at play in the Aldara model, the model results in a well-established pro-inflammatory neural environment and behavioural changes (McColl et al., 2016, Nerurkar et al., 2017b, Sharma et al., 2024). To study consequences of a particular central or peripheral mode of neuroinflammation induction, other models would be more useful than Aldara. However, the Aldara model is sufficient and useful for answering questions surrounding the consequences of neuroinflammation and impact on neural networks, particularly with TLR7 and IFNγ driven inflammation. This IFN-driven mechanism may be useful to further understand anti-viral responses within brain parenchyma and the type II IFN's involvement in neuropsychiatric conditions including MDD (Monteiro et al., 2017).

As previously discussed, separating microglial and myeloid populations from each other is a difficult technical task for the neuroimmunology field. The 2 broad cell populations share many common surface markers. This commonality makes distinction between the 2 and their contribution to a pro-inflammatory environment challenging to delineate (Greter et al., 2015, Honarpisheh et al., 2020). This becomes even more challenging when microglia are known to shift surface markers, such as CD45, from an intermediate to macrophage-like high expression. This possibility shift in CD45 phenotype was justification for, via flow

cytometry, only characterising the CD45^{int} populations which would mainly contain microglia rather than other myeloid populations such as BAMs or monocytes.

Findings from the current experiments detail a range of reactivity statuses of CNS-resident immune populations via a range of scientific techniques including flow cytometry and spatial transcriptomics. Both techniques lack true morphological detail of these myeloid cells which is the best distinguisher between myeloids and microglia with the latter being relatively more complex in their cellular boundaries (Vidal-Itriago et al., 2022). Microglia have been shown to change their morphology to a less ramified state following Aldara treatment (Sharma et al., 2024). Spatial transcriptomics does not currently hold the ability to drive this area of myeloid research forward until more microglia-specific markers are incorporated into RNA panels. Increased microglia-specific RNA targets coupled with more accurate cellular segmentation could advance microglia identification via spatial transcriptomics.

The spatial transcriptomics platform CosMx was used in this thesis as a tool to investigate cellular contributions *in situ* within the TLR7-driven neuroinflammation paradigm. However, following this in-depth analysis of the platform and the data outputs currently available from this software, some limitations are met particularly with CNS tissue. The pre-determined 1000-plex mouse neuroscience panel is limited in nature with an estimated 25 times fewer targets than a whole-transcriptomic experiment (Breschi et al., 2017). As suggested by its title, the target probes included in this panel focus more on neuroscience biology and, even though a vital compartment of the neural landscape, the immunological functions of microglia cannot be entirely characterised by the current panel.

Further limitations exist with the CosMx platform surrounding cell segmentation. Other fields including immunology and oncology have found great success with the spatial transcriptomics system, utilising an immunology-focused panel. Some of this success may be attributed to the relatively more uniform and spherical cell morphology displayed by immune cells compared to that of CNS-resident cells (Denisenko et al., 2024, Weber et al., 2024). CNS cells do not adopt this defined spherical morphology as neurons, glial and oligodendrocytes possess a complex

and far-reaching cell boundary. This complexity displayed by CNS-resident cells is a difficult parameter to capture *in situ*. The CosMx platform does not employ a protein membrane markers and cell morphology is determined on an mRNA estimation method completed by cell segmentation algorithm (He et al., 2022). This absence of membrane marker however can be explained by the great cell diversity expressed in the brain and no one marker being all to label and capture all cell types present. The difficulty in capturing the full cell membrane boundary is increased by using 6μm thick sections which does not encompass many CNS cells. These limitations surrounding accurate cell segmentation of CNS cells restricts the conclusions that can be drawn from this dataset.

7.8 Conclusions

In conclusion, this thesis has expanded the transcriptomic understanding of the TLR7-driven Aldara neuroinflammation model, identified cytokine contributions from microglia and $CD4^+$ and $CD8^+$ T cell populations. Additionally, this work has begun to unravel the inflammation-induced anhedonia-like behavioural phenotype exhibited by Aldara-treated mice. This experimental work could evolve in a variety of ways. Future experiments could focus on delineating contributions from brain-resident to infiltrating immune populations, expanding the spatial transcriptomic landscape within the brain as technologies improve to tackle relatively complex cell morphologies and further characterising the anhedonia-like phenotype. All experimental avenues that may be explored in the future with regards to the Aldara model will strive to grow understanding of neuroinflammation-driven changes to aid translational work to the neuropsychiatric field. This thesis presents the Aldara model a useful research tool to study the mechanisms underpinning neuroinflammation including consequences to cellular reactivity and functional behavioural output.

7.9 Future directions

There is a variety of avenues this work could explore to expand the understanding of TLR7-driven neuroinflammation and its biological consequences. Future work could compare its effects to other neuroinflammatory models including

tamoxifen-driven cell-specific cytokine expressing mice and CUMS. Comparing the Aldara model to relatively more chronic neuroinflammatory models would allow for a clearer understanding of the sequence of events following different stimuli. This would include differences and similarities across various neuroinflammatory models. Detailing sequence of events following a neuroinflammatory stimulus may present different intervention points for novel therapeutics.

To address the question of what TLR7 trigger is driving the neuroinflammation observed in the Aldara model, teasing apart the peripheral and central responses within animals would prove beneficial. For the dermal inflammation exhibited in the model, it is suspected the isostearic acid in the cream preparation may contribute to the local cutaneous inflammation as this compound has been shown to be an irritant to skin if applied topically (Strass et al., 2023). Attempts to create a 'home-made' IMQ topical cream with soluble IMQ and aqueous cream were carried out, however, no comparable dermal or neural inflammation responses to the 'traditional' Aldara model were captured (Kirstyn Gardner-Stephen, unpublished data). Preliminary experiments with 5% IMQ cream without the isostearic acid contained in the Aldara preparation did not show promising results to induce the same level of neuroinflammation compared to the original mouse model. Instead of trying to improve the model to eliminate the psoriasis-like dermal inflammation, teasing apart the peripheral and central immune compartments would prove beneficial. To delineate these 2 pro-inflammatory responses within the model, one approach to this would be to separate the brain-resident microglia response from peripheral macrophage populations.

Several pro-inflammatory cytokines were found to be at play in the Aldara model with both transcriptional and flow cytometric cell-specific evidence presented in all results chapters of this thesis. Both microglia and T cells were found to be primary producers of these pro-inflammatory cytokines. To further investigate the consequence of these cellular origins of cytokines, transgenic mice with both cell and cytokine specific promoters would prove useful in future experiments. In the context of microglia, I propose cytokine-specific promoters for TNFα and IFNγ would provide crucial insight to these pro-inflammatory cytokines' responsibilities in this TLR7-driven neuroinflammatory environment. Both cytokines are implicated in the pathophysiology of neuropsychiatric conditions including MDD

(Bortolato et al., 2015, Daria et al., 2020). The ability to control the cell-specific expression of these pro-inflammatory cytokines would allow for mapping of their consequences and downstream actions in a TLR7-driven neuroinflammatory environment. This would further characterise the molecular steps which is relatively unknown for neuroinflammation pathophysiology.

All the work present in this thesis used female mice and no males. This was as male mice have been found to have different skin morphology which hinders the pro-inflammatory nature of the Aldara model psoriasis-like reaction (Azzi et al., 2005, McColl et al., 2016). However, exploring TLR7-driven neuroinflammation and its consequences in both sexes is essential in evaluating clinical outcomes of inflammation-induced changes. Particularly when investigating immune cell populations which a variety of both innate and adaptive cells being shown to express sex-specific hormonal receptors that can alter their functions (Sciarra et al., 2023). Providing this thesis focused on microglial, it has been long established that the brain-resident immune population expressed receptors for and alter their physiology in response to oestrogen (Mor et al., 1999). Recent work has shown, particularly in neuroinflammatory environments, these oestrogen-related microglial changes include increased immunoreactivity, altered transcriptional signatures and increased pro-inflammatory cytokine production (Acosta-Martinez, 2020). Furthermore, this exploration of possible sex differences in a neuroinflammatory model would be useful for translational work as sex has been found to impact symptoms experienced with neuropsychiatric conditions (Thibaut, 2016). Future experiments may involve optimising the Aldara model, including altering doses and duration, for male mice inclusion.

This thesis focused on transcriptional changes in brain regions involved in the prefrontal-thalamostriatal circuit which underpins reward behaviours. To fully understand inflammation-induced changes to circuitry, future experiments would plan to include electrophysiology to investigate synaptic signalling perturbations. Other anhedonia-presenting neuroinflammatory models such as chronic stress have used electrophysiological methods to detail synaptic changes (Lim et al., 2012). This functional evaluation of how neurons are communicating following Aldara treatment would build on the transcriptional evidence of changes to neurotransmission present in chapters 3 and 6 of this thesis.

Dopamine and its effects were studied in this thesis at the regional transcriptional level using CosMx in chapter 6. Minimal transcriptional changes were uncovered for the reward-modulating neurotransmitter even though reward-deficits were recorded in Aldara-treated mice. To fully investigate dopamine and its changes in the TLR7-driven neuroinflammatory environment, optogenetics would prove a useful research tool. Successful selection and activation of dopaminergic neurons in the VTA has been achieved in previous studies (Taylor et al., 2016). Transcriptional evidence of a downregulation of synaptic signalling following Aldara treatment was shown via CosMx in chapter 6 of the thesis. To fully understand dopamine's role in the manifestation of anhedonia-like behaviours in the Aldara model, optogenetics could be used to inhibit dopaminergic neurons in the ACC and NAc. If this dopamine-specific neuronal inhibition in the reward-related regions results in similar behavioural outputs as observed in the model, this would strengthen dopamine's involvement in the anhedonia-like change following TLR7-driven neuroinflammation.

Evidence of cytokine-producing $CD4^+$ and $CD8^+$ T cells was shown in chapter 5 of this thesis. Other work surrounding the Aldara model shows presence of other peripheral immune cells within the brain parenchyma (Sharma et al., 2024). However, the question concerning the mechanism of entry of these immune populations into the brain and their role in neuroinflammation and behavioural changes remains unanswered. Transcriptional changes presented in the thesis suggests a chemokine-driven mechanism to this cellular entry. To test chemokine involvement of cellular recruitment to brain parenchyma in Aldara mice, inflammatory chemokine receptor (iCCR) KO mice could be utilised. Specifically mice lacking CCR 1, 2, 3 and 5. Preliminary experiments with these iCCR KO mice have shown a potential decrease in monocytic recruitment to the brain in Aldara-treated mice (Sharma et al., 2024). However, these iCCR deficient mice still displayed weight loss and sucrose preference deficits following Aldara treatment.

Alternative methods of removing a specific cell type from the inflammatory physiology involves the use of antibody blockers. Hexb was previously discussed as, from the limited availability, one of the most microglia-specific markers to delineate from other myeloid populations (Shah et al., 2022). Antibody-driven silencing of this microglia-specific marker could eliminate the brain's innate

immune cell from an organism. This could then indirectly evaluate microglia's contribution to the TLR7-driven neuroinflammation and contrast it with other myeloid populations including BAMs and infiltrating monocytes.

One element of the Aldara model which was not explored in depth was the consequence of changes to the BBB. Disruption of the circulation-tissue interface following the TLR7-driven inflammation has been shown via entry of systemically administered Evan's blue dye into the brain (*Maria Suessmilch, unpublished)*. Additionally, some transcriptional evidence of BBB remodelling was suggested by the CosMx data for both microglia-specific changes and regions involved in reward behaviours. The spatial transcriptomic identification of unique immune-rich neighbourhoods in Aldara-treated mice which appear to map to the neural vasculature show immune-driven changes potentially effecting the barrier's integrity. Loss of BBB integrity is a common consequence of neuroinflammatory environments including neuropsychiatric conditions such as anxiety and MDD (Kealy et al., 2020, Wu et al., 2022a). As changes to the BBB is thought to both be a result of and contribute to worsening of neuroinflammation in neuropsychiatric conditions, novel therapeutics have been designed to try and strengthen the barrier's integrity (Bicker et al., 2020). Future work utilising the Aldara model could use the previously identified NVU cells from the CosMx dataset in chapter 4 of the thesis. Exploring the transcriptomic changes to these BBB-associated cells following TLR7 stimulation could strengthen the use of Aldara as a neuroinflammatory model with BBB disruption. This may lead to the TLR7-driven neuroinflammatory model being useful as a non-invasive model to study these novel BBB-promoting drugs. Some of these therapeutics involve increasing expression of crucial proteins expressed in the NVU cells such as aquaporin-4 and various endothelial integrins (Bicker et al., 2020).

CosMx spatial transcriptomic platform provided a novel approach to assessing the Aldara model's TLR7-driven neuroinflammation. The 1000-plex RNA panel, although comparatively limited to whole-transcriptome studies, cell- and region-specific changes during pro-inflammatory neural environments. Greater transcriptional understanding of these identified cells would be achieved through other techniques including whole-transcriptome single-nuclei RNA sequencing

(Han et al., 2025). This would expand the current 1000-plex understanding of cellular drivers within the Aldara model to their whole transcriptional profile.

In conclusion, a variety of experiments could be explored in the future to further detail cellular and molecular changes exhibited in the Aldara model. Building understanding of the TLR7-driven neuroinflammation and consequential changes to systems presents potential novel therapeutic targets for the psychoneuroimmunology field.

List of References

ABBAOUI, A., FATOBA, O. & YAMASHITA, T. 2023. Meningeal T cells function in the central nervous system homeostasis and neurodegenerative diseases. *Front Cell Neurosci,* 17**,** 1181071.

ACOSTA-MARTINEZ, M. 2020. Shaping Microglial Phenotypes Through Estrogen Receptors: Relevance to Sex-Specific Neuroinflammatory Responses to Brain Injury and Disease. *J Pharmacol Exp Ther,* 375**,** 223-236.

ADRIAN, M., WEBER, M., TSAI, M. C., GLOCK, C., KAHN, O. I., PHU, L., CHEUNG, T. K., MEILANDT, W. J., ROSE, C. M. & HOOGENRAAD, C. C. 2023. Polarized microtubule remodeling transforms the morphology of reactive microglia and drives cytokine release. *Nat Commun,* 14**,** 6322.

AGRAWAL, S., BAULCH, J. E., MADAN, S., SALAH, S., CHEEKS, S. N., KRATTLI, R. P., JR., SUBRAMANIAN, V. S., ACHARYA, M. M. & AGRAWAL, A. 2022. Impact of IL-21-associated peripheral and brain crosstalk on the Alzheimer's disease neuropathology. *Cell Mol Life Sci,* 79**,** 331.

AHN, J. J., ABU-RUB, M. & MILLER, R. H. 2021. B Cells in Neuroinflammation: New Perspectives and Mechanistic Insights. *Cells,* 10.

AKAMATSU, Y. & OETTINGER, M. A. 1998. Distinct roles of RAG1 and RAG2 in binding the V(D)J recombination signal sequences. *Mol Cell Biol,* 18**,** 4670-8.

AL-HARBI, K. S. 2012. Treatment-resistant depression: therapeutic trends, challenges, and future directions. *Patient Prefer Adherence,* 6**,** 369-88.

ALKABIE, S., BASIVIREDDY, J., ZHOU, L., ROSKAMS, J., RIECKMANN, P. & QUANDT, J. A. 2016. SPARC expression by cerebral microvascular endothelial cells in vitro and its influence on blood-brain barrier properties. *J Neuroinflammation,* 13**,** 225.

ALLIOT, F., GODIN, I. & PESSAC, B. 1999. Microglia derive from progenitors, originating from the yolk sac, and which proliferate in the brain. *Brain Res Dev Brain Res,* 117**,** 145-52.

ALQUICIRA-HERNANDEZ, J. & POWELL, J. E. 2021. Nebulosa recovers single-cell gene expression signals by kernel density estimation. *Bioinformatics,* 37**,** 2485-2487.

ALQURASHI, G. K., HINDI, E. A., ZAYED, M. A., ABD EL-AZIZ, G. S., ALTURKISTANI, H. A., IBRAHIM, R. F., AL-THEPYANI, M. A., BAKHLGI, R., ALZAHRANI, N. A., ASHRAF, G. M. & ALGHAMDI, B. S. 2022. The Impact of Chronic Unpredictable Mild Stress-Induced Depression on Spatial, Recognition and

Reference Memory Tasks in Mice: Behavioral and Histological Study. *Behav Sci (Basel),* 12.

ALVES DE LIMA, K., RUSTENHOVEN, J., DA MESQUITA, S., WALL, M., SALVADOR, A. F., SMIRNOV, I., MARTELOSSI CEBINELLI, G., MAMULADZE, T., BAKER, W., PAPADOPOULOS, Z., LOPES, M. B., CAO, W. S., XIE, X. S., HERZ, J. & KIPNIS, J. 2020. Meningeal γδ T cells regulate anxiety-like behavior via IL-17a signaling in neurons. *Nature Immunology,* 21**,** 1421-1429.

ANGLIN, R. E., TARNOPOLSKY, M. A., MAZUREK, M. F. & ROSEBUSH, P. I. 2012. The psychiatric presentation of mitochondrial disorders in adults. *J Neuropsychiatry Clin Neurosci,* 24**,** 394-409.

ANNUNZIATO, F., ROMAGNANI, C. & ROMAGNANI, S. 2015. The 3 major types of innate and adaptive cell-mediated effector immunity. *J Allergy Clin Immunol,* 135**,** 626-35.

ARELLANO, G., ACUNA, E., REYES, L. I., OTTUM, P. A., DE SARNO, P., VILLARROEL, L., CIAMPI, E., URIBE-SAN MARTIN, R., CARCAMO, C. & NAVES, R. 2017. Th1 and Th17 Cells and Associated Cytokines Discriminate among Clinically Isolated Syndrome and Multiple Sclerosis Phenotypes. *Front Immunol,* 8**,** 753.

ASAMU, M. O., OLADIPO, O. O., ABAYOMI, O. A. & ADEBAYO, A. A. 2023. Alzheimer's disease: The role of T lymphocytes in neuroinflammation and neurodegeneration. *Brain Res,* 1821**,** 148589.

AUBERT, A. 1999. Sickness and behaviour in animals: a motivational perspective. *Neurosci Biobehav Rev,* 23**,** 1029-36.

AUCOTT, H., LUNDBERG, J., SALO, H., KLEVENVALL, L., DAMBERG, P., OTTOSSON, L., ANDERSSON, U., HOLMIN, S. & ERLANDSSON HARRIS, H. 2018. Neuroinflammation in Response to Intracerebral Injections of Different HMGB1 Redox Isoforms. *J Innate Immun,* 10**,** 215-227.

AYASOUFI, K., WOLF, D. M., NAMEN, S. L., JIN, F., TRITZ, Z. P., PFALLER, C. K., ZHENG, J., GODDERY, E. N., FAIN, C. E., GULBICKI, L. R., BORCHERS, A. L., REESMAN, R. A., YOKANOVICH, L. T., MAYNES, M. A., BAMKOLE, M. A., KHADKA, R. H., HANSEN, M. J., WU, L. J. & JOHNSON, A. J. 2023. Brain resident memory T cells rapidly expand and initiate neuroinflammatory responses following CNS viral infection. *Brain Behav Immun,* 112**,** 51-76.

AYDIN, S., PAREJA, J., SCHALLENBERG, V. M., KLOPSTEIN, A., GRUBER, T., PAGE, N., BOUILLET, E., BLANCHARD, N., LIBLAU, R., KORBELIN, J., SCHWANINGER, M., JOHNSON, A. J., SCHENK, M., DEUTSCH, U., MERKLER, D. & ENGELHARDT, B. 2023. Antigen recognition detains CD8(+) T cells at the blood-brain barrier and contributes to its breakdown. *Nat Commun,* 14**,** 3106.

AZZI, L., EL-ALFY, M., MARTEL, C. & LABRIE, F. 2005. Gender differences in mouse skin morphology and specific effects of sex steroids and dehydroepiandrosterone. *J Invest Dermatol,* 124**,** 22-7.

BABICKI, S., ARNDT, D., MARCU, A., LIANG, Y., GRANT, J. R., MACIEJEWSKI, A. & WISHART, D. S. 2016. Heatmapper: web-enabled heat mapping for all. *Nucleic Acids Res,* 44**,** W147-53.

BALLAZ, S. & BOURIN, M. 2023. Anti-Inflammatory Therapy as a Promising Target in Neuropsychiatric Disorders. *Adv Exp Med Biol,* 1411**,** 459-486.

BANKS, W. A., GRAY, A. M., ERICKSON, M. A., SALAMEH, T. S., DAMODARASAMY, M., SHEIBANI, N., MEABON, J. S., WING, E. E., MOROFUJI, Y., COOK, D. G. & REED, M. J. 2015. Lipopolysaccharide-induced blood-brain barrier

disruption: roles of cyclooxygenase, oxidative stress, neuroinflammation, and elements of the neurovascular unit. *J Neuroinflammation,* 12**,** 223.

BARCIA, C., SR., MITXITORENA, I., CARRILLO-DE SAUVAGE, M. A., GALLEGO, J. M., PEREZ-VALLES, A. & BARCIA, C., JR. 2013. Imaging the microanatomy of astrocyte-T-cell interactions in immune-mediated inflammation. *Front Cell Neurosci,* 7**,** 58.

BARROCA, N. C. B., DELLA SANTA, G., SUCHECKI, D., GARCIA-CAIRASCO, N. & UMEOKA, E. H. L. 2022. Challenges in the use of animal models and perspectives for a translational view of stress and psychopathologies. *Neurosci Biobehav Rev,* 140**,** 104771.

BARTHEL, A. L., PINAIRE, M. A., CURTISS, J. E., BAKER, A. W., BROWN, M. L., HOEPPNER, S. S., BUI, E., SIMON, N. M. & HOFMANN, S. G. 2020. Anhedonia is central for the association between quality of life, metacognition, sleep, and affective symptoms in generalized anxiety disorder: A complex network analysis. *J Affect Disord,* 277**,** 1013-1021.

BASSI, G. S., KANASHIRO, A., SANTIN, F. M., DE SOUZA, G. E., NOBRE, M. J. & COIMBRA, N. C. 2012. Lipopolysaccharide-induced sickness behaviour evaluated in different models of anxiety and innate fear in rats. *Basic Clin Pharmacol Toxicol,* 110**,** 359-69.

BAULCH, J. E., ACHARYA, M. M., AGRAWAL, S., APODACA, L. A., MONTEIRO, C. & AGRAWAL, A. 2020. Immune and Inflammatory Determinants Underlying Alzheimer's Disease Pathology. *J Neuroimmune Pharmacol,* 15**,** 852-862.

BAUMEISTER, A. A., HAWKINS, M. F. & UZELAC, S. M. 2003. The myth of reserpine-induced depression: role in the historical development of the monoamine hypothesis. *J Hist Neurosci,* 12**,** 207-20.

BAYRAMGURLER, D., KARSON, A., OZER, C. & UTKAN, T. 2013. Effects of long-term etanercept treatment on anxiety- and depression-like neurobehaviors in rats. *Physiol Behav,* 119**,** 145-8.

BEHL, S., MEHTA, S. & PANDEY, M. K. 2023. The role of selenoproteins in neurodevelopment and neurological function: Implications in autism spectrum disorder. *Front Mol Neurosci,* 16**,** 1130922.

BELLETTATO, C. M. & SCARPA, M. 2018. Possible strategies to cross the blood–brain barrier. *Italian Journal of Pediatrics,* 44**,** 131.

BELOVICOVA, K., BOGI, E., CSATLOSOVA, K. & DUBOVICKY, M. 2017. Animal tests for anxiety-like and depression-like behavior in rats. *Interdiscip Toxicol,* 10**,** 40-43.

BENAKIS, C., SIMATS, A., TRITSCHLER, S., HEINDL, S., BESSON-GIRARD, S., LLOVERA, G., PINKHAM, K., KOLZ, A., RICCI, A., THEIS, F. J., BITTNER, S., GOKCE, O., PETERS, A. & LIESZ, A. 2022. T cells modulate the microglial response to brain ischemia. *Elife,* 11.

BENALLEGUE, N., KEBIR, H. & ALVAREZ, J. I. 2022. Neuroinflammation: Extinguishing a blaze of T cells. *Immunol Rev,* 311**,** 151-176.

BENDER, A. T., TZVETKOV, E., PEREIRA, A., WU, Y., KASAR, S., PRZETAK, M. M., VLACH, J., NIEWOLD, T. B., JENSEN, M. A. & OKITSU, S. L. 2020. TLR7 and TLR8 Differentially Activate the IRF and NF-κB Pathways in Specific Cell Types to Promote Inflammation. *Immunohorizons,* 4**,** 93-107.

BENNETT, M. L. & VIAENE, A. N. 2021. What are activated and reactive glia and what is their role in neurodegeneration? *Neurobiol Dis,* 148**,** 105172.

BENSKEY, M. J., SELLNOW, R. C., SANDOVAL, I. M., SORTWELL, C. E., LIPTON, J. W. & MANFREDSSON, F. P. 2018. Silencing Alpha Synuclein in Mature Nigral

Neurons Results in Rapid Neuroinflammation and Subsequent Toxicity. *Front Mol Neurosci,* 11**,** 36.

BICKER, J., ALVES, G., FONSECA, C., FALCAO, A. & FORTUNA, A. 2020. Repairing blood-CNS barriers: Future therapeutic approaches for neuropsychiatric disorders. *Pharmacol Res,* 162**,** 105226.

BISSIERE, S., MCALLISTER, K. H., OLPE, H. R. & CRYAN, J. F. 2006. The rostral anterior cingulate cortex modulates depression but not anxiety-related behaviour in the rat. *Behav Brain Res,* 175**,** 195-9.

BLUTHE, R. M., MICHAUD, B., POLI, V. & DANTZER, R. 2000. Role of IL-6 in cytokine-induced sickness behavior: a study with IL-6 deficient mice. *Physiol Behav,* 70**,** 367-73.

BOBOTIS, B. C., HALVORSON, T., CARRIER, M. & TREMBLAY, M. E. 2024. Established and emerging techniques for the study of microglia: visualization, depletion, and fate mapping. *Front Cell Neurosci,* 18**,** 1317125.

BORTOLATO, B., CARVALHO, A. F., SOCZYNSKA, J. K., PERINI, G. I. & MCINTYRE, R. S. 2015. The Involvement of TNF-alpha in Cognitive Dysfunction Associated with Major Depressive Disorder: An Opportunity for Domain Specific Treatments. *Curr Neuropharmacol,* 13**,** 558-76.

BOULAND, G. A., MAHFOUZ, A. & REINDERS, M. J. T. 2023. Consequences and opportunities arising due to sparser single-cell RNA-seq datasets. *Genome Biol,* 24**,** 86.

BOURGOGNON, J. M. & CAVANAGH, J. 2020. The role of cytokines in modulating learning and memory and brain plasticity. *Brain Neurosci Adv,* 4**,** 2398212820979802.

BRANDENBURG, S., BLANK, A., BUNGERT, A. D. & VAJKOCZY, P. 2020. Distinction of Microglia and Macrophages in Glioblastoma: Close Relatives, Different Tasks? *Int J Mol Sci,* 22.

BRESCHI, A., GINGERAS, T. R. & GUIGO, R. 2017. Comparative transcriptomics in human and mouse. *Nat Rev Genet,* 18**,** 425-440.

BROMBERG-MARTIN, E. S., MATSUMOTO, M. & HIKOSAKA, O. 2010. Dopamine in motivational control: rewarding, aversive, and alerting. *Neuron,* 68**,** 815-34.

BRUMMER, T., SCHILLNER, M., STEFFEN, F., KNEILMANN, F., WASSER, B., UPHAUS, T., ZIPP, F. & BITTNER, S. 2023. Spatial transcriptomics and neurofilament light chain reveal changes in lesion patterns in murine autoimmune neuroinflammation. *J Neuroinflammation,* 20**,** 262.

BRYMER, K. J., FENTON, E. Y., KALYNCHUK, L. E. & CARUNCHO, H. J. 2018. Peripheral Etanercept Administration Normalizes Behavior, Hippocampal Neurogenesis, and Hippocampal Reelin and GABA(A) Receptor Expression in a Preclinical Model of Depression. *Front Pharmacol,* 9**,** 121.

BURMEISTER, A. R. & MARRIOTT, I. 2018. The Interleukin-10 Family of Cytokines and Their Role in the CNS. *Front Cell Neurosci,* 12**,** 458.

BURRE, J. 2015. The Synaptic Function of alpha-Synuclein. *J Parkinsons Dis,* 5**,** 699-713.

BURROWS, K., STEWART, J. L., KUPLICKI, R., FIGUEROA-HALL, L., SPECHLER, P. A., ZHENG, H., GUINJOAN, S. M., TULSA, I., SAVITZ, J. B., KENT TEAGUE, T. & PAULUS, M. P. 2021. Elevated peripheral inflammation is associated with attenuated striatal reward anticipation in major depressive disorder. *Brain Behav Immun,* 93**,** 214-225.

BUTOVSKY, O. & WEINER, H. L. 2018. Microglial signatures and their role in health and disease. *Nat Rev Neurosci,* 19**,** 622-635.

CALABRESI, P., MECHELLI, A., NATALE, G., VOLPICELLI-DALEY, L., DI LAZZARO, G. & GHIGLIERI, V. 2023. Alpha-synuclein in Parkinson's disease and other synucleinopathies: from overt neurodegeneration back to early synaptic dysfunction. *Cell Death Dis,* 14**,** 176.

CAMPBELL, D., GREEN, M. J., DAVIES, N., DEMOU, E., HOWE, L. D., HARRISON, S., SMITH, D. J., HOWARD, D. M., MCINTOSH, A. M., MUNAFO, M. & KATIKIREDDI, S. V. 2022. Effects of depression on employment and social outcomes: a Mendelian randomisation study. *J Epidemiol Community Health,* 76**,** 563-571.

CAMPBELL, L. R., PANG, Y., OJEDA, N. B., ZHENG, B., RHODES, P. G. & ALEXANDER, B. T. 2012. Intracerebral lipopolysaccharide induces neuroinflammatory change and augmented brain injury in growth-restricted neonatal rats. *Pediatr Res,* 71**,** 645-52.

CAO, B., ZHU, J., ZUCKERMAN, H., ROSENBLAT, J. D., BRIETZKE, E., PAN, Z., SUBRAMANIEAPILLAI, M., PARK, C., LEE, Y. & MCINTYRE, R. S. 2019. Pharmacological interventions targeting anhedonia in patients with major depressive disorder: A systematic review. *Prog Neuropsychopharmacol Biol Psychiatry,* 92**,** 109-117.

CAPURON, L., HAUSER, P., HINZE-SELCH, D., MILLER, A. H. & NEVEU, P. J. 2002. Treatment of cytokine-induced depression. *Brain Behav Immun,* 16**,** 575-80.

CARPINELLI, L., BUCCI, C., SANTONICOLA, A., ZINGONE, F., CIACCI, C. & IOVINO, P. 2019. Anhedonia in irritable bowel syndrome and in inflammatory bowel diseases and its relationship with abdominal pain. *Neurogastroenterol Motil,* 31**,** e13531.

CARREGOSA, D., LONCAREVIC-VASILJKOVIC, N., FELICIANO, R., MOURA-LOURO, D., MENDES, C. S. & DOS SANTOS, C. N. 2024. Locomotor and gait changes in the LPS model of neuroinflammation are correlated with inflammatory cytokines in blood and brain. *J Inflamm (Lond),* 21**,** 39.

CHANDRASEKHARAN, B., NEZAMI, B. G. & SRINIVASAN, S. 2013. Emerging neuropeptide targets in inflammation: NPY and VIP. *Am J Physiol Gastrointest Liver Physiol,* 304**,** G949-57.

CHEN, J., LIU, X. & ZHONG, Y. 2020. Interleukin-17A: The Key Cytokine in Neurodegenerative Diseases. *Frontiers in Aging Neuroscience,* 12.

CHEN, L., LU, Y., HUA, X., ZHANG, H., SUN, S. & HAN, C. 2024. Three methods of behavioural testing to measure anxiety - A review. *Behav Processes,* 215**,** 104997.

CHEN, M., REED, R. R. & LANE, A. P. 2019. Chronic Inflammation Directs an Olfactory Stem Cell Functional Switch from Neuroregeneration to Immune Defense. *Cell Stem Cell,* 25**,** 501-513 e5.

CHEN, P., LIN, W. L., LIU, X. Y., LI, S. J., CHEN, R. F., HU, Z. H., LIN, P. T., LIN, M. H., SHI, M. Y., WU, W., WANG, Y., LIN, Q. S. & YE, Z. C. 2025. D30 Alleviates beta2-Microglobulin-Facilitated Neurotoxic Microglial Responses in Isoflurane/Surgery-Induced Cognitive Dysfunction in Aged Mice. *Lab Invest,* 105**,** 102190.

CHEN, Y., JIANG, T., CHEN, P., OUYANG, J., XU, G., ZENG, Z. & SUN, Y. 2011. Emerging tendency towards autoimmune process in major depressive patients: a novel insight from Th17 cells. *Psychiatry Res,* 188**,** 224-30.

CHEN, Y. H., WANG, W. M., LI, I. H., KAO, H. H., YEH, C. B. & KAO, L. T. 2021. Major depressive disorder increased risk of psoriasis: A propensity score matched cohort study. *J Affect Disord,* 278**,** 407-412.

CHIU, C. C., LIAO, Y. E., YANG, L. Y., WANG, J. Y., TWEEDIE, D., KARNATI, H. K., GREIG, N. H. & WANG, J. Y. 2016. Neuroinflammation in animal models of traumatic brain injury. *J Neurosci Methods,* 272**,** 38-49.

CHUCAIR-ELLIOTT, A. J., CONRADY, C., ZHENG, M., KROLL, C. M., LANE, T. E. & CARR, D. J. 2014. Microglia-induced IL-6 protects against neuronal loss following HSV-1 infection of neural progenitor cells. *Glia,* 62**,** 1418-34.

CHUNG, Y. W., JEONG, D., NOH, O. J., PARK, Y. H., KANG, S. I., LEE, M. G., LEE, T. H., YIM, M. B. & KIM, I. Y. 2009. Antioxidative role of selenoprotein W in oxidant-induced mouse embryonic neuronal cell death. *Mol Cells,* 27**,** 609-13.

CIUBUC-BATCU, M. T., STAPELBERG, N. J. C., HEADRICK, J. P. & RENSHAW, G. M. C. 2024. A mitochondrial nexus in major depressive disorder: Integration with the psycho-immune-neuroendocrine network. *Biochim Biophys Acta Mol Basis Dis,* 1870**,** 166920.

COLE, J. J., FAYDACI, B. A., MCGUINNESS, D., SHAW, R., MACIEWICZ, R. A., ROBERTSON, N. A. & GOODYEAR, C. S. 2021. Searchlight: automated bulk RNA-seq exploration and visualisation using dynamically generated R scripts. *BMC Bioinformatics,* 22**,** 411.

COLONNA, M. & BUTOVSKY, O. 2017. Microglia Function in the Central Nervous System During Health and Neurodegeneration. *Annu Rev Immunol,* 35**,** 441-468.

CONTALDI, E., MAGISTRELLI, L. & COMI, C. 2022. T Lymphocytes in Parkinson's Disease. *J Parkinsons Dis,* 12**,** S65-S74.

COOPER, J. A., ARULPRAGASAM, A. R. & TREADWAY, M. T. 2018. Anhedonia in depression: biological mechanisms and computational models. *Curr Opin Behav Sci,* 22**,** 128-135.

CORNELL, J., SALINAS, S., HUANG, H. Y. & ZHOU, M. 2022. Microglia regulation of synaptic plasticity and learning and memory. *Neural Regen Res,* 17**,** 705-716.

CORRALIZA-GOMEZ, M., BENDITO, B., SANDONIS-CAMARERO, D., MONDEJAR-DURAN, J., VILLA, M., PONCELA, M., VALERO, J., SANCHEZ, D. & GANFORNINA, M. D. 2023. Dual role of Apolipoprotein D as long-term instructive factor and acute signal conditioning microglial secretory and phagocytic responses. *Front Cell Neurosci,* 17**,** 1112930.

CUI, L., LI, S., WANG, S., WU, X., LIU, Y., YU, W., WANG, Y., TANG, Y., XIA, M. & LI, B. 2024. Major depressive disorder: hypothesis, mechanism, prevention and treatment. *Signal Transduct Target Ther,* 9**,** 30.

DAGLAS, M., DRAXLER, D. F., HO, H., MCCUTCHEON, F., GALLE, A., AU, A. E., LARSSON, P., GREGORY, J., ALDERUCCIO, F., SASHINDRANATH, M. & MEDCALF, R. L. 2019. Activated CD8(+) T Cells Cause Long-Term Neurological Impairment after Traumatic Brain Injury in Mice. *Cell Rep,* 29**,** 1178-1191 e6.

DAI, B., LI, T., CAO, J., ZHAO, X., JIANG, Y., SHI, L. & WEI, J. 2024. CD4(+) T-cell subsets are associated with chronic stress effects in newly diagnosed anxiety disorders. *Neurobiol Stress,* 31**,** 100661.

DANTZER, R. 2009. Cytokine, sickness behavior, and depression. *Immunol Allergy Clin North Am,* 29**,** 247-64.

DANTZER, R. 2023. Evolutionary Aspects of Infections: Inflammation and Sickness Behaviors. *Curr Top Behav Neurosci,* 61**,** 1-14.

DANTZER, R., O'CONNOR, J. C., FREUND, G. G., JOHNSON, R. W. & KELLEY, K. W. 2008. From inflammation to sickness and depression: when the immune system subjugates the brain. *Nat Rev Neurosci,* 9**,** 46-56.

DANTZER, R. & WALKER, A. K. 2014. Is there a role for glutamate-mediated excitotoxicity in inflammation-induced depression? *J Neural Transm (Vienna),* 121**,** 925-32.

DARIA, S., PROMA, M. A., SHAHRIAR, M., ISLAM, S. M. A., BHUIYAN, M. A. & ISLAM, M. R. 2020. Serum interferon-gamma level is associated with drug-naive major depressive disorder. *SAGE Open Med,* 8**,** 2050312120974169.

DAS, R., EMON, M. P. Z., SHAHRIAR, M., NAHAR, Z., ISLAM, S. M. A., BHUIYAN, M. A., ISLAM, S. N. & ISLAM, M. R. 2021. Higher levels of serum IL-1beta and TNF-alpha are associated with an increased probability of major depressive disorder. *Psychiatry Res,* 295**,** 113568.

DAUBNER, S. C., LE, T. & WANG, S. 2011. Tyrosine hydroxylase and regulation of dopamine synthesis. *Arch Biochem Biophys,* 508**,** 1-12.

DAVAMI, M. H., BAHARLOU, R., AHMADI VASMEHJANI, A., GHANIZADEH, A., KESHTKAR, M., DEZHKAM, I. & ATASHZAR, M. R. 2016. Elevated IL-17 and TGF-beta Serum Levels: A Positive Correlation between T-helper 17 Cell-Related Pro-Inflammatory Responses with Major Depressive Disorder. *Basic Clin Neurosci,* 7**,** 137-42.

DEACON, R. M. 2006. Assessing nest building in mice. *Nat Protoc,* 1**,** 1117-9.

DECARIE-SPAIN, L., SHARMA, S., HRYHORCZUK, C., ISSA-GARCIA, V., BARKER, P. A., ARBOUR, N., ALQUIER, T. & FULTON, S. 2018. Nucleus accumbens inflammation mediates anxiodepressive behavior and compulsive sucrose seeking elicited by saturated dietary fat. *Mol Metab,* 10**,** 1-13.

DENISENKO, E., DE KOCK, L., TAN, A., BEASLEY, A. B., BEILIN, M., JONES, M. E., HOU, R., MUIRI, D. O., BILIC, S., MOHAN, G., SALFINGER, S., FOX, S., HMON, K. P. W., YEOW, Y., KIM, Y., JOHN, R., GILDERMAN, T. S., KILLINGBECK, E., GRAY, E. S., COHEN, P. A., YU, Y. & FORREST, A. R. R. 2024. Spatial transcriptomics reveals discrete tumour microenvironments and autocrine loops within ovarian cancer subclones. *Nat Commun,* 15**,** 2860.

DEPAULA-SILVA, A. B., GORBEA, C., DOTY, D. J., LIBBEY, J. E., SANCHEZ, J. M. S., HANAK, T. J., CAZALLA, D. & FUJINAMI, R. S. 2019. Differential transcriptional profiles identify microglial- and macrophage-specific gene markers expressed during virus-induced neuroinflammation. *J Neuroinflammation,* 16**,** 152.

DER-AVAKIAN, A. & MARKOU, A. 2012. The neurobiology of anhedonia and other reward-related deficits. *Trends Neurosci,* 35**,** 68-77.

DERMITZAKIS, I., THEOTOKIS, P., EVANGELIDIS, P., DELILAMPOU, E., EVANGELIDIS, N., CHATZISAVVIDOU, A., AVRAMIDOU, E. & MANTHOU, M. E. 2023. CNS Border-Associated Macrophages: Ontogeny and Potential Implication in Disease. *Curr Issues Mol Biol,* 45**,** 4285-4300.

DHABHAR, F. S., BURKE, H. M., EPEL, E. S., MELLON, S. H., ROSSER, R., REUS, V. I. & WOLKOWITZ, O. M. 2009. Low serum IL-10 concentrations and loss of regulatory association between IL-6 and IL-10 in adults with major depression. *J Psychiatr Res,* 43**,** 962-9.

DISABATO, D. J., QUAN, N. & GODBOUT, J. P. 2016. Neuroinflammation: the devil is in the details. *J Neurochem,* 139 Suppl 2**,** 136-153.

DOMINGUES, H. S., MUES, M., LASSMANN, H., WEKERLE, H. & KRISHNAMOORTHY, G. 2010. Functional and pathogenic differences of Th1 and Th17 cells in experimental autoimmune encephalomyelitis. *PLoS One,* 5**,** e15531.

DONINI, M., FONTANA, S., SAVOLDI, G., VERMI, W., TASSONE, L., GENTILI, F., ZENARO, E., FERRARI, D., NOTARANGELO, L. D., PORTA, F., FACCHETTI, F., NOTARANGELO, L. D., DUSI, S. & BADOLATO, R. 2007. G-CSF treatment of severe congenital neutropenia reverses neutropenia but does not correct the underlying functional deficiency of the neutrophil in defending against microorganisms. *Blood,* 109**,** 4716-23.

DOWLATI, Y., HERRMANN, N., SWARDFAGER, W., LIU, H., SHAM, L., REIM, E. K. & LANCTOT, K. L. 2010. A meta-analysis of cytokines in major depression. *Biol Psychiatry,* 67**,** 446-57.

DRABKIN, H. J., BLAKE, J. A. & MOUSE GENOME INFORMATICS, D. 2012. Manual Gene Ontology annotation workflow at the Mouse Genome Informatics Database. *Database (Oxford),* 2012**,** bas045.

DRAPER, A., KOCH, R. M., VAN DER MEER, J. W., AJ APPS, M., PICKKERS, P., HUSAIN, M. & VAN DER SCHAAF, M. E. 2018. Effort but not Reward Sensitivity is Altered by Acute Sickness Induced by Experimental Endotoxemia in Humans. *Neuropsychopharmacology,* 43**,** 1107-1118.

DRESP-LANGLEY, B. 2023. From Reward to Anhedonia-Dopamine Function in the Global Mental Health Context. *Biomedicines,* 11.

DUARTE, J. M., NGUYEN, R., KYPROU, M., LI, K., MILENTIJEVIC, A., CERQUETELLA, C., FORRO, T. & CIOCCHI, S. 2024. Hippocampal contextualization of social rewards in mice. *Nat Commun,* 15**,** 9493.

DUDEK, K. A., DION-ALBERT, L., LEBEL, M., LECLAIR, K., LABRECQUE, S., TUCK, E., FERRER PEREZ, C., GOLDEN, S. A., TAMMINGA, C., TURECKI, G., MECHAWAR, N., RUSSO, S. J. & MENARD, C. 2020. Molecular adaptations of the blood–brain barrier promote stress resilience vs. depression. *Proceedings of the National Academy of Sciences,* 117**,** 3326-3336.

DUKAY, B., CSOBOZ, B. & TOTH, M. E. 2019. Heat-Shock Proteins in Neuroinflammation. *Front Pharmacol,* 10**,** 920.

DUNN, G. A., LOFTIS, J. M. & SULLIVAN, E. L. 2020. Neuroinflammation in psychiatric disorders: An introductory primer. *Pharmacol Biochem Behav,* 196**,** 172981.

EDISON, P. 2024. Astroglial activation: Current concepts and future directions. *Alzheimers Dement,* 20**,** 3034-3053.

EITMANN, S., FUREDI, N., GASZNER, B., KORMOS, V., BERTA, G., POLAI, F., KOVACS, D. K., BALASKO, M. & PETERVARI, E. 2024. Activity of the hypothalamic neuropeptide Y increases in adult and decreases in old rats. *Sci Rep,* 14**,** 22676.

EL-ZAYAT, S. R., SIBAII, H. & MANNAA, F. A. 2019. Toll-like receptors activation, signaling, and targeting: an overview. *Bulletin of the National Research Centre,* 43**,** 187.

ELGELLAIE, A., THOMAS, S. J., KAELLE, J., BARTSCHI, J. & LARKIN, T. 2023. Pro-inflammatory cytokines IL-1alpha, IL-6 and TNF-alpha in major depressive disorder: Sex-specific associations with psychological symptoms. *Eur J Neurosci,* 57**,** 1913-1928.

EME-SCOLAN, E. & DANDO, S. J. 2020. Tools and Approaches for Studying Microglia In vivo. *Front Immunol,* 11**,** 583647.

ERTA, M., QUINTANA, A. & HIDALGO, J. 2012. Interleukin-6, a major cytokine in the central nervous system. *Int J Biol Sci,* 8**,** 1254-66.

EVANS, F. L., DITTMER, M., DE LA FUENTE, A. G. & FITZGERALD, D. C. 2019. Protective and Regenerative Roles of T Cells in Central Nervous System Disorders. *Front Immunol,* 10**,** 2171.

FELGER, J. C., LI, Z., HAROON, E., WOOLWINE, B. J., JUNG, M. Y., HU, X. & MILLER, A. H. 2016. Inflammation is associated with decreased functional connectivity within corticostriatal reward circuitry in depression. *Mol Psychiatry,* 21**,** 1358-65.

FELGER, J. C. & LOTRICH, F. E. 2013. Inflammatory cytokines in depression: neurobiological mechanisms and therapeutic implications. *Neuroscience,* 246**,** 199-229.

FERNANDEZ-PUJALS, A. M., ADAMS, M. J., THOMSON, P., MCKECHANIE, A. G., BLACKWOOD, D. H., SMITH, B. H., DOMINICZAK, A. F., MORRIS, A. D., MATTHEWS, K., CAMPBELL, A., LINKSTED, P., HALEY, C. S., DEARY, I. J., PORTEOUS, D. J., MACINTYRE, D. J. & MCINTOSH, A. M. 2015. Epidemiology and Heritability of Major Depressive Disorder, Stratified by Age of Onset, Sex, and Illness Course in Generation Scotland: Scottish Family Health Study (GS:SFHS). *PLoS One,* 10**,** e0142197.

FESHARAKI-ZADEH, A., MIYAUCHI, J. T., ST LAURENT-ARRIOT, K., TSIRKA, S. E. & BERGOLD, P. J. 2020. Increased Behavioral Deficits and Inflammation in a Mouse Model of Co-Morbid Traumatic Brain Injury and Post-Traumatic Stress Disorder. *ASN Neuro,* 12**,** 1759091420979567.

FILLATREAU, S., MANFROI, B. & DÖRNER, T. 2021. Toll-like receptor signalling in B cells during systemic lupus erythematosus. *Nature Reviews Rheumatology,* 17**,** 98-108.

FINKELMAN, F. D., MALEK, T. R., SHEVACH, E. M. & MOND, J. J. 1986. In vivo and in vitro expression of an interleukin 2 receptor by murine B and T lymphocytes. *J Immunol,* 137**,** 2252-9.

FINTER, N. B., CHAPMAN, S., DOWD, P., JOHNSTON, J. M., MANNA, V., SARANTIS, N., SHERON, N., SCOTT, G., PHUA, S. & TATUM, P. B. 1991. The use of interferon-alpha in virus infections. *Drugs,* 42**,** 749-65.

FLETCHER, J. M., LALOR, S. J., SWEENEY, C. M., TUBRIDY, N. & MILLS, K. H. 2010. T cells in multiple sclerosis and experimental autoimmune encephalomyelitis. *Clin Exp Immunol,* 162**,** 1-11.

FLORIS, G., ZANDA, M. T., DABROWSKI, K. R. & DAWS, S. E. 2024. Neuroinflammatory history results in overlapping transcriptional signatures with heroin exposure in the nucleus accumbens and alters responsiveness to heroin in male rats. *Transl Psychiatry,* 14**,** 500.

FOIADELLI, T., LODDO, N., SACCHI, L., SANTI, V., D'IMPORZANO, G., SPREAFICO, E., ORSINI, A., FERRETTI, A., DE AMICI, M., TESTA, G., MARSEGLIA, G. L. & SAVASTA, S. 2025. IL-17 in serum and cerebrospinal fluid of pediatric patients with acute neuropsychiatric disorders: Implications for PANDAS and PANS. *Eur J Paediatr Neurol,* 54**,** 1-7.

FRICKER, M., NEHER, J. J., ZHAO, J. W., THERY, C., TOLKOVSKY, A. M. & BROWN, G. C. 2012. MFG-E8 mediates primary phagocytosis of viable neurons during neuroinflammation. *J Neurosci,* 32**,** 2657-66.

FUNAYAMA, Y., LI, H., ISHIMORI, E., KAWATAKE-KUNO, A., INABA, H., YAMAGATA, H., SEKI, T., NAKAGAWA, S., WATANABE, Y., MURAI, T., OISHI, N. & UCHIDA, S. 2023. Antidepressant Response and Stress Resilience Are Promoted by CART Peptides in GABAergic Neurons of the Anterior Cingulate Cortex. *Biol Psychiatry Glob Open Sci,* 3**,** 87-98.

GALEA, I., BECHMANN, I. & PERRY, V. H. 2007. What is immune privilege (not)? *Trends Immunol,* 28**,** 12-8.

GALECKA, M., BLIZNIEWSKA-KOWALSKA, K., ORZECHOWSKA, A., SZEMRAJ, J., MAES, M., BERK, M., SU, K. P. & GALECKI, P. 2021. Inflammatory versus Anti-inflammatory Profiles in Major Depressive Disorders-The Role of IL-17, IL-21, IL-23, IL-35 and Foxp3. *J Pers Med,* 11.

GAO, H., DANZI, M. C., CHOI, C. S., TAHERIAN, M., DALBY-HANSEN, C., ELLMAN, D. G., MADSEN, P. M., BIXBY, J. L., LEMMON, V. P., LAMBERTSEN, K. L. & BRAMBILLA, R. 2017. Opposing Functions of Microglial and Macrophagic TNFR2 in the Pathogenesis of Experimental Autoimmune Encephalomyelitis. *Cell Rep,* 18**,** 198-212.

GAO, Y. & WILLIAMS, A. P. 2015. Role of Innate T Cells in Anti-Bacterial Immunity. *Front Immunol,* 6**,** 302.

GASKILL, B. N., KARAS, A. Z., GARNER, J. P. & PRITCHETT-CORNING, K. R. 2013. Nest building as an indicator of health and welfare in laboratory mice. *J Vis Exp,* 51012.

GELOSO, M. C., ZUPO, L. & CORVINO, V. 2024. Crosstalk between peripheral inflammation and brain: Focus on the responses of microglia and astrocytes to peripheral challenge. *Neurochem Int,* 180**,** 105872.

GENCTURK, S. & UNAL, G. 2024. Rodent tests of depression and anxiety: Construct validity and translational relevance. *Cogn Affect Behav Neurosci,* 24**,** 191-224.

GERLOFF, C., KNOTH, R. & VOLK, B. 1993. Cytoplasmic expression of the leu-4 (CD3) antigen in developing Purkinje cells in the rat cerebellum. *Neuropathol Appl Neurobiol,* 19**,** 313-23.

GODDERY, E. N., FAIN, C. E., LIPOVSKY, C. G., AYASOUFI, K., YOKANOVICH, L. T., MALO, C. S., KHADKA, R. H., TRITZ, Z. P., JIN, F., HANSEN, M. J. & JOHNSON, A. J. 2021. Microglia and Perivascular Macrophages Act as Antigen Presenting Cells to Promote CD8 T Cell Infiltration of the Brain. *Front Immunol,* 12**,** 726421.

GOLDSMITH, D. R., BEKHBAT, M., MEHTA, N. D. & FELGER, J. C. 2023. Inflammation-Related Functional and Structural Dysconnectivity as a Pathway to Psychopathology. *Biol Psychiatry,* 93**,** 405-418.

GOMES, C., HUANG, K. C., HARKIN, J., BAKER, A., HUGHES, J. M., PAN, Y., TUTROW, K., VANDERWALL, K. B., LAVEKAR, S. S., HERNANDEZ, M., CUMMINS, T. R., CANFIELD, S. G. & MEYER, J. S. 2024. Induction of astrocyte reactivity promotes neurodegeneration in human pluripotent stem cell models. *Stem Cell Reports,* 19**,** 1122-1136.

GOMEZ-ARBOLEDAS, A., CARVALHO, K., BALDERRAMA-GUTIERREZ, G., CHU, S. H., LIANG, H. Y., SCHARTZ, N. D., SELVAN, P., PETRISKO, T. J., PAN, M. A., MORTAZAVI, A. & TENNER, A. J. 2022. C5aR1 antagonism alters microglial polarization and mitigates disease progression in a mouse model of Alzheimer's disease. *Acta Neuropathol Commun,* 10**,** 116.

GONZALEZ CALDITO, N. 2023. Role of tumor necrosis factor-alpha in the central nervous system: a focus on autoimmune disorders. *Front Immunol,* 14**,** 1213448.

GONZALEZ, H. & PACHECO, R. 2014. T-cell-mediated regulation of neuroinflammation involved in neurodegenerative diseases. *J Neuroinflammation,* 11**,** 201.

GORMAN, J. M. & KENT, J. M. 1999. SSRIs and SNRIs: broad spectrum of efficacy beyond major depression. *J Clin Psychiatry,* 60 Suppl 4**,** 33-8; discussion 39.

GOSSELIN, D. & RIVEST, S. 2007. Role of IL-1 and TNF in the brain: twenty years of progress on a Dr. Jekyll/Mr. Hyde duality of the innate immune system. *Brain Behav Immun,* 21**,** 281-9.

GRAFF, L. A., WALKER, J. R. & BERNSTEIN, C. N. 2009. Depression and Anxiety in Inflammatory Bowel Disease:A Review of Comorbidity and Management. *Inflammatory Bowel Diseases,* 15**,** 1105-1118.

GREEN, T. R. F. & ROWE, R. K. 2024. Quantifying microglial morphology: an insight into function. *Clin Exp Immunol,* 216**,** 221-229.

GREENE, R. K., WALSH, E., MOSNER, M. G. & DICHTER, G. S. 2019. A potential mechanistic role for neuroinflammation in reward processing impairments in autism spectrum disorder. *Biol Psychol,* 142**,** 1-12.

GRETER, M., LELIOS, I. & CROXFORD, A. L. 2015. Microglia Versus Myeloid Cell Nomenclature during Brain Inflammation. *Front Immunol,* 6**,** 249.

GRINE, L., DEJAGER, L., LIBERT, C. & VANDENBROUCKE, R. E. 2015. Dual Inhibition of TNFR1 and IFNAR1 in Imiquimod-Induced Psoriasiform Skin Inflammation in Mice. *J Immunol,* 194**,** 5094-102.

GROH, J., FENG, R., YUAN, X., LIU, L., KLEIN, D., HUTAHAEAN, G., BUTZ, E., WANG, Z., STEINBRECHER, L., NEHER, J., MARTINI, R. & SIMONS, M. 2025. Microglia activation orchestrates CXCL10-mediated CD8(+) T cell recruitment to promote aging-related white matter degeneration. *Nat Neurosci,* 28**,** 1160-1173.

GROSCURTH, P. & FILGUEIRA, L. 1998. Killing Mechanisms of Cytotoxic T Lymphocytes. *News Physiol Sci,* 13**,** 17-21.

GUO, J., ZHANG, H., LIN, W., LU, L., SU, J. & CHEN, X. 2024. Correction: Signaling pathways and targeted therapies for psoriasis. *Signal Transduct Target Ther,* 9**,** 25.

GUO, L., TIAN, J. & DU, H. 2017. Mitochondrial Dysfunction and Synaptic Transmission Failure in Alzheimer's Disease. *J Alzheimers Dis,* 57**,** 1071-1086.

GURREA-RUBIO, M., FOX, D. A. & CASTRESANA, J. S. 2025. CD6 in Human Disease. *Cells,* 14.

GUSEL'NIKOVA, V. V. & KORZHEVSKIY, D. E. 2015. NeuN As a Neuronal Nuclear Antigen and Neuron Differentiation Marker. *Acta Naturae,* 7**,** 42-7.

GUVENEK, A., PARIKSHAK, N., ZAMOLODCHIKOV, D., GELFMAN, S., MOSCATI, A., DOBBYN, L., STAHL, E., SHULDINER, A. & COPPOLA, G. 2024. Transcriptional profiling in microglia across physiological and pathological states identifies a transcriptional module associated with neurodegeneration. *Commun Biol,* 7**,** 1168.

HAILE, Y., CARMINE-SIMMEN, K., OLECHOWSKI, C., KERR, B., BLEACKLEY, R. C. & GIULIANI, F. 2015. Granzyme B-inhibitor serpina3n induces neuroprotection in vitro and in vivo. *J Neuroinflammation,* 12**,** 157.

HAMMOND, T. R., DUFORT, C., DISSING-OLESEN, L., GIERA, S., YOUNG, A., WYSOKER, A., WALKER, A. J., GERGITS, F., SEGEL, M., NEMESH, J., MARSH, S. E., SAUNDERS, A., MACOSKO, E., GINHOUX, F., CHEN, J., FRANKLIN, R. J. M., PIAO, X., MCCARROLL, S. A. & STEVENS, B. 2019. Single-Cell RNA Sequencing of Microglia throughout the Mouse Lifespan and in the Injured Brain Reveals Complex Cell-State Changes. *Immunity,* 50**,** 253-271 e6.

HAN, L., LIU, Z., JING, Z., LIU, Y., PENG, Y., CHANG, H., LEI, J., WANG, K., XU, Y., LIU, W., WU, Z., LI, Q., SHI, X., ZHENG, M., WANG, H., DENG, J., ZHONG, Y., PAN, H., LIN, J., ZHANG, R., CHEN, Y., WU, J., XU, M., REN, B., CHENG, M., YU, Q., SONG, X., LU, Y., TANG, Y., YUAN, N., SUN, S., AN,

Y., DING, W., SUN, X., WEI, Y., ZHANG, S., DOU, Y., ZHAO, Y., HAN, L., ZHU, Q., XU, J., WANG, S., WANG, D., BAI, Y., LIANG, Y., LIU, Y., CHEN, M., XIE, C., BO, B., LI, M., ZHANG, X., TING, W., CHEN, Z., FANG, J., LI, S., JIANG, Y., TAN, X., ZUO, G., XIE, Y., LI, H., TAO, Q., LI, Y., LIU, J., LIU, Y., HAO, M., WANG, J., WEN, H., LIU, J., YAN, Y., ZHANG, H., SHENG, Y., YU, S., LIAO, X., JIANG, X., WANG, G., LIU, H., WANG, C., FENG, N., LIU, X., MA, K., XU, X., HAN, T., CAO, H., ZHENG, H., CHEN, Y., LU, H., YU, Z., ZHANG, J., WANG, B., WANG, Z., XIE, Q., PAN, S., LIU, C., XU, C., CUI, L., LI, Y., LIU, S., LIAO, S., CHEN, A., WU, Q. F., et al. 2025. Single-cell spatial transcriptomic atlas of the whole mouse brain. *Neuron*.

HAN, X., CHEN, M., WANG, F., WINDREM, M., WANG, S., SHANZ, S., XU, Q., OBERHEIM, N. A., BEKAR, L., BETSTADT, S., SILVA, A. J., TAKANO, T., GOLDMAN, S. A. & NEDERGAARD, M. 2013. Forebrain engraftment by human glial progenitor cells enhances synaptic plasticity and learning in adult mice. *Cell Stem Cell,* 12**,** 342-53.

HANKE, M. L. & KIELIAN, T. 2011. Toll-like receptors in health and disease in the brain: mechanisms and therapeutic potential. *Clin Sci (Lond),* 121**,** 367-87.

HAO, Y., STUART, T., KOWALSKI, M. H., CHOUDHARY, S., HOFFMAN, P., HARTMAN, A., SRIVASTAVA, A., MOLLA, G., MADAD, S., FERNANDEZ-GRANDA, C. & SATIJA, R. 2024. Dictionary learning for integrative, multimodal and scalable single-cell analysis. *Nat Biotechnol,* 42**,** 293-304.

HAROON, E., MILLER, A. H. & SANACORA, G. 2017. Inflammation, Glutamate, and Glia: A Trio of Trouble in Mood Disorders. *Neuropsychopharmacology,* 42**,** 193-215.

HART, O. M., ATHIE-MORALES, V., O'CONNOR, G. M. & GARDINER, C. M. 2005. TLR7/8-mediated activation of human NK cells results in accessory cell-dependent IFN-gamma production. *J Immunol,* 175**,** 1636-42.

HART, P. H., VITTI, G. F., BURGESS, D. R., WHITTY, G. A., PICCOLI, D. S. & HAMILTON, J. A. 1989. Potential antiinflammatory effects of interleukin 4: suppression of human monocyte tumor necrosis factor alpha, interleukin 1, and prostaglandin E2. *Proc Natl Acad Sci U S A,* 86**,** 3803-7.

HAYNES, S. E., HOLLOPETER, G., YANG, G., KURPIUS, D., DAILEY, M. E., GAN, W. B. & JULIUS, D. 2006. The P2Y12 receptor regulates microglial activation by extracellular nucleotides. *Nat Neurosci,* 9**,** 1512-9.

HE, L. W., ZENG, L., TIAN, N., LI, Y., HE, T., TAN, D. M., ZHANG, Q. & TAN, Y. 2020. Optimization of food deprivation and sucrose preference test in SD rat model undergoing chronic unpredictable mild stress. *Animal Model Exp Med,* 3**,** 69-78.

HE, S., BHATT, R., BROWN, C., BROWN, E. A., BUHR, D. L., CHANTRANUVATANA, K., DANAHER, P., DUNAWAY, D., GARRISON, R. G., GEISS, G., GREGORY, M. T., HOANG, M. L., KHAFIZOV, R., KILLINGBECK, E. E., KIM, D., KIM, T. K., KIM, Y., KLOCK, A., KORUKONDA, M., KUTCHMA, A., LEWIS, Z. R., LIANG, Y., NELSON, J. S., ONG, G. T., PERILLO, E. P., PHAN, J. C., PHAN-EVERSON, T., PIAZZA, E., RANE, T., REITZ, Z., RHODES, M., ROSENBLOOM, A., ROSS, D., SATO, H., WARDHANI, A. W., WILLIAMS-WIETZIKOSKI, C. A., WU, L. & BEECHEM, J. M. 2022. High-plex imaging of RNA and proteins at subcellular resolution in fixed tissue by spatial molecular imaging. *Nat Biotechnol,* 40**,** 1794-1806.

HE, Y., REN, Y., CHEN, X., WANG, Y., YU, H., CAI, J., WANG, P., REN, Y. & XIE, P. 2024. Neural and molecular investigation into the paraventricular

thalamus for chronic restraint stress induced depressive-like behaviors. *J Adv Res*.

HEALY, L. M., ZIA, S. & PLEMEL, J. R. 2022. Towards a definition of microglia heterogeneity. *Commun Biol,* 5**,** 1114.

HEDEMANN, T. L., LIU, X., KANG, C. N. & HUSAIN, M. I. 2022. Associations between psoriasis and mental illness: an update for clinicians. *Gen Hosp Psychiatry,* 75**,** 30-37.

HEIR, R. & STELLWAGEN, D. 2020. TNF-Mediated Homeostatic Synaptic Plasticity: From in vitro to in vivo Models. *Front Cell Neurosci,* 14**,** 565841.

HEMMI, H., KAISHO, T., TAKEUCHI, O., SATO, S., SANJO, H., HOSHINO, K., HORIUCHI, T., TOMIZAWA, H., TAKEDA, K. & AKIRA, S. 2002. Small anti-viral compounds activate immune cells via the TLR7 MyD88-dependent signaling pathway. *Nat Immunol,* 3**,** 196-200.

HENNING, L., ANTONY, H., BREUER, A., MULLER, J., SEIFERT, G., AUDINAT, E., SINGH, P., BROSSERON, F., HENEKA, M. T., STEINHAUSER, C. & BEDNER, P. 2023. Reactive microglia are the major source of tumor necrosis factor alpha and contribute to astrocyte dysfunction and acute seizures in experimental temporal lobe epilepsy. *Glia,* 71**,** 168-186.

HESDORFFER, D. C. 2016. Comorbidity between neurological illness and psychiatric disorders. *CNS Spectr,* 21**,** 230-8.

HESHMATI, M. & RUSSO, S. J. 2015. Anhedonia and the brain reward circuitry in depression. *Curr Behav Neurosci Rep,* 2**,** 146-153.

HICKMAN, S. E., KINGERY, N. D., OHSUMI, T. K., BOROWSKY, M. L., WANG, L. C., MEANS, T. K. & EL KHOURY, J. 2013. The microglial sensome revealed by direct RNA sequencing. *Nat Neurosci,* 16**,** 1896-905.

HIMMERICH, H., PATSALOS, O., LICHTBLAU, N., IBRAHIM, M. A. A. & DALTON, B. 2019. Cytokine Research in Depression: Principles, Challenges, and Open Questions. *Front Psychiatry,* 10**,** 30.

HOFBAUER, D., MOUGIAKAKOS, D., BROGGINI, L., ZAISS, M., BUTTNER-HEROLD, M., BACH, C., SPRIEWALD, B., NEUMANN, F., BISHT, S., NOLTING, J., ZEISER, R., HAMARSHEH, S., EBERHARDT, M., VERA, J., VISENTIN, C., DE LUCA, C. M. G., MODA, F., HASKAMP, S., FLAMANN, C., BOTTCHER, M., BITTERER, K., VOLKL, S., MACKENSEN, A., RICAGNO, S. & BRUNS, H. 2021. beta(2)-microglobulin triggers NLRP3 inflammasome activation in tumor-associated macrophages to promote multiple myeloma progression. *Immunity,* 54**,** 1772-1787 e9.

HOFLICH, A., MICHENTHALER, P., KASPER, S. & LANZENBERGER, R. 2019. Circuit Mechanisms of Reward, Anhedonia, and Depression. *Int J Neuropsychopharmacol,* 22**,** 105-118.

HOLCMANN, M., DROBITS, B. & SIBILIA, M. 2012. How imiquimod licenses plasmacytoid dendritic cells to kill tumors. *Oncoimmunology,* 1**,** 1661-1663.

HOLLANDER, J. A., CORY-SLECHTA, D. A., JACKA, F. N., SZABO, S. T., GUILARTE, T. R., BILBO, S. D., MATTINGLY, C. J., MOY, S. S., HAROON, E., HORNIG, M., LEVIN, E. D., PLETNIKOV, M. V., ZEHR, J. L., MCALLISTER, K. A., DZIERLENGA, A. L., GARTON, A. E., LAWLER, C. P. & LADD-ACOSTA, C. 2020. Beyond the looking glass: recent advances in understanding the impact of environmental exposures on neuropsychiatric disease. *Neuropsychopharmacology,* 45**,** 1086-1096.

HONARPISHEH, P., LEE, J., BANERJEE, A., BLASCO-CONESA, M. P., HONARPISHEH, P., D'AIGLE, J., MAMUN, A. A., RITZEL, R. M., CHAUHAN, A., GANESH, B. P. & MCCULLOUGH, L. D. 2020. Potential caveats of putative microglia-

specific markers for assessment of age-related cerebrovascular neuroinflammation. *J Neuroinflammation,* 17**,** 366.

HOOK, G., REINHECKEL, T., NI, J., WU, Z., KINDY, M., PETERS, C. & HOOK, V. 2022. Cathepsin B Gene Knockout Improves Behavioral Deficits and Reduces Pathology in Models of Neurologic Disorders. *Pharmacol Rev,* 74**,** 600-629.

HOZUMI, Y. & GOTO, K. 2012. Diacylglycerol kinase beta in neurons: functional implications at the synapse and in disease. *Adv Biol Regul,* 52**,** 315-25.

HSING, L. C. & RUDENSKY, A. Y. 2005. The lysosomal cysteine proteases in MHC class II antigen presentation. *Immunol Rev,* 207**,** 229-41.

HU, R. K., ZUO, Y., LY, T., WANG, J., MEERA, P., WU, Y. E. & HONG, W. 2021. An amygdala-to-hypothalamus circuit for social reward. *Nat Neurosci,* 24**,** 831-842.

HUANG, J. W., CAO, C. A., ZHENG, W. H., JIA, C. R., LIU, X., GAO, S. Q. & GUO, Y. 2024. The mechanism of cancer-depression comorbidity. *Neuroscience,* 556**,** 25-30.

HUANG, Y., LIU, Z., CAO, B. B., QIU, Y. H. & PENG, Y. P. 2020. Treg Cells Attenuate Neuroinflammation and Protect Neurons in a Mouse Model of Parkinson's Disease. *J Neuroimmune Pharmacol,* 15**,** 224-237.

HUWART, S. J. P., FAYT, C., GANGAROSSA, G., LUQUET, S., CANI, P. D. & EVERARD, A. 2024. TLR4-dependent neuroinflammation mediates LPS-driven food-reward alterations during high-fat exposure. *J Neuroinflammation,* 21**,** 305.

HWANG, C. K., CHAURASIA, S. S., JACKSON, C. R., CHAN, G. C., STORM, D. R. & IUVONE, P. M. 2013. Circadian rhythm of contrast sensitivity is regulated by a dopamine-neuronal PAS-domain protein 2-adenylyl cyclase 1 signaling pathway in retinal ganglion cells. *J Neurosci,* 33**,** 14989-97.

ITO, D., IMAI, Y., OHSAWA, K., NAKAJIMA, K., FUKUUCHI, Y. & KOHSAKA, S. 1998. Microglia-specific localisation of a novel calcium binding protein, Iba1. *Brain Res Mol Brain Res,* 57**,** 1-9.

ITO, H. & NAGATA, K. I. 2022. Functions of CNKSR2 and Its Association with Neurodevelopmental Disorders. *Cells,* 11.

ITO, M., KOMAI, K., MISE-OMATA, S., IIZUKA-KOGA, M., NOGUCHI, Y., KONDO, T., SAKAI, R., MATSUO, K., NAKAYAMA, T., YOSHIE, O., NAKATSUKASA, H., CHIKUMA, S., SHICHITA, T. & YOSHIMURA, A. 2019. Brain regulatory T cells suppress astrogliosis and potentiate neurological recovery. *Nature,* 565**,** 246-250.

JACK, C. S., ARBOUR, N., MANUSOW, J., MONTGRAIN, V., BLAIN, M., MCCREA, E., SHAPIRO, A. & ANTEL, J. P. 2005. TLR signaling tailors innate immune responses in human microglia and astrocytes. *J Immunol,* 175**,** 4320-30.

JAMES, M. H., MCNALLY, G. P. & LI, X. 2021. Editorial: Role of the Thalamus in Motivated Behavior. *Front Behav Neurosci,* 15**,** 720592.

JANGALWE, S., KAPOOR, V. N., XU, J., GIRNIUS, N., KENNEDY, N. J., EDWARDS, Y. J. K., WELSH, R. M., DAVIS, R. J. & BREHM, M. A. 2019. Cutting Edge: Early Attrition of Memory T Cells during Inflammation and Costimulation Blockade Is Regulated Concurrently by Proapoptotic Proteins Fas and Bim. *J Immunol,* 202**,** 647-651.

JIANG, Y., ZOU, M., WANG, Y. & WANG, Y. 2023. Nucleus accumbens in the pathogenesis of major depressive disorder: A brief review. *Brain Res Bull,* 196**,** 68-75.

JIE, Z., KO, C. J., WANG, H., XIE, X., LI, Y., GU, M., ZHU, L., YANG, J. Y., GAO, T., RU, W., TANG, S. J., CHENG, X. & SUN, S. C. 2021. Microglia promote

autoimmune inflammation via the noncanonical NF-kappaB pathway. *Sci Adv,* 7**,** eabh0609.

JIN, R., SUN, S., HU, Y., ZHANG, H. & SUN, X. 2023. Neuropeptides Modulate Feeding via the Dopamine Reward Pathway. *Neurochem Res,* 48**,** 2622-2643.

JIN, X. & YAMASHITA, T. 2016. Microglia in central nervous system repair after injury. *J Biochem,* 159**,** 491-6.

JIRKOF, P. 2014. Burrowing and nest building behavior as indicators of well-being in mice. *J Neurosci Methods,* 234**,** 139-46.

JOFFE, R. T., LEVITT, A. J. & SOKOLOV, S. T. 1996. Augmentation strategies: focus on anxiolytics. *J Clin Psychiatry,* 57 Suppl 7**,** 25-31; discussion 32-3.

JOHNSON, J. D., BARNARD, D. F., KULP, A. C. & MEHTA, D. M. 2019. Neuroendocrine Regulation of Brain Cytokines After Psychological Stress. *J Endocr Soc,* 3**,** 1302-1320.

JU, H., PARK, K. W., KIM, I. D., CAVE, J. W. & CHO, S. 2022. Phagocytosis converts infiltrated monocytes to microglia-like phenotype in experimental brain ischemia. *J Neuroinflammation,* 19**,** 190.

JUNG, H., LEE, D., YOU, H., LEE, M., KIM, H., CHEONG, E. & UM, J. W. 2023. LPS induces microglial activation and GABAergic synaptic deficits in the hippocampus accompanied by prolonged cognitive impairment. *Sci Rep,* 13**,** 6547.

JUNG, S., ALIBERTI, J., GRAEMMEL, P., SUNSHINE, M. J., KREUTZBERG, G. W., SHER, A. & LITTMAN, D. R. 2000. Analysis of fractalkine receptor CX(3)CR1 function by targeted deletion and green fluorescent protein reporter gene insertion. *Mol Cell Biol,* 20**,** 4106-14.

JURGA, A. M., PALECZNA, M. & KUTER, K. Z. 2020. Overview of General and Discriminating Markers of Differential Microglia Phenotypes. *Front Cell Neurosci,* 14**,** 198.

KAHL, K. G., KRUSE, N., FALLER, H., WEISS, H. & RIECKMANN, P. 2002. Expression of tumor necrosis factor-alpha and interferon-gamma mRNA in blood cells correlates with depression scores during an acute attack in patients with multiple sclerosis. *Psychoneuroendocrinology,* 27**,** 671-81.

KAMEI, R., URATA, S., MARUOKA, H. & OKABE, S. 2022. In vivo Chronic Two-Photon Imaging of Microglia in the Mouse Hippocampus. *J Vis Exp*.

KAPPELMANN, N., DANTZER, R. & KHANDAKER, G. M. 2021. Interleukin-6 as potential mediator of long-term neuropsychiatric symptoms of COVID-19. *Psychoneuroendocrinology,* 131**,** 105295.

KAWANOKUCHI, J., MIZUNO, T., TAKEUCHI, H., KATO, H., WANG, J., MITSUMA, N. & SUZUMURA, A. 2006. Production of interferon-gamma by microglia. *Mult Scler,* 12**,** 558-64.

KAWASAKI, T. & KAWAI, T. 2014. Toll-Like Receptor Signaling Pathways. *Frontiers in Immunology,* 5.

KAYA, T., MATTUGINI, N., LIU, L., JI, H., CANTUTI-CASTELVETRI, L., WU, J., SCHIFFERER, M., GROH, J., MARTINI, R., BESSON-GIRARD, S., KAJI, S., LIESZ, A., GOKCE, O. & SIMONS, M. 2022. CD8(+) T cells induce interferon-responsive oligodendrocytes and microglia in white matter aging. *Nat Neurosci,* 25**,** 1446-1457.

KEALY, J., GREENE, C. & CAMPBELL, M. 2020. Blood-brain barrier regulation in psychiatric disorders. *Neurosci Lett,* 726**,** 133664.

KEBIR, H., KREYMBORG, K., IFERGAN, I., DODELET-DEVILLERS, A., CAYROL, R., BERNARD, M., GIULIANI, F., ARBOUR, N., BECHER, B. & PRAT, A. 2007.

Human TH17 lymphocytes promote blood-brain barrier disruption and central nervous system inflammation. *Nature Medicine,* 13**,** 1173-1175.

KEDIA, S., JI, H., FENG, R., ANDROVIC, P., SPIETH, L., LIU, L., FRANZ, J., ZDIARSTEK, H., ANDERSON, K. P., KABOGLU, C., LIU, Q., MATTUGINI, N., CHERIF, F., PRTVAR, D., CANTUTI-CASTELVETRI, L., LIESZ, A., SCHIFFERER, M., STADELMANN, C., TAHIROVIC, S., GOKCE, O. & SIMONS, M. 2024. T cell-mediated microglial activation triggers myelin pathology in a mouse model of amyloidosis. *Nat Neurosci,* 27**,** 1468-1474.

KELLEY, K. W. & KENT, S. 2020. The Legacy of Sickness Behaviors. *Front Psychiatry,* 11**,** 607269.

KEREN-SHAUL, H., SPINRAD, A., WEINER, A., MATCOVITCH-NATAN, O., DVIR-SZTERNFELD, R., ULLAND, T. K., DAVID, E., BARUCH, K., LARA-ASTAISO, D., TOTH, B., ITZKOVITZ, S., COLONNA, M., SCHWARTZ, M. & AMIT, I. 2017. A Unique Microglia Type Associated with Restricting Development of Alzheimer's Disease. *Cell,* 169**,** 1276-1290 e17.

KIANI SHABESTARI, S., MORABITO, S., DANHASH, E. P., MCQUADE, A., SANCHEZ, J. R., MIYOSHI, E., CHADAREVIAN, J. P., CLAES, C., COBURN, M. A., HASSELMANN, J., HIDALGO, J., TRAN, K. N., MARTINI, A. C., CHANG ROTHERMICH, W., PASCUAL, J., HEAD, E., HUME, D. A., PRIDANS, C., DAVTYAN, H., SWARUP, V. & BLURTON-JONES, M. 2022. Absence of microglia promotes diverse pathologies and early lethality in Alzheimer's disease mice. *Cell Rep,* 39**,** 110961.

KIM, D. G., GONZALES, E. L., KIM, S., KIM, Y., ADIL, K. J., JEON, S. J., CHO, K. S., KWON, K. J. & SHIN, C. Y. 2019. Social Interaction Test in Home Cage as a Novel and Ethological Measure of Social Behavior in Mice. *Exp Neurobiol,* 28**,** 247-260.

KIM, J., SUH, Y.-H. & CHANG, K.-A. 2021a. Interleukin-17 induced by cumulative mild stress promoted depression-like behaviors in young adult mice. *Molecular Brain,* 14**,** 11.

KIM, J., SUH, Y. H. & CHANG, K. A. 2021b. Interleukin-17 induced by cumulative mild stress promoted depression-like behaviors in young adult mice. *Mol Brain,* 14**,** 11.

KIM, Y. K., NA, K. S., MYINT, A. M. & LEONARD, B. E. 2016. The role of pro-inflammatory cytokines in neuroinflammation, neurogenesis and the neuroendocrine system in major depression. *Prog Neuropsychopharmacol Biol Psychiatry,* 64**,** 277-84.

KINDY, M. S., YU, J., ZHU, H., EL-AMOURI, S. S., HOOK, V. & HOOK, G. R. 2012. Deletion of the cathepsin B gene improves memory deficits in a transgenic ALZHeimer's disease mouse model expressing AbetaPP containing the wild-type beta-secretase site sequence. *J Alzheimers Dis,* 29**,** 827-40.

KLEIDONAS, D., KIRSCH, M., ANDRIEUX, G., PFEIFER, D., BOERRIES, M. & VLACHOS, A. 2023. Microglia modulate TNFalpha-mediated synaptic plasticity. *Glia,* 71**,** 2117-2136.

KOCH, C. M., CHIU, S. F., AKBARPOUR, M., BHARAT, A., RIDGE, K. M., BARTOM, E. T. & WINTER, D. R. 2018. A Beginner's Guide to Analysis of RNA Sequencing Data. *Am J Respir Cell Mol Biol,* 59**,** 145-157.

KOLBERG, L., RAUDVERE, U., KUZMIN, I., ADLER, P., VILO, J. & PETERSON, H. 2023. g:Profiler-interoperable web service for functional enrichment analysis and gene identifier mapping (2023 update). *Nucleic Acids Res,* 51**,** W207-W212.

KONSMAN, J. P. 2022. Cytokines in the Brain and Neuroinflammation: We Didn't Starve the Fire! *Pharmaceuticals (Basel),* 15.

KOOL, M. J., PROIETTI ONORI, M., BORGESIUS, N. Z., VAN DE BREE, J. E., ELGERSMA-HOOISMA, M., NIO, E., BEZSTAROSTI, K., BUITENDIJK, G. H. S., AGHADAVOUD JOLFAEI, M., DEMMERS, J. A. A., ELGERSMA, Y. & VAN WOERDEN, G. M. 2019. CAMK2-Dependent Signaling in Neurons Is Essential for Survival. *J Neurosci,* 39**,** 5424-5439.

KORSUNSKY, I., MILLARD, N., FAN, J., SLOWIKOWSKI, K., ZHANG, F., WEI, K., BAGLAENKO, Y., BRENNER, M., LOH, P. R. & RAYCHAUDHURI, S. 2019. Fast, sensitive and accurate integration of single-cell data with Harmony. *Nat Methods,* 16**,** 1289-1296.

KRAEUTER, A. K., GUEST, P. C. & SARNYAI, Z. 2019. The Open Field Test for Measuring Locomotor Activity and Anxiety-Like Behavior. *Methods Mol Biol,* 1916**,** 99-103.

KRETZSCHMAR, F., PIECHA, R., JAHN, J., POTRU, P. S. & SPITTAU, B. 2021. Characterization of the Leucocyte Immunoglobulin-like Receptor B4 (Lilrb4) Expression in Microglia. *Biology (Basel),* 10.

KRONFOL, Z. & REMICK, D. G. 2000. Cytokines and the brain: implications for clinical psychiatry. *Am J Psychiatry,* 157**,** 683-94.

KUMMER, K. K., ZEIDLER, M., KALPACHIDOU, T. & KRESS, M. 2021. Role of IL-6 in the regulation of neuronal development, survival and function. *Cytokine,* 144**,** 155582.

KUNKL, M., AMORMINO, C., TEDESCHI, V., FIORILLO, M. T. & TUOSTO, L. 2022. Astrocytes and Inflammatory T Helper Cells: A Dangerous Liaison in Multiple Sclerosis. *Front Immunol,* 13**,** 824411.

KUNO, R., WANG, J., KAWANOKUCHI, J., TAKEUCHI, H., MIZUNO, T. & SUZUMURA, A. 2005. Autocrine activation of microglia by tumor necrosis factor-alpha. *J Neuroimmunol,* 162**,** 89-96.

KYRKANIDES, S., BROUXHON, S. M., TALLENTS, R. H., MILLER, J. N., OLSCHOWKA, J. A. & O'BANION, M. K. 2012. Conditional expression of human beta-hexosaminidase in the neurons of Sandhoff disease rescues mice from neurodegeneration but not neuroinflammation. *J Neuroinflammation,* 9**,** 186.

LADA, G., CHINOY, H., HEAL, C., WARREN, R. B., TALBOT, P. S. & KLEYN, C. E. 2022. Depression and Suicidality in Patients With Psoriasis and the Role of Psoriatic Arthritis: A Cross-sectional Study in a Tertiary Setting. *J Acad Consult Liaison Psychiatry,* 63**,** 372-383.

LAFEVER, B. J., KAWASAWA, Y. I., ITO, A. & IMAMURA, F. 2022. Pathological consequences of chronic olfactory inflammation on neurite morphology of olfactory bulb projection neurons. *Brain Behav Immun Health,* 21**,** 100451.

LAI, J. Y., HO, J. X., KOW, A. S. F., LIANG, G., THAM, C. L., HO, Y. C. & LEE, M. T. 2023. Interferon therapy and its association with depressive disorders - A review. *Front Immunol,* 14**,** 1048592.

LAMBERTSEN, K. L., CLAUSEN, B. H., BABCOCK, A. A., GREGERSEN, R., FENGER, C., NIELSEN, H. H., HAUGAARD, L. S., WIRENFELDT, M., NIELSEN, M., DAGNAES-HANSEN, F., BLUETHMANN, H., FAERGEMAN, N. J., MELDGAARD, M., DEIERBORG, T. & FINSEN, B. 2009. Microglia protect neurons against ischemia by synthesis of tumor necrosis factor. *J Neurosci,* 29**,** 1319-30.

LANE, A. P., TURNER, J., MAY, L. & REED, R. 2010. A genetic model of chronic rhinosinusitis-associated olfactory inflammation reveals reversible

functional impairment and dramatic neuroepithelial reorganization. *J Neurosci,* 30**,** 2324-9.

LAUMET, G., EDRALIN, J. D., DANTZER, R., HEIJNEN, C. J. & KAVELAARS, A. 2020. CD3(+) T cells are critical for the resolution of comorbid inflammatory pain and depression-like behavior. *Neurobiol Pain,* 7**,** 100043.

LAURENT, C., DOROTHEE, G., HUNOT, S., MARTIN, E., MONNET, Y., DUCHAMP, M., DONG, Y., LEGERON, F. P., LEBOUCHER, A., BURNOUF, S., FAIVRE, E., CARVALHO, K., CAILLIEREZ, R., ZOMMER, N., DEMEYER, D., JOUY, N., SAZDOVITCH, V., SCHRAEN-MASCHKE, S., DELARASSE, C., BUEE, L. & BLUM, D. 2017. Hippocampal T cell infiltration promotes neuroinflammation and cognitive decline in a mouse model of tauopathy. *Brain,* 140**,** 184-200.

LEE, H. G., CHO, M. J. & CHOI, J. M. 2020. Bystander CD4(+) T cells: crossroads between innate and adaptive immunity. *Exp Mol Med,* 52**,** 1255-1263.

LEE, K., BAKHURIN, K. I., CLAAR, L. D., HOLLEY, S. M., CHONG, N. C., CEPEDA, C., LEVINE, M. S. & MASMANIDIS, S. C. 2019. Gain Modulation by Corticostriatal and Thalamostriatal Input Signals during Reward-Conditioned Behavior. *Cell Rep,* 29**,** 2438-2449 e4.

LEE, S., JEONG, J., KWAK, Y. & PARK, S. K. 2010. Depression research: where are we now? *Mol Brain,* 3**,** 8.

LEE, Y., SUBRAMANIAPILLAI, M., BRIETZKE, E., MANSUR, R. B., HO, R. C., YIM, S. J. & MCINTYRE, R. S. 2018. Anti-cytokine agents for anhedonia: targeting inflammation and the immune system to treat dimensional disturbances in depression. *Ther Adv Psychopharmacol,* 8**,** 337-348.

LEONARD, B. T., KARK, S. M., GRANGER, S. J., ADAMS, J. G., MCMILLAN, L. & YASSA, M. A. 2024. Anhedonia is associated with higher functional connectivity between the nucleus accumbens and paraventricular nucleus of thalamus. *J Affect Disord,* 366**,** 1-7.

LESNIAK, M., LIPNIARSKA, J., MAJKA, P., KOPYT, W., LEJMAN, M. & ZAWITKOWSKA, J. 2023. The Role of TRL7/8 Agonists in Cancer Therapy, with Special Emphasis on Hematologic Malignancies. *Vaccines (Basel),* 11.

LEZAK, K. R., MISSIG, G. & CARLEZON, W. A., JR. 2017. Behavioral methods to study anxiety in rodents. *Dialogues Clin Neurosci,* 19**,** 181-191.

LI, J., LU, C., GAO, Z., FENG, Y., LUO, H., LU, T., SUN, X., HU, J. & LUO, Y. 2020. SNRIs achieve faster antidepressant effects than SSRIs by elevating the concentrations of dopamine in the forebrain. *Neuropharmacology,* 177**,** 108237.

LI, L., DONG, M. & WANG, X. G. 2016. The Implication and Significance of Beta 2 Microglobulin: A Conservative Multifunctional Regulator. *Chin Med J (Engl),* 129**,** 448-55.

LI, Q., YAN, Y., LIU, J., HUANG, X., ZHANG, X., KIRSCHNING, C., XU, H. C., LANG, P. A., DITTMER, U., ZHANG, E. & LU, M. 2019. Toll-Like Receptor 7 Activation Enhances CD8+ T Cell Effector Functions by Promoting Cellular Glycolysis. *Front Immunol,* 10**,** 2191.

LI, S., FANG, Y., ZHANG, Y., SONG, M., ZHANG, X., DING, X., YAO, H., CHEN, M., SUN, Y., DING, J., WANG, Q., LU, M., WU, G. & HU, G. 2022a. Microglial NLRP3 inflammasome activates neurotoxic astrocytes in depression-like mice. *Cell Rep,* 41**,** 111532.

LI, S. & JAKOBS, T. C. 2022. Secreted phosphoprotein 1 slows neurodegeneration and rescues visual function in mouse models of aging and glaucoma. *Cell Rep,* 41**,** 111880.

LI, S., LIU, H., LV, P., YAO, Y., PENG, L., XIA, T., YAN, C., MA, Z., CHEN, Z. P., ZHAO, C. & GU, X. 2024. Microglia mediate memory dysfunction via excitatory synaptic elimination in a fracture surgery mouse model. *J Neuroinflammation,* 21**,** 227.

LI, Y., LI, Z., YANG, M., WANG, F., ZHANG, Y., LI, R., LI, Q., GONG, Y., WANG, B., FAN, B., WANG, C., CHEN, L., LI, H., ONG, J., TENG, Z., JIN, L., WANG, Y. L., DU, P. & JIAO, J. 2022b. Decoding the temporal and regional specification of microglia in the developing human brain. *Cell Stem Cell,* 29**,** 620-634 e6.

LI, Z., WANG, T., LIU, P. & HUANG, Y. 2023. SpatialDM for rapid identification of spatially co-expressed ligand-receptor and revealing cell-cell communication patterns. *Nat Commun,* 14**,** 3995.

LIDDELOW, S. A., GUTTENPLAN, K. A., CLARKE, L. E., BENNETT, F. C., BOHLEN, C. J., SCHIRMER, L., BENNETT, M. L., MUNCH, A. E., CHUNG, W. S., PETERSON, T. C., WILTON, D. K., FROUIN, A., NAPIER, B. A., PANICKER, N., KUMAR, M., BUCKWALTER, M. S., ROWITCH, D. H., DAWSON, V. L., DAWSON, T. M., STEVENS, B. & BARRES, B. A. 2017. Neurotoxic reactive astrocytes are induced by activated microglia. *Nature,* 541**,** 481-487.

LIER, J., STREIT, W. J. & BECHMANN, I. 2021. Beyond Activation: Characterizing Microglial Functional Phenotypes. *Cells,* 10.

LIM, B. K., HUANG, K. W., GRUETER, B. A., ROTHWELL, P. E. & MALENKA, R. C. 2012. Anhedonia requires MC4R-mediated synaptic adaptations in nucleus accumbens. *Nature,* 487**,** 183-9.

LIN, G., MELA, A., GUILFOYLE, E. M. & GOLDMAN, J. E. 2009. Neonatal and adult O4(+) oligodendrocyte lineage cells display different growth factor responses and different gene expression patterns. *J Neurosci Res,* 87**,** 3390-402.

LISTON, A., DOOLEY, J. & YSHII, L. 2022. Brain-resident regulatory T cells and their role in health and disease. *Immunol Lett,* 248**,** 26-30.

LISTON, A., PASCIUTO, E., FITZGERALD, D. C. & YSHII, L. 2024. Brain regulatory T cells. *Nat Rev Immunol,* 24**,** 326-337.

LIU, K., AIERKEN, A., LIU, M., PARHAT, N., KONG, W., YIN, X., LIU, G., YU, D., HONG, J., NI, J., QUAN, Z., LIU, X., JI, S., MAO, J., PENG, W., CHEN, C., YAN, Y. & QING, H. 2024. The decreased astrocyte-microglia interaction reflects the early characteristics of Alzheimer's disease. *iScience,* 27**,** 109281.

LIU, P. P., LIU, X. H., REN, M. J., LIU, X. T., SHI, X. Q., LI, M. L., LI, S. A., YANG, Y., WANG, D. D., WU, Y., YIN, F. X., GUO, Y. H., YANG, R. Z., CHENG, M., XIN, Y. J., KANG, J. S., HUANG, B. & REN, K. D. 2025. Neuronal cathepsin S increases neuroinflammation and causes cognitive decline via CX3CL1-CX3CR1 axis and JAK2-STAT3 pathway in aging and Alzheimer's disease. *Aging Cell,* 24**,** e14393.

LIU, Y. N., PENG, Y. L., LIU, L., WU, T. Y., ZHANG, Y., LIAN, Y. J., YANG, Y. Y., KELLEY, K. W., JIANG, C. L. & WANG, Y. X. 2015. TNFalpha mediates stress-induced depression by upregulating indoleamine 2,3-dioxygenase in a mouse model of unpredictable chronic mild stress. *Eur Cytokine Netw,* 26**,** 15-25.

LIU, Z., LI, Y., CUI, Y., ROBERTS, C., LU, M., WILHELMSSON, U., PEKNY, M. & CHOPP, M. 2014. Beneficial effects of gfap/vimentin reactive astrocytes for axonal remodeling and motor behavioral recovery in mice after stroke. *Glia,* 62**,** 2022-33.

LLOYD, C. E., NOUWEN, A., SARTORIUS, N., AHMED, H. U., ALVAREZ, A., BAHENDEKA, S., BASANGWA, D., BOBROV, A. E., BODEN, S., BULGARI, V., BURTI, L., CHATURVEDI, S. K., CIMINO, L. C., GAEBEL, W., DE GIROLAMO, G., GONDEK, T. M., DE BRAUDE, M. G., GUNTUPALLI, A., HEINZE, M. G., JI, L., HONG, X., KHAN, A., KIEJNA, A., KOKOSZKA, A., KAMALA, T., LALIC, N. M., LECIC TOSEVSKI, D., MANKOVSKY, B., LI, M., MUSAU, A., MUSSIG, K., NDETEI, D., RABBANI, G., SRIKANTA, S. S., STAROSTINA, E. G., SHEVCHUK, M., TAJ, R., VUKOVIC, O., WOLWER, W. & XIN, Y. 2018. Prevalence and correlates of depressive disorders in people with Type 2 diabetes: results from the International Prevalence and Treatment of Diabetes and Depression (INTERPRET-DD) study, a collaborative study carried out in 14 countries. *Diabet Med,* 35**,** 760-769.

LOBO-SILVA, D., CARRICHE, G. M., CASTRO, A. G., ROQUE, S. & SARAIVA, M. 2016. Balancing the immune response in the brain: IL-10 and its regulation. *J Neuroinflammation,* 13**,** 297.

LOPEZ-FERRERAS, L., LONGO, F., RICHARD, J. E., EEROLA, K., SHEVCHOUK, O. T., TUZINOVIC, M. & SKIBICKA, K. P. 2021. Key role for hypothalamic interleukin-6 in food-motivated behavior and body weight regulation. *Psychoneuroendocrinology,* 131**,** 105284.

LOVE, M. I., HUBER, W. & ANDERS, S. 2014. Moderated estimation of fold change and dispersion for RNA-seq data with DESeq2. *Genome Biol,* 15**,** 550.

LU, J., LI, H., YU, Z., CAO, C., XU, Z., PENG, L., ZHANG, J. H. & CHEN, G. 2024. Cathepsin B as a key regulator of ferroptosis in microglia following intracerebral hemorrhage. *Neurobiol Dis,* 194**,** 106468.

LU, L., HU, X. & JIN, X. 2023a. IL-4 as a potential biomarker for differentiating major depressive disorder from bipolar depression. *Medicine (Baltimore),* 102**,** e33439.

LU, Y., ZHANG, P., XU, F., ZHENG, Y. & ZHAO, H. 2023b. Advances in the study of IL-17 in neurological diseases and mental disorders. *Front Neurol,* 14**,** 1284304.

MA, H., LI, H., ZHANG, Y., ZHOU, Y., LIU, H., XU, H., ZHU, L., ZHANG, G., WANG, J., LI, Z., HONG, B., ZHOU, W., YANG, P. & LIU, J. 2023. Microglia Exhibit Distinct Heterogeneity Rather than M1/M2 Polarization within the Early Stage of Acute Ischemic Stroke. *Aging Dis,* 14**,** 2284-2302.

MA, R., XIE, Q., LI, Y., CHEN, Z., REN, M., CHEN, H., LI, H., LI, J. & WANG, J. 2020. Animal models of cerebral ischemia: A review. *Biomed Pharmacother,* 131**,** 110686.

MACHHI, J., YEAPURI, P., LU, Y., FOSTER, E., CHIKHALE, R., HERSKOVITZ, J., NAMMINGA, K. L., OLSON, K. E., ABDELMOATY, M. M., GAO, J., QUADROS, R. M., KIYOTA, T., JINGJING, L., KEVADIYA, B. D., WANG, X., LIU, Y., POLUEKTOVA, L. Y., GURUMURTHY, C. B., MOSLEY, R. L. & GENDELMAN, H. E. 2021. CD4+ effector T cells accelerate Alzheimer's disease in mice. *J Neuroinflammation,* 18**,** 272.

MAES, M., BERK, M., GOEHLER, L., SONG, C., ANDERSON, G., GAŁECKI, P. & LEONARD, B. 2012. Depression and sickness behavior are Janus-faced responses to shared inflammatory pathways. *BMC Med,* 10**,** 66.

MANCINI, M., NATOLI, S., GARDONI, F., DI LUCA, M. & PISANI, A. 2023. Dopamine Transmission Imbalance in Neuroinflammation: Perspectives on Long-Term COVID-19. *Int J Mol Sci,* 24.

MAO, P. 2011. Potential Antidepressant Role of Neurotransmitter CART: Implications for Mental Disorders. *Depress Res Treat,* 2011**,** 762139.

MARKOV, D. D. 2022. Sucrose Preference Test as a Measure of Anhedonic Behavior in a Chronic Unpredictable Mild Stress Model of Depression: Outstanding Issues. *Brain Sci,* 12.

MARQUES, C. P., CHEERAN, M. C., PALMQUIST, J. M., HU, S., URBAN, S. L. & LOKENSGARD, J. R. 2008. Prolonged microglial cell activation and lymphocyte infiltration following experimental herpes encephalitis. *J Immunol,* 181**,** 6417-26.

MARSLAND, A. L., GIANAROS, P. J., ABRAMOWITCH, S. M., MANUCK, S. B. & HARIRI, A. R. 2008. Interleukin-6 covaries inversely with hippocampal grey matter volume in middle-aged adults. *Biol Psychiatry,* 64**,** 484-90.

MARTENS, L. H., ZHANG, J., BARMADA, S. J., ZHOU, P., KAMIYA, S., SUN, B., MIN, S. W., GAN, L., FINKBEINER, S., HUANG, E. J. & JR, R. V. F. 2022. Progranulin deficiency promotes neuroinflammation and neuron loss following toxin-induced injury. *J Clin Invest,* 132.

MARTIN, E., EL-BEHI, M., FONTAINE, B. & DELARASSE, C. 2017. Analysis of Microglia and Monocyte-derived Macrophages from the Central Nervous System by Flow Cytometry. *J Vis Exp*.

MASUDA, T., AMANN, L., SANKOWSKI, R., STASZEWSKI, O., LENZ, M., P, D. E., SNAIDERO, N., COSTA JORDAO, M. J., BOTTCHER, C., KIERDORF, K., JUNG, S., PRILLER, J., MISGELD, T., VLACHOS, A., MEYER-LUEHMANN, M., KNOBELOCH, K. P. & PRINZ, M. 2020a. Novel Hexb-based tools for studying microglia in the CNS. *Nat Immunol,* 21**,** 802-815.

MASUDA, T., SANKOWSKI, R., STASZEWSKI, O. & PRINZ, M. 2020b. Microglia Heterogeneity in the Single-Cell Era. *Cell Rep,* 30**,** 1271-1281.

MATCHAM, F., RAYNER, L., STEER, S. & HOTOPF, M. 2013. The prevalence of depression in rheumatoid arthritis: a systematic review and meta-analysis. *Rheumatology (Oxford),* 52**,** 2136-48.

MAVROGIORGOU, P., FISCHER, L., BURGY, M. & JUCKEL, G. 2025. The phenomenon of despair in patients with depression. *J Psychiatr Res,* 181**,** 648-652.

MAZZITELLI, J. A., PULOUS, F. E., SMYTH, L. C. D., KAYA, Z., RUSTENHOVEN, J., MOSKOWITZ, M. A., KIPNIS, J. & NAHRENDORF, M. 2023. Skull bone marrow channels as immune gateways to the central nervous system. *Nat Neurosci,* 26**,** 2052-2062.

MCCARTHY, R. C., SOSA, J. C., GARDECK, A. M., BAEZ, A. S., LEE, C. H. & WESSLING-RESNICK, M. 2018. Inflammation-induced iron transport and metabolism by brain microglia. *J Biol Chem,* 293**,** 7853-7863.

MCCOLL, A., THOMSON, C. A., NERURKAR, L., GRAHAM, G. J. & CAVANAGH, J. 2016. TLR7-mediated skin inflammation remotely triggers chemokine expression and leukocyte accumulation in the brain. *J Neuroinflammation,* 13**,** 102.

MCCOY, M. K. & TANSEY, M. G. 2008. TNF signaling inhibition in the CNS: implications for normal brain function and neurodegenerative disease. *J Neuroinflammation,* 5**,** 45.

MCCULLOCH, T. R., ROSSI, G. R., ALIM, L., LAM, P. Y., WONG, J. K. M., COLEBORN, E., KUMARI, S., KEANE, C., KUEH, A. J., HEROLD, M. J., WILHELM, C., KNOLLE, P. A., KANE, L., WELLS, T. J. & SOUZA-FONSECA-GUIMARAES, F. 2024. Dichotomous outcomes of TNFR1 and TNFR2 signaling in NK cell-mediated immune responses during inflammation. *Nat Commun,* 15**,** 9871.

MENDES, M. S. & MAJEWSKA, A. K. 2021. An overview of microglia ontogeny and maturation in the homeostatic and pathological brain. *Eur J Neurosci,* 53**,** 3525-3547.

MESQUITA, S. D., FERREIRA, A. C., GAO, F., COPPOLA, G., GESCHWIND, D. H., SOUSA, J. C., CORREIA-NEVES, M., SOUSA, N., PALHA, J. A. & MARQUES, F. 2015. The choroid plexus transcriptome reveals changes in type I and II interferon responses in a mouse model of Alzheimer's disease. *Brain Behav Immun,* 49**,** 280-92.

MICHAELIS, K. A., NORGARD, M. A., LEVASSEUR, P. R., OLSON, B., BURFEIND, K. G., BUENAFE, A. C., ZHU, X., JENG, S., MCWEENEY, S. K. & MARKS, D. L. 2019. Persistent Toll-like receptor 7 stimulation induces behavioral and molecular innate immune tolerance. *Brain Behav Immun,* 82**,** 338-353.

MIKOCKA-WALUS, A., KNOWLES, S. R., KEEFER, L. & GRAFF, L. 2016. Controversies Revisited: A Systematic Review of the Comorbidity of Depression and Anxiety with Inflammatory Bowel Diseases. *Inflamm Bowel Dis,* 22**,** 752-62.

MILDNER, A., SCHMIDT, H., NITSCHE, M., MERKLER, D., HANISCH, U. K., MACK, M., HEIKENWALDER, M., BRUCK, W., PRILLER, J. & PRINZ, M. 2007. Microglia in the adult brain arise from Ly-6ChiCCR2+ monocytes only under defined host conditions. *Nat Neurosci,* 10**,** 1544-53.

MILLER, A. H. 2009. Norman Cousins Lecture. Mechanisms of cytokine-induced behavioral changes: psychoneuroimmunology at the translational interface. *Brain Behav Immun,* 23**,** 149-58.

MILLET, A., LEDO, J. H. & TAVAZOIE, S. F. 2024. An exhausted-like microglial population accumulates in aged and APOE4 genotype Alzheimer's brains. *Immunity,* 57**,** 153-170 e6.

MIN, X., WANG, G., CUI, Y., MENG, P., HU, X., LIU, S. & WANG, Y. 2023. Association between inflammatory cytokines and symptoms of major depressive disorder in adults. *Front Immunol,* 14**,** 1110775.

MINOGUE, A. M. 2017. Role of infiltrating monocytes/macrophages in acute and chronic neuroinflammation: Effects on cognition, learning and affective behaviour. *Prog Neuropsychopharmacol Biol Psychiatry,* 79**,** 15-18.

MITTAL, K., EREMENKO, E., BERNER, O., ELYAHU, Y., STROMINGER, I., APELBLAT, D., NEMIROVSKY, A., SPIEGEL, I. & MONSONEGO, A. 2019. CD4 T Cells Induce A Subset of MHCII-Expressing Microglia that Attenuates Alzheimer Pathology. *iScience,* 16**,** 298-311.

MOHRI, I., TANIIKE, M., TANIGUCHI, H., KANEKIYO, T., ARITAKE, K., INUI, T., FUKUMOTO, N., EGUCHI, N., KUSHI, A., SASAI, H., KANAOKA, Y., OZONO, K., NARUMIYA, S., SUZUKI, K. & URADE, Y. 2006. Prostaglandin D2-mediated microglia/astrocyte interaction enhances astrogliosis and demyelination in twitcher. *J Neurosci,* 26**,** 4383-93.

MOMBAERTS, P., IACOMINI, J., JOHNSON, R. S., HERRUP, K., TONEGAWA, S. & PAPAIOANNOU, V. E. 1992. RAG-1-deficient mice have no mature B and T lymphocytes. *Cell,* 68**,** 869-77.

MONCRIEFF, J., COOPER, R. E., STOCKMANN, T., AMENDOLA, S., HENGARTNER, M. P. & HOROWITZ, M. A. 2023. The serotonin theory of depression: a systematic umbrella review of the evidence. *Mol Psychiatry,* 28**,** 3243-3256.

MONTEIRO, S., ROQUE, S., MARQUES, F., CORREIA-NEVES, M. & CERQUEIRA, J. J. 2017. Brain interference: Revisiting the role of IFNgamma in the central nervous system. *Prog Neurobiol,* 156**,** 149-163.

MOR, G., NILSEN, J., HORVATH, T., BECHMANN, I., BROWN, S., GARCIA-SEGURA, L. M. & NAFTOLIN, F. 1999. Estrogen and microglia: A regulatory system that affects the brain. *J Neurobiol,* 40**,** 484-96.

MOULTON, C. D., PAVLIDIS, P., NORTON, C., NORTON, S., PARIANTE, C., HAYEE, B. & POWELL, N. 2019. Depressive symptoms in inflammatory bowel

disease: an extraintestinal manifestation of inflammation? *Clin Exp Immunol,* 197**,** 308-318.

MOUSA, A. & BAKHIET, M. 2013. Role of cytokine signaling during nervous system development. *Int J Mol Sci,* 14**,** 13931-57.

MRDJEN, D., PAVLOVIC, A., HARTMANN, F. J., SCHREINER, B., UTZ, S. G., LEUNG, B. P., LELIOS, I., HEPPNER, F. L., KIPNIS, J., MERKLER, D., GRETER, M. & BECHER, B. 2018. High-Dimensional Single-Cell Mapping of Central Nervous System Immune Cells Reveals Distinct Myeloid Subsets in Health, Aging, and Disease. *Immunity,* 48**,** 599.

MUDA, R., KICIA, M., MICHALAK-WOJNOWSKA, M., GINSZT, M., FILIP, A., GAWDA, P. & MAJCHER, P. 2018. The Dopamine Receptor D4 Gene (DRD4) and Financial Risk-Taking: Stimulating and Instrumental Risk-Taking Propensity and Motivation to Engage in Investment Activity. *Front Behav Neurosci,* 12**,** 34.

MULLER, L., DI BENEDETTO, S. & MULLER, V. 2025. From Homeostasis to Neuroinflammation: Insights into Cellular and Molecular Interactions and Network Dynamics. *Cells,* 14.

MURPHY, A. C., LALOR, S. J., LYNCH, M. A. & MILLS, K. H. 2010. Infiltration of Th1 and Th17 cells and activation of microglia in the CNS during the course of experimental autoimmune encephalomyelitis. *Brain Behav Immun,* 24**,** 641-51.

MUZIO, L., VIOTTI, A. & MARTINO, G. 2021. Microglia in Neuroinflammation and Neurodegeneration: From Understanding to Therapy. *Front Neurosci,* 15**,** 742065.

NA, K. S., JUNG, H. Y. & KIM, Y. K. 2014. The role of pro-inflammatory cytokines in the neuroinflammation and neurogenesis of schizophrenia. *Prog Neuropsychopharmacol Biol Psychiatry,* 48**,** 277-86.

NAHRENDORF, M. & SWIRSKI, F. K. 2016. Abandoning M1/M2 for a Network Model of Macrophage Function. *Circ Res,* 119**,** 414-7.

NAZEM, A., SANKOWSKI, R., BACHER, M. & AL-ABED, Y. 2015. Rodent models of neuroinflammation for Alzheimer's disease. *J Neuroinflammation,* 12**,** 74.

NERURKAR, L., MCCOLL, A., GRAHAM, G. & CAVANAGH, J. 2017a. The Systemic Response to Topical Aldara Treatment is Mediated Through Direct TLR7 Stimulation as Imiquimod Enters the Circulation. *Sci Rep,* 7**,** 16570.

NERURKAR, L., MCCOLL, A., GRAHAM, G. & CAVANAGH, J. 2017b. The Systemic Response to Topical Aldara Treatment is Mediated Through Direct TLR7 Stimulation as Imiquimod Enters the Circulation. *Scientific Reports,* 7**,** 16570.

NERURKAR, L., SIEBERT, S., MCINNES, I. B. & CAVANAGH, J. 2019. Rheumatoid arthritis and depression: an inflammatory perspective. *Lancet Psychiatry,* 6**,** 164-173.

NEVALAINEN, T., AUTIO, A. & HURME, M. 2022. Composition of the infiltrating immune cells in the brain of healthy individuals: effect of aging. *Immun Ageing,* 19**,** 45.

NI CHASAIDE, C. & LYNCH, M. A. 2020. The role of the immune system in driving neuroinflammation. *Brain Neurosci Adv,* 4**,** 2398212819901082.

NI, P., MA, Y. & CHUNG, S. 2024. Mitochondrial dysfunction in psychiatric disorders. *Schizophr Res,* 273**,** 62-77.

NICHOLSON, T. E. & RENTON, K. W. 2002. The role of cytokines in the depression of CYP1A activity using cultured astrocytes as an in vitro model of inflammation in the central nervous system. *Drug Metab Dispos,* 30**,** 42-6.

NIMMERJAHN, A., KIRCHHOFF, F. & HELMCHEN, F. 2005. Resting microglial cells are highly dynamic surveillants of brain parenchyma in vivo. *Science,* 308**,** 1314-8.

NOMURA, K., VILALTA, A., ALLENDORF, D. H., HORNIK, T. C. & BROWN, G. C. 2017. Activated Microglia Desialylate and Phagocytose Cells via Neuraminidase, Galectin-3, and Mer Tyrosine Kinase. *J Immunol,* 198**,** 4792-4801.

NORDEN, D. M., TROJANOWSKI, P. J., VILLANUEVA, E., NAVARRO, E. & GODBOUT, J. P. 2016. Sequential activation of microglia and astrocyte cytokine expression precedes increased Iba-1 or GFAP immunoreactivity following systemic immune challenge. *Glia,* 64**,** 300-16.

NOTHDURFTER, C., MILENKOVIC, V. M., SARUBIN, N., HILBERT, S., MANOOK, A., WEIGL, J., ALMEQBAALI, K., WETZEL, C. H., RUPPRECHT, R. & BAGHAI, T. C. 2021. The cytokine IL-17A as a marker of treatment resistance in major depressive disorder? *Eur J Neurosci,* 53**,** 172-182.

NUTMA, E., GEBRO, E., MARZIN, M. C., VAN DER VALK, P., MATTHEWS, P. M., OWEN, D. R. & AMOR, S. 2021. Activated microglia do not increase 18 kDa translocator protein (TSPO) expression in the multiple sclerosis brain. *Glia,* 69**,** 2447-2458.

O'CONNOR, J. C., LAWSON, M. A., ANDRE, C., MOREAU, M., LESTAGE, J., CASTANON, N., KELLEY, K. W. & DANTZER, R. 2009. Lipopolysaccharide-induced depressive-like behavior is mediated by indoleamine 2,3-dioxygenase activation in mice. *Mol Psychiatry,* 14**,** 511-22.

OLAH, M., MENON, V., HABIB, N., TAGA, M. F., MA, Y., YUNG, C. J., CIMPEAN, M., KHAIRALLAH, A., CORONAS-SAMANO, G., SANKOWSKI, R., GRUN, D., KROSHILINA, A. A., DIONNE, D., SARKIS, R. A., COSGROVE, G. R., HELGAGER, J., GOLDEN, J. A., PENNELL, P. B., PRINZ, M., VONSATTEL, J. P. G., TEICH, A. F., SCHNEIDER, J. A., BENNETT, D. A., REGEV, A., ELYAMAN, W., BRADSHAW, E. M. & DE JAGER, P. L. 2020. Single cell RNA sequencing of human microglia uncovers a subset associated with Alzheimer's disease. *Nat Commun,* 11**,** 6129.

OLIVEROS, J. C. 2024. Venny. An interactive tool for comparing lists with Venn's diagrams.

OSIMO, E. F., PILLINGER, T., RODRIGUEZ, I. M., KHANDAKER, G. M., PARIANTE, C. M. & HOWES, O. D. 2020. Inflammatory markers in depression: A meta-analysis of mean differences and variability in 5,166 patients and 5,083 controls. *Brain Behav Immun,* 87**,** 901-909.

OSTINELLI, E. G., CHIOCCHIA, V., MACLEOD, M., BROWNING, M., HARMER, C., SIAFIS, S., STANSFIELD, C., FRIEDRICH, C., WRIGHT, S., CHIKAURA, T., MILLIGAN, L., THOMAS, J., MORENO, C., FURUKAWA, T. A., SEEDAT, S., POTTS, J., SALANTI, G., CIPRIANI, A. & TEAM, G. 2023. Pro-dopaminergic pharmacological interventions for anhedonia in depression: protocol for a living systematic review of human and non-human studies. *Wellcome Open Res,* 8**,** 425.

OU, Q., POWER, R. & GRIFFIN, M. D. 2023. Revisiting regulatory T cells as modulators of innate immune response and inflammatory diseases. *Front Immunol,* 14**,** 1287465.

OWENS, M. L., BRIDSON, W. E., SMITH, S. L., MYERS, J. A., FOX, T. L. & WELLS, T. M. 1998. Percutaneous penetration of Aldara cream, 5% during the topical treatment of genital and perianal warts. *Prim Care Update Ob Gyns,* 5**,** 151.

OYAMADA, H., YING, Y., AGRAWAL, S., LIU, A., SUBRAMANIAN, V. S., DE MELO BENTO, C. A. & AGRAWAL, A. 2025. Chronic IL-21 drives neuroinflammation and promotes lipid accumulation in microglia. *Immun Ageing,* 22**,** 15.

PAPAZIAN, I., TSOUKALA, E., BOUTOU, A., KARAMITA, M., KAMBAS, K., ILIOPOULOU, L., FISCHER, R., KONTERMANN, R. E., DENIS, M. C., KOLLIAS, G., LASSMANN, H. & PROBERT, L. 2021. Fundamentally different roles of neuronal TNF receptors in CNS pathology: TNFR1 and IKKbeta promote microglial responses and tissue injury in demyelination while TNFR2 protects against excitotoxicity in mice. *J Neuroinflammation,* 18**,** 222.

PAREL, Y. & CHIZZOLINI, C. 2004. CD4+ CD8+ double positive (DP) T cells in health and disease. *Autoimmun Rev,* 3**,** 215-20.

PARLINDUNGAN, F., HIDAYAT, R., ARIANE, A. & SHATRI, H. 2023. Association between Proinflammatory Cytokines and Anxiety and Depression Symptoms in Rheumatoid Arthritis Patients: A Cross-sectional Study. *Clin Pract Epidemiol Ment Health,* 19**,** e174501792304261.

PASCIUTO, E., BURTON, O. T., ROCA, C. P., LAGOU, V., RAJAN, W. D., THEYS, T., MANCUSO, R., TITO, R. Y., KOUSER, L., CALLAERTS-VEGH, Z., DE LA FUENTE, A. G., PREZZEMOLO, T., MASCALI, L. G., BRAJIC, A., WHYTE, C. E., YSHII, L., MARTINEZ-MURIANA, A., NAUGHTON, M., YOUNG, A., MOUDRA, A., LEMAITRE, P., POOVATHINGAL, S., RAES, J., DE STROOPER, B., FITZGERALD, D. C., DOOLEY, J. & LISTON, A. 2020. Microglia Require CD4 T Cells to Complete the Fetal-to-Adult Transition. *Cell,* 182**,** 625-640 e24.

PENKOWA, M., GIRALT, M., CARRASCO, J., HADBERG, H. & HIDALGO, J. 2000. Impaired inflammatory response and increased oxidative stress and neurodegeneration after brain injury in interleukin-6-deficient mice. *Glia,* 32**,** 271-85.

PERALTA, M. F., GUZMÁN, M. L., PÉREZ, A. P., APEZTEGUIA, G. A., FÓRMICA, M. L., ROMERO, E. L., OLIVERA, M. E. & CARRER, D. C. 2018. Liposomes can both enhance or reduce drugs penetration through the skin. *Scientific Reports,* 8**,** 13253.

PERUZZOTTI-JAMETTI, L., WILLIS, C. M., KRZAK, G., HAMEL, R., PIRVAN, L., IONESCU, R. B., REISZ, J. A., PRAG, H. A., GARCIA-SEGURA, M. E., WU, V., XIANG, Y., BARLAS, B., CASEY, A. M., VAN DEN BOSCH, A. M. R., NICAISE, A. M., ROTH, L., BATES, G. R., HUANG, H., PRASAD, P., VINCENT, A. E., FREZZA, C., VISCOMI, C., BALMUS, G., TAKATS, Z., MARIONI, J. C., D'ALESSANDRO, A., MURPHY, M. P., MOHORIANU, I. & PLUCHINO, S. 2024. Mitochondrial complex I activity in microglia sustains neuroinflammation. *Nature,* 628**,** 195-203.

PETTAS, S., KARAGIANNI, K., KANATA, E., CHATZIEFSTATHIOU, A., CHRISTOUDIA, N., XANTHOPOULOS, K., SKLAVIADIS, T. & DAFOU, D. 2022. Profiling Microglia through Single-Cell RNA Sequencing over the Course of Development, Aging, and Disease. *Cells,* 11.

PIANO, I., VOTTA, A., COLUCCI, P., CORSI, F., VITOLO, S., CERRI, C., PUPPI, D., LAI, M., MAYA-VETENCOURT, J. F., LEIGHEB, M., GABELLINI, C. & FERRARO, E. 2023. Anti-inflammatory reprogramming of microglia cells by metabolic modulators to counteract neurodegeneration; a new role for Ranolazine. *Sci Rep,* 13**,** 20138.

PINTO, E. F. & ANDRADE, C. 2016. Interferon-Related Depression: A Primer on Mechanisms, Treatment, and Prevention of a Common Clinical Problem. *Curr Neuropharmacol,* 14**,** 743-8.

PIRES-AFONSO, Y., MULLER, A., GRZYB, K., OUDIN, A., YABO, Y. A., SOUSA, C., SCAFIDI, A., POLI, A., COSMA, A., HALDER, R., COOWAR, D., GOLEBIEWSKA, A., SKUPIN, A., NICLOU, S. P. & MICHELUCCI, A. 2022. Elucidating tumour-associated microglia/macrophage diversity along glioblastoma progression and under ACOD1 deficiency. *Mol Oncol,* 16**,** 3167-3191.

POBOR, G., PETTERSSON, S., BANDEIRA, A., MARTINEZ, A. C. & COUTINHO, A. 1984. B lymphocyte activation upon exclusive recognition of major histocompatibility antigens by T helper cells. *Eur J Immunol,* 14**,** 222-7.

POCOCK, J. M. & PIERS, T. M. 2018. Modelling microglial function with induced pluripotent stem cells: an update. *Nat Rev Neurosci,* 19**,** 445-452.

POPE, B. S. & WOOD, S. K. 2020. Advances in understanding mechanisms and therapeutic targets to treat comorbid depression and cardiovascular disease. *Neurosci Biobehav Rev,* 116**,** 337-349.

POTTER, W. Z. & MANJI, H. K. 1994. Catecholamines in depression: an update. *Clin Chem,* 40**,** 279-87.

PRAJEETH, C. K., KRONISCH, J., KHOROOSHI, R., KNIER, B., TOFT-HANSEN, H., GUDI, V., FLOESS, S., HUEHN, J., OWENS, T., KORN, T. & STANGEL, M. 2017. Effectors of Th1 and Th17 cells act on astrocytes and augment their neuroinflammatory properties. *J Neuroinflammation,* 14**,** 204.

PREISSLER, J., GROSCHE, A., LEDE, V., LE DUC, D., KRUGEL, K., MATYASH, V., SZULZEWSKY, F., KALLENDRUSCH, S., IMMIG, K., KETTENMANN, H., BECHMANN, I., SCHONEBERG, T. & SCHULZ, A. 2015. Altered microglial phagocytosis in GPR34-deficient mice. *Glia,* 63**,** 206-15.

PRIMO, M. J., FONSECA-RODRIGUES, D., ALMEIDA, A., TEIXEIRA, P. M. & PINTO-RIBEIRO, F. 2023. Sucrose preference test: A systematic review of protocols for the assessment of anhedonia in rodents. *Eur Neuropsychopharmacol,* 77**,** 80-92.

PRINZ, M. & PRILLER, J. 2014. Microglia and brain macrophages in the molecular age: from origin to neuropsychiatric disease. *Nat Rev Neurosci,* 15**,** 300-12.

QIAN, W., YU, C., WANG, S., NIU, A., SHI, G., CHENG, Y., XU, N., JIN, Q. & JING, X. 2020. Depressive-Like Behaviors Induced by Chronic Social Defeat Stress Are Associated With HDAC7 Reduction in the Nucleus Accumbens. *Front Psychiatry,* 11**,** 586904.

QIAN, Z., XIA, M., ZHAO, T., LI, Y., LI, G., ZHANG, Y., LI, H. & YANG, L. 2024. ACOD1, rather than itaconate, facilitates p62-mediated activation of Nrf2 in microglia post spinal cord contusion. *Clin Transl Med,* 14**,** e1661.

QIN, L., WU, X., BLOCK, M. L., LIU, Y., BREESE, G. R., HONG, J. S., KNAPP, D. J. & CREWS, F. T. 2007. Systemic LPS causes chronic neuroinflammation and progressive neurodegeneration. *Glia,* 55**,** 453-62.

RADEMACHER, L., LASSELIN, J., KARSHIKOFF, B., HUNDT, J. E., ENGLER, H. & LANGE, T. 2021. Editorial: The Different Faces of Sickness. *Front Psychiatry,* 12**,** 735337.

RAFFAELE, S., LOMBARDI, M., VERDERIO, C. & FUMAGALLI, M. 2020. TNF Production and Release from Microglia via Extracellular Vesicles: Impact on Brain Functions. *Cells,* 9.

RAFFAELE, S., THOUGAARD, E., LAURSEN, C. C. H., GAO, H., ANDERSEN, K. M., NIELSEN, P. V., ORTI-CASAN, N., BLICHFELDT-ECKHARDT, M., KOCH, S., DEB-CHATTERJI, M., MAGNUS, T., STUBBE, J., MADSEN, K., MEYER, M., DEGN, M., EISEL, U. L. M., WLODARCZYK, A., FUMAGALLI, M., CLAUSEN, B. H., BRAMBILLA, R. & LAMBERTSEN, K. L. 2024. Microglial TNFR2 signaling

regulates the inflammatory response after CNS injury in a sex-specific fashion. *Brain Behav Immun,* 116**,** 269-285.

RAMINENI, S. K., CUNNINGHAM, L. L., JR., DZIUBLA, T. D. & PULEO, D. A. 2013. Development of imiquimod-loaded mucoadhesive films for oral dysplasia. *J Pharm Sci,* 102**,** 593-603.

RANSOHOFF, R. M. & ENGELHARDT, B. 2012. The anatomical and cellular basis of immune surveillance in the central nervous system. *Nat Rev Immunol,* 12**,** 623-35.

REAGIN, K. L. & FUNK, K. E. 2022. The role of antiviral CD8(+) T cells in cognitive impairment. *Curr Opin Neurobiol,* 76**,** 102603.

REBEJAC, J., EME-SCOLAN, E. & RUA, R. 2024. Role of meningeal immunity in brain function and protection against pathogens. *J Inflamm (Lond),* 21**,** 3.

REDDAWAY, J., RICHARDSON, P. E., BEVAN, R. J., STONEMAN, J. & PALOMBO, M. 2023. Microglial morphometric analysis: so many options, so little consistency. *Front Neuroinform,* 17**,** 1211188.

REIMAND, J., ISSERLIN, R., VOISIN, V., KUCERA, M., TANNUS-LOPES, C., ROSTAMIANFAR, A., WADI, L., MEYER, M., WONG, J., XU, C., MERICO, D. & BADER, G. D. 2019. Pathway enrichment analysis and visualization of omics data using g:Profiler, GSEA, Cytoscape and EnrichmentMap. *Nat Protoc,* 14**,** 482-517.

REMUS, J. L. & DANTZER, R. 2016. Inflammation Models of Depression in Rodents: Relevance to Psychotropic Drug Discovery. *Int J Neuropsychopharmacol,* 19.

RENGASAMY, M., NANCE, M., ECKSTRAND, K. & FORBES, E. 2023. Splitting the reward: Differences in inflammatory marker associations with neural connectivity between reward anticipation and reward outcome in adolescents at high risk for depression. *J Affect Disord,* 327**,** 128-136.

RHINN, H., TATTON, N., MCCAUGHEY, S., KURNELLAS, M. & ROSENTHAL, A. 2022. Progranulin as a therapeutic target in neurodegenerative diseases. *Trends Pharmacol Sci,* 43**,** 641-652.

RITZEL, R. M., PATEL, A. R., GRENIER, J. M., CRAPSER, J., VERMA, R., JELLISON, E. R. & MCCULLOUGH, L. D. 2015. Functional differences between microglia and monocytes after ischemic stroke. *J Neuroinflammation,* 12**,** 106.

ROBINSON, L., DREESEN, E., MONDESIR, M., HARRINGTON, C., WISCHIK, C. & RIEDEL, G. 2024. Apathy-like behaviour in tau mouse models of Alzheimer's disease and frontotemporal dementia. *Behav Brain Res,* 456**,** 114707.

ROGGE, G., JONES, D., HUBERT, G. W., LIN, Y. & KUHAR, M. J. 2008. CART peptides: regulators of body weight, reward and other functions. *Nat Rev Neurosci,* 9**,** 747-58.

ROJO, R., RAPER, A., OZDEMIR, D. D., LEFEVRE, L., GRABERT, K., WOLLSCHEID-LENGELING, E., BRADFORD, B., CARUSO, M., GAZOVA, I., SANCHEZ, A., LISOWSKI, Z. M., ALVES, J., MOLINA-GONZALEZ, I., DAVTYAN, H., LODGE, R. J., GLOVER, J. D., WALLACE, R., MUNRO, D. A. D., DAVID, E., AMIT, I., MIRON, V. E., PRILLER, J., JENKINS, S. J., HARDINGHAM, G. E., BLURTON-JONES, M., MABBOTT, N. A., SUMMERS, K. M., HOHENSTEIN, P., HUME, D. A. & PRIDANS, C. 2019. Deletion of a Csf1r enhancer selectively impacts CSF1R expression and development of tissue macrophage populations. *Nat Commun,* 10**,** 3215.

RUAN, C. & ELYAMAN, W. 2022. A New Understanding of TMEM119 as a Marker of Microglia. *Front Cell Neurosci,* 16**,** 902372.

RUAN, C., SUN, L., KROSHILINA, A., BECKERS, L., DE JAGER, P., BRADSHAW, E. M., HASSON, S. A., YANG, G. & ELYAMAN, W. 2020. A novel Tmem119-tdTomato

reporter mouse model for studying microglia in the central nervous system. *Brain Behav Immun,* 83**,** 180-191.

RUFFO, E., WU, R. C., BRUNO, T. C., WORKMAN, C. J. & VIGNALI, D. A. A. 2019. Lymphocyte-activation gene 3 (LAG3): The next immune checkpoint receptor. *Semin Immunol,* 42**,** 101305.

RUSSO, P. A., ILCHEF, R. & COOPER, A. J. 2004. Psychiatric morbidity in psoriasis: a review. *Australas J Dermatol,* 45**,** 155-9; quiz 160-1.

SAKAI, K., SANDERS, K. M., YOUSSEF, M. R., YANUSHEFSKI, K. M., JENSEN, L., YOSIPOVITCH, G. & AKIYAMA, T. 2016. Mouse model of imiquimod-induced psoriatic itch. *Pain,* 157**,** 2536-2543.

SAKATA, K., NAKAYAMADA, S., MIYAZAKI, Y., KUBO, S., ISHII, A., NAKANO, K. & TANAKA, Y. 2018. Up-Regulation of TLR7-Mediated IFN-alpha Production by Plasmacytoid Dendritic Cells in Patients With Systemic Lupus Erythematosus. *Front Immunol,* 9**,** 1957.

SALCUDEAN, A., BODO, C. R., POPOVICI, R. A., COZMA, M. M., PACURAR, M., CRACIUN, R. E., CRISAN, A. I., ENATESCU, V. R., MARINESCU, I., CIMPIAN, D. M., NAN, A. G., SASU, A. B., ANCULIA, R. C. & STRETE, E. G. 2025. Neuroinflammation-A Crucial Factor in the Pathophysiology of Depression-A Comprehensive Review. *Biomolecules,* 15.

SALEM, G., COPE, N., GARMENDIA, M., PU, A., SOMENHALLI, A., KRYNITSKY, J., CUBERT, N., JONES, T., DOLD, G., FLETCHER, A., KRAVITZ, A., POHIDA, T. & DENNIS, J. 2024. MouseVUER: video based open-source system for laboratory mouse home-cage monitoring. *Sci Rep,* 14**,** 2662.

SANTOS, R. F., DE SOUSA LINHARES, A., STEINBERGER, P., DAVIS, S. J., OLIVEIRA, L. & CARMO, A. M. 2024. The CD6 interactome orchestrates ligand-independent T cell inhibitory signaling. *Cell Commun Signal,* 22**,** 286.

SARAIVA, M. & O'GARRA, A. 2010. The regulation of IL-10 production by immune cells. *Nat Rev Immunol,* 10**,** 170-81.

SARMIN, N., ROKNUZZAMAN, A. S. M., SARKER, R., OR-RASHID, M., QUSAR, M. S., BACHAR, S. C., KABIR, E. R., ISLAM, M. R. & AL MAHMUD, Z. 2024. Association of interleukin-2 and interleukin-10 with the pathophysiology and development of generalized anxiety disorder: a case-control study. *BMC Psychiatry,* 24**,** 462.

SARTORIUS, N. 2018. Depression and diabetes. *Dialogues Clin Neurosci,* 20**,** 47-52.

SCHEGGI, S., DE MONTIS, M. G. & GAMBARANA, C. 2018. Making Sense of Rodent Models of Anhedonia. *Int J Neuropsychopharmacol,* 21**,** 1049-1065.

SCHETTERS, S. T. T., GOMEZ-NICOLA, D., GARCIA-VALLEJO, J. J. & VAN KOOYK, Y. 2017. Neuroinflammation: Microglia and T Cells Get Ready to Tango. *Front Immunol,* 8**,** 1905.

SCHINDELIN, J., ARGANDA-CARRERAS, I., FRISE, E., KAYNIG, V., LONGAIR, M., PIETZSCH, T., PREIBISCH, S., RUEDEN, C., SAALFELD, S., SCHMID, B., TINEVEZ, J. Y., WHITE, D. J., HARTENSTEIN, V., ELICEIRI, K., TOMANCAK, P. & CARDONA, A. 2012. Fiji: an open-source platform for biological-image analysis. *Nat Methods,* 9**,** 676-82.

SCHWABENLAND, M., BRUCK, W., PRILLER, J., STADELMANN, C., LASSMANN, H. & PRINZ, M. 2021. Analyzing microglial phenotypes across neuropathologies: a practical guide. *Acta Neuropathol,* 142**,** 923-936.

SCIARRA, F., CAMPOLO, F., FRANCESCHINI, E., CARLOMAGNO, F. & VENNERI, M. A. 2023. Gender-Specific Impact of Sex Hormones on the Immune System. *Int J Mol Sci,* 24.

SEDGWICK, J. D., SCHWENDER, S., IMRICH, H., DORRIES, R., BUTCHER, G. W. & TER MEULEN, V. 1991. Isolation and direct characterization of resident microglial cells from the normal and inflamed central nervous system. *Proc Natl Acad Sci U S A,* 88**,** 7438-42.

SEIBENHENER, M. L. & WOOTEN, M. C. 2015. Use of the Open Field Maze to measure locomotor and anxiety-like behavior in mice. *J Vis Exp***,** e52434.

SELMAJ, K. W. & RAINE, C. S. 1988. Tumor necrosis factor mediates myelin and oligodendrocyte damage in vitro. *Ann Neurol,* 23**,** 339-46.

SERRETTI, A. 2023. Anhedonia and Depressive Disorders. *Clin Psychopharmacol Neurosci,* 21**,** 401-409.

SERRETTI, A. 2025. Anhedonia: Current and future treatments. *PCN Rep,* 4**,** e70088.

SHAH, S., WONG, L. M., ELLIS, K., BODNAR, B., SARIBAS, S., TING, J., WEI, Z., TANG, Y., WANG, X., WANG, H., LING, B., MARGOLIS, D. M., GARCIA, J. V., HU, W. & JIANG, G. 2022. Microglia-Specific Promoter Activities of HEXB Gene. *Front Cell Neurosci,* 16**,** 808598.

SHARMA, D., ANDRIANOVA, L., MCGONIGAL, R., GARDNER-STEPHEN, K., AL FADHEL, H., BARRIE, J. A., HOHNE, R., SAATHOFF, M., KARABALCI, Y., BOURGOGNON, J.-M., COLE, J. J., CRAIG, M. T. & CAVANAGH, J. T. 2024. Anhedonic behaviour in a TLR7-driven neuroinflammation mouse model is associated with impaired thalamostriatal signalling and immune cell ingress into the brain. *bioRxiv***,** 2024.06.26.600791.

SHARMA, S. & FULTON, S. 2013. Diet-induced obesity promotes depressive-like behaviour that is associated with neural adaptations in brain reward circuitry. *Int J Obes (Lond),* 37**,** 382-9.

SHAW, G. A., HYER, M. M., TARGETT, I., COUNCIL, K. R., DYER, S. K., TURKSON, S., BURNS, C. M. & NEIGH, G. N. 2020. Traumatic stress history interacts with sex and chronic peripheral inflammation to alter mitochondrial function of synaptosomes. *Brain Behav Immun,* 88**,** 203-219.

SHI, W., ZHANG, S., LU, Y., WANG, Y., ZHAO, J. & LI, L. 2022. T cell responses in depressed mice induced by chronic unpredictable mild stress. *J Affect Disord,* 296**,** 150-156.

SHI, W., ZHANG, S., YAO, K., MENG, Q., LU, Y., REN, Y., LI, L. & ZHAO, J. 2024. Breakdown of the blood-brain barrier in depressed mice induced by chronic unpredictable mild stress. *J Psychiatr Res,* 180**,** 138-146.

SHI, Z., WANG, X., WANG, J., CHEN, H., DU, Q., LANG, Y., KONG, L., LUO, W., QIU, Y., ZHANG, Y., LI, C., WEN, D., YAO, J., CHENG, X., CAI, L., LIN, X., WANG, R., MOU, Z., LI, S., LIU, D., ZHOU, H., ZHOU, H. & YANG, M. 2023. Granzyme B + CD8 + T cells with terminal differentiated effector signature determine multiple sclerosis progression. *J Neuroinflammation,* 20**,** 138.

SHINKAI, Y., RATHBUN, G., LAM, K. P., OLTZ, E. M., STEWART, V., MENDELSOHN, M., CHARRON, J., DATTA, M., YOUNG, F., STALL, A. M. & ET AL. 1992. RAG-2-deficient mice lack mature lymphocytes owing to inability to initiate V(D)J rearrangement. *Cell,* 68**,** 855-67.

SHIPPY, D. C. & ULLAND, T. K. 2023. Lipid metabolism transcriptomics of murine microglia in Alzheimer's disease and neuroinflammation. *Sci Rep,* 13**,** 14800.

SHUKURI, M., UCHINO, M., SAKAMAKI, T., ONOE, S., HOSOI, R., TODOROKI, K., ARANO, Y., SAKAI, T., AKIZAWA, H. & INOUE, O. 2021. Ex vivo imaging and analysis of ROS generation correlated with microglial activation in rat model with acute neuroinflammation induced by intrastriatal injection of LPS. *Biochem Biophys Res Commun,* 584**,** 101-106.

SMITH, C. L., BLAKE, J. A., KADIN, J. A., RICHARDSON, J. E., BULT, C. J. & MOUSE GENOME DATABASE, G. 2018. Mouse Genome Database (MGD)-2018: knowledgebase for the laboratory mouse. *Nucleic Acids Res,* 46**,** D836-D842.

SMITH, K. J., NORRIS, S., O'FARRELLY, C. & O'MARA, S. M. 2011. Risk factors for the development of depression in patients with hepatitis C taking interferon-alpha. *Neuropsychiatr Dis Treat,* 7**,** 275-92.

SONG, N., LIU, Z., GAO, Y., LU, S., YANG, S. & YUAN, C. 2024. NAc-DBS corrects depression-like behaviors in CUMS mouse model via disinhibition of DA neurons in the VTA. *Mol Psychiatry,* 29**,** 1550-1566.

SOUSA, C., BIBER, K. & MICHELUCCI, A. 2017. Cellular and Molecular Characterization of Microglia: A Unique Immune Cell Population. *Front Immunol,* 8**,** 198.

SRAKOCIC, S., JOSIC, P., TRIFUNOVIC, S., GAJOVIC, S., GRCEVIC, D. & GLASNOVIC, A. 2022. Proposed practical protocol for flow cytometry analysis of microglia from the healthy adult mouse brain: Systematic review and isolation methods' evaluation. *Front Cell Neurosci,* 16**,** 1017976.

STAHL, P. L., SALMEN, F., VICKOVIC, S., LUNDMARK, A., NAVARRO, J. F., MAGNUSSON, J., GIACOMELLO, S., ASP, M., WESTHOLM, J. O., HUSS, M., MOLLBRINK, A., LINNARSSON, S., CODELUPPI, S., BORG, A., PONTEN, F., COSTEA, P. I., SAHLEN, P., MULDER, J., BERGMANN, O., LUNDEBERG, J. & FRISEN, J. 2016. Visualization and analysis of gene expression in tissue sections by spatial transcriptomics. *Science,* 353**,** 78-82.

STAHL, S. M. 1998. Mechanism of action of serotonin selective reuptake inhibitors. Serotonin receptors and pathways mediate therapeutic effects and side effects. *J Affect Disord,* 51**,** 215-35.

STANLEY, B. G., KYRKOULI, S. E., LAMPERT, S. & LEIBOWITZ, S. F. 1986. Neuropeptide Y chronically injected into the hypothalamus: a powerful neurochemical inducer of hyperphagia and obesity. *Peptides,* 7**,** 1189-92.

STEELAND, S., VAN RYCKEGHEM, S., VAN IMSCHOOT, G., DE RYCKE, R., TOUSSAINT, W., VANHOUTTE, L., VANHOVE, C., DE VOS, F., VANDENBROUCKE, R. E. & LIBERT, C. 2017. TNFR1 inhibition with a Nanobody protects against EAE development in mice. *Sci Rep,* 7**,** 13646.

STRASS, S., GEIGER, J., MARTORELLI, M., GEIGER, S., CLOOS, N., KEPPLER, M., FISCHER, T., RIEXINGER, L., SCHWAMBORN, A., GUEZGUEZ, J., SPATH, N., CRUCES, S., GUSE, J. H., SANDRI, T. L., BURNET, M. & LAUFER, S. 2023. Isostearic acid is an active component of imiquimod formulations used to induce psoriaform disease models. *Inflammopharmacology,* 31**,** 799-812.

STRAWBRIDGE, R., JAVED, R. R., CAVE, J., JAUHAR, S. & YOUNG, A. H. 2023. The effects of reserpine on depression: A systematic review. *J Psychopharmacol,* 37**,** 248-260.

SUI, X., LO, J. A., LUO, S., HE, Y., TANG, Z., LIN, Z., ZHOU, Y., WANG, W. X., LIU, J. & WANG, X. 2024. Scalable spatial single-cell transcriptomics and translatomics in 3D thick tissue blocks. *bioRxiv*.

SUN, L., LI, Y., JIA, X., WANG, Q., LI, Y., HU, M., TIAN, L., YANG, J., XING, W., ZHANG, W., WANG, J., XU, H., WANG, L., ZHANG, D. & REN, H. 2017. Neuroprotection by IFN-gamma via astrocyte-secreted IL-6 in acute neuroinflammation. *Oncotarget,* 8**,** 40065-40078.

SUN, L., SU, Y., JIAO, A., WANG, X. & ZHANG, B. 2023. T cells in health and disease. *Signal Transduct Target Ther,* 8**,** 235.

SUN, R. & JIANG, H. 2024a. Border-associated macrophages in the central nervous system. *Clin Immunol***,** 109921.

SUN, R. & JIANG, H. 2024b. Border-associated macrophages in the central nervous system. *J Neuroinflammation,* 21**,** 67.

SURENDRANATHAN, A., SU, L., MAK, E., PASSAMONTI, L., HONG, Y. T., ARNOLD, R., VAZQUEZ RODRIGUEZ, P., BEVAN-JONES, W. R., BRAIN, S. A. E., FRYER, T. D., AIGBIRHIO, F. I., ROWE, J. B. & O'BRIEN, J. T. 2018. Early microglial activation and peripheral inflammation in dementia with Lewy bodies. *Brain,* 141**,** 3415-3427.

SUZUKI, H., TOHYAMA, K., NAGATA, K., TAKETANI, S. & ARAKI, M. 2007. Regulatory expression of Neurensin-1 in the spinal motor neurons after mouse sciatic nerve injury. *Neurosci Lett,* 421**,** 152-7.

SWAIN, S. L. 1983. T cell subsets and the recognition of MHC class. *Immunol Rev,* 74**,** 129-42.

TAYLOR, N. E., VAN DORT, C. J., KENNY, J. D., PEI, J., GUIDERA, J. A., VLASOV, K. Y., LEE, J. T., BOYDEN, E. S., BROWN, E. N. & SOLT, K. 2016. Optogenetic activation of dopamine neurons in the ventral tegmental area induces reanimation from general anesthesia. *Proc Natl Acad Sci U S A,* 113**,** 12826-12831.

TEAM, R. C. 2024a. R: A Language and Environment for Statistical Computing. 4.4.1 ed.: R Foundation for Statistical Computing.

TEAM, R. S. 2024b. RStudio: Integrated Development Environment for R. 2024.12.1+563 ed.: Posit Software, PBC.

TEELING, J. L., FELTON, L. M., DEACON, R. M., CUNNINGHAM, C., RAWLINS, J. N. & PERRY, V. H. 2007. Sub-pyrogenic systemic inflammation impacts on brain and behavior, independent of cytokines. *Brain Behav Immun,* 21**,** 836-50.

THIBAUT, F. 2016. The role of sex and gender in neuropsychiatric disorders. *Dialogues Clin Neurosci,* 18**,** 351-352.

THOMSON, C. A., MCCOLL, A., CAVANAGH, J. & GRAHAM, G. J. 2014. Peripheral inflammation is associated with remote global gene expression changes in the brain. *J Neuroinflammation,* 11**,** 73.

TIGNER, A., IBRAHIM, S. A. & MURRAY, I. V. 2025. Histology, White Blood Cell. *StatPearls.* Treasure Island (FL) ineligible companies. Disclosure: Sherif Ibrahim declares no relevant financial relationships with ineligible companies. Disclosure: Ian Murray declares no relevant financial relationships with ineligible companies.

TREADWAY, M. T. 2023. Treating Motivational and Consummatory Aspects of Anhedonia. *Focus (Am Psychiatr Publ),* 21**,** 278-280.

TSIKIS, S. T., FLIGOR, S. C., HIRSCH, T. I., PAN, A., YU, L. J., KISHIKAWA, H., JOINER, M. M., MITCHELL, P. D. & PUDER, M. 2022. Lipopolysaccharide-induced murine lung injury results in long-term pulmonary changes and downregulation of angiogenic pathways. *Sci Rep,* 12**,** 10245.

TURKHEIMER, F. E., VERONESE, M., MONDELLI, V., CASH, D. & PARIANTE, C. M. 2023. Sickness behaviour and depression: An updated model of peripheral-central immunity interactions. *Brain Behav Immun,* 111**,** 202-210.

UBOGU, E. E., CALLAHAN, M. K., TUCKY, B. H. & RANSOHOFF, R. M. 2006. Determinants of CCL5-driven mononuclear cell migration across the blood-brain barrier. Implications for therapeutically modulating neuroinflammation. *J Neuroimmunol,* 179**,** 132-44.

UNGER, M. S., LI, E., SCHARNAGL, L., POUPARDIN, R., ALTENDORFER, B., MROWETZ, H., HUTTER-PAIER, B., WEIGER, T. M., HENEKA, M. T., ATTEMS, J. & AIGNER, L. 2020. CD8(+) T-cells infiltrate Alzheimer's disease brains

and regulate neuronal- and synapse-related gene expression in APP-PS1 transgenic mice. *Brain Behav Immun,* 89**,** 67-86.

UTZ, S. G., SEE, P., MILDENBERGER, W., THION, M. S., SILVIN, A., LUTZ, M., INGELFINGER, F., RAYAN, N. A., LELIOS, I., BUTTGEREIT, A., ASANO, K., PRABHAKAR, S., GAREL, S., BECHER, B., GINHOUX, F. & GRETER, M. 2020. Early Fate Defines Microglia and Non-parenchymal Brain Macrophage Development. *Cell,* 181**,** 557-573 e18.

VAN DER FITS, L., MOURITS, S., VOERMAN, J. S., KANT, M., BOON, L., LAMAN, J. D., CORNELISSEN, F., MUS, A. M., FLORENCIA, E., PRENS, E. P. & LUBBERTS, E. 2009. Imiquimod-induced psoriasis-like skin inflammation in mice is mediated via the IL-23/IL-17 axis. *J Immunol,* 182**,** 5836-45.

VAN HOVE, H., MARTENS, L., SCHEYLTJENS, I., DE VLAMINCK, K., POMBO ANTUNES, A. R., DE PRIJCK, S., VANDAMME, N., DE SCHEPPER, S., VAN ISTERDAEL, G., SCOTT, C. L., AERTS, J., BERX, G., BOECKXSTAENS, G. E., VANDENBROUCKE, R. E., VEREECKE, L., MOECHARS, D., GUILLIAMS, M., VAN GINDERACHTER, J. A., SAEYS, Y. & MOVAHEDI, K. 2019. A single-cell atlas of mouse brain macrophages reveals unique transcriptional identities shaped by ontogeny and tissue environment. *Nat Neurosci,* 22**,** 1021-1035.

VAN WAGENINGEN, T. A., VLAAR, E., KOOIJ, G., JONGENELEN, C. A. M., GEURTS, J. J. G. & VAN DAM, A. M. 2019. Regulation of microglial TMEM119 and P2RY12 immunoreactivity in multiple sclerosis white and grey matter lesions is dependent on their inflammatory environment. *Acta Neuropathol Commun,* 7**,** 206.

VANKRIEKELSVENNE, E., CHRZANOWSKI, U., MANZHULA, K., GREINER, T., WREE, A., HAWLITSCHKA, A., LLOVERA, G., ZHAN, J., JOOST, S., SCHMITZ, C., PONSAERTS, P., AMOR, S., NUTMA, E., KIPP, M. & KADDATZ, H. 2022. Transmembrane protein 119 is neither a specific nor a reliable marker for microglia. *Glia,* 70**,** 1170-1190.

VASCONCELLOS, L. R. C., MARTIMIANO, L., DANTAS, D. P., FONSECA, F. M., MATA-SANTOS, H., TRAVASSOS, L., MENDEZ-OTERO, R., BOZZA, M. T. & PIMENTEL-COELHO, P. M. 2021. Intracerebral Injection of Heme Induces Lipid Peroxidation, Neuroinflammation, and Sensorimotor Deficits. *Stroke,* 52**,** 1788-1797.

VASEK, M. J., MUELLER, S. M., FASS, S. B., DEAJON-JACKSON, J. D., LIU, Y., CROSBY, H. W., KOESTER, S. K., YI, J., LI, Q. & DOUGHERTY, J. D. 2023. Local translation in microglial processes is required for efficient phagocytosis. *Nat Neurosci,* 26**,** 1185-1195.

VAZQUEZ-VILLOLDO, N., DOMERCQ, M., MARTIN, A., LLOP, J., GOMEZ-VALLEJO, V. & MATUTE, C. 2014. P2X4 receptors control the fate and survival of activated microglia. *Glia,* 62**,** 171-84.

VERSELE, R., SEVIN, E., GOSSELET, F., FENART, L. & CANDELA, P. 2022. TNF-alpha and IL-1beta Modulate Blood-Brain Barrier Permeability and Decrease Amyloid-beta Peptide Efflux in a Human Blood-Brain Barrier Model. *Int J Mol Sci,* 23.

VICHAYA, E. G. & DANTZER, R. 2018. Inflammation-induced motivational changes: Perspective gained by evaluating positive and negative valence systems. *Curr Opin Behav Sci,* 22**,** 90-95.

VICHAYA, E. G., HUNT, S. C. & DANTZER, R. 2014. Lipopolysaccharide reduces incentive motivation while boosting preference for high reward in mice. *Neuropsychopharmacology,* 39**,** 2884-90.

VIDAL-ITRIAGO, A., RADFORD, R. A. W., ARAMIDEH, J. A., MAUREL, C., SCHERER, N. M., DON, E. K., LEE, A., CHUNG, R. S., GRAEBER, M. B. & MORSCH, M. 2022. Microglia morphophysiological diversity and its implications for the CNS. *Front Immunol,* 13**,** 997786.

VIGNALI, D. A., COLLISON, L. W. & WORKMAN, C. J. 2008. How regulatory T cells work. *Nat Rev Immunol,* 8**,** 523-32.

VILLEMIN, J. P., BASSAGANYAS, L., POURQUIER, D., BOISSIERE, F., CABELLO-AGUILAR, S., CRAPEZ, E., TANOS, R., CORNILLOT, E., TURTOI, A. & COLINGE, J. 2023. Inferring ligand-receptor cellular networks from bulk and spatial transcriptomic datasets with BulkSignalR. *Nucleic Acids Res,* 51**,** 4726-44.

VOLKOW, N. D., WANG, G. J. & BALER, R. D. 2011. Reward, dopamine and the control of food intake: implications for obesity. *Trends Cogn Sci,* 15**,** 37-46.

VON MUCKE-HEIM, I. A., URBINA-TREVINO, L., BORDES, J., RIES, C., SCHMIDT, M. V. & DEUSSING, J. M. 2023. Introducing a depression-like syndrome for translational neuropsychiatry: a plea for taxonomical validity and improved comparability between humans and mice. *Mol Psychiatry,* 28**,** 329-340.

VOSS, S. D., SONDEL, P. M. & ROBB, R. J. 1992. Characterization of the interleukin 2 receptors (IL-2R) expressed on human natural killer cells activated in vivo by IL-2: association of the p64 IL-2R gamma chain with the IL-2R beta chain in functional intermediate-affinity IL-2R. *J Exp Med,* 176**,** 531-41.

WAGNON, I. M., JABUR, L. J., NIEDERMAYER, G., MUNCH, G., KARL, T., CHESWORTH, R. & GYENGESI, E. 2023. Chronic interleukin-6 mediated neuroinflammation decreases anxiety, and impaires spatial memory in aged female mice. *Front Neurosci,* 17**,** 1267818.

WAGSTAFF, A. J. & PERRY, C. M. 2007. Topical imiquimod: a review of its use in the management of anogenital warts, actinic keratoses, basal cell carcinoma and other skin lesions. *Drugs,* 67**,** 2187-210.

WALF, A. A. & FRYE, C. A. 2007. The use of the elevated plus maze as an assay of anxiety-related behavior in rodents. *Nat Protoc,* 2**,** 322-8.

WALTER, A., SCHAFER, M., CECCONI, V., MATTER, C., UROSEVIC-MAIWALD, M., BELLONI, B., SCHONEWOLF, N., DUMMER, R., BLOCH, W., WERNER, S., BEER, H. D., KNUTH, A. & VAN DEN BROEK, M. 2013. Aldara activates TLR7-independent immune defence. *Nat Commun,* 4**,** 1560.

WAN, C., XIA, Y., YAN, J., LIN, W., YAO, L., ZHANG, M., GAISLER-SALOMON, I., MEI, L., YIN, D. M. & CHEN, Y. 2024. nNOS in Erbb4-positive neurons regulates GABAergic transmission in mouse hippocampus. *Cell Death Dis,* 15**,** 167.

WANG, F., BONAM, S. R., SCHALL, N., KUHN, L., HAMMANN, P., CHALOIN, O., MADINIER, J. B., BRIAND, J. P., PAGE, N. & MULLER, S. 2018a. Blocking nuclear export of HSPA8 after heat shock stress severely alters cell survival. *Sci Rep,* 8**,** 16820.

WANG, H., CHENG, Z., XU, Z., WANG, M., SUN, X., LIU, W., WANG, J., YANG, Q., ZHANG, T., SONG, J., DU, Y. & ZHANG, X. 2025. Systemic Inflammatory Factors and Neuropsychiatric Disorders: A Bidirectional Mendelian Randomization Study. *Brain Behav,* 15**,** e70478.

WANG, J., DENG, X., XIE, Y., TANG, J., ZHOU, Z., YANG, F., HE, Q., CAO, Q., ZHANG, L. & HE, L. 2020a. An Integrated Transcriptome Analysis Reveals IGFBP7 Upregulation in Vasculature in Traumatic Brain Injury. *Front Genet,* 11**,** 599834.

WANG, J., HE, W. & ZHANG, J. 2023a. A richer and more diverse future for microglia phenotypes. *Heliyon,* 9**,** e14713.

WANG, J., HORLACHER, M., CHENG, L. & WINTHER, O. 2023b. RNA trafficking and subcellular localization-a review of mechanisms, experimental and predictive methodologies. *Brief Bioinform,* 24.

WANG, J., JIA, Y., LI, G., WANG, B., ZHOU, T., ZHU, L., CHEN, T. & CHEN, Y. 2018b. The Dopamine Receptor D3 Regulates Lipopolysaccharide-Induced Depressive-Like Behavior in Mice. *Int J Neuropsychopharmacol,* 21**,** 448-460.

WANG, J., WANG, L., WU, Q., CAI, Y., CUI, C., YANG, M., SUN, B., MAO, L. & WANG, Y. 2024. Interleukin-4 Modulates Neuroinflammation by Inducing Phenotypic Transformation of Microglia Following Subarachnoid Hemorrhage. *Inflammation,* 47**,** 390-403.

WANG, Q., DING, S. L., LI, Y., ROYALL, J., FENG, D., LESNAR, P., GRADDIS, N., NAEEMI, M., FACER, B., HO, A., DOLBEARE, T., BLANCHARD, B., DEE, N., WAKEMAN, W., HIROKAWA, K. E., SZAFER, A., SUNKIN, S. M., OH, S. W., BERNARD, A., PHILLIPS, J. W., HAWRYLYCZ, M., KOCH, C., ZENG, H., HARRIS, J. A. & NG, L. 2020b. The Allen Mouse Brain Common Coordinate Framework: A 3D Reference Atlas. *Cell,* 181**,** 936-953 e20.

WANG, Y., SADIKE, D., HUANG, B., LI, P., WU, Q., JIANG, N., FANG, Y., SONG, G., XU, L., WANG, W. & XIE, M. 2023c. Regulatory T cells alleviate myelin loss and cognitive dysfunction by regulating neuroinflammation and microglial pyroptosis via TLR4/MyD88/NF-kappaB pathway in LPC-induced demyelination. *J Neuroinflammation,* 20**,** 41.

WANG, Y. L., HAN, Q. Q., GONG, W. Q., PAN, D. H., WANG, L. Z., HU, W., YANG, M., LI, B., YU, J. & LIU, Q. 2018c. Microglial activation mediates chronic mild stress-induced depressive- and anxiety-like behavior in adult rats. *J Neuroinflammation,* 15**,** 21.

WEBER, A. A., YANG, X., MENNILLO, E., WONG, S., LE, S., ASHLEY TEO, J. Y., CHANG, M., BENNER, C. W., DING, J., JAIN, M., CHEN, S., KARIN, M. & TUKEY, R. H. 2024. Triclosan administration to humanized UDP-glucuronosyltransferase 1 neonatal mice induces UGT1A1 through a dependence on PPARalpha and ATF4. *J Biol Chem,* 300**,** 107340.

WEI, W., ZHANG, L., XIN, W., PAN, Y., TATENHORST, L., HAO, Z., GERNER, S. T., HUBER, S., JUENEMANN, M., BUTZ, M., HUTTNER, H. B., BAHR, M., FITZNER, D., JIA, F. & DOEPPNER, T. R. 2024. TREM2 regulates microglial lipid droplet formation and represses post-ischemic brain injury. *Biomed Pharmacother,* 170**,** 115962.

WEI, Y. & LI, X. 2022. Different phenotypes of microglia in animal models of Alzheimer disease. *Immun Ageing,* 19**,** 44.

WENZEL, J., UERLICH, M., HALLER, O., BIEBER, T. & TUETING, T. 2005. Enhanced type I interferon signaling and recruitment of chemokine receptor CXCR3-expressing lymphocytes into the skin following treatment with the TLR7-agonist imiquimod. *J Cutan Pathol,* 32**,** 257-62.

WILLIAMS, C. G., LEE, H. J., ASATSUMA, T., VENTO-TORMO, R. & HAQUE, A. 2022. An introduction to spatial transcriptomics for biomedical research. *Genome Med,* 14**,** 68.

WILLIAMS, G. P., SCHONHOFF, A. M., JURKUVENAITE, A., GALLUPS, N. J., STANDAERT, D. G. & HARMS, A. S. 2021. CD4 T cells mediate brain inflammation and neurodegeneration in a mouse model of Parkinson's disease. *Brain,* 144**,** 2047-2059.

WOHLEB, E. S., MCKIM, D. B., SHERIDAN, J. F. & GODBOUT, J. P. 2014. Monocyte trafficking to the brain with stress and inflammation: a novel axis of immune-to-brain communication that influences mood and behavior. *Front Neurosci,* 8**,** 447.

WOHN, C. T., PANTELYUSHIN, S., OBER-BLOBAUM, J. L. & CLAUSEN, B. E. 2014. Aldara-induced psoriasis-like skin inflammation: isolation and characterization of cutaneous dendritic cells and innate lymphocytes. *Methods Mol Biol,* 1193**,** 171-85.

WON, E. & KIM, Y. K. 2020. Neuroinflammation-Associated Alterations of the Brain as Potential Neural Biomarkers in Anxiety Disorders. *Int J Mol Sci,* 21.

WONG, P., FOLTZ, J. A., CHANG, L., NEAL, C. C., YAO, T., CUBITT, C. C., TRAN, J., KERSTING-SCHADEK, S., PALAKURTY, S., JAEGER, N., RUSSLER-GERMAIN, D. A., MARIN, N. D., GANG, M., WAGNER, J. A., ZHOU, A. Y., JACOBS, M. T., FOSTER, M., SCHAPPE, T., MARSALA, L., MCCLAIN, E., PENCE, P., BECKER-HAPAK, M., FISK, B., PETTI, A. A., GRIFFITH, O. L., GRIFFITH, M., BERRIEN-ELLIOTT, M. M. & FEHNIGER, T. A. 2023. T-BET and EOMES sustain mature human NK cell identity and antitumor function. *J Clin Invest,* 133.

WU, H., WILLIAMS, J. & NATHANS, J. 2014. Complete morphologies of basal forebrain cholinergic neurons in the mouse. *Elife,* 3**,** e02444.

WU, L., JI, N. N., WANG, H., HUA, J. Y., SUN, G. L., CHEN, P. P., HUA, R. & ZHANG, Y. M. 2021. Domino Effect of Interleukin-15 and CD8 T-Cell-Mediated Neuronal Apoptosis in Experimental Traumatic Brain Injury. *J Neurotrauma,* 38**,** 1450-1463.

WU, Q., CARLOS, A. R., BRAZA, F., BERGMAN, M. L., KITOKO, J. Z., BASTOS-AMADOR, P., CUADRADO, E., MARTINS, R., OLIVEIRA, B. S., MARTINS, V. C., SCICLUNA, B. P., LANDRY, J. J., JUNG, F. E., ADEMOLUE, T. W., PEITZSCH, M., ALMEIDA-SANTOS, J., THOMPSON, J., CARDOSO, S., VENTURA, P., SLOT, M., RONTOGIANNI, S., RIBEIRO, V., DOMINGUES, V. D. S., CABRAL, I. A., WEIS, S., GROTH, M., AMENEIRO, C., FIDALGO, M., WANG, F., DEMENGEOT, J., AMSEN, D. & SOARES, M. P. 2024. Ferritin heavy chain supports stability and function of the regulatory T cell lineage. *EMBO J,* 43**,** 1445-1483.

WU, S., YIN, Y. & DU, L. 2022a. Blood-Brain Barrier Dysfunction in the Pathogenesis of Major Depressive Disorder. *Cell Mol Neurobiol,* 42**,** 2571-2591.

WU, X., SHEN, Q., CHANG, H., LI, J. & XING, D. 2022b. Promoted CD4(+) T cell-derived IFN-gamma/IL-10 by photobiomodulation therapy modulates neurogenesis to ameliorate cognitive deficits in APP/PS1 and 3xTg-AD mice. *J Neuroinflammation,* 19**,** 253.

XENI, F., MARANGONI, C. & JACKSON, M. G. 2024. Validation of a non-food or water motivated effort-based foraging task as a measure of motivational state in male mice. *Neuropsychopharmacology,* 49**,** 1883-1891.

XIAO, J., ADKINSON, J. A., MYERS, J., ALLAWALA, A. B., MATHURA, R. K., PIRTLE, V., NAJERA, R., PROVENZA, N. R., BARTOLI, E., WATROUS, A. J., OSWALT, D., GADOT, R., ANAND, A., SHOFTY, B., MATHEW, S. J., GOODMAN, W. K., POURATIAN, N., PITKOW, X., BIJANKI, K. R., HAYDEN, B. & SHETH, S. A. 2024. Beta activity in human anterior cingulate cortex mediates reward biases. *Nat Commun,* 15**,** 5528.

XIAO, J., MENG, Z., LU, Y., NIE, Z., LIU, Y., YAO, Z., ZHANG, Y. & LI, L. 2025. Targeting microglia-Th17 feed-forward loop to suppress autoimmune neuroinflammation. *J Neuroinflammation,* 22**,** 118.

XIONG, B., LI, A., LOU, Y., CHEN, S., LONG, B., PENG, J., YANG, Z., XU, T., YANG, X., LI, X., JIANG, T., LUO, Q. & GONG, H. 2017. Precise Cerebral Vascular Atlas in Stereotaxic Coordinates of Whole Mouse Brain. *Front Neuroanat,* 11**,** 128.

XU, L., YE, X., WANG, Q., XU, B., ZHONG, J., CHEN, Y. Y. & WANG, L. L. 2021. T-cell infiltration, contribution and regulation in the central nervous system post-traumatic injury. *Cell Prolif,* 54**,** e13092.

XU, S. & CAO, X. 2010. Interleukin-17 and its expanding biological functions. *Cellular & Molecular Immunology,* 7**,** 164-174.

XU, Y., LIN, Y., YU, M. & ZHOU, K. 2024. The nucleus accumbens in reward and aversion processing: insights and implications. *Front Behav Neurosci,* 18**,** 1420028.

XU, Y. J., AU, N. P. B. & MA, C. H. E. 2022. Functional and Phenotypic Diversity of Microglia: Implication for Microglia-Based Therapies for Alzheimer's Disease. *Front Aging Neurosci,* 14**,** 896852.

XUE, F. & DU, H. 2021. TREM2 Mediates Microglial Anti-Inflammatory Activations in Alzheimer's Disease: Lessons Learned from Transcriptomics. *Cells,* 10.

YAN, L., LI, Y., TAN, T., QI, J., FANG, J., GUO, H., REN, Z., GOU, L., GENG, Y., CUI, H., SHEN, L., YU, S., WANG, Z. & ZUO, Z. 2023. RAGE-TLR4 Crosstalk Is the Key Mechanism by Which High Glucose Enhances the Lipopolysaccharide-Induced Inflammatory Response in Primary Bovine Alveolar Macrophages. *Int J Mol Sci,* 24.

YANG, A., XIN, X., YANG, W., LI, M., YANG, W., LI, L. & LIU, X. 2019. Etanercept reduces anxiety and depression in psoriasis patients, and sustained depression correlates with reduced therapeutic response to etanercept. *Ann Dermatol Venereol,* 146**,** 363-371.

YANG, I., HAN, S. J., KAUR, G., CRANE, C. & PARSA, A. T. 2010. The role of microglia in central nervous system immunity and glioma immunology. *J Clin Neurosci,* 17**,** 6-10.

YANG, R., WANG, X., LIU, H., CHEN, J., TAN, C., CHEN, H. & WANG, X. 2024. Egr-1 is a key regulator of the blood-brain barrier damage induced by meningitic Escherichia coli. *Cell Commun Signal,* 22**,** 44.

YANG, S. C., SHIEH, K. R. & LI, H. Y. 2005. Cocaine- and amphetamine-regulated transcript in the nucleus accumbens participates in the regulation of feeding behavior in rats. *Neuroscience,* 133**,** 841-51.

YAO, Z., VAN VELTHOVEN, C. T. J., KUNST, M., ZHANG, M., MCMILLEN, D., LEE, C., JUNG, W., GOLDY, J., ABDELHAK, A., BAKER, P., BARKAN, E., BERTAGNOLLI, D., CAMPOS, J., CAREY, D., CASPER, T., CHAKKA, A. B., CHAKRABARTY, R., CHAVAN, S., CHEN, M., CLARK, M., CLOSE, J., CRICHTON, K., DANIEL, S., DOLBEARE, T., ELLINGWOOD, L., GEE, J., GLANDON, A., GLOE, J., GOULD, J., GRAY, J., GUILFORD, N., GUZMAN, J., HIRSCHSTEIN, D., HO, W., JIN, K., KROLL, M., LATHIA, K., LEON, A., LONG, B., MALTZER, Z., MARTIN, N., MCCUE, R., MEYERDIERKS, E., NGUYEN, T. N., PHAM, T., RIMORIN, C., RUIZ, A., SHAPOVALOVA, N., SLAUGHTERBECK, C., SULC, J., TIEU, M., TORKELSON, A., TUNG, H., CUEVAS, N. V., WADHWANI, K., WARD, K., LEVI, B., FARRELL, C., THOMPSON, C. L., MUFTI, S., PAGAN, C. M., KRUSE, L., DEE, N., SUNKIN, S. M., ESPOSITO, L., HAWRYLYCZ, M. J., WATERS, J., NG, L., SMITH, K. A., TASIC, B., ZHUANG, X. & ZENG, H. 2023. A high-resolution transcriptomic and spatial atlas of cell types in the whole mouse brain. *bioRxiv*.

YAQUBI, M., GROH, A. M. R., DORION, M. F., AFANASIEV, E., LUO, J. X. X., HASHEMI, H., SINHA, S., KIERAN, N. W., BLAIN, M., CUI, Q. L., BIERNASKIE, J., SROUR, M., DUDLEY, R., HALL, J. A., SONNEN, J. A., ARBOUR, N., PRAT, A., STRATTON, J. A., ANTEL, J. & HEALY, L. M. 2023. Analysis of the microglia transcriptome across the human lifespan using single cell RNA sequencing. *J Neuroinflammation,* 20**,** 132.

YATES, A. D., ACHUTHAN, P., AKANNI, W., ALLEN, J., ALLEN, J., ALVAREZ-JARRETA, J., AMODE, M. R., ARMEAN, I. M., AZOV, A. G., BENNETT, R., BHAI, J., BILLIS, K., BODDU, S., MARUGAN, J. C., CUMMINS, C., DAVIDSON, C., DODIYA, K., FATIMA, R., GALL, A., GIRON, C. G., GIL, L., GREGO, T., HAGGERTY, L., HASKELL, E., HOURLIER, T., IZUOGU, O. G., JANACEK, S. H., JUETTEMANN, T., KAY, M., LAVIDAS, I., LE, T., LEMOS, D., MARTINEZ, J. G., MAUREL, T., MCDOWALL, M., MCMAHON, A., MOHANAN, S., MOORE, B., NUHN, M., OHEH, D. N., PARKER, A., PARTON, A., PATRICIO, M., SAKTHIVEL, M. P., ABDUL SALAM, A. I., SCHMITT, B. M., SCHUILENBURG, H., SHEPPARD, D., SYCHEVA, M., SZUBA, M., TAYLOR, K., THORMANN, A., THREADGOLD, G., VULLO, A., WALTS, B., WINTERBOTTOM, A., ZADISSA, A., CHAKIACHVILI, M., FLINT, B., FRANKISH, A., HUNT, S. E., G, I. I., KOSTADIMA, M., LANGRIDGE, N., LOVELAND, J. E., MARTIN, F. J., MORALES, J., MUDGE, J. M., MUFFATO, M., PERRY, E., RUFFIER, M., TREVANION, S. J., CUNNINGHAM, F., HOWE, K. L., ZERBINO, D. R. & FLICEK, P. 2020. Ensembl 2020. *Nucleic Acids Res,* 48**,** D682-D688.

YEH, C. Y., AGUIRRE, K., LAVERONI, O., KIM, S., WANG, A., LIANG, B., ZHANG, X., HAN, L. M., VALBUENA, R., BASSIK, M. C., KIM, Y. M., PLEVRITIS, S. K., SNYDER, M. P., HOWITT, B. E. & JERBY, L. 2024. Mapping spatial organization and genetic cell-state regulators to target immune evasion in ovarian cancer. *Nat Immunol,* 25**,** 1943-1958.

YIN, R., ZHANG, K., LI, Y., TANG, Z., ZHENG, R., MA, Y., CHEN, Z., LEI, N., XIONG, L., GUO, P., LI, G. & XIE, Y. 2023a. Lipopolysaccharide-induced depression-like model in mice: meta-analysis and systematic evaluation. *Front Immunol,* 14**,** 1181973.

YIN, S., MA, X. Y., SUN, Y. F., YIN, Y. Q., LONG, Y., ZHAO, C. L., MA, J. W., LI, S., HU, Y., LI, M. T., HU, G. & ZHOU, J. W. 2023b. RGS5 augments astrocyte activation and facilitates neuroinflammation via TNF signaling. *J Neuroinflammation,* 20**,** 203.

YIRMIYA, R. 2024. The inflammatory underpinning of depression: An historical perspective. *Brain Behav Immun,* 122**,** 433-443.

YOGEV, N., BEDKE, T., KOBAYASHI, Y., BROCKMANN, L., LUKAS, D., REGEN, T., CROXFORD, A. L., NIKOLAV, A., HOVELMEYER, N., VON STEBUT, E., PRINZ, M., UBEDA, C., MALOY, K. J., GAGLIANI, N., FLAVELL, R. A., WAISMAN, A. & HUBER, S. 2022. CD4(+) T-cell-derived IL-10 promotes CNS inflammation in mice by sustaining effector T cell survival. *Cell Rep,* 38**,** 110565.

YONG, H. Y. F., RAWJI, K. S., GHORBANI, S., XUE, M. & YONG, V. W. 2019. The benefits of neuroinflammation for the repair of the injured central nervous system. *Cell Mol Immunol,* 16**,** 540-546.

YOU, J. E., KIM, E. J., KIM, H. W., KIM, J. S., KIM, K. & KIM, P. H. 2024. Exploring the Role of Guanylate-Binding Protein-2 in Activated Microglia-Mediated Neuroinflammation and Neuronal Damage. *Biomedicines,* 12.

YOUSEFI, B., ESLAMI, M., GHASEMIAN, A., KOKHAEI, P., SALEK FARROKHI, A. & DARABI, N. 2019. Probiotics importance and their immunomodulatory properties. *J Cell Physiol,* 234**,** 8008-8018.

YSHII, L., GEBAUER, C., BERNARD-VALNET, R. & LIBLAU, R. 2015. Neurons and T cells: Understanding this interaction for inflammatory neurological diseases. *Eur J Immunol,* 45**,** 2712-20.

YU, C., ZHOU, X., FU, Q., PENG, Q., OH, K. W. & HU, Z. 2017. A New Insight into the Role of CART in Cocaine Reward: Involvement of CaMKII and Inhibitory G-Protein Coupled Receptor Signaling. *Front Cell Neurosci,* 11**,** 244.

YU, J., ZHU, H., TAHERI, S., MONDY, W., BONILHA, L., MAGWOOD, G. S., LACKLAND, D., ADAMS, R. J. & KINDY, M. S. 2019. Serum Amyloid A-Mediated Inflammasome Activation of Microglial Cells in Cerebral Ischemia. *J Neurosci,* 39**,** 9465-9476.

ZAISS, D. M., VAN LOOSDREGT, J., GORLANI, A., BEKKER, C. P., GRONE, A., SIBILIA, M., VAN BERGEN EN HENEGOUWEN, P. M., ROOVERS, R. C., COFFER, P. J. & SIJTS, A. J. 2013. Amphiregulin enhances regulatory T cell-suppressive function via the epidermal growth factor receptor. *Immunity,* 38**,** 275-84.

ZANNO, A. E., ROMER, M. A., FOX, L., GOLDEN, T., JAECKLE-SANTOS, L., SIMMONS, R. A. & GRINSPAN, J. B. 2019. Reducing Th2 inflammation through neutralizing IL-4 antibody rescues myelination in IUGR rat brain. *J Neurodev Disord,* 11**,** 34.

ZHANG, C., DULINSKAS, R., INEICHEN, C., GRETER, A., SIGRIST, H., LI, Y., ALANIS-LOBATO, G., HENGERER, B. & PRYCE, C. R. 2024. Chronic stress deficits in reward behaviour co-occur with low nucleus accumbens dopamine activity during reward anticipation specifically. *Commun Biol,* 7**,** 966.

ZHANG, Y., CHEN, K., SLOAN, S. A., BENNETT, M. L., SCHOLZE, A. R., O'KEEFFE, S., PHATNANI, H. P., GUARNIERI, P., CANEDA, C., RUDERISCH, N., DENG, S., LIDDELOW, S. A., ZHANG, C., DANEMAN, R., MANIATIS, T., BARRES, B. A. & WU, J. Q. 2014. An RNA-sequencing transcriptome and splicing database of glia, neurons, and vascular cells of the cerebral cortex. *J Neurosci,* 34**,** 11929-47.

ZHANG, Z., GAN, Q., HAN, J., TAO, Q., QIU, W. Q. & MADRI, J. A. 2023a. CD31 as a probable responding and gate-keeping protein of the blood-brain barrier and the risk of Alzheimer's disease. *J Cereb Blood Flow Metab,* 43**,** 1027-1041.

ZHANG, Z., LI, Y., JIANG, S., SHI, F. D., SHI, K. & JIN, W. N. 2023b. Targeting CCL5 signaling attenuates neuroinflammation after seizure. *CNS Neurosci Ther,* 29**,** 317-330.

ZHAO, Y., HUANG, Y., CAO, Y. & YANG, J. 2024. Astrocyte-Mediated Neuroinflammation in Neurological Conditions. *Biomolecules,* 14.

ZHOU, X., SONG, H., HE, J., HAN, W. & LI, Q. 2024. Deciphering microglial activation and neuronal apoptosis post-traumatic brain injury: The role of TYROBP in inflammation regulation networks. *Mol Med Rep,* 29.

ZHU, J., LI, S., ZHANG, Y., DING, G., ZHU, C., HUANG, S., ZHANG, A., JIA, Z. & LI, M. 2018. COX-2 contributes to LPS-induced Stat3 activation and IL-6 production in microglial cells. *Am J Transl Res,* 10**,** 966-974.

ZHU, Y., ZHANG, Y., HE, S., YI, S., FENG, H., XIA, X., FANG, X., GONG, X. & ZHAO, P. 2024. Integrating single-nucleus RNA sequencing and spatial transcriptomics to elucidate a specialized subpopulation of astrocytes, microglia and vascular cells in brains of mouse model of lipopolysaccharide-induced sepsis-associated encephalopathy. *J Neuroinflammation,* 21**,** 169.

ZOLLINGER, D. R., LINGLE, S. E., SORG, K., BEECHEM, J. M. & MERRITT, C. R. 2020. GeoMx RNA Assay: High Multiplex, Digital, Spatial Analysis of RNA in FFPE Tissue. *Methods Mol Biol,* 2148**,** 331-345.

ZRZAVY, T., HAMETNER, S., WIMMER, I., BUTOVSKY, O., WEINER, H. L. & LASSMANN, H. 2017. Loss of 'homeostatic' microglia and patterns of their activation in active multiple sclerosis. *Brain,* 140**,** 1900-1913.

Appendices

Appendix 1: Isolated RNA samples (for whole-brain bulk RNA sequencing) concentrations and quality ratios

Sample ID	Analysis ID	Conc. (ng/uL)	260/230 Ratio	260/280 Ratio
Control 0	S1	786.5053333	3.515333333*	2.624**
Control 1	S2	1151.894167	2.272666667	2.108333333
Control 2	S3	868.384	3.214*	2.576**
Control 3	S4	1182.2285	2.243	2.090166667
Control 4	S5	1060.994	3.047333333*	2.446333333
Aldara 0	S6	1133.249667	1.859666667	2.120833333
Aldara 1	S7	1168.485333	2.877	2.381333333
Aldara 2	S8	1154.128167	2.448166667	2.089166667
Aldara 3	S9	1087.262333	2.981	2.429666667
Aldara 4	S10	917.9905	1.761166667	2.097833333

Appendix 2: CosMx mouse neuroscience 1000-plex RNA panel

Gene	Human Gene	Gene	Human Gene	Gene	Human Gene	Gene	Human Gene	Gene	Human Gene	Gene	Human Gene	Gene	Human Gene	Gene	Human Gene	Gene	Human Gene	Gene	Human Gene	Gene	Human Gene
4930486L24R	CTSL	Bcl2	BCL2	Cpix1	CPLX1	F13a1	F13A1	H2-Ab1	HLA-DQB1	Lrrc7	LRRC7	Nsg1	NSG1	Prkce	PRKCE	Scn2a	SCN2A	Tab2	TAB2	Wwp2	WWP2
6330403K07I	LOC728392	Bcl2l1	BCL2L1	Cr1l	CR1L	Fa2h	FA2H	H2-Ea	HLA-DRA	Lrrk2	LRRK2	Ntm	NTM	Prkcq	PRKCQ	Scn8a	SCN8A	Tac1	TAC1	Xist	XIST
Abca2	ABCA2	Bdnf	BDNF	Creb5	CREB5	Fabp7	FABP7	H3f3b	H3-3A	Lrrtm3	LRRTM3	Ntrk2	NTRK2	Prkg1	PRKG1	Sec24b	SEC24B	Tacr1	TACR1	Xpo1	XPO1
Abi1	ABI1	Bex1/2	BEX1/2	Crebbp	CREBBP	Fau	FAU	H6pd	H6PD	Lsr	LSR	Ntrk3	NTRK3	Prkn	PRKN	Selenow	SELENOW	Tacr2	TACR2	Ybx1	YBX1
Abi2	ABI2	Bin1	BIN1	Crh	CRH	Fbln5	FBLN5	Hc	C5	Ltbp1	LTBP1	Ntsr2	NTSR2	Prnp	PRNP	Selplg	SELPLG	Tacr3	TACR3	Ywhae	YWHAE
Abl1	ABL1	Birc6	BIRC6	Crhr1	CRHR1	Fbn1	FBN1	Hdac4	HDAC4	Lynx1	LYNX1	Nup160	NUP160	Pros1	PROS1	Sem1	SEM1	Tagln	TAGLN	Ywhag	YWHAG
Abl2	ABL2	Bmpr1a	BMPR1A	Crhr2	CRHR2	Fbxo33	FBXO33	Hdac9	HDAC9	Lyz1/2	LYZ	Nup214	NUP214	Prps2	PRPS2	Sema5a	SEMA5A	Taldo1	TALDO1	Ywhaq	YWHAQ
Acaca	ACACA	Bmpr1b	BMPR1B	Crip1	CRIP1	Fbxw11	FBXW11	Hecw1	HECW1	Mag	MAG	Olfm1	OLFM1	Psap	PSAP	Sema6d	SEMA6D	Tank	TANK	Ywhaz	YWHAZ
Acacb	ACACB	Bmpr2	BMPR2	Crp	CRP	Fbxw7	FBXW7	Herc1	HERC1	Maged1	MAGED1	Olig1	OLIG1	Psen1	PSEN1	Serinc3	SERINC3	Taok3	TAOK3	Zbtb20	ZBTB20
Ace2	ACE2	Braf	BRAF	Cryab	CRYAB	Fgf1	FGF1	Herc4	HERC4	Magi1	MAGI1	Olig2	OLIG2	Psma1	PSMA1	Serinc5	SERINC5	Tardbp	TARDBP	Zeb1	ZEB1
Acer3	ACER3	Brwd1	BRWD1	Csf1	CSF1	Fgf2	FGF2	Hexb	HEXB	Malat1	MALAT1	Opa1	OPA1	Psmd1	PSMD1	Serpine2	SERPINE2	Tbl1x	TBL1X	Zfyve16	ZFYVE16
Acta2	ACTA2	Bsg	BSG	Csf1r	CSF1R	Fgfr2	FGFR2	Higd1b	HIGD1B	Maml2	MAML2	Oprd1	OPRD1	Psmd14	PSMD14	Serping1	SERPING1	Tbl1xr1	TBL1XR1	Zfyve9	ZFYVE9
Ada	ADA	Btrc	BTRC	Csmd3	CSMD3	Flt1	FLT1	Hip1	HIP1	Maml3	MAML3	Oprk1	OPRK1	Psme4	PSME4	Setx	SETX	Tcf12	TCF12	Znrf3	ZNRF3
Adam10	ADAM10	C1qb	C1QB	Csnk1a1	CSNK1A1	Fnip2	FNIP2	Hipk2	HIPK2	Man1a	MAN1A1	Oprm1	OPRM1	Pten	PTEN	Sgk1	SGK1	Tcf4	TCF4	Zwint	ZWINT
Adam22	ADAM22	C1qc	C1QC	Csnk2a1	CSNK2A1	Foxo1	FOXO1	Hmgb1	HMGB1	Man1a2	MAN1A2	P2rx4	P2RX4	Ptgds	PTGDS	Sgk3	SGK3	Tcf7l2	TCF7L2		
Adar	ADAR	C1s1/2	C1S	Cspg5	CSPG5	Foxo3	FOXO3	Hnrnpa2b1	HNRNPA2B1	Man1c1	MAN1C1	P2rx7	P2RX7	Ptgs2	PTGS2	Sh3gl2	SH3GL2	Tenm2	TENM2		
Adcy1	ADCY1	C2	C2	Cst3	CST3	Fpr2	FPR2	Homer1	HOMER1	Man2a1	MAN2A1	P2ry12	P2RY12	Ptk2	PTK2	Sh3gl3	SH3GL3	Tenm4	TENM4		
Adcy2	ADCY2	C3	C3	Cst7	CST7	Fpr3	FPR2	Hsp90aa1	HSP90AA1	Maoa	MAOA	P2ry14	P2RY14	Ptn	PTN	Sh3tc2	SH3TC2	Terf2ip	TERF2IP		
Adcy5	ADCY5	C5ar1	C5AR1	Ctbp2	CTBP2	Frs2	FRS2	Hsp90ab1	HSP90AB1	Maob	MAOB	P2ry2	P2RY2	Ptpn1	PTPN1	Shc3	SHC3	Tfdp2	TFDP2		
Adcy8	ADCY8	Cab39	CAB39	Ctnna1	CTNNA1	Fth1	FTH1	Hspa1a	HSPA1A	Map1b	MAP1B	Pak1	PAK1	Ptpn11	PTPN11	Shprh	SHPRH	Tgfb1	TGFB1		
Adcy9	ADCY9	Cab39l	CAB39L	Ctnna2	CTNNA2	Ftl1	FTL	Hspa1b	HSPA1B	Map2k1	MAP2K1	Pak2	PAK2	Ptpn13	PTPN13	Shtn1	SHTN1	Tgfb2	TGFB2		
Add1	ADD1	Cacna1a	CACNA1A	Ctnnb1	CTNNB1	Fus	FUS	Hspa4l	HSPA4L	Map2k4	MAP2K4	Pak3	PAK3	Ptpn4	PTPN4	Sil1	SIL1	Tgfbr1	TGFBR1		
Adgrg1	ADGRG1	Cacna1b	CACNA1B	Ctnnd2	CTNND2	Fxyd6	FXYD6	Hspa8	HSPA8	Map2k5	MAP2K5	Pard3	PARD3	Ptprg	PTPRG	Sipa1l1	SIPA1L1	Thrb	THRB		
Adgrl2	ADGRL2	Cacna1c	CACNA1C	Ctsb	CTSB	Fyn	FYN	Hsph1	HSPH1	Map2k6	MAP2K6	Park7	PARK7	Ptprj	PTPRJ	Skil	SKIL	Thsd4	THSD4		
Adgrl3	ADGRL3	Cacna1d	CACNA1D	Ctsd	CTSD	Fzd3	FZD3	Htr1a	HTR1A	Map3k5	MAP3K5	Parn	PARN	Ptpro	PTPRO	Slc10a6	SLC10A6	Thy1	THY1		
Adgrv1	ADGRV1	Cacna1e	CACNA1E	Ctss	CTSS	Gab1	GAB1	Htr2a	HTR2A	Map4k4	MAP4K4	Pbx1	PBX1	Ptprr	PTPRR	Slc11a2	SLC11A2	Tiam1	TIAM1		
Adora1	ADORA1	Cacna2d1	CACNA2D1	Ctxn1	CTXN1	Gab2	GAB2	Htr2c	HTR2C	Mapk1	MAPK1	Pcdh15	PCDH15	Ptprs	PTPRS	Slc12a2	SLC12A2	Timp2	TIMP2		
Adora2a	ADORA2A	Cacna2d3	CACNA2D3	Cul1	CUL1	Gabbr2	GABBR2	Htr3a	HTR3A	Mapk10	MAPK10	Pcp2	PCP2	Ptprz1	PTPRZ1	Slc13a3	SLC13A3	Tjp1	TJP1		
Adra1d	ADRA1D	Cacnb2	CACNB2	Cul5	CUL5	Gabra2	GABRA2	Htr6	HTR6	Mapk14	MAPK14	Pcp4	PCP4	Pvalb	PVALB	Slc17a7	SLC17A7	Tkt	TKT		
Adrb2	ADRB2	Cacnb4	CACNB4	Cx3cr1	CX3CR1	Gabrb1	GABRB1	Htt	HTT	Mapk8	MAPK8	Pcsk1n	PCSK1N	Rab1a	RAB1A	Slc18a2	SLC18A2	Tle4	TLE4		
Ago2	AGO2	Cacng3	CACNG3	Cxcl14	CXCL14	Gabrb2	GABRB2	Iapp	IAPP	Mapkap1	MAPKAP1	Pcsk5	PCSK5	Rab31	RAB31	Slc1a2	SLC1A2	Tlr4	TLR4		
Ago3	AGO3	Calb1	CALB1	Cyfip1	CYFIP1	Gabrb3	GABRB3	Icmt	ICMT	Mapt	MAPT	Pcsk6	PCSK6	Rab6a	RAB6A	Slc1a3	SLC1A3	Tmem119	TMEM119		
Agt	AGT	Calb2	CALB2	Cyfip2	CYFIP2	Gabrg3	GABRG3	Idnk	IDNK	Mark3	MARK3	Pde10a	PDE10A	Rab7	RAB7A	Slc24a3	SLC24A3	Tmsb10	TMSB10		
Agtr1a	AGTR1	Calca	CALCB	Daam1	DAAM1	Gad1	GAD1	Ifnar1	IFNAR1	Masp1	MASP1	Pde1a	PDE1A	Raf1	RAF1	Slc25a12	SLC25A12	Tmsb4x	TMSB4X		
Agtr1b	AGTR1	Calcr	CALCR	Daam2	DAAM2	Gad2	GAD2	Ifngr1	IFNGR1	Mbp	MBP	Pde1c	PDE1C	Ramp1	RAMP1	Slc25a4	SLC25A4	Tnc	TNC		
Agtr2	AGTR2	Calm1	CALM1	Dab1	DAB1	Gal	GAL	Ifngr2	IFNGR2	Mc1r	MC1R	Pde3b	PDE3B	Ranbp2	RGPD5	Slc2a1	SLC2A1	Tnf	TNF		
Ahcyl1	AHCYL1	Calm2	CALM2	Dapk1	DAPK1	Galr1	GALR1	Ift88	IFT88	Mc2r	MC2R	Pde4d	PDE4D	Rap1a	RAP1A	Slc2a13	SLC2A13	Tnik	TNIK		
Akt1	AKT1	Calm3	CALM1	Dapk2	DAPK2	Galr2	GALR2	Igf1r	IGF1R	Mc3r	MC3R	Pde7b	PDE7B	Rapgef1	RAPGEF1	Slc32a1	SLC32A1	Tnks	TNKS		
Akt3	AKT3	Camk1d	CAMK1D	Dbi	DBI	Galr3	GALR3	Igfbp7	IGFBP7	Mc4r	MC4R	Pde8a	PDE8A	Rapgef2	RAPGEF2	Slc38a9	SLC38A9	Tnr	TNR		
Alcam	ALCAM	Camk2a	CAMK2A	Dcc	DCC	Gap43	GAP43	Il10	IL10	Mc5r	MC5R	Pdgfd	PDGFD	Rasa1	RASA1	Slc39a10	SLC39A10	Tnrc6a	TNRC6A		
Aldh1l1	ALDH1L1	Camk2b	CAMK2B	Ddt	DDT	Gas2	GAS2	Il1b	IL1B	Mcm5	MCM5	Pdgfra	PDGFRA	Rasal2	RASAL2	Slc39a11	SLC39A11	Tnrc6b	TNRC6B		
Aldoa	ALDOA	Camk2d	CAMK2D	Deptor	DEPTOR	Gba	GBA	Il1rap	IL1RAP	Mcu	MCU	Pdyn	PDYN	Rasgrf2	RASGRF2	Slc44a1	SLC44A1	Tnrc6c	TNRC6C		
Aldoc	ALDOC	Camk2g	CAMK2G	Dera	DERA	Gbp2	GBP2	Il1rapl2	IL1RAPL2	Mdga2	MDGA2	Pecam1	PECAM1	Rb1	RB1	Slc4a4	SLC4A4	Tph2	TPH2		
Ambp	AMBP	Camk2n1	CAMK2N1	Des	DES	Gbp2b	GBP3	Il6	IL6	Mdh1	MDH1	Peli2	PELI2	Rb1cc1	RB1CC1	Slc4a8	SLC4A8	Traf3	TRAF3		
Ambra1	AMBRA1	Camk4	CAMK4	Dgkb	DGKB	Gcg	GCG	Inpp5a	INPP5A	Mef2a	MEF2A	Penk	PENK	Rbfox3	RBFOX3	Slc6a1	SLC6A1	Trem2	TREM2		
Anapc16	ANAPC16	Car8	CA8	Dgkg	DGKG	Gcgr	GCGR	Insr	INSR	Mef2c	MEF2C	Pfkl	PFKL	Rbks	RBKS	Slc6a3	SLC6A3	Trim2	TRIM2		
Ano6	ANO6	Cartpt	CARTPT	Dgki	DGKI	Gdnf	GDNF	Invs	INVS	Meg3	MEG3	Pfkm	PFKM	Rbp4	RBP4	Slc8a1	SLC8A1	Trim33	TRIM33		
Apba1	APBA1	Casp3	CASP3	Dicer1	DICER1	Gfap	GFAP	Ip6k2	IP6K2	Megf11	MEGF11	Pfkp	PFKP	Rbpj	RBPJ	Slc9a3r1	SLC9A3R1	Trim62	TRIM62		
Apc	APC	Cast	CAST	Dlg1	DLG1	Gfod1	GFOD1	Irf2	IRF2	Mertk	MERTK	Pgd	PGD	Reln	RELN	Slit2	SLIT2	Trio	TRIO		
Apela	APELA	Cblb	CBLB	Dlg4	DLG4	Ghr	GHR	Irf6	IRF6	Mfge8	MFGE8	Pgls	PGLS	Rgl1	RGL1	Sln	SLN	Trip12	TRIP12		
Aph1b/c	APH1B	Cbln2	CBLN2	Dlgap2	DLGAP2	Gja1	GJA1	Irs2	IRS2	Mib1	MIB1	Pgm1	PGM1	Rgn	RGN	Smad2	SMAD2	Trp53	TP53		
Aplnr	APLNR	Cck	CCK	Dlk1	DLK1	Gjb1	GJB1	Itch	ITCH	Mid1	MID1	Phactr1	PHACTR1	Rgs12	RGS12	Smad3	SMAD3	Trpm7	TRPM7		
Aplp2	APLP2	Cckar	CCKAR	Dmd	DMD	Glp1r	GLP1R	Itga2	ITGA2	Mll11	MLLT11	Phc2	PHC2	Rgs5	RGS5	Smurf1	SMURF1	Trpv1	TRPV1		
Apoe	APOE	Cckbr	CCKBR	Dnah14	DNAH14	Glp2r	GLP2R	Itga8	ITGA8	Mobp	MOBP	Phc3	PHC3	Rgs6	RGS6	Snap25	SNAP25	Tspan3	TSPAN3		
App	APP	Ccnf	CCNF	Dnah6	DNAH6	Gls	GLS	Itga9	ITGA9	Mog	MOG	Phkb	PHKB	Rgs7	RGS7	Snca	SNCA	Tspan5	TSPAN5		
Aqp4	AQP4	Cd109	CD109	Dnah7a/b/c	DNAH7	Glul	GLUL	Itgav	ITGAV	Msr1	MSR1	Phlpp1	PHLPP1	Rhobtb1	RHOBTB1	Sncb	SNCB	Tspan7	TSPAN7		
Arhgef7	ARHGEF7	Cd14	CD14	Dnajc1	DNAJC1	Gm2a	GM2A	Itgax	ITGAX	Mt1	MT1A	Pias1	PIAS1	Rictor	RICTOR	Snhg11	SNHG11	Tspo	TSPO		
Arih1	ARIH1	Cd44	CD44	Dner	DNER	Gnai1	GNAI1	Itgb8	ITGB8	Mt3	MT3	Pik3c3	PIK3C3	Rims1	RIMS1	Snn	SNN	Ttc3	TTC3		
Arpp21	ARPP21	Cd46	CD46	Dnm1	DNM1	Gnai2	GNAI2	Itm2a	ITM2A	Mtmr3	MTMR3	Pik3ca	PIK3CA	Rims2	RIMS2	Snrpn	SNRPN	Ttr	TTR		
Arrb1	ARRB1	Cd55	CD55	Dnm1l	DNM1L	Gnal	GNAL	Itm2b	ITM2B	Myl6	MYL6	Pik3cb	PIK3CB	Rit2	RIT2	Sod1	SOD1	Tuba1a/b/c	TUBA1A/B/C		
Artn	ARTN	Cd74	CD74	Dnm2	DNM2	Gnao1	GNAO1	Itm2c	ITM2C	Myl9	MYL9	Pik3r1	PIK3R1	Rnf144a	RNF144A	Sorbs1	SORBS1	Tubb5	TUBB		
Aspa	ASPA	Cd81	CD81	Dnm3	DNM3	Gnaq	GNAQ	Itpr1	ITPR1	Myo6	MYO6	Pink1	PINK1	Robo1	ROBO1	Sorl1	SORL1	Tusc3	TUSC3		
Astn2	ASTN2	Cd9	CD9	Dock1	DOCK1	Gnas	GNAS	Itpr2	ITPR2	Myrf	MYRF	Pip5k1b	PIP5K1B	Robo2	ROBO2	Sort1	SORT1	Tyrobp	TYROBP		
Atf6	ATF6	Cdc14b	CDC14B	Dock10	DOCK10	Gnb1	GNB1	Jak1	JAK1	Nap1l5	NAP1L5	Pirb	LILRB3	Rock1	ROCK1	Sos1	SOS1	Ube2e1	UBE2E1		
Atg10	ATG10	Cdc27	CDC27	Dock3	DOCK3	Gng7	GNG7	Jak2	JAK2	Nav3	NAV3	Pkn2	PKN2	Rock2	ROCK2	Sos2	SOS2	Ube2e2	UBE2E2		
Atg13	ATG13	Cdc6	CDC6	Dok6	DOK6	Gphn	GPHN	Jam3	JAM3	Nbea	NBEA	Pla2g4c	PLA2G4C	Ror1	ROR1	Sox5	SOX5	Ube2e3	UBE2E3		
Atg2b	ATG2B	Cdk6	CDK6	Drd1	DRD1	Gpi1	GPI	Jun	JUN	Ncam1	NCAM1	Plcb1	PLCB1	Rora	RORA	Sox6	SOX6	Ube2g1	UBE2G1		
Atg4c	ATG4C	Cdk8	CDK8	Drd2	DRD2	Gpm6a	GPM6A	Kalrn	KALRN	Nckap1	NCKAP1	Plcb4	PLCB4	Rpe	RPE	Sox9	SOX9	Ube2h	UBE2H		
Atg5	ATG5	Cfh	CFH	Drd4	DRD4	Gpm6b	GPM6B	Kat2b	KAT2B	Ncor1	NCOR1	Plcl1	PLCL1	Rpia	RPIA	Spag9	SPAG9	Ube2k	UBE2K		
Atg7	ATG7	Chchd10	CHCHD10	Dscam	DSCAM	Gpnmb	GPNMB	Kcna2	KCNA2	Ncor2	NCOR2	Pllp	PLLP	Rpl10	RPL10	Sparc	SPARC	Ube2r2	UBE2R2		
Atm	ATM	Chl1	CHL1	Dscaml1	DSCAML1	Gpr158	GPR158	Kcnd2	KCND2	Ndrg1	NDRG1	Plp1	PLP1	Rpl13a	RPL13A	Sparcl1	SPARCL1	Ube3c	UBE3C		
Atp1a2	ATP1A2	Chrm1	CHRM1	Dtl	DTL	Gpr17	GPR17	Kcnj3	KCNJ3	Ndrg2	NDRG2	Plpp3	PLPP3	Rpl14	RPL14	Spg11	SPG11	Ube4b	UBE4B		
Atp1b1	ATP1B1	Chrm2	CHRM2	Dync1h1	DYNC1H1	Gpr37	GPR37	Kcnq3	KCNQ3	Ndrg4	NDRG4	Plppr1	PLPPR1	Rpl32	RPL32	Spock1	SPOCK1	Ubr5	UBR5		
Atp2a2	ATP2A2	Chrm3	CHRM3	Dync1i1	DYNC1I1	Gpr37l1	GPR37L1	Kcnq5	KCNQ5	Ndufa10	NDUFA10	Pltp	PLTP	Rpl37	RPL37	Spp1	SPP1	Ugt2	UGGT2		
Atp2b1	ATP2B1	Chrm5	CHRM5	Dync1i2	DYNC1I2	Grb10	GRB10	Kdm4a	KDM4A	Ndufa13	NDUFA13	Plxna4	PLXNA4	Rplp0	RPLP0	Spp2	SPP2	Ugt8a	UGT8		
Atp2b2	ATP2B2	Chrna4	CHRNA4	Dync1li2	DYNC1LI2	Grb2	GRB2	Kidins220	KIDINS220	Ndufa4	NDUFA4	Pmch	PMCH	Rps14	RPS14	Sptan1	SPTAN1	Ulk2	ULK2		
Atp2b4	ATP2B4	Chrna7	CHRNA7	Dynll1	DYNLL1	Gria1	GRIA1	Kif5c	KIF5C	Ndufs1	NDUFS1	Polr2f	POLR2F	Rps27	RPS27	Sptbn1	SPTBN1	Unc5c	UNC5C		
Atp6v0a1	ATP6V0A1	Ckb	CKB	Dynll2	DYNLL2	Gria2	GRIA2	Kirrel3	KIRREL3	Nedd4l	NEDD4L	Pomc	POMC	Rps4x	RPS4Y1	Sptbn4	SPTBN4	Unc5d	UNC5D		
Atp6v1a	ATP6V1A	Clasp2	CLASP2	Eda	EDA	Gria3	GRIA3	Ksr2	KSR2	Negr1	NEGR1	Pou2f1	POU2F1	Rps5	RPS5	Srgn	SRGN	Uqcr10	UQCR10		
Atp6v1h	ATP6V1H	Cldn5	CLDN5	Edn1	EDN1	Gria4	GRIA4	Lama2	LAMA2	Nell2	NELL2	Ppargc1a	PPARGC1A	Rps6ka2	RPS6KA2	Ssh2	SSH2	Uqcrq	UQCRQ		
Atp8a1	ATP8A1	Clec7a	CLEC7A	Edn2	EDN2	Grid1	GRID1	Lamc2	LAMC2	Neo1	NEO1	Ppfia2	PPFIA2	Rps6ka3	RPS6KA3	Sspo	SSPOP	Ush1g	USH1G		
Atpif1	ATPIF1	Clip1	CLIP1	Edn3	EDN3	Grid2	GRID2	Lamp2	LAMP2	Neu4	NEU4	Ppp1r13b	PPP1R13B	Rps6ka5	RPS6KA5	Sst	SST	Usp15	USP15		
Atr	ATR	Clstn1	CLSTN1	Ednra	EDNRA	Grik1	GRIK1	Lancl1	LANCL1	Nf1	NF1	Ppp1r1b	PPP1R1B	Rps9	RPS9	Sstr1	SSTR1	Usp34	USP34		
Atrn	ATRN	Clu	CLU	Ednrb	EDNRB	Grik2	GRIK2	Lep	LEP	Nfasc	NFASC	Ppp2r2a	PPP2R2A	Rptor	RPTOR	Sstr2	SSTR2	Usp9x	USP9X		
Atxn1	ATXN1	Cmip	CMIP	Eef2k	EEF2K	Grin1	GRIN1	Lepr	LEPR	Nfe2l2	NFE2L2	Ppp2r2c	PPP2R2C	Rspo2	RSPO2	Sstr3	SSTR3	Uvrag	UVRAG		
Atxn2	ATXN2	Cnksr2	CNKSR2	Efna5	EFNA5	Grin2a	GRIN2A	Lgi2	LGI2	Nfkb1	NFKB1	Ppp2r3a	PPP2R3A	Rtn1	RTN1	Sstr4	SSTR4	Vav3	VAV3		
Auts2	AUTS2	Cnr1	CNR1	Egfr	EGFR	Grin2b	GRIN2B	Lgr4	LGR4	Nlgn4l	NLGN4X	Ppp2r5c	PPP2R5C	Rtn3	RTN3	St3gal6	ST3GAL6	Vcan	VCAN		
Avp	AVP	Cntn1	CNTN1	Egr1	EGR1	Grip1	GRIP1	Lgr5	LGR5	Nlk	NLK	Ppp2r5e	PPP2R5E	Rtn4	RTN4	Stat2	STAT2	Vegfa	VEGFA		
Avpr1a	AVPR1A	Cntn2	CNTN2	Eif4a2	EIF4A2	Grk3	GRK3	Lifr	LIFR	Nnat	NNAT	Ppp3ca	PPP3CA	Runx1	RUNX1	Stat3	STAT3	Vim	VIM		
Avpr1b	AVPR1B	Cntn4	CNTN4	Eif4g3	EIF4G3	Grm1	GRM1	Lilra5	LILRA5	Nos1	NOS1	Ppp3cb	PPP3CB	Ryr2	RYR2	Stk3	STK3	Vip	VIP		
Avpr2	AVPR2	Cntn5	CNTN5	Elmo1	ELMO1	Grm3	GRM3	Lilrb4a/b	LILRB4	Npy	NPY	Ppp3cc	PPP3CC	Ryr3	RYR3	Stmn2	STMN2	Vipr1	VIPR1		
Axl	AXL	Col4a5	COL4A5	Emcn	EMCN	Grm5	GRM5	Lpar1	LPAR1	Npy1r	NPY1R	Prex1	PREX1	S100a16	S100A16	Stmn3	STMN3	Vipr2	VIPR2		
B2m	B2M	Comt	COMT	Emp1	EMP1	Grm7	GRM7	Lpar2	LPAR2	Npy2r	NPY2R	Prickle1	PRICKLE1	S100b	S100B	Sulf2	SULF2	Vmp1	VMP1		
B3gnt5	B3GNT5	Cop1	COP1	Entpd2	ENTPD2	Grm8	GRM8	Lpar3	LPAR3	Nr3c1	NR3C1	Prickle2	PRICKLE2	Sall1	SALL1	Sv2a	SV2A	Vtn	VTN		
Bace1	BACE1	Cox4i1	COX4I1	Ep300	EP300	Grn	GRN	Lpar6	LPAR6	Nrcam	NRCAM	Prkacb	PRKACB	Samhd1	SAMHD1	Syn2	SYN2	Wac	WAC		
Bace2	BACE2	Cox6c	COX6C	Epb41l2	EPB41L2	Gsk3b	GSK3B	Lpin1	LPIN1	Nrf1	NRF1	Prkag2	PRKAG2	Sbf2	SBF2	Syn3	SYN3	Wasf1	WASF1		
Bcan	BCAN	Cox7c	COX7C	Epb41l3	EPB41L3	Gsn	GSN	Lpl	LPL	Nrg1	NRG1	Prkar1b	PRKAR1B	Scd2	SCD	Synpr	SYNPR	Wdr41	WDR41		
Bcas1	BCAS1	Cox8a	COX8A	Ephb6	EPHA6	Gstm1	GSTM5	Lrp2	LRP2	Nrg2	NRG2	Prkar2a	PRKAR2A	Scg2	SCG2	Syp	SYP	Wdr59	WDR59		
Bche	BCHE	Cpb2	CPB2	Epn2	EPN2	Gucy1a2	GUCY1A2	Lrp6	LRP6	Nrgn	NRGN	Prkar2b	PRKAR2B	Scg5	SCG5	Syt1	SYT1	Wscd1	WSCD1		
Bcl2	BCL2	Cpe	CPE	Esam	ESAM	H2-Aa	HLA-DQA1	Lrrc4c	LRRC4C	Nrsn1	NRSN1	Prkca	PRKCA			Syt11	SYT11	Wwp1	WWP1		

Appendix 3: Flow cytometry gating strategy and FMO controls for microglia and T cell subset identification

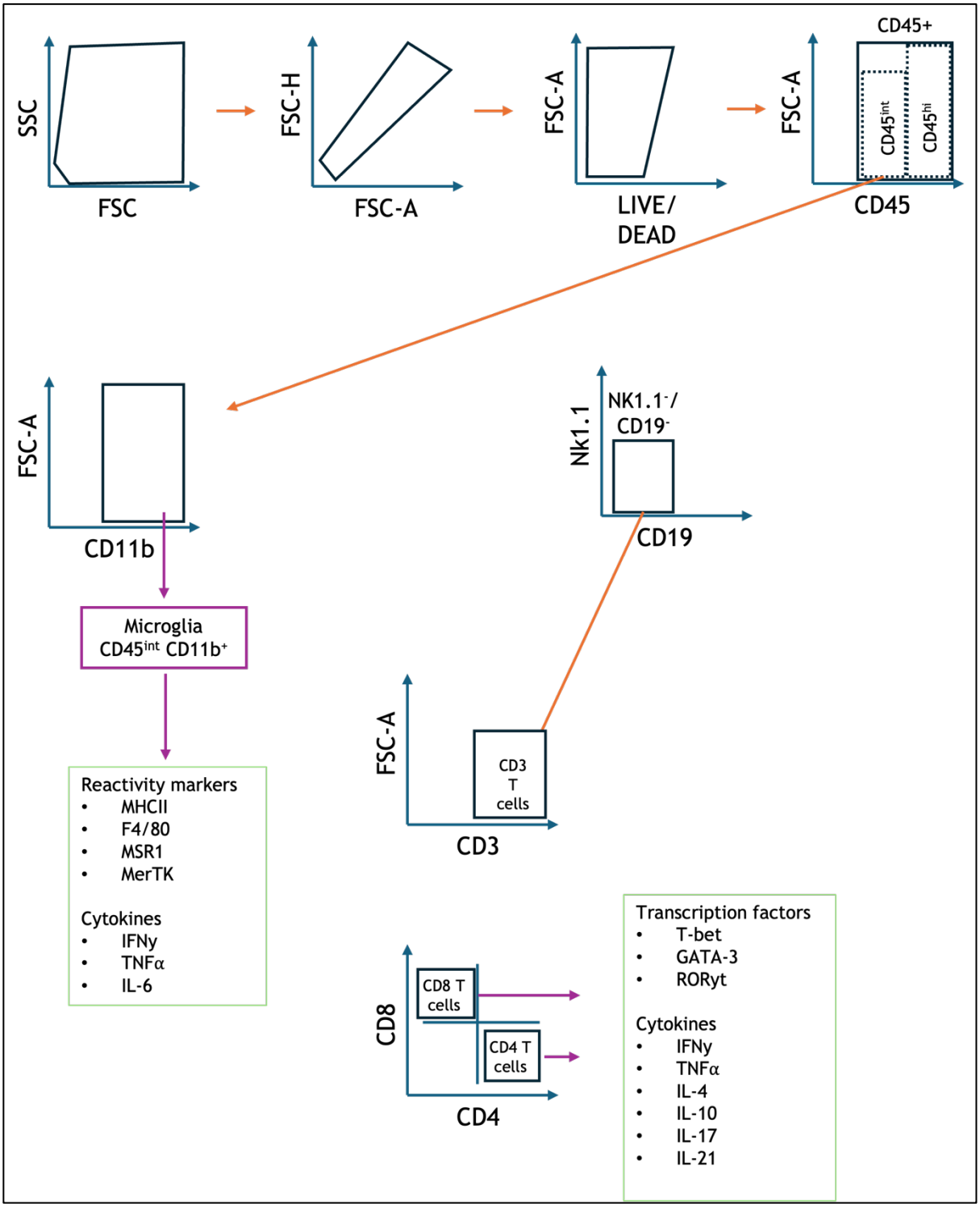

Immune cell (CD45+) gating strategy with FMO

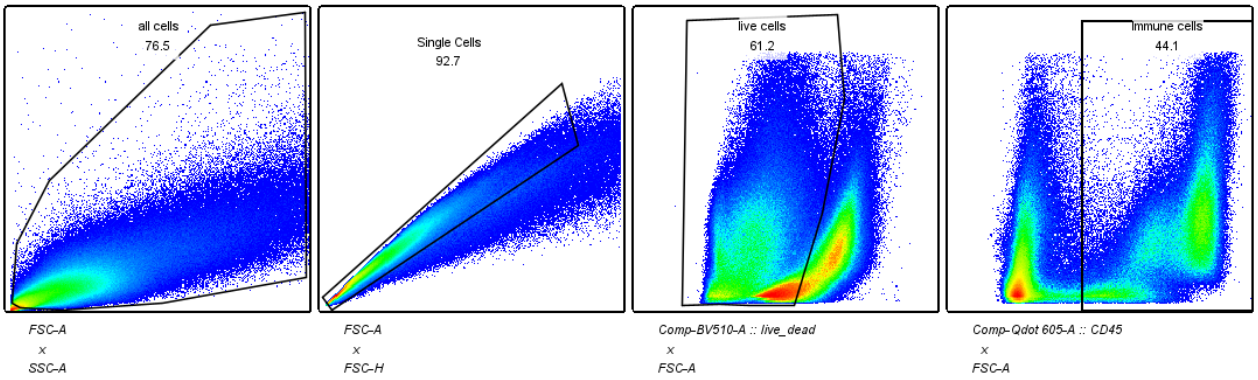

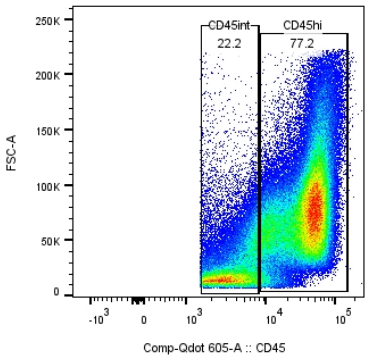

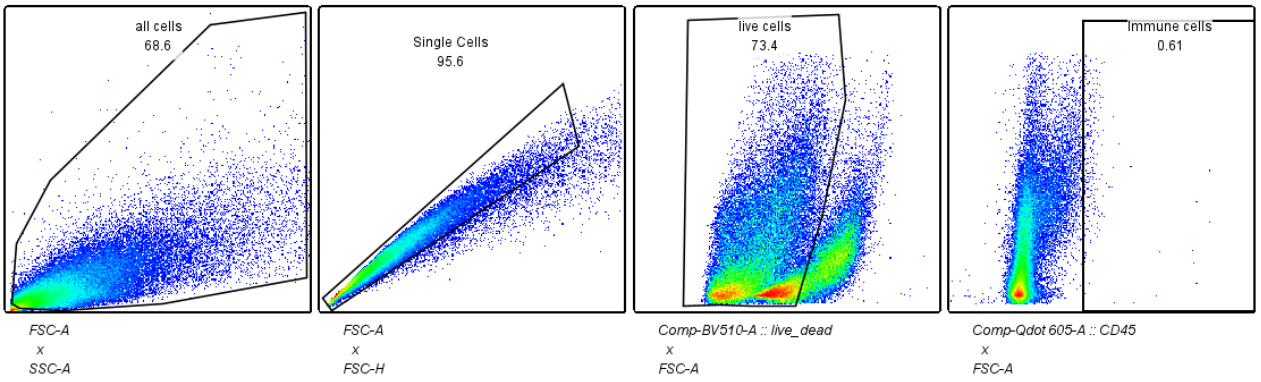

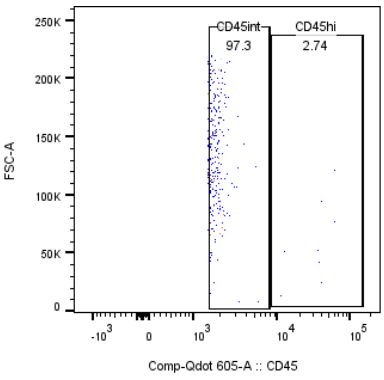

CD3 T cell gating and FMO

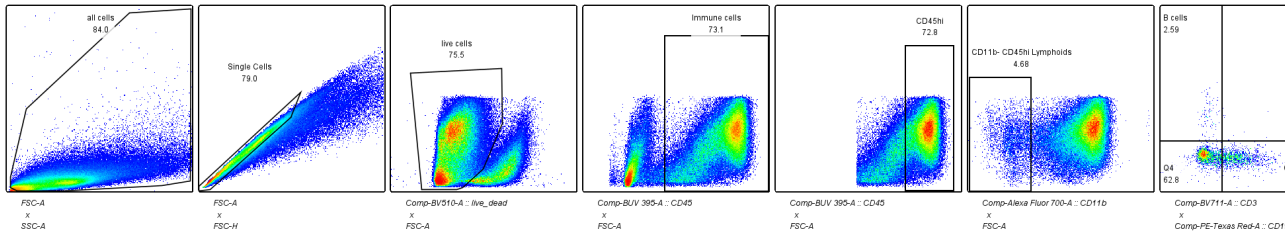

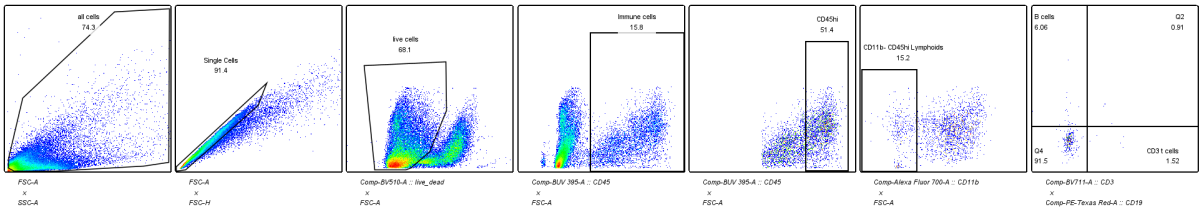

CD4 gating and FMO

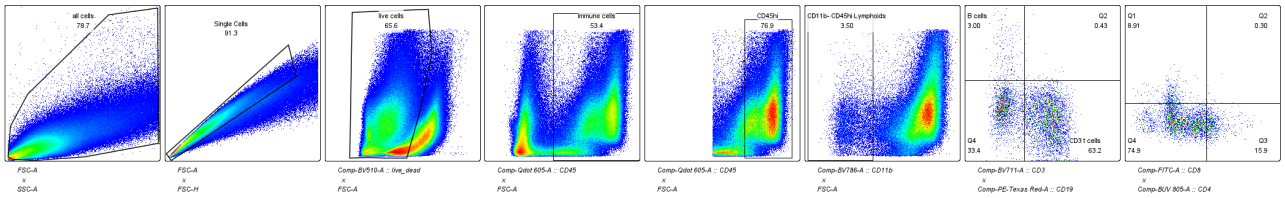

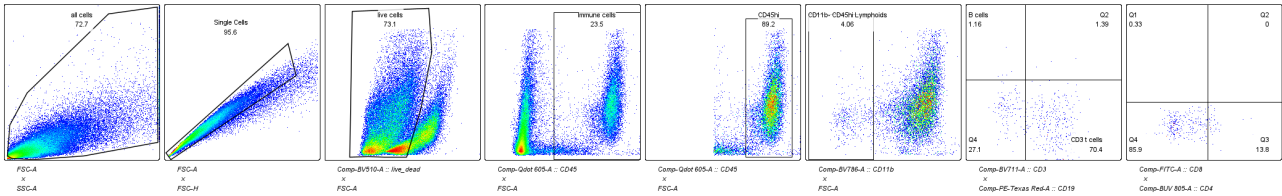

CD8 gating and FMO

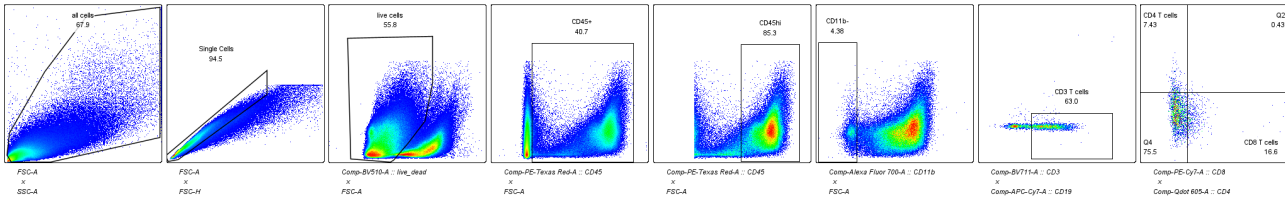

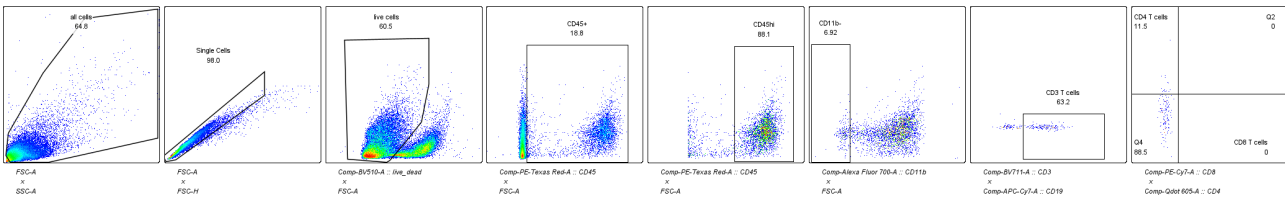

Microglia gating and FMO

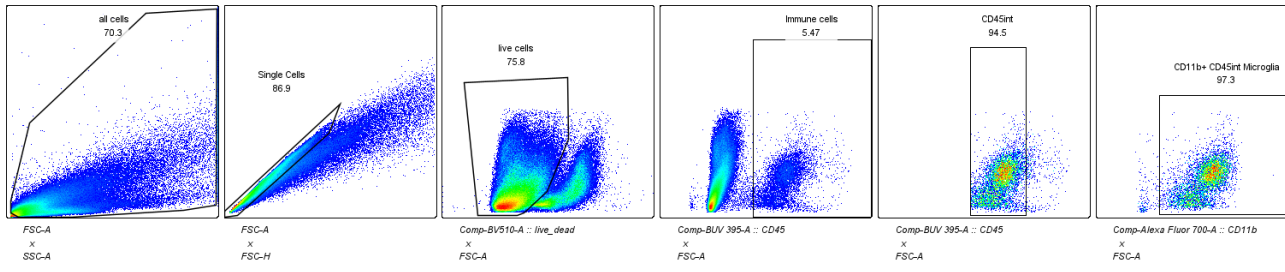

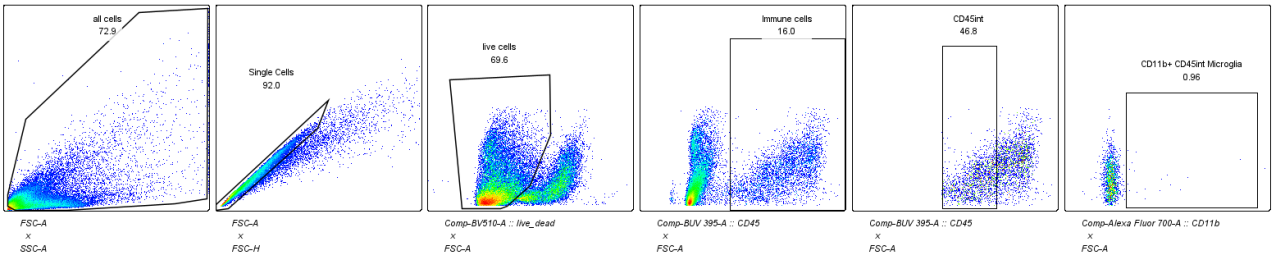
all cells
72.9
FSC-A
x
SSC-A
Single Cells
92.0
FSC-A
x
FSC-H
live cells
69.6
Comp-BV510-A :: live_dead
x
FSC-A
Immune cells
16.0
Comp-BUV 395-A :: CD45
x
FSC-A
CD45int
46.8
Comp-BUV 395-A :: CD45
x
FSC-A
CD11b+ CD45int Microglia
0.96
Comp-Alexa Fluor 700-A :: CD11b
x
FSC-A